

**Coordination Chemistry of Vanadium(IV) and Vanadium(V) with Amidoxime Ligands
and its Role in Sequestering Uranium from Seawater**

A Dissertation

Presented in Partial Fulfillment of the Requirements for the

Degree of Doctorate of Philosophy

with a

Major in Chemistry

in the

College of Graduate Studies

University of Idaho

by

Ruma Joshi

Major Professor: Chien M. Wai, Ph.D.

Committee Members: Thomas E. Bitterwolf, Ph.D., I. Francis Cheng, Ph.D.,
Thomas Williams, Ph.D.

Department Administrator: Ray von Wandruszka, Ph.D.

May 2017

Authorization to Submit Dissertation

This dissertation of Ruma Joshi, submitted for the degree of Doctorate of Philosophy with a Major in Chemistry and titled “Coordination Chemistry of Vanadium(IV) and Vanadium(V) with Amidoxime Ligands and its Role in Sequestering Uranium from Seawater,” has been reviewed in final form. Permission, as indicated by the signatures and dates below, is now granted to submit final copies to the College of Graduate Studies for approval.

Major Professor: _____ Date: _____
Chien M. Wai, Ph.D.

Committee Members: _____ Date: _____
Thomas E. Bitterwolf, Ph.D.

_____ Date: _____
I. Francis Cheng, Ph.D.

_____ Date: _____
Thomas Williams, Ph.D.

Department Administrator: _____ Date: _____
Ray von Wandruszka, Ph.D.

Abstract

Nuclear power is a significant alternative energy resource because it is free of carbon emissions and hence prevents global warming and climate change. Uranium is an essential fuel used for the generation of nuclear power. Since the current uranium deposits of about 63 million metric tons present in terrestrial sources might be exhausted by the end of this century, active research has been done in the past and is still under development for the establishment of a cost-effective technique for the extraction of uranium from seawater.

Chapter one provides an outlook on different energy resources and the importance of nuclear energy. Chapter two highlights the novel approaches explored by various research groups for the extraction of uranium from seawater using amidoxime-based polymer adsorbents. Competition of vanadium with uranium in seawater for adsorption to the amidoxime-based adsorbent is discussed. Chapter three examines the solution phase complexation of glutarimidedioxime and glutardiamidoxime with UO_2^{+2} , VO_2^+ , and VO^{+2} because the knowledge gained will aid in understanding the adsorption of uranium and vanadium using amidoxime-based adsorbents for the extraction of uranium from seawater.

Chapter four uses ^{13}C CP/MAS solid state NMR (SSNMR) spectroscopy for the characterization of a newly synthesized LCW polymer adsorbent derived from acrylic fiber and the Oak Ridge National Lab adsorbent (ORNL-AF1). According to the SSNMR results, the former contains primarily the open-chain glutardiamidoxime groups, whereas the latter contains mainly the cyclic glutarimidedioxime groups. The vanadium uptake by the adsorbents was examined in simulated seawater conditions using the ICP-MS technique. The ORNL-AF1 adsorbent has a higher vanadium adsorption capacity relative to the LCW adsorbent. The result is consistent with the observation made in the solution phase

complexation study, which shows that vanadium has a much higher affinity for cyclic glutarimidedioxime than the open-chain glutardiamidoxime.

It should be cautioned that the coordination behavior of metal ions with free ligand molecules may not be the same as the ligand attached to a polymer adsorbent. Nevertheless, the information obtained from the solution phase chemistry of the metal/ligand complexes presented in Chapter three of the dissertation is still valuable for designing new amidoxime-based adsorbents with higher uranium adsorption capacity.

Curriculum Vitae

Ruma Joshi

EDUCATION

Ph.D. (Analytical Chemistry)	University of Idaho, Moscow, Idaho	Spring 2017
M.Sc. (Organic Chemistry) First Rank Holder	Kumaun University Nainital, India	June 2006
B.Sc. (Chemistry, Botany, Zoology) First Rank Holder	Kumaun University Nainital, India	July 2004

PROFESSIONAL EXPERIENCE

Research Assistant, University of Idaho (Aug. 2015 – Aug. 2016, Moscow, ID) Worked on the following projects.

Coordination chemistry of vanadium(IV) and vanadium(V) with amidoxime ligands and its role in sequestering uranium from seawater. Spectroscopic characterization of amidoxime based polymer adsorbents and probing vanadium adsorption by ICP-MS.

The effect of tributylphosphate and tributyl phosphine oxide on hydrogen bonding interactions between water and 1-ethyl-3-methylimidazolium cation in 1-ethyl-3-methylimidazolium bis(trifluoromethylsulfonyl)imide. Investigation of lanthanum (III) complexes with tributylphosphine oxide in imidazolium-based room temperature ionic liquid.

Teaching Assistant, University of Idaho (Aug. 2012–Aug. 2015, Aug. 2016 - Dec. 2016 Moscow, ID)

Research Associate, ITC R&D Centre, Bangalore, India (Sep. 2006 – June 2012)

AWARDS AND RECOGNITION

- Teaching Assistant of the Year, University of Idaho, Department of Chemistry, 2015
- 2nd place, Innovation Showcase, University of Idaho, Graduate Research Oral presentation category, 2014
- Gold Medal, debate competition held at National Cadet Corps Battalion, Almora
- Member of 1st place team, Quiz Competition, World Environment Day at ITC R&D Centre, 2007, 2008
- Member of 1st place team, Quiz Competition, National Safety Day at ITC R&D Centre, 2008

- 2nd prize, Quiz Competition organized by Information and Broadcasting Ministry, Government of India, at Haldwani, Nainital, 2004

RESEARCH PUBLICATIONS

Joshi, R.; Pasilis, S. P. The effect of tributylphosphate and tributyl phosphine oxide on hydrogen bonding interactions between water and the 1-ethyl-3-methylimidazolium cation in 1-ethyl-3-methylimidazolium bis(trifluoromethylsulfonyl)imide. *J. Mol. Liq.* **2015**, *209*, 381–386.

Pan, H.B.; Kuo, L.; Wai, C. M.; Miyamoto, N.; **Joshi, R.;** Wood, J. R.; Strivens, J. E.; Janke, C. J.; Oyola, Y.; Das, S.; Mayes, R. T.; Gill, G. A. Elution of Uranium and Transition Metals from Amidoxime-Based Polymer Adsorbents for Sequestering Uranium from Seawater. *Ind. Eng. Chem. Res.* **2016**, *55*, 4313–4320.

Joshi, R.; Porter, J. C.; Pasilis, S. P. Investigation of Lanthanum (III) Complexes with Tributylphosphine Oxide in Imidazolium-based Room Temperature Ionic Liquid. Manuscript in progress.

Joshi, R.; Pan, H.B.; Wai, C. M. Vanadium and Uranium Coordination with Amidoxime Molecules in Aqueous Solutions. Manuscript in progress.

Joshi, R.; Pan, H.B.; Wai, C. M. Spectroscopic Characterization of Amidoxime Based Polymer Adsorbents and Probing Vanadium adsorption by ICP-MS. Manuscript in progress.

CONFERENCE PRESENTATIONS

- Oral presentation at 248th American Chemical Society (ACS) National Meeting & Exposition, San Francisco, California, United States, August 10-14, 2014.
- Oral presentation of research work, at Innovation Showcase, University of Idaho, April 16, 2014.
- Oral presentation of research work at the Idaho Academy of Sciences meeting in Moscow ID, March 21, 2014.
- Poster Presentation at 247th American Chemical Society (ACS) National Meeting & Exposition, Dallas, TX, United States, March 16-20, 2014.

PROFESSIONAL ACTIVITIES

- Member, American Chemical Society (ACS)
- Graduate student member, Tenure and Promotion Committee of Assistant Professor, 2015
- National Cadet Corps (NCC) “C” Certificate holder, Rank Senior Under Officer, 2004
- NCC “B” Certificate holder, Rank Under Officer, 2003
- Internal Auditor, DET NORSKE VERITAS - audited the labs on EMS Systems as per ISO 14001:2004 standard

Acknowledgements

I would like to thank God Almighty from the bottom of my heart for being with me all the way and for making possible my childhood dream and ambition of pursuing this doctoral program and for approval and support in writing this doctoral dissertation.

I would like to express my devoted thanks to my PhD. advisor Dr. Chien M. Wai for his help during my program. I am very lucky to have had you as my major advisor. I thank you for your patience and understanding. Your mentoring has made me develop into a good research scientist.

I would also like to thank my committee members Drs. Thomas E. Bitterwolf, I. Francis Cheng, and Thomas Williams for serving on my committee. Your suggestions have been invaluable to my research work. I sincerely thank Dr. Alexander Blumenfeld for his time in teaching me NMR spectroscopy, operating the NMR instrument, and engaging in research discussions and advice. Without his support, I would not have had the opportunity to become the chemist I am today. I would also like to thank Dr. Jean'ne M. Shreeve for helping with chemicals when needed and Dr. Lee Deobald for his help in obtaining the mass spec data.

To all the students that I have worked with in the lab: Dr. Horng-Bin Pan, Dr. Clive H Yen, Wen-Lung Chang, Hsieh Hsiang, Anup Tuladhar, as well as all of the chemistry departmental staff: Cindy Ball, Ashley Bogar, Terry Evans, Wells Travis, William Whittaker, Dave Sergent, and others. I thank you all for your patience in dealing with me and your contributions to the success of this dissertation. Special thanks to Deb Cissell and my friends Jesse and Justin for their support and encouragement during my time at UI.

I would like to acknowledge Dr. and Mrs. Renfrew for the Malcolm Renfrew summer scholarships I received each summer, as well as the Graduate and Professional Students Associations of the University of Idaho (GPSA-UI).

Finally, I have to specially thank my brothers Sanjay Kumar Joshi and Sunil Kumar Joshi, my sisters Neha and Lata Joshi, and Dr. Shashank Vaman Dhalewadikar for guiding, protecting, and providing for me. I also thank all of my friends here in Moscow, Idaho, and my department. Thank you everyone for your help.

Dedication

*This dissertation is dedicated to my parents, Pooran Chandra Joshi and Pushpa Joshi, my brothers Sanjay Kumar Joshi and Sunil Kumar Joshi, my sisters Lata Joshi and Neha Joshi, and Dr. Shashank Vaman Dhalewadikar.
Thank you all for your prayers.*

Table of Contents

Authorization to Submit Dissertation	ii
Abstract.....	iii
Curriculum Vitae	v
Acknowledgements.....	vii
Dedication.....	ix
Table of Contents.....	x
List of Figures.....	xiii
List of Tables	xxiv
List of Abbreviations	xxv
Chapter 1: Introduction.....	1
1.1 Outlook on Different Energy Resources.....	1
1.2 The Nuclear Fuel Cycle	3
1.3 Uranium from Oceans	6
1.4 Objectives of This Thesis.....	9
1.5 Achievements of This Thesis	10
References.....	15
Chapter 2: Literature Review.....	23
2.1 Introduction.....	23
2.2 Speciation of Uranyl(VI), Vanadium(V) and Vanadium(IV) in Presence of Amidoxime Ligands.....	26
2.3 Adsorbents for Uranium Extraction from Seawater	34
2.4 Comparison of Different Metal Elution Approaches	39

2.5	Cost Analysis	40
2.6	Conclusions.....	41
	References.....	43
Chapter 3: Vanadium and Uranium Coordination with Amidoxime Ligands in Aqueous Solutions		
		53
3.1	Abstract.....	53
3.2	Introduction.....	53
3.3	Experimental.....	55
3.3.1	Chemicals and reagents.....	55
3.3.2	Instrumentation	55
3.3.3	Sample preparation.....	56
3.4	Results and Discussion	57
3.4.1	Complexation of vanadium(V) with glutarimidedioxime.....	61
3.4.2	Complexation of vanadium(V) with glutarimidedioxime in presence of UO_2^{+2} at the pH of 8.3.....	76
3.4.3	Glutarimidedioxime complexation with UO_2^{+2}	79
3.4.4	Complexation of vanadium(V) with glutarimidedioxime in presence of UO_2^{+2}	85
3.4.5	Open-chain glutardiamidoxime complexation with UO_2^{+2}	93
3.4.6	Competition of glutardiamidoxime and carbonate for complexation with UO_2^{+2}	100
3.4.7	Vanadium(V) complexation with open-chain glutardiamidoxime	104
3.4.8	Vanadium(IV) complexation with glutarimidedioxime and glutardiamidoxime	108
3.4.9	Glutarimidedioxime complexation with vanadium(V) using LC-MS and formation of polynuclear vanadium species	121
3.5	Conclusions.....	126

References.....	129
Chapter 4: Spectroscopic Characterization of Amidoxime Based Polymer Adsorbents and Probing Vanadium Adsorption by ICP-MS.....	135
4.1 Abstract.....	135
4.2 Introduction.....	136
4.2.1 Type of interactions in solid state NMR.....	139
4.2.2 Techniques used in solid state NMR.....	141
4.2.3 Advantages and drawbacks of using solid state NMR.....	143
4.2.4 Applications of solid state NMR.....	144
4.3 Experimental.....	144
4.3.1 Chemicals and reagents.....	144
4.3.2 Instrumentation.....	145
4.3.3 Sample preparation.....	146
4.4 Results and Discussion.....	151
4.4.1 Characterization of glutarimidedioxime and glutardiamidoxime using ¹³ C CP/MAS solid state NMR spectroscopy.....	151
4.4.2 Characterization of amidoxime and carboxylate containing polymer adsorbents using ¹³ C CP/MAS solid state NMR and FTIR spectroscopy.....	154
4.4.3 Vanadium adsorbtion in simulated seawater by the LCW adsorbent without and with NaOH treatment.....	164
4.4.4 Vanadium adsorbtion in simulated seawater by ORNL adsorbent after KOH conditioning.....	169
4.5 Conclusions.....	172
References.....	174

List of Figures

Figure 2.1 Different modes of amidoxime functional group binding to UO_2^{+2} ($\text{M} = \text{UO}_2^{+2}$) (a) monodentate, (b) bidentate, and (c) η^2 binding. (Figure adapted from reference 23).....	28
Figure 2.2 Formation and coordination modes of Glutarimidedioxime and Glutardiamidoxime complexes with uranyl. (Figure adapted from reference 21)	30
Figure 3.1 Structures of open-chain diamidoxime (left) and cyclic imidedioxime (right)...	58
Figure 3.2 ^{51}V NMR spectra of 0.2 mM vanadium(V) in simulated seawater (a) without any ligand, (b) with 0.2 mM of cyclic glutarimidedioxime, and (c) with 0.2 mM of open- chain glutardiamidoxime.....	59
Figure 3.3 ^{51}V NMR spectra of 0.2 mM vanadium(V) followed by addition of different concentrations of cyclic glutarimidedioxime. All samples in 0.5 M NaCl aqueous solution at pH 8.3.	60
Figure 3.4 ^{51}V NMR spectra of 0.2 mM vanadium(V) followed by addition of different molar concentrations of glutarimidedioxime, (a) 0.4 mM, (b) 0.8 mM, (c) 1.2 mM, and (d) 2.0 mM. All samples in 0.05 M NaCl aqueous solution at pH 8.3.....	61
Figure 3.5 Positive-ion ESI mass spectrum of a solution containing 0.2 mM vanadium(V) and 0.2 mM glutarimidedioxime in 0.05 M NaCl aqueous solution at pH 8.3.	63
Figure 3.6 Chromatogram for solutions containing 0.2 mM glutarimidedioxime only, and 0.2 mM glutarimidedioxime:0.2 mM vanadium(V) in 0.05 M NaCl aqueous solution at pH 8.3.	64
Figure 3.7 Positive-ion ESI-MS mass spectrum acquired from a solution containing 0.1 mM glutarimidedioxime in 0.05 M NaCl aqueous solution at pH 8.3.....	64

- Figure 3.8 ^{13}C NMR spectra of (a) 5 mM glutarimidedioxime, and (b) 5 mM vanadium(V):5 mM glutarimidedioxime. All samples in 0.05 M NaCl aqueous solution at pH 8.3. The ^{13}C NMR signal at 128.3 ppm is due to benzene-d₆ used for magnetic field lock. 66
- Figure 3.9 ^1H NMR spectra of (a) 5 mM glutarimidedioxime, and (b) 5 mM vanadium(V):5 mM glutarimidedioxime. All samples in 0.05 M NaCl aqueous solution at pH 8.3. 67
- Figure 3.10 ^{51}V NMR spectra of 0.5 mM vanadium(V) followed by addition of different millimolar concentrations of glutarimidedioxime (a) 1.0 mM, (b) 2.0 mM, (c) 3.0 mM, and (d) 5.0 mM. All samples in 0.05 M NaCl aqueous solution at pH 8.3. 68
- Figure 3.11 ^{51}V NMR spectra of a solution containing 0.5 mM vanadium(V):1 mM glutarimidedioxime observed with time. All samples in 0.05 M NaCl aqueous solution at pH 8.3. 69
- Figure 3.12 ^{13}C NMR spectra of solution containing (a) 1 mM glutarimidedioxime only, (b) 0.5 mM vanadium(V):1 mM glutarimidedioxime, and (c) spectrum b, zoomed in the region of 15-35 ppm. All samples in 0.05 M NaCl aqueous solution at pH 8.3. The signal at 128.3 is due to benzene d₆ insert used for magnetic field lock. 71
- Figure 3.13 Positive-ion ESI mass spectrum acquired from a solution containing 0.5 mM vanadium(V), and 1 mM glutarimidedioxime in 0.05 M NaCl, at pH 8.3. 72
- Figure 3.14 Chromatogram of a solution containing 0.5 mM vanadium(V) and 1 mM glutarimidedioxime analyzed immediately (0 hours) and after 2 days in 0.05 M NaCl aqueous solution at pH 8.3. 73
- Figure 3.15 Positive-ion ESI mass spectrum of a solution containing 0.5 mM vanadium(V) and 1 mM glutarimidedioxime in 0.05 M NaCl aqueous solution at pH 8.3. The

- spectrum shows m/z 333.1 for the peak at the retention time of 2.65 minutes shown in Figure 3.14..... 74
- Figure 3.16 ^{51}V NMR spectra of 0.5 mM vanadium(V) followed by the addition of 1.0 mM glutarimidedioxime showing the formation of (a) 1:1, and (b) 1:2, vanadium(V)-glutarimidedioxime complex in 0.05 M NaCl aqueous solution at pH 8.3..... 75
- Figure 3.17 ^1H NMR spectra demonstrating vanadium(V)-glutarimidedioxime complex formation in the presence of UO_2^{+2} . Solutions labels (a) 0.2 mM UO_2^{+2} :0.2 mM glutarimidedioxime, (b) 0.2 mM UO_2^{+2} :0.2 mM glutarimidedioxime upon the addition of 0.2 mM vanadium(V). All samples in 0.05 M NaCl in D_2O at pH 8.3..... 77
- Figure 3.18 ^{51}V NMR spectrum demonstrating vanadium(V)-glutarimidedioxime complex formation in the presence of UO_2^{+2} upon the addition of 0.2 mM vanadium(V) to a solution containing 0.2 mM UO_2^{+2} :0.2 mM glutarimidedioxime, at pH 8.3..... 78
- Figure 3.19 ^{51}V NMR spectrum demonstrating vanadium(V)-glutarimidedioxime complex formation in presence of UO_2^{+2} , upon addition of 0.2 mM vanadium(V) to a solution containing 0.1 mM UO_2^{+2} : 0.1 mM glutarimidedioxime, at pH 8.3. 79
- Figure 3.20 ^1H NMR spectra of solutions containing 0.2 mM glutarimidedioxime with (a) no UO_2^{+2} , at pH 3.4, (b) 0.2 mM UO_2^{+2} , at pH 2.3, (c) 0.2 mM UO_2^{+2} , at pH 3.4, (d) 0.2 mM UO_2^{+2} , at pH 4.4, (e) 0.2 mM UO_2^{+2} , at pH 5.4, and (f) 0.2 mM UO_2^{+2} , at pH 8.2. All samples in 0.05 M NaCl in D_2O 81
- Figure 3.21 ^1H NMR spectra of solutions containing 0.2 mM UO_2^{+2} and 0.1 mM glutarimidedioxime after (a) 24 hours, and (b) 7 days. All samples in 0.05 M NaCl in D_2O at pH 3.4. 82

Figure 3.22 ^1H NMR spectra of (a) 0.2 mM cyclic glutarimidedioxime only, (b) 0.2 mM UO_2^{+2} :0.05 mM cyclic glutarimidedioxime, and (c) 0.3 UO_2^{+2} :0.05 mM cyclic glutarimidedioxime in 0.05 M NaCl in D_2O at pH 3.4. 84

Figure 3.23 Heteronuclear Multiple Bond Coherence (HMBC) spectra for 0.2 mM UO_2^{+2} :0.2 mM cyclic glutarimidedioxime in 0.05 M NaCl in D_2O at pH 3.4. 85

Figure 3.24 ^1H NMR spectra of (a) 0.2 mM cyclic glutarimidedioxime only, at pH \sim 3.4, (b) 0.2 mM UO_2^{+2} :0.05 mM cyclic glutarimidedioxime, at pH \sim 3.4, (c) 0.2 mM UO_2^{+2} :0.05 mM cyclic glutarimidedioxime:0.2 mM vanadium(V), at pH \sim 6.5, (d) 0.2 mM UO_2^{+2} :0.1 mM cyclic glutarimidedioxime, at pH \sim 3.4, (e) 0.2 mM UO_2^{+2} :0.1 mM cyclic glutarimidedioxime:0.2 mM vanadium(V), at pH \sim 7.1, (f) 0.2 mM UO_2^{+2} :0.2 mM cyclic glutarimidedioxime, at pH \sim 3.4, (g) 0.2 mM UO_2^{+2} :0.2 mM cyclic glutarimidedioxime:0.2 mM vanadium(V), at pH \sim 6.8, (h) 0.2 mM UO_2^{+2} :0.3 mM cyclic glutarimidedioxime, at pH \sim 3.4, (i) 0.2 mM UO_2^{+2} :0.3 mM cyclic glutarimidedioxime:0.2 mM vanadium(V), at pH \sim 7.1. 87

Figure 3.25 ^1H NMR spectra of (a) 0.2 mM cyclic glutarimidedioxime only, at pH \sim 3.4, (b) 0.2 mM UO_2^{+2} :0.4 mM cyclic glutarimidedioxime, at pH \sim 3.4, (c) 0.2 mM UO_2^{+2} :0.4 mM cyclic glutarimidedioxime:0.2 mM vanadium(V), at pH \sim 6.8, (d) 0.2 mM UO_2^{+2} :0.5 mM cyclic glutarimidedioxime, at pH \sim 3.4, (e) 0.2 mM UO_2^{+2} :0.5 mM cyclic glutarimidedioxime: 0.2 mM vanadium(V), at pH \sim 7.3, (f) 0.2 mM UO_2^{+2} :0.6 mM cyclic glutarimidedioxime, at pH \sim 3.4, (g) 0.2 mM UO_2^{+2} :0.6 mM cyclic glutarimidedioxime:0.2 mM vanadium(V), at pH \sim 7.24, (h) 0.2 mM UO_2^{+2} :0.8 cyclic glutarimidedioxime, at pH \sim 3.4, and (i) 0.2 mM UO_2^{+2} :0.8 cyclic glutarimidedioxime:0.2 mM vanadium(V), at pH \sim 7.4. 88

Figure 3.26 ^{51}V NMR spectra of (a) 0.2 mM UO_2^{+2} :0.05 mM cyclic glutarimidedioxime: 0.2 mM vanadium(V), at pH \sim 6.5, (b) 0.2 mM UO_2^{+2} :0.1 mM cyclic glutarimidedioxime:0.2 mM vanadium(V), at pH \sim 7.1, (c) 0.2 mM UO_2^{+2} :0.2 mM cyclic glutarimidedioxime:0.2 mM vanadium(V), at pH \sim 6.8, and (d) 0.2 mM UO_2^{+2} :0.3 mM cyclic glutarimidedioxime:0.2 mM vanadium(V), at pH \sim 7.1. 90

Figure 3.27 ^{51}V NMR spectra of (a) 0.2 mM UO_2^{+2} :0.4 mM cyclic glutarimidedioxime: 0.2 mM vanadium(V), at pH \sim 6.8, (b) 0.2 mM UO_2^{+2} :0.5 mM cyclic glutarimidedioxime:0.2 mM vanadium(V), at pH \sim 7.3, (c) 0.2 mM UO_2^{+2} :0.6 mM cyclic glutarimidedioxime:0.2 mM vanadium(V), at pH \sim 7.24, and (d) 0.2 mM UO_2^{+2} :0.8 mM cyclic glutarimidedioxime:0.2 mM vanadium(V), at pH \sim 7.4. 90

Figure 3.28 UV-Visible absorption spectra showing complexation of UO_2^{+2} with glutarimidedioxime, and effect of vanadium(V) upon complexation of UO_2^{+2} with glutarimidedioxime at pH 8.3. 92

Figure 3.29 UV-Visible absorption spectra acquired at pH 8.3 from solutions containing (a) 0.05 mM vanadium(V):0.1 mM glutarimidedioxime to which 0.05 mM UO_2^{+2} was added, (b) 0.05 mM vanadium(V):0.05 mM glutarimidedioxime to which 0.05 mM UO_2^{+2} was added. 93

Figure 3.30 ^1H NMR spectra of solutions containing (a) 0.2 mM open-chain glutardiamidoxime, at pH 8.2, (b) 0.2 UO_2^{+2} :0.2 mM open-chain glutardiamidoxime, at pH 8.2, (c) 0.2 mM open-chain glutardiamidoxime, at pH 4.4, (d) 0.2 mM UO_2^{+2} :0.2 mM open-chain glutardiamidoxime, at pH 4.4, (e) 0.2 mM open-chain glutardiamidoxime, at pH 3.4, (f) 0.2 mM UO_2^{+2} :0.2 mM open-chain

- glutarimidedioxime, at pH 3.4, and (g) 0.2 mM UO_2^{+2} :0.2 mM open-chain glutardiamidoxime, at pH 2.3. All samples in 0.05 M NaCl in D_2O 95
- Figure 3.31 ^1H NMR spectra of solutions containing 0.2 mM UO_2^{+2} and 0.2 mM open-chain glutardiamidoxime in 0.05 M NaCl in D_2O at pH 3.4 (a) 5 minutes, (b) 24 hours, and (c) 7 days. 97
- Figure 3.32 ^1H NMR spectra of solutions containing (a) 0.2 mM open-chain glutardiamidoxime, (b) 0.05 mM open-chain glutardiamidoxime:0.2 mM UO_2^{+2} , and (c) 0.1 mM open-chain glutardiamidoxime:0.2 mM UO_2^{+2} . All samples in 0.05 M NaCl in D_2O at pH 3.4. 98
- Figure 3.33 ^{13}C NMR spectra of solution containing (a) 1 mM open-chain glutardiamidoxime, (b) 1 mM UO_2^{+2} :1 mM open-chain glutardiamidoxime in 0.05 M NaCl in D_2O at pH 3.4..... 99
- Figure 3.34 ^{13}C NMR spectra of (a) open-chain glutardiamidoxime, (b) Na_2CO_3 at pH 11, and (c) Na_2CO_3 at pH 8. The ^{13}C signals at 206.6 ppm and 29.9 ppm are due to acetone- d_6 insert used for magnetic field lock. 101
- Figure 3.35 ^{13}C NMR spectra of (a) $\text{UO}_2(\text{CO}_3)_3^{4-}$ prepared using 10 mM uranyl (VI) nitrate hexahydrate and 30 mM Na_2CO_3 , (b) $\text{UO}_2(\text{CO}_3)_3^{4-}$ in 10 mM open-chain glutardiamidoxime, (c) $\text{UO}_2(\text{CO}_3)_3^{4-}$ in 20 mM open-chain glutardiamidoxime, (d) $\text{UO}_2(\text{CO}_3)_3^{4-}$ in 100 mM open-chain glutardiamidoxime, and (e) $\text{UO}_2(\text{CO}_3)_3^{4-}$ in 140 mM open-chain glutardiamidoxime at pH 8 and +3 °C. 103
- Figure 3.36 ^1H NMR spectra demonstrating no formation of vanadium(V)-(open-chain glutardiamidoxime) complex. Solutions labels (a) 5 mM open-chain glutardiamidoxime only, and (b) 5 mM vanadium(V):5 mM open-chain glutardiamidoxime. 105

- Figure 3.37 ^{13}C NMR spectra demonstrating no formation of vanadium(V)-(open-chain glutardiamidoxime) complex. Solutions labels (a) 5 mM open-chain glutardiamidoxime only, and (b) 5 mM vanadium(V):5 mM open-chain glutardiamidoxime. 106
- Figure 3.38 ^1H NMR spectra demonstrating no formation of vanadium(V)-(open-chain glutardiamidoxime) complex in the presence of UO_2^{+2} . Solutions labels (a) 0.2 mM open-chain glutardiamidoxime only, and (b) 0.2 mM UO_2^{+2} :0.2 mM open-chain glutardiamidoxime:0.2 mM vanadium(V). All samples in 0.05 M NaCl in D_2O at pH 3.4. 107
- Figure 3.39 ^{51}V NMR spectra acquired from a solution containing 0.2 mM UO_2^{+2} :0.2 mM vanadium(V):0.2 mM open-chain glutardiamidoxime observed after (a) 5 minutes, and (b) 24 hours. Sample was prepared in 0.05 M NaCl in D_2O at pH 3.4. 108
- Figure 3.40 UV-Visible absorption spectra using vanadium(IV) and its complexation with glutarimidedioxime. 110
- Figure 3.41 ^{51}V NMR spectra of (a) 0.5 mM vanadium(IV) in 2 mM glutarimidedioxime, and (b) 2 mM vanadium(IV) in 2 mM glutarimidedioxime. 111
- Figure 3.42 ^{51}V NMR spectra in the absence of NaOH (a) 0.5 mM vanadium(IV) in 2 mM glutarimidedioxime, (b) 1 mM vanadium(IV) in 2.0 mM glutarimidedioxime, and (c) 2.0 mM vanadium(IV) in 2 mM glutarimidedioxime. 112
- Figure 3.43 ^{51}V NMR spectra of (a) 2 mM vanadium(IV):2 mM fulvic acid, at pH 8.0, (b) 2 mM vanadium(IV):2 mM fulvic acid, at pH 3.14, (c) 10 mM vanadium(IV):10 mM catechol, at pH 8.0, and (d) 10 mM vanadium(IV):10 mM catechol, at pH 3.2. 113

- Figure 3.44 ^{51}V NMR spectra of (a) 10 mM vanadium(IV) in water, at pH 8.3, (b) 10 mM vanadium(IV) in ethylenediaminetetraacetic acid (EDTA), at pH 8.3, and (c) 10 mM vanadium(IV) in diethylenetriaminepentaacetic acid (DTPA), at pH 8.3..... 114
- Figure 3.45 EPR spectrum of 5 mM vanadium(IV):5 mM EDTA in water at pH 8.0. ... 115
- Figure 3.46 UV-Visible absorption spectra acquired upon the addition of UO_2^{+2} to vanadium(IV)-EDTA solution, showing complexation of UO_2^{+2} with glutarimidedioxime. 117
- Figure 3.47 UV-Visible absorption spectra showing the effect of increasing vanadium(IV) concentrations on UO_2^{+2} complexation with glutarimidedioxime. 118
- Figure 3.48 UV-Visible absorption spectra acquired for vanadium(IV)-EDTA solution, showing its complexation with glutarimidedioxime. 119
- Figure 3.49 UV-Visible absorption spectra using vanadium(IV):DTPA solution and its complexation with glutarimidedioxime..... 120
- Figure 3.50 UV-Visible absorption spectrum acquired from a solution containing 2 mM vanadium(IV):2 mM EDTA:2 mM open-chain glutardiamidoxime at pH 8.0. 121
- Figure 3.51 ^{51}V NMR spectra acquired from solutions containing varying concentrations of vanadium(V). All samples in 0.05 M NaCl aqueous solution at pH 8.3. 123
- Figure 3.52 Chromatogram acquired from solutions containing 0.2 mM vanadium(V) and varying concentrations of glutarimidedioxime. The vanadium(V):glutarimidedioxime molar ratio of 1:1.5, 1:2, 1:4, and 1:10 were used in this study. All samples in 0.05 M NaCl aqueous solution at pH 8.3..... 124
- Figure 3.53 Positive-ion ESI mass spectrum acquired from a solution containing 0.2 mM vanadium(V) and 2 mM glutarimidedioxime showing m/z 333.13 for the peak at the

retention time of 2.76 minutes. Sample was prepared in 0.05 M NaCl aqueous solution at pH 8.3.	125
Figure 3.54 Chromatogram acquired from solutions containing 0.5 mM vanadium(V) and varying concentrations of glutarimidedioxime. The vanadium(V):glutarimidedioxime molar ratio of 1:2, 1:4, 1:6, and 1:10 were used in this study. All samples in 0.05 M NaCl aqueous solution at pH 8.3.....	126
Figure 4.1 Geometry of sample showing magic angle ($\beta = 54.74^\circ$) with respect to the applied magnetic field. (Figure adapted from reference 14)	142
Figure 4.2 Reaction scheme for preparation of amidoxime-based ORNL-AF1 polyethylene fibers. (Figure adapted from reference 39)	147
Figure 4.3 Chemical structure of (a) pure acrylic fiber, (b) amidoximated LCW adsorbent, and (c) alkaline treated LCW adsorbent. (From Horng-Bin Pan unpublished).....	149
Figure 4.4 Sample preparation accessories for solid state NMR (SSNMR).....	150
Figure 4.5 ^{13}C CP/MAS solid state NMR spectrum of Adamantane.....	151
Figure 4.6 ^{13}C CP/MAS solid state NMR spectra of (a) open-chain glutardiamidoxime, and (b) cyclic glutarimidedioxime.	152
Figure 4.7 ^{51}V solid state NMR spectrum of sodium orthovanadate (Na_3VO_4)	154
Figure 4.8 ^{13}C CP/MAS solid state NMR spectra of (a) pure acrylic fiber, (b) amidoximated (using 3 wt% hydroxylamine) LCW adsorbent, and (c) alkaline treated LCW adsorbent.	156
Figure 4.9 ^{13}C CP/MAS solid state NMR spectra of (a) pure acrylic fiber, (b) amidoximated (using 6 wt% hydroxylamine) LCW adsorbent, and (c) alkaline treated LCW adsorbent.	158

- Figure 4.10 ^{13}C CP/MAS solid state NMR spectra of (a) ORNL-AF1 adsorbent, (b) amidoximated (using 3 wt% hydroxylamine) and alkaline treated LCW adsorbent, and (c) amidoximated (using 6 wt% hydroxylamine) and alkaline treated LCW adsorbent. 160
- Figure 4.11 FTIR spectra showing the characteristic absorption bands for the LCW adsorbent prepared using 3 wt% hydroxylamine. 163
- Figure 4.12 FTIR spectra showing the characteristic absorption bands for the LCW adsorbent prepared using 6 wt% hydroxylamine. 164
- Figure 4.13 LCW adsorbent without NaOH treatment in simulated seawater spiked with 10 ppm vanadium. 166
- Figure 4.14 Colours of the LCW fiber at different stages. Left, LCW fiber with NaOH treatment in water, hydrophilic forming hydrogel; middle, LCW fibers after ~1-2 hours of exposure in 10 ppm vanadium solution in simulated seawater (yellowish); right, LCW fibers after 24 hours of exposure in 10 ppm vanadium solution in simulated seawater (light brown)..... 167
- Figure 4.15 Time dependent measurements of vanadium adsorption capacity (mg vanadium/g of adsorbent) by LCW adsorbent exposed to 10 ppm vanadium in simulated seawater. 169
- Figure 4.16 Colours of the ORNL-AF1 fiber at different stages. Left, ORNL-AF1 fiber (white); middle, ORNL-AF1 after ~1-2 hours of exposure in 10 ppm vanadium solution in simulated seawater (light brownish); right, ORNL-AF1 fibers after 24 hours of exposure in 10 ppm vanadium solution in simulated seawater (dark brown) 170

Figure 4.17 Time dependent measurements of vanadium adsorption capacity (mg vanadium/g of adsorbent) by the ORNL-AF1 adsorbent exposed to 10 ppm vanadium in simulated seawater.	172
---------------------------------------------------------------------------------------------------------------------------------------------------------------------------------------	-----

List of Tables

Table 2.1	Common metal ions in seawater and their concentrations. (Table reproduced from references 7 and 18).....	26
Table 2.2	Formation constants for Glutardiamidoxime and Glutarimidedioxime with uranyl. (Table adapted from references 20 and 21).....	29
Table 4.1	ICP-MS results on mg of vanadium adsorbtion by the LCW adsorbent without NaOH treatment in simulated seawater spiked with 10 ppm vanadium.	165
Table 4.2	Time dependent vanadium uptake by LCW adsorbent exposed to 10 ppm vanadium in simulated seawater.....	168
Table 4.3	Time dependent vanadium uptake by the ORNL-AF1 adsorbent exposed to 10 ppm of vanadium in simulated seawater.	171

List of Abbreviations

CCD	Charge Coupled Device
CP/MAS	Cross Polarization with Magic Angle Spinning
CPP	Clean Power Plan
DFT	Density Functional Theory
DTPA	Diethylenetriaminepentaacetic acid
DMSO	Dimethyl Sulfoxide
DMF	N-N dimethylformamide
DOE	Department of Energy
DTGS	Deuterated Triglycine Sulfate
DOPA	3, 4 dihydroxyphenylalanine
EDTA	Ethylenediaminetetraacetic acid
EPR	Electron Paramagnetic Resonance
ESI-MS	Electrospray Ionization Mass Spectrometry
EFG	Electric Field Gradient
FTIR	Fourier Transform Infrared Spectroscopy
HMBC	Heteronuclear Multiple Bond Coherence
ICP-MS	Inductively Coupled Plasma Mass Spectrometry
ICP-OES	Inductively Coupled Plasma Optical Emission Spectrometry
IEO	International Energy Outlook
LC-MS	Liquid Chromatography Mass Spectrometry
MSL	Marine Sciences Laboratory

<i>m/z</i>	Mass-to-charge ratio
NMR	Nuclear Magnetic Resonance
ORNL	Oak Ridge National Laboratory
PNNL	Pacific Northwest National Laboratory
PUREX	Plutonium Uranium Reduction Extraction
RIGP	Radiation Induced Graft Polymerization
SSNMR	Solid State NMR
SAMs	Self-Assembled Monolayers
UV-Vis	Ultraviolet-Visible
WHOI	Woods Hall Oceanographic Institution
XRD	X-Ray Diffraction

Chapter 1: Introduction

1.1 Outlook on Different Energy Resources

It is of major interest to review an outlook on different energy resources, worldwide energy consumption, and the future of global energy use.¹ The major energy resources include fossil fuels, such as coal, oil, and natural gas, which are used by power plants, furnaces, motors, and jet engines. Renewable energy resources include wind used by wind turbines, water used for the generation of hydroelectric power, and sunlight used by solar cells and solar panels to convert solar energy into electricity. Uranium is used as a fuel for the generation of nuclear energy. Most of the worldwide energy comes from fossil fuels, which accounts for an 83% share among all other energy resources.² The burning of fossil fuels in the past has caused a dramatic increase in the emission of CO₂ into earth's atmosphere, leading to global warming and climate change.³ Among the fossil fuels, coal is the major source of CO₂ emission,³⁻⁵ while natural gas is the least carbon-intensive fossil fuel. World energy demand will increase significantly with time due to economic growth and expanding population. As the living standards of the population increase, the demand for the usage of electric power also increases due to the use of electronic devices in industries, in office buildings, in homes, and in commercial or public service buildings, such as hospitals and malls. Renewable energy resources, which include solar, geothermal, wind, hydroelectric, and biomass are not very harmful to the environment⁶ due to their very little to no CO₂ emission. They can therefore potentially contribute to a reliable solution to current energy problems.

One challenge associated with renewable energy resources is their levels of availability. For example, solar collectors require sunshine in order to make electricity, hydropower generators need rain or other water sources to fill dams with flowing water, and

wind turbines need wind. It would take a very long time to transition to exclusive use of renewable energy sources, and in considering such a case, nuclear energy plays an important role.

Nuclear power is one of the most energy-intensive and carbon-free sources of power. The worldwide energy consumption outlook and the future trend of global energy use presented in the International Energy Outlook (IEO) in 2016⁷ projects an increase in the consumption of energy from 2012 to 2040 from the different energy resources. In the future, non-fossil fuel consumption will exceed fossil fuel consumption. In order to reach a low carbon emission society⁸ by replacing fossil fuels with low carbon-emitting sources,⁹ renewable energy would be the fastest-growing energy resource, and nuclear power would be the second fastest-growing energy source. Energy resources that are not harmful to the environment need to be the main energy resources in future.

The recently proposed Clean Power Plan (CPP) policy in the United States projects the reduction in CO₂ emission^{10,11} from different energy resources. Due to the implementation of the US CPP and concerns about energy security; the harmful effects of fossil fuel emissions upon the environment; and the high price of oil; the use of fossil fuels will decrease with time, and the use of coal as the dominant fuel for electric power generation will decline. Therefore, in the long term, the electricity generation from renewable energy resources and nuclear power will play a crucial role.¹² Indeed, promising technology and economic analysis indicate nuclear energy as one of the substantial sources of electricity for the 21st century.

Like other energy resources, there are challenges associated with the use of nuclear energy. The most important challenge is associated with the storage of nuclear waste.¹³ The stored nuclear waste may leak and contaminate the soil and water.¹⁴ Storage tanks are buried

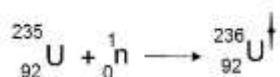
at the Hanford site in Washington state; Clark County, southern Nevada; West Valley, New York; Morris, Illinois; the Savannah River site in South Carolina; and at Idaho National Laboratory (INL) in Idaho Falls, Idaho.

The next challenge associated with the use of nuclear energy is the reprocessing of spent fuel. The United States banned reprocessing spent nuclear fuel because the process produces about 1% of plutonium along with some residual uranium. Therefore, the spent nuclear fuel is radioactive and contains plutonium, a poisonous chemical. Moreover, separating plutonium from the spent nuclear fuel can make it available for the production of nuclear weapons and could lead to their proliferation. The impacts of the Fukushima Daiichi nuclear disaster^{8, 15} due to the massive tsunami and earthquake in Japan on March 11, 2011, as well as the Chernobyl nuclear accident in Ukraine, Pripyat, on April 26, 1986, have raised major concern with the safety associated with the performance of nuclear reactors. However, the Department of Energy (DOE) is developing technology and solutions to improve and sustain the safety associated with energy production from nuclear reactors. If safety guidelines associated with nuclear energy production and storage are followed, the electricity generation from nuclear energy will provide a safer source than that of fossil fuels. This is because a comparison of the impacts of the waste present in the air we breathe every day (emitted CO₂ from the burning of fossil fuels) to the probable impacts of appropriately stored nuclear waste, the safer option remains the storage of nuclear waste.

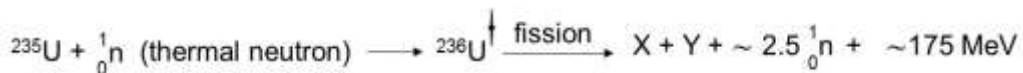
1.2 The Nuclear Fuel Cycle

In the nuclear fuel cycle, the conversion of nuclear energy is achieved by the nuclear fission reaction. A material is considered a fissile material if the fission occurs by thermal or slow neutrons. However, a material is considered as “fertile” if that material is converted to a

“fissile” material by irradiation. Uranium is a fissile material used as an essential fuel for nuclear power generation in nuclear reactors. The uranium that is mined naturally contains 99.24% ^{238}U , 0.72% ^{235}U , and 0.0054% ^{234}U . The abundant isotope of uranium ^{238}U can be activated by fast neutrons to initiate fission. However, ^{235}U is a fissile isotope of uranium, and it requires absorption of slow neutrons to undergo fission. The slow neutrons have energy < 0.4 eV. ^{235}U absorbs neutrons and transfers to an excited state, $^{236}\text{U}^\dagger$, according to the following reaction.



The excited state $^{236}\text{U}^\dagger$ possesses excess energy and experiences intense oscillations, deforms, and becomes highly distorted. As a consequence, the nucleus splits into two pieces and emits several neutrons during this operation. The fission reaction is shown below.



For nuclear power generation, a continuous and self-sustaining fission reaction is needed. A critical mass of about 50 kg of ^{235}U is used in the nuclear reactor for this purpose, and for each megawatt day of thermal energy¹⁶, 1.3 g of ^{235}U is consumed.

Uranium is an important component in the nuclear fuel rods that are used in nuclear reactors. In the nuclear fuel cycle, the first stage is mining the fuel ore. The mines can be underground or open pit. Some of the mine companies use in situ leaching of the ore without deep excavation and drilling of the earth's surface. During the in situ leaching, acidic or alkaline leaching agents that contain hydrogen peroxide are used. The porous surface of the ore is then exposed to the leaching agent by pumping the leaching agent into the ore deposits. The leached out uranium solution is used for further processing.

Heap leaching is also used. During this processes, excavated ores are collected as heaps. Then, a low concentration of sulphuric acid used as a leaching agent is sprayed upon the heaps. The uranium is then leached out, and the drained solution containing uranium is further processed. The nuclear fuel cycle ends with the reprocessing step, although a cycle without reprocessing is called a once-through nuclear cycle. In the nuclear fuel cycle, uranium in the form of U_3O_8 , known as yellow cake, is first purified. An ion exchange process or solvent extraction is used for its purification.

The pure U_3O_8 forms uranyl nitrate [$UO_2(NO_3)_2$] when it is treated with nitric acid. Then, the uranyl nitrate is treated with ammonia, and it produces ammoniumdiuranate [$(NH_4)_2U_2O_7$]. Uranite (UO_2) is then formed by the reduction of ammoniumdiuranate in hydrogen atmosphere. After that, this UO_2 is enriched with the fissile isotope of ^{235}U (0.7% to >3% enrichment) because, in order to have a stable operation in the nuclear reactor, a fissile nucleus that uses thermal neutrons to undergo fission is required. For the process of enrichment, the uranium needs to be in the gaseous phase. The UO_2 is subsequently converted to UF_6 by fluorination using hydrogen fluoride (HF) for enrichment.¹⁷The UF_6 is then used for enrichment. After enrichment, the UF_6 is reconverted to UO_2 .

In order to have a stable power generation, the ratio between the fissile ^{235}U and non-fissile ^{238}U should be high. The ^{235}U content of the fuel should be greater than 3.5%. The uranium is then converted to fuel pellets to be used in the reactor for the generation of energy in the nuclear reactor. Finally, the nuclear waste is either stored or reprocessed and reused in the nuclear fuel cycle. According to current estimates, there are around 63 million metric tons of uranium ore worldwide, but there is a concern that the uranium deposits present in the land

might be exhausted by the end of this century.^{18, 19} Hence, a reasonable supply of nuclear fuel uranium is important for nuclear energy to remain sustainable.

1.3 Uranium from Oceans

Oceans are a rich source of uranium, as they contain about 4.5 billion metric tons of uranium.²⁰ The amount of uranium in the ocean is much greater than in terrestrial sources. It is an inexhaustible uranium resource because natural mechanisms, such as exchange from sea bed or run-off from fresh water, can restore uranium in the ocean. However, uranium in the ocean is present at a low concentration of 3 ppb. It is expensive to extract uranium from this expansive uranium resource due to the low uranium concentration. For decades, study on uranium recovery from seawater has been conducted by different research groups. In the 1960's, Japanese researchers started working on the prospect of recovering uranium from seawater.²¹ However, the technology for recovering uranium from seawater has not flourished economically due to the associated challenges.

To achieve efficient uranium recovery at such low concentrations (3 ppb), a large volume of seawater is required to be in contact with the adsorbent. The adsorbent is deployed in seawater and picks up some grams of uranium per kg of the adsorbent. Therefore, an inexpensive adsorbent is required for developing a cost-efficient process for uranium extraction from seawater. Different extraction techniques were tested²² for the recovery of uranium from seawater in the past. During the 1960's and 1980's, hydrous titanium dioxide adsorbent was used for uranium extraction from seawater.²³⁻²⁷ This adsorbent material adsorbed ~0.1 g U/kg of adsorbent.²⁶ Adsorption capacity is one of the greatest factors that controls the cost of uranium extraction from seawater. It determines the proficiency of an adsorbent material. Greater adsorption capacity makes an adsorbent attractive. Hydrous

titanium dioxide adsorbent was not economically viable because of its low adsorption capacity and enormous energy requirements. It also required active water pumping²⁷ for complete uranium recovery. The 1980's represented a turning point when a transition occurred from hydrous titanium dioxide adsorbent to poly(acrylamidoxime) adsorbent.²⁶ In poly(acrylamidoxime) adsorbent the amidoxime groups were grafted in a substrate of acrylic fiber.^{26,28} Poly(acrylamidoxime) adsorbent demonstrated a higher uranium loading capacity than hydrous titanium dioxide adsorbent. It was easily used with different type of polymer substrates and continues to receive focus since the 1980's.²⁹⁻³⁴ Extensive research has continued since the 1980's towards the search for different adsorbent materials and an attractive ligand.^{26,35-38} Amidoxime ligands continued to be used because of their high adsorption capacity. In the 1990's Japanese researchers pioneered polyethylene-based substrates because they were inexpensive and more durable than acrylic substrates.²⁶ Later, there was an advancement in the 20th century towards a kelp field concept using braid type adsorbent material.^{26, 39, 40} These kelp braid adsorbents were moored in the sea bed standing upwards like kelp, and ships or work boats were used to winch the braid adsorbents.^{26, 41}

In 2011, the Department of Energy (DOE) built a team including national laboratories, universities, and research institutes⁴² in order to evaluate the economic feasibility of extracting uranium from seawater. The goal was to reduce the cost of uranium extraction from seawater through the development of an adsorbent with high adsorption capacity. The work done by different research groups and the challenges associated with the technology of uranium extraction from seawater is summarized in Chapter 2.

The synthesis and design of ligands that possess higher selectivity for uranium than competing metal ions present in seawater, such as K^+ , Ca^{2+} , Na^+ , Mg^{2+} , Fe^{3+} , Ni^{2+} , $V(V)$ etc.

is challenging. These metal ions limit binding sites present in the adsorbent and decrease its uranium adsorption efficiency. Research is ongoing in synthesizing new ligands^{38, 43-45} with high uranium selectivity. Calculations using density functional theory are used for designing and screening of new ligands based on their uranium binding affinity.^{38, 45}

Synthesized ligands can be readily tested in laboratory conditions using artificial seawater because seawater chemical composition can be reproduced. However, it is crucial to test the synthesized ligand in real seawater conditions⁴⁶ because biofouling on the adsorbent cannot be replicated in a laboratory environment. The accumulation of microorganism on prolonged deployment of the adsorbent in seawater significantly decreases its uranium adsorption efficiency. Testing of different adsorbent materials is performed using column and flume setups. Marine tests are conducted at the Marine Science Lab (MSL) in Sequim, Washington; University of Miami's Broad Key Island Research Facility; and the Woods Hole Oceanographic Institution (WHOI), Massachusetts. It takes ~28 to ~56 days for the conduction of real seawater tests because of the slow adsorption process.

The life cycle of uranium adsorption begins from adsorbent synthesis. The steps include the production of polymer fiber, the use of electron beam irradiation to open grafting sites, the grafting of the functional group that grabs uranium, and the addition of hydrophilic functional group. The hydrophilic functional group enhances contact between seawater and adsorbent. After adsorbent synthesis, the adsorbent is deployed in seawater for uranium uptake. After uranium adsorption, the adsorbent is removed from seawater; uranium and other metal ions are then eluted from the adsorbent.^{47, 48} The adsorbent is then reconditioned⁴⁹ and reused for multiple metal adsorption cycles. Techniques like fourier transform infrared spectroscopy (FTIR) and scanning electron microscopy (SEM) provide valuable information

about the alteration of functional groups and damages in adsorbent during adsorption-desorption experiments. Inductively coupled plasma optical emission spectrometry (ICP-OES), and inductively coupled plasma mass spectrometry (ICP-MS)⁵⁰ are used for quantification of adsorbed elements. Considerable cost is involved in uranium extraction from seawater. One solution for decreasing this cost is higher uranium adsorption capacity, which can be achieved by increasing adsorbent surface area. Research is being conducted on synthesis and development of adsorbents with high surface area.⁵¹

1.4 Objectives of This Thesis

- 1) The overall aim of this research is to investigate the complexation of vanadium(IV) and vanadium(V) with glutarimidedioxime and glutardiamidoxime and their competition with UO_2^{+2} for complexation. This will be accomplished based on the following sub objectives.
 - a) Investigate the interactions of amidoxime ligands cyclic glutarimidedioxime and open-chain glutardiamidoxime with UO_2^{+2} , with vanadium(IV) and vanadium(V).
 - b) Examine the effectiveness of uranium complexation with cyclic glutarimidedioxime and open-chain glutardiamidoxime in the presence of vanadium(IV) and vanadium(V).
- 2) Understanding the application of spectroscopic techniques, such as UV-Visible, NMR, FTIR, and LC/MS, to identify complex formation between metal ions and ligands. These techniques were used to investigate the competitive interactions of UO_2^{+2} , vanadium(V) and vanadium(IV) with amidoxime ligands cyclic glutarimidedioxime and open-chain glutardiamidoxime.

- 3) To characterize newly developed amidoxime-carboxylate containing LCW adsorbent and the ORNL-AF1 adsorbent using solid state NMR (SSNMR) and FTIR spectroscopy.
- 4) To study and compare vanadium uptake by LCW adsorbent and ORNL-AF1 adsorbent in simulated seawater conditions using ICP-MS spectrometry.

1.5 Achievements of This Thesis

This thesis reports results from different spectroscopic studies used for probing complexation of vanadium and uranyl ions with amidoxime ligands, and their competition for complexation. This work is focused upon a) understanding coordination chemistry and complexation of vanadium species with amidoxime ligands in presence of UO_2^{+2} and b) comparing vanadium adsorption between newly developed LCW adsorbent and ORNL-AF1 adsorbent. This study presents a first look at solution state NMR studies of UO_2^{+2} complexation with glutarimidedioxime and glutardiamidoxime system in the absence and presence of vanadium. Understanding competitive adsorption of UO_2^{+2} and vanadium on amidoxime-based adsorbents in seawater is crucial for designing new adsorbents with higher uranium adsorption capacity.

According to the literature, amidoxime-based adsorbents have been shown to be the most effective material for sequestering uranium from seawater. They possess good mechanical strength and high uranium adsorption capacity. Amidoxime-based adsorbents are very effective for extracting vanadium from seawater. On a molar basis, vanadium adsorption is much greater than uranium upon using them for uranium extraction from seawater. Vanadium competes with UO_2^{+2} for binding sites in the adsorbent, and affects its UO_2^{+2} extraction efficiency. Little information is available in the literature regarding the distribution

of vanadium species in seawater and complexation of vanadium with amidoxime ligands glutarimidedioxime and glutardiamidoxime.

Vanadium(IV) and vanadium(V) govern aquatic chemistry of vanadium in seawater. The aquatic species⁵² of vanadium(IV) are VO^{+2} and $\text{VO}(\text{OH})^+$, and for vanadium(V) they are $\text{H}_2\text{VO}_4^{-1}$ and HVO_4^{-2} . In natural water the most stable form of vanadium is a mobile metavanadate anion VO_3^- . Vanadyl (VO^{+2}), forms strong complexes with organic chelating agents because it can coordinate very strongly with oxygen donor ligands. It is the most stable oxidation state and a hard Lewis acid due to central +4 charge and d^1 electronic configuration. The relative abundance of vanadium in open oxygenated seawater is about 34–45 nM.⁵³ The concentrations of vanadium are very high in anoxic sediments ranging from 4–8 mmol/kg.⁵⁴ Vanadium chemistry is fascinating because valence of vanadium changes in response to the redox potential of environment. The stability of vanadium(IV) and vanadium(V) oxidation states vary with the environment. In an oxidized marine environment, vanadium(V) is stable. However, in a reducing environment vanadium(IV) is stable. Vanadium(V) reduces to a smaller cation, vanadyl (VO^{+2}), in mild reducing or suboxic conditions. In comparison to large vanadate (VO_2^+), vanadyl (VO^{+2}) is smaller and binds more effectively to chelating groups.⁵⁵ Suboxic areas are created during summer hypoxia, when concentration of dissolved oxygen is less than 2 mg/litre. Vanadyl is adsorbed into organic particles and removed from seawater. Vanadyl occurs in shale and carbonaceous sediments because of the reducing environment. Suitable places with suboxic or anoxic conditions for studying vanadium(IV) speciation include the water of Long Island Sound (LIS), and head of the Peconic River estuary in New York.

In aqueous solution vanadium(V) undergoes hydrolysis, and polynuclear species, such as $H_xV_{10}O_{28}^{(6-x)}$ decavanadates, are formed.⁵² These polynuclear species are not present in seawater because of the low vanadium concentration (1.6 ppb) in seawater. The concentration of vanadium varies according to different seasons and is determined by physico-chemical parameters, such as the temperature of the water, redox conditions, and biological activity in seawater. The levels of vanadium in seawater are high during the summer, vanadium(IV) = 2.2 ± 1.7 nM and vanadium(V) = 22.4 ± 3.9 nM⁵⁶ because the high water temperature during summer enhances the release of vanadium from sediments. Sources for increased vanadium(IV) in seawater include inputs of vanadium(IV) from sewage, fluvial discharge, sedimentary release, and reduction of vanadium(V) to vanadium(IV), caused by decrease in redox potential. Vanadium(IV) is also produced by oxidation of vanadium(III) in western Long Island Sound (LIS). Vanadium(IV) complexes with organic matter, is readily adsorbed by particles, and deposits in sediments. The concentration of vanadium in seawater is lower in spring, V(IV) = 1.4 ± 1.4 nM and V(V) = 11.1 ± 2.6 nM⁵⁶ because of input of freshwater in the ocean from rivers increase and cause dilution effect. During cold spring conditions, vanadium(IV) is removed from water due to its adsorption by particles. Biological uptake of vanadium(IV) is more than vanadium(V). Vanadium(IV) is important for phytoplankton metabolism and reacts with their nucleic acids, Adenosine diphosphate (ADP), Adenosine triphosphate (ATP), Guanosine diphosphate (GDP), glutathione, and amino acids. Biological uptake of vanadium(IV) by phytoplankton reduces total concentration of vanadium(IV) in seawater.

The following chapter is a literature review, and it summarizes current knowledge and investigations by different research groups on extraction of uranium from seawater. It provides information about different chelating agents used for uranium extraction, their binding modes, coordination environments, different type of adsorbents, and their synthesis. Information about adsorbent deployment process, the process for elution of adsorbed metal, and a cost analysis for the whole life cycle of adsorbent is also described in Chapter 2.

Chapter 3 describes spectroscopic results obtained regarding complexation of vanadium and UO_2^{+2} with glutarimidedioxime and glutardiamidoxime in aqueous solutions. ^{51}V NMR, ^1H NMR, ^{13}C NMR, LC-MS, and UV-Visible spectroscopic techniques were used to understand vanadium complexation with glutarimidedioxime and glutardiamidoxime. ^{51}V NMR gives information about vanadium environment upon complexation with ligands glutarimidedioxime and glutardiamidoxime. ^1H NMR and ^{13}C NMR give information about ligand environment upon complexation with vanadium and UO_2^{+2} . The effect of changes in solution pH upon UO_2^{+2} -glutarimidedioxime and UO_2^{+2} -glutardiamidoxime complexes was observed. The competitive interaction study reveals that ease of complex formation with glutarimidedioxime is much higher for vanadium than UO_2^{+2} . It was observed that vanadium(V) and vanadium(IV) do not complex with open-chain glutardiamidoxime. However, UO_2^{+2} complexes with both glutarimidedioxime and open-chain glutardiamidoxime. It was observed that UO_2^{+2} -glutarimidedioxime complex does not form in the presence of vanadium(V) because of the more stable vanadium(V)-glutarimidedioxime complex. This observation indicates high affinity of vanadium(V) for glutarimidedioxime than UO_2^{+2} .

In Chapter 4 characterization of an amidoxime and carboxylate containing LCW polymer adsorbent using ^{13}C CP/MAS, solid state NMR spectroscopy is discussed. The synthesis of the LCW adsorbent is described in Chapter 4. The ^{13}C CP/MAS results show that LCW polymer adsorbent mainly contains glutardiamidoxime. The synthesized LCW adsorbent was tested for vanadium adsorption using ICP-MS spectrometry. The vanadium uptake was studied for the Oak Ridge National Lab (ORNL)-AF1 adsorbent produced by the Radiation Induced Graft Polymerization (RIGP) technique. The ^{13}C CP/MAS characterization of the ORNL adsorbent shows that it mainly contains cyclic glutarimidedioxime. Results of vanadium uptake analysis by the LCW and the ORNL adsorbents show higher vanadium adsorption for the ORNL adsorbent than the LCW adsorbent.

References

1. Klapp, J.; Cervantes-Cota, J.L.; Longoria-Gandara, L.C.; Gabbasov, R. Energy for the Present and Future: A World Energy Overview. In *Towards a Cleaner Planet* ; Alcala, J.F.C., Klapp, J., Cervantes-Cota, J.L., Eds.; Springer Berlin Heidelberg: 2007; pp 3-34.
2. U.S. Energy Information Administration. Trends in Renewable Energy Consumption and Electricity, 2012. www.eia.gov/renewable/annual/trends/ (accessed Feb 9, 2017).
3. Emissions of greenhouse gases in the United States 1985-1990, Department of Energy/Energy Information Administration, Washington, DC, 1993.
4. Hong, B.D.; Slatick, E.R. Carbon Dioxide Emission Factors for Coal U.S. Energy Information Administration.
https://www.eia.gov/coal/production/quarterly/co2_article/co2.html#N_1_ (accessed Feb 9, 2017).
5. U.S. Energy Information Administration. How Much of U.S. Carbon Dioxide Emissions are Associated with Electricity Generation?, 2016.
<http://www.eia.gov/tools/faqs/faq.cfm?id=77&t=11> (accessed Feb 9, 2017).
6. McCombie, C.; Jefferson, M. Renewable and nuclear electricity: Comparison of environmental impacts. *Energy Policy*. **2016**, *96*, 758-769.
7. U.S. Energy Information Administration. World Energy Demand and Economic Outlook. In *International Energy Outlook 2016*.
<https://www.eia.gov/forecasts/ieo/world.cfm> (accessed Feb 9, 2017).
8. Suzuki, T.; Kobayashi, T.; Kobayashi, H.; Iwata, K. Aiming at a Low Carbon Society in Japan by 2050: Impact of the Fukushima Nuclear Accident and CO₂ Reduction Target. *Economics of Energy & Environmental Policy*. **2016**, *5* (1), 89-103.

9. Scott, K.; Daly, H.; Barrett, J.; Strachan, N. National climate policy implications of mitigating embodied energy system emissions. *Climatic Change*. **2016**, *136* (2), 325-338.
10. Lu, L.; Preckel, P.V.; Gotham, D.; Liu, A.L. An assessment of alternative carbon mitigation policies for achieving the emissions reduction of the Clean Power Plan: Case study for the state of Indiana. *Energy Policy*. **2016**, *96*, 661-672.
11. Davis, C.; Bollinger, L.A.; Dijkema, G.P.J. The state of the states Data-driven analysis of the US Clean Power Plan. *Renewable & Sustainable Energy Reviews*. **2016**, *60*, 631-652.
12. Nuclear Energy: Assuring Future Energy Supplies. *ORNL Review*. **2002**, *35*(2), 2-3.
13. Petroll, M. USA: Energy policy and spent fuel and waste management. *Atw-Internationale Zeitschrift Fur Kernenergie*. **2001**, *46* (5), 342.
14. Um, W.; Icenhower, J.P.; Brown, C.F.; Serne, R.J.; Wang, Z.; Dodge, C.J.; Francis, A.J. Characterization of uranium-contaminated sediments from beneath a nuclear waste storage tank from Hanford, Washington: Implications for contaminant transport and fate. *Geochimica Et Cosmochimica Acta*. **2010**, *74* (4), 1363-1380.
15. Hirose, K. Fukushima Daiichi Nuclear Plant accident: Atmospheric and oceanic impacts over the five years. *Journal of Environmental Radioactivity*. **2016**, *157*, 113-130.
16. Knief, R.A. *Nuclear Engineering: Theory and Technology of Commercial Nuclear Power*. Hemisphere Publishing Corporation: Washington, DC, USA, 1992.
17. Morss, L.R.; Edelstein, N.; Fuger, J.; Katz, J.J. *The Chemistry of the Actinide and Transactinide Elements*, 3rd ed.; Springer: Netherlands, 2006.
18. IAEA; OECD, *Uranium 2014: Resources, Production and Demand*; OECD/NEA Publishing: Paris, 2014.

19. Kim, J.; Tsouris, C.; Mayes, R. T.; Oyola, Y.; Saito, T.; Janke, C. J.; Dai, S.; Schneider, E.; Sachde, D. Recovery of Uranium from Seawater: A Review of Current Status and Future Research Needs. *Separation Science and Technology*. **2013**, *48* (3), 367-387.
20. Davies, R.V.; Kennedy, J.; Hill, K.M.; McIlroy, R.W.; Spence, R. Extraction of uranium from sea water. *Nature*. **1964**, *203* (495), 1110.
21. Kanno, M. Design and cost studies on the extraction of uranium from seawater. *Separation science and technology*. **1981**, *16*(9), 999-1018.
22. Bitte, J.; Kellner, A.; Ludwig, K.P. Comparison of different extraction concepts for the recovery of uranium from sea water. AESJ, Japan, 1984.
23. Keen, N.J. Studies on the extraction of uranium from seawater. *J. Brit. Nucl. Energy Soc.* **1968**, *7*, 178.
24. Jaffrezicrenault, N.; Poirier-Andrade, H.; Trang, D. H. Models for the adsorption of uranium on titanium-dioxide. *Journal of Chromatography*. **1980**, *201*, 187-192.
25. Yamashita, H.; Ozawa, Y.; Nakajima, F.; Murata, T. The collection of uranium from seawater with hydrous metal oxide.III.The effects of diverse ions in seawater on uranium adsorption by hydrous titanium(IV) oxide. *Bulletin of the Chemical Society of Japan*. **1980**, *53* (5), 1331-1334.
26. Lindner, H.; Schneider, E. Review of cost estimates for uranium recovery from seawater. *Energy Economics*. **2015**, *49*, 9-22.
27. Kanno, M. Present status of study on extraction of uranium from seawater. *Journal of Nuclear Science and Technology*. **1984**, *21* (1), 1-9.
28. Driscoll, M.J. Recent work at MIT on uranium recovery from seawater. AESJ, Japan, 1984.

29. Kago, T.; Goto, A.; Kusakabe, K.; Morooka, S. Preparation and performance of amidoxime fiber adsorbents for recovery of uranium from seawater. *Industrial & Engineering Chemistry Research*. **1992**, *31* (1), 204-209.
30. Das, S.; Pandey, A.K.; Athawale, A.; Kumar, V.; Bhardwaj, Y.K.; Sabharwal, S.; Manchanda, V.K. Chemical aspects of uranium recovery from seawater by amidoximated electron-beam-grafted polypropylene membranes. *Desalination*. **2008**, *232* (1-3), 243-253.
31. Egawa, H.; Kabay, N.; Shuto, T.; Jyo, A. Recovery of uranium from seawater.13. Long term stability tests for high performance chelating resins containing amidoxime groups and evaluation of elution process. *Industrial & Engineering Chemistry Research*. **1993**, *32* (3), 540-547.
32. Egawa, H.; Kabay, N.; Jyo, A.; Hirono, M.; Shuto, T. Recovery of uranium from seawater.15. Development of amidoxime resins with high sedimentation velocity for passively driver fluidized bed adsorbers. *Industrial & Engineering Chemistry Research*. **1994**, *33* (3), 657-661.
33. Astheimer, L.; Schenk, H.J.; Witte, E.G.; Schwochau, K. Development of sorbers for the recovery of uranium from seawater. Part 2. The accumulation of uranium from seawater by resins containing amidoxime and imidoxime functional groups. *Separation Science and Technology*. **1983**, *18* (4), 307-339.
34. Liu, X.Y.; Liu, H.Z.; Ma, H.J.; Cao, C.Q.; Yu, M.; Wang, Z.Q.; Deng, B.; Wang, M.; Li, J.Y. Adsorption of the uranyl ions on an amidoxime based polyethylene nonwoven fabric prepared by preirradiation induced emulsion graft polymerization. *Industrial and Engineering Chemistry Research*. **2012**, *51* (46), 15089-15095.

35. Brown, S.; Chatterjee, S.; Li, M.J.; Yue, Y.F.; Tsouris, C.; Janke, C.J.; Saito, T.; Dai, S. Uranium Adsorbent Fibers Prepared by Atom-Transfer Radical Polymerization from Chlorinated Polypropylene and Polyethylene Trunk Fibers. *Industrial & Engineering Chemistry Research*. **2016**, *55* (15), 4130-4138.
36. Saito, T.; Brown, S.; Chatterjee, S.; Kim, J.; Tsouris, C.; Mayes, R.T.; Kuo, L.J.; Gill, G.; Oyola, Y.; Janke, C.J.; Dai, S. Uranium recovery from seawater: development of fiber adsorbents prepared via atom-transfer radical polymerization. *Journal of Materials Chemistry A*. **2014**, *2* (35), 14674-14681.
37. Brown, S.; Yue, Y.F.; Kuo, L.J.; Mehio, N.; Li, M.; Gill, G.; Tsouris, C.; Mayes, R. T.; Saito, T.; Dai, S. Uranium Adsorbent Fibers Prepared by Atom-Transfer Radical Polymerization (ATRP) from Poly(vinyl chloride)-co-chlorinated Poly(vinyl chloride) (PVC-co-CPVC) Fiber. *Industrial & Engineering Chemistry Research*. **2016**, *55* (15), 4139-4148.
38. Chatterjee, S.; Bryantsev, V.S.; Brown, S.; Johnson, J.C.; Grant, C.D.; Mayes, R. T.; Hay, B.P.; Dai, S.; Saito, T. Synthesis of Naphthalimidedioxime Ligand-Containing Fibers for Uranium Adsorption from Seawater. *Industrial & Engineering Chemistry Research*. **2016**, *55* (15), 4161-4169.
39. Tamada, M. Current Status of Technology for Collection of Uranium from Sea water. Proceedings of the Erice seminar: JAEA, 2009, 1-9.
http://nuclearinfo.net/twiki/pub/Nuclearpower/WebHomeAvailabilityOfUsableUranium/2009_Tamada.pdf (Accessed 02/09/2017).
40. Sachde, D.; Schneider, E. The cost of recovering uranium from seawater by a braided polymer adsorbent system. *Science & Global Security*. **2013**, *21*(2), 134-163.

41. Tamada, M.; Seko, N.; Kasai, N.; Shimizu, T. Cost estimation of uranium recovery from seawater with system of braid type adsorbent. *Trans. At. Energ. Soc. Japan.* **2006**, *5*, 358-363.
42. Alexandratos, S.D.; Kung, S. Preface to the special Issue: Uranium in Seawater. *Ind. Eng. Chem. Res.* **2016**, *55* (15), 4101-4102.
43. Beauvais, R.A.; Alexandratos, S.D. Polymer-supported reagents for the selective complexation of metal ions: an overview. *Reactive & Functional Polymers.* **1998**, *36* (2), 113-123.
44. Alexandratos, S.D.; Zhu, X.P.; Florent, M.; Sellin, R. Polymer-Supported Bifunctional Amidoximes for the Sorption of Uranium from Seawater. *Industrial & Engineering Chemistry Research.* **2016**, *55* (15), 4208-4216.
45. Piechowicz, M.; Abney, C.W.; Zhou, X.; Thacker, N.C.; Li, Z.; Lin, W.B. Design, Synthesis, and Characterization of a Bifunctional Chelator with Ultrahigh Capacity for Uranium Uptake from Seawater Simulant. *Industrial & Engineering Chemistry Research.* **2016**, *55* (15), 4170-4178.
46. Gill, G.A.; Kuo, L.J.; Janke, C.J.; Park, J.; Jeters, R.T.; Bonheyo, G.T.; Pan, H. B.; Wai, C.M.; Khangaonkar, T.; Bianucci, L.; Wood, J.R.; Warner, M.G.; Peterson, S.; Abrecht, D.G.; Mayes, R.T.; Tsouris, C.; Oyola, Y.; Strivens, J.E.; Schlafer, N. J.; Addleman, R.S.; Chouyyok, W.; Das, S.; Kim, J.; Buessler, K.; Breier, C.; D'Alessandro, E. The Uranium from Seawater Program at the Pacific Northwest National Laboratory: Overview of Marine Testing, Adsorbent Characterization, Adsorbent Durability, Adsorbent Toxicity, and Deployment Studies. *Industrial & Engineering Chemistry Research.* **2016**, *55* (15), 4264-4277.

47. Pan, H.B.; Liao, W.S.; Wai, C.M.; Oyola, Y.; Janke, C.J.; Tian, G.X.; Rao, L.F. Carbonate-H₂O₂ leaching for sequestering uranium from seawater. *Dalton Transactions*. **2014**, 43 (28), 10713-10718.
48. Pan, H.B.; Kuo, L.J.; Wai, C.M.; Miyamoto, N.; Joshi, R.; Wood, J.R.; Strivens, J. E.; Janke, C.J.; Oyola, Y.; Das, S.; Mayes, R.T.; Gill, G.A. Elution of Uranium and Transition Metals from Amidoxime-Based Polymer Adsorbents for Sequestering Uranium from Seawater. *Industrial & Engineering Chemistry Research*. **2016**, 55 (15), 4313-4320.
49. Pan, H.B.; Kuo, L.J.; Wood, J.R.; Strivens, J.; Gill, G.A.; Janke, C.J.; Wai, C.M. Towards understanding KOH conditioning of amidoxime-based polymer adsorbents for sequestering uranium from seawater. *Rsc Advances*. **2015**, 5 (122), 100715-100721.
50. Wood, J.R.; Gill, G.A.; Kuo, L.J.; Strivens, J.E.; Choe, K.Y. Comparison of Analytical Methods for the Determination of Uranium in Seawater Using Inductively Coupled Plasma Mass Spectrometry. *Industrial & Engineering Chemistry Research*. **2016**, 55 (15), 4344-4350.
51. Oyola, Y.; Janke, C.J.; Dai, S. Synthesis, Development, and Testing of High-Surface-Area Polymer-Based Adsorbents for the Selective Recovery of Uranium from Seawater. *Industrial & Engineering Chemistry Research*. **2016**, 55 (15), 4149-4160.
52. Wehrli, B.; Stumm, W. Vanadyl in natural-waters-adsorption and hydrolysis promote oxygenation. *Geochimica Et Cosmochimica Acta*. **1989**, 53 (1), 69-77.
53. Wang, D.; Sanudo-Wilhelmy, S.A. Development of an analytical protocol for the determination of V(IV) and V(V) in seawater: Application to coastal environments. *Marine Chemistry*. **2008**, 112 (1-2), 72-80.
54. Emerson, S.R.; Husted, S.S. Ocean anoxia and the concentrations of molybdenum and vanadium in seawater. *Marine Chemistry*. **1991**, 34 (3-4), 177-196.

55. Mason, R. *Trace Metals in Aquatic Systems*, Wiley-blackwell: 2013.
56. Wang, D.; Sanudo-Wilhelmy, S.A. Vanadium speciation and cycling in coastal waters. *Marine Chemistry*. **2009**, *117* (1-4), 52-58.

Chapter 2: Literature Review

2.1 Introduction

Recent advancements related to conservation of environment and plans and policies^{1,2} to combat climate change have placed interest in nuclear energy as an important energy source for future generations.³⁻⁵ Uranium is an important metal required for the generation of nuclear energy. The terrestrial sources of uranium may not last beyond this century.^{6,7} To maintain a sustainable supply of uranium, alternative uranium resources are required. The Department of Energy (DOE) Fuel Resource Program is developing strategies to ensure a sustainable supply of uranium for nuclear reactors in the United States.⁸ A potential alternative source of uranium is seawater. The estimated amount of uranium in seawater is 4.5 billion metric tons, which is thousands of times greater than land sources, containing up to 63 million tons of uranium. In seawater, uranium uniformly exists at a concentration of 3 ppb, as uranyl tris-carbonato complex $[\text{UO}_2(\text{CO}_3)_3]^{4-}$. In seawater, UO_2^{+2} also complexes with calcium forming, $\text{Ca}_2[\text{UO}_2(\text{CO}_3)_3]$, $\text{Ca}[\text{UO}_2(\text{CO}_3)_3]^{-2}$ complexes, and with magnesium forming $\text{Mg}[\text{UO}_2(\text{CO}_3)_3]^{-2}$ complex^{9,10}. Ternary Ca-U- CO_3 and $\text{Ca}_2\text{UO}_2(\text{CO}_3)_2$ complexes are dominant species in seawater.

Amidoxime-based adsorbents have been recognized since the 1980's.¹¹ They are most attractive and efficient among other adsorbents that have been explored since the 1960's¹¹ for uranium extraction from seawater.^{12, 13} Amidoxime functional groups can remove and substitute the carbonate present in uranyl tris-carbonato complex $[\text{UO}_2(\text{CO}_3)_3]^{4-}$, forming a unique UO_2^{+2} -amidoxime complex. This is caused through greater binding ability and stability of amidoxime functional group at seawater pH of 8.3. Amidoxime-based adsorbent contains

ligands glutarimidedioxime and glutardiamidoxime as complexing agents for uranium extraction from seawater (Figure 2.2).

A recent report¹⁴ suggests that salicyldoxime possess high selectivity for UO_2^{+2} over competing metal ions in seawater. Vanadium(V) and Iron(III), present in seawater, are two major transition metals which affect UO_2^{+2} complexation with glutarimidedioxime and glutardiamidoxime. Decrease in UO_2^{+2} adsorption capacity occurs because vanadium(V) and iron(III) compete with UO_2^{+2} and occupy more binding sites on the adsorbent. Different techniques, such as electrospray ionization mass spectrometry (ESI-MS), nuclear magnetic resonance (NMR), liquid chromatography mass spectrometry (LC-MS), potentiometry, UV-Visible absorption spectroscopy, and X-ray diffraction, are used to study vanadium and UO_2^{+2} complexation with glutarimidedioxime, and glutardiamidoxime. The effect on NMR spectra upon changes in metal/ligand mole ratio and metal/ligand concentration is examined in the following chapter. The effect of changes in solution pH upon complexation was also studied. At high pH, UO_2^{+2} -glutarimidedioxime complex was not detected because more hydroxide ions are present at high pH, and they participate in complexation with UO_2^{+2} , resulting in precipitation of uranyl hydroxides.¹⁵ UO_2^{+2} -glutarimidedioxime complex was not detected at lower pH because, at low pH, H^+ ions compete with glutarimidedioxime for complexation.

Radiation Induced Graft Polymerization (RIGP) technique is used by the Oak Ridge National Lab (ORNL) to develop more durable and reusable adsorbent with high adsorption capacity, enhanced uranium selectivity, and high adsorption kinetics. This technique includes four steps. The steps are explained in section 4.3.3, Chapter 4, and the reaction scheme is shown in Figure 4.2 Chapter 4. The development of an efficient, robust, and cost-effective

adsorbent for uranium extraction from seawater is the focus of a research team brought together by Department of Energy (DOE) in 2011.⁸

Tamada et al.^{11, 16} demonstrated the efficiency of using braid type adsorbent tied to chains anchored in seabed. Adsorbent braids were used to float in the surface of seawater, standing upwards like kelp. Boats were used to lift the adsorbent after uranium uptake, uranium was then eluted from them at seashore, and they were redeployed to seawater for further uranium uptake. The total cost of UO_2^{+2} recovery estimated by Tamada using this system was \$1000 per kg of uranium.¹¹ In their study, 2g U/kg of adsorbent was collected in a 60-day seawater exposure. The adsorbent was reusable for 6 times with 5% loss in adsorption capacity upon each reuse.

Another study on the improvement of UO_2^{+2} recovery from seawater was reported in 2014 for adsorbents developed at the Oak Ridge National Laboratory (ORNL). The adsorbent was submerged in ocean for 8 weeks, and then it was tested for UO_2^{+2} adsorption at the Pacific Northwest National Laboratory (PNNL). The adsorbent showed an increase in uranium uptake to about 3.3g/kg of adsorbent.¹⁷ Overall cost of UO_2^{+2} extraction using this adsorbent was reduced to \$610 per kg of uranium. The objective of scientists in Japan and the United States is to explore practical methods for making UO_2^{+2} extraction from seawater more economical by enhancing uranium adsorption capacity, developing better elution techniques, and increasing adsorbent reusability. Increase in uranium uptake can also be achieved by improving the adsorbent selectivity for UO_2^{+2} relative to competitive elements in seawater.

2.2 Speciation of Uranyl(VI), Vanadium(V) and Vanadium(IV) in Presence of Amidoxime Ligands

Understanding complexation of UO_2^{+2} and vanadium, present in seawater with amidoxime ligands, will aid in designing adsorbents with high UO_2^{+2} adsorption efficiency. The metal ions shown in Table 2.1, participate for binding with amidoxime-based adsorbent, and impede UO_2^{+2} adsorption. This results in low UO_2^{+2} uptake and contributes to high cost of UO_2^{+2} extraction.

Table 2.1 Common metal ions in seawater and their concentrations. (Table reproduced from references 7 and 18)

Elements	Symbol	Concentration (ppb)	Elements	Symbol	Concentration (ppb)
Sodium	Na	1.08×10^7	Iron	Fe	1–3.4
Magnesium	Mg	1.33×10^6	Nickel	Ni	0.5–6.6
Calcium	Ca	4.22×10^5	Vanadium	V	1.5-1.6
Chlorine	Cl	1.91×10^7	Titanium	Ti	1
Potassium	K	3.80×10^5	Copper	Cu	0.6-0.9
Lithium	Li	170	Manganese	Mn	0.25
Zinc	Zn	4	Cobalt	Co	0.05
Uranium	U	3–3.3	Lead	Pb	0.03
Aluminum	Al	2			

Investigation of complexation and stability constants of other metal ions, such as copper(II), lead(II), calcium(II), magnesium(II), nickel(II), and iron(III) present in seawater was done previously.^{7,9,18} The stability constants for some complexes of glutarimidedioxime with these metal ions are low, but their complexes outpace UO_2^{+2} complexes because of their high concentration. They capture most of the binding sites on the adsorbent and decrease its UO_2^{+2} extraction capacity.

Over the years, the development of adsorbents, interaction of various ligands with UO_2^{+2} , and their coordination modes has been examined by different research groups.^{12, 13, 15, 19-23} One of the objectives was to discern UO_2^{+2} uptake by amidoxime-based adsorbents that peaked in the 1980's and have been steadily used till today.¹¹ A previous report by Vukovic et al.²³ showed three possible binding motifs for acetamidoximate (AO) ligand forming $[\text{UO}_2(\text{AO})_x(\text{OH})_y]^{2-x}$ complexes.

Three categories of UO_2^{+2} complexes were identified: a cationic complex involving one acetamidoximate (AO) ligand $[\text{UO}_2[(\text{AO})(\text{OH})_2]_3]^{1+}$; a neutral complex with two acetamidoximate (AO) ligands $[\text{UO}_2(\text{AO})_2(\text{OH})_2]$; and an anionic complex with three acetamidoximate ligands $[\text{UO}_2(\text{AO})_3]^-$. Basically, UO_2^{+2} binds to two adjacent amidoximate ligands on the adsorbent forming a chelate complex. The various mechanisms by which amidoxime group approaches and binds with UO_2^{+2} are monodentate binding, bidentate approach, and η^2 fashion. Density functional theory calculations were used for understanding different types of coordination. In such UO_2^{+2} -acetamidoximate complexes, monodentate binding shows interaction of amidoxime ligand to UO_2^{+2} through nitrogen/oxygen of oxime functional group. Bidentate coordination approach involves binding through oxime oxygen as well as with amide nitrogen. Theoretical studies using density functional theory calculation predicted η^2 type of binding to be the most energetically favourable configuration, which involves binding through N-O chemical bond in such UO_2^{+2} -acetamidoximate complexes. Different modes of UO_2^{+2} binding with amidoxime groups are illustrated in Figure 2.1.

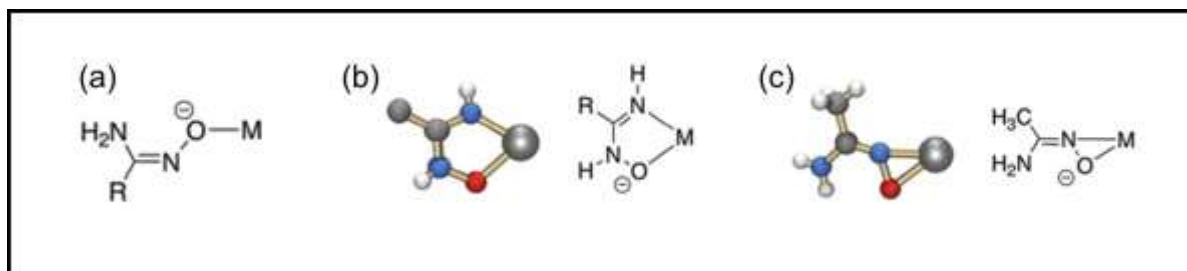


Figure 2.1 Different modes of amidoxime functional group binding to UO_2^{+2} ($M = \text{UO}_2^{+2}$) (a) monodentate, (b) bidentate, and (c) η^2 binding. (Figure adapted from reference 23)

Glutarimidedioxime and glutardiamidoxime are principal ligands present in amidoxime functionalized adsorbents. The structures of glutarimidedioxime and glutardiamidoxime are shown in Chapter 3, Figure 3.1. Kang et al.²² studied formation and hydrolytic stability of glutarimidedioxime and glutardiamidoxime. NMR experiments were used to understand stability of glutarimidedioxime and glutardiamidoxime under basic and acidic conditions at room temperature and a high temperature of 80 °C. Exposing glutardiamidoxime to strong alkaline conditions at 80 °C showed complete degradation to glutarate after 2 days. Under strong acidic conditions (1M DCl), glutardiamidoxime was stable at room temperature for weeks, but, at high temperature it degraded to carboxylic acid product. Cyclic glutarimidedioxime was unstable at room temperature and degraded to glutaric acid, via glutarimidedioxime intermediate.

At room temperature, no conversion of glutardiamidoxime to glutarimidedioxime was observed. However, a recent report by Das et al.²⁴ using solid state NMR spectroscopy shows conversion of glutardiamidoxime to glutarimidedioxime, at a high temperature of 130 °C, for 3 hours, in dimethyl sulfoxide-d₆. A recent report²⁵ shows that open-chain glutardiamidoxime can be converted to a new ligand 2,6-diiminopiperidin-1-ol in situ at room temperature. The open-chain glutardiamidoxime was exposed to UO_2^{+2} and other dissolved transition metals, such as Cu^{+2} and Ni^{+2} . A dinuclear UO_2^{+2} complex, $[(\text{UO}_2^{+2})_2(\text{H}_2\text{L}_1)(\mu\text{-O})_2(\text{NO}_3)_2]$ connected

by μ -O bridges and multinuclear $\text{Cu}^{+2}[(\text{Cu})_3(\text{H}_2\text{L}^1)(\mu\text{-O})_2(\text{H}_2\text{O})_6](\text{NO}_3)_3$ and $\text{Ni}^{+2}[(\text{Ni})_3(\text{H}_2\text{L}^1)_3(\mu\text{-O})_3(\text{H}_2\text{O})_6]\text{Cl}_3$, μ -O bridged complexes, were isolated in aqueous solutions, where H_2L^1 stands for 2,6 diiminopiperidin-1-ol.

A report by Xian and coworkers²⁶ showed that glutarimidedioxime is a reducing and complexing reagent used for recovering plutonium in Plutonium Uranium Reduction Extraction (PUREX) process. Formation constants for glutarimidedioxime and glutardiamidoxime complex with UO_2^{+2} are calculated by Rao and coworkers.^{9, 20, 21} The formation constants for UO_2^{+2} -glutarimidedioxime and UO_2^{+2} -glutardiamidoxime are shown in Table 2.2.

Table 2.2 Formation constants for Glutardiamidoxime and Glutarimidedioxime with uranyl. (Table adapted from references 20 and 21)

Ligand	Reaction	$\log \beta$
Glutardiamidoxime (H_2B)	$\text{H}^+ + \text{B}^{2-} = \text{HB}^-$	12.13 ± 0.12
	$2\text{H}^+ + \text{B}^{2-} = \text{H}_2\text{B}$	24.19 ± 0.07
	$3\text{H}^+ + \text{B}^{2-} = \text{H}_3\text{B}^+$	29.98 ± 0.07
	$4\text{H}^+ + \text{B}^{2-} = \text{H}_4\text{B}^{2+}$	34.77 ± 0.07
	$\text{UO}_2^{2+} + \text{B}^{2-} = \text{UO}_2\text{B}$	17.3 ± 0.3
	$2\text{H}^+ + \text{UO}_2^{2+} + \text{B}^{2-} = \text{UO}_2(\text{H}_2\text{B})^{2+}$	29.2 ± 0.3
	$\text{UO}_2^{2+} + 2\text{B}^{2-} = \text{UO}_2\text{B}_2^{2-}$	26.1 ± 0.3
	$\text{H}^+ + \text{UO}_2^{2+} + 2\text{B}^{2-} = \text{UO}_2(\text{HB})\text{B}^-$	36.4 ± 0.3
	$4\text{H}^+ + \text{UO}_2^{2+} + 2\text{B}^{2-} = \text{UO}_2(\text{H}_2\text{B})_2^{2+}$	56.3 ± 1.0
	Glutarimidedioxime (H_2A) ^d	$\text{H}^+ + \text{A}^{2-} = \text{HA}^-$
$2\text{H}^+ + \text{A}^{2-} = \text{H}_2\text{A}$		22.76 ± 0.31
$3\text{H}^+ + \text{A}^{2-} = \text{H}_3\text{A}^+$		24.88 ± 0.35
$\text{UO}_2^{2+} + \text{A}^{2-} = \text{UO}_2\text{A}$		17.8 ± 1.1
$\text{H}^+ + \text{UO}_2^{2+} + \text{A}^{2-} = \text{UO}_2(\text{HA})^+$		22.7 ± 1.3
$\text{UO}_2^{2+} + 2\text{A}^{2-} = \text{UO}_2\text{A}_2^{2-}$		27.5 ± 2.3
$\text{H}^+ + \text{UO}_2^{2+} + 2\text{A}^{2-} = \text{UO}_2(\text{HA})\text{A}^-$		36.8 ± 2.1
$2\text{H}^+ + \text{UO}_2^{2+} + 2\text{A}^{2-} = \text{UO}_2(\text{HA})_2$		43.0 ± 1.1

A previous report²⁷ about comparison of UO_2^{+2} binding with glutarimidedioxime, and glutardiamidoxime, shows glutarimidedioxime binds to UO_2^{+2} more effectively than glutardiamidoxime, based upon gas phase complexes investigated using electrospray ionization mass spectrometry (ESI-MS).

Formation of UO_2^{+2} -glutarimidedioxime and UO_2^{+2} -glutardiamidoxime complexes, and their different modes of coordination, is shown in Figure 2.2. Cyclic glutarimidedioxime can complex with UO_2^{+2} more efficiently than open-chain glutardiamidoxime because it can form a tridentate complex with UO_2^{+2} as shown in Figure 2.2. However, open-chain glutardiamidoxime can only form either a monodentate or a bidentate complex with UO_2^{+2} .

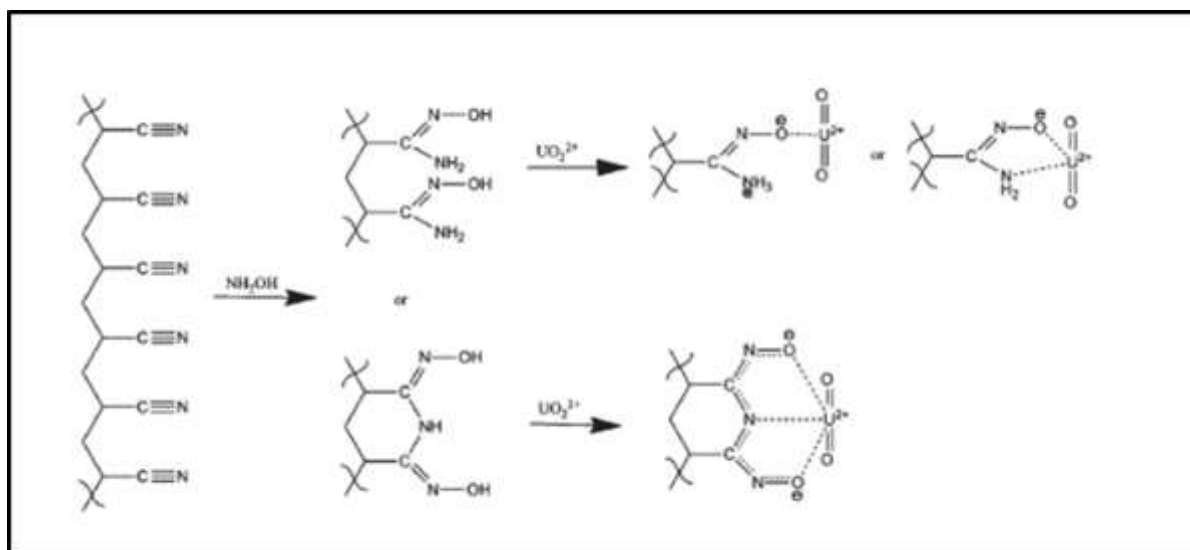


Figure 2.2 Formation and coordination modes of Glutarimidedioxime and Glutardiamidoxime complexes with uranyl. (Figure adapted from reference 21)

Previous reports^{28, 29} show complexation of vanadium with amidoxime ligands. Vanadium, can be found as oxovanadium(IV), (VO^{+2}), and oxovanadium(V), (VO_2^+), cation in seawater. It impedes UO_2^{+2} adsorption capacity of amidoxime-functionalized adsorbent by decreasing adsorption sites available for UO_2^{+2} binding.^{7, 30} Elution of vanadium from amidoxime-based adsorbents is very difficult because of its intense binding ability to amidoxime groups.²⁹ Overall, vanadium adsorption decreases extraction efficiency of uranium and has critical impact upon economic feasibility of uranium extraction from ocean. Vanadium(V) forms 1:1 vanadium(V)-glutarimidedioxime complex at low vanadium

concentration and 1:2 vanadium(V)-glutarimidedioxime complex at high vanadium concentration, as discussed in the following chapter. This observation suggests that presence of VO_2^+ will influence UO_2^{+2} extraction from seawater using amidoxime-based adsorbents.

A recent report³¹ shows formation of vanadium-glutarimidedioxime complex with stoichiometry of 1:2. This complex possesses distorted octahedral geometry and two fully deprotonated glutarimidedioxime ligand binding to the bare V^{+5} species, via tridentate mode. The formation of such strong complex of bare V^{+5} species may be the reason behind the high adsorption of vanadium on the amidoxime-based adsorbents. ^{17}O , ^{51}V , ^1H , ^{13}C NMR, and ESI-MS spectroscopic techniques were used for characterization of this complex. The structure of the complex was determined by X-Ray diffraction technique.

Solution state complexation of UO_2^{+2} with glutarimidedioxime and glutardiamidoxime has been explored widely, and formation of UO_2^{+2} -glutarimidedioxime complexes in 1:1, and 1:2 UO_2^{+2} :glutarimidedioxime molar ratios have been described in the literature.^{20, 21} A previous report²⁷ suggests formation of metal/ligand complex in 2:3 stoichiometry, along with metal/ligand complex in stoichiometries of 1:1, and 1:2. Excess glutarimidedioxime was required for formation of metal/ligand complex in 1:2 stoichiometry. There have been many studies in which ^{51}V NMR has been used to study vanadium(V) species and their complex with ligands in aqueous solution. Mahmoud and coworkers³² used ^{51}V NMR to investigate vanadium(V) species, such as $\text{V}_3\text{O}_9^{-3}$, $\text{V}_4\text{O}_{12}^{-4}$, $\text{V}_6\text{O}_{17}^{-4}$ formed in aqueous solutions of sodium metavanadate. ^{51}V NMR peak for both $\text{V}_3\text{O}_9^{-3}$ and $\text{V}_4\text{O}_{12}^{-4}$ species was observed at 574 ppm, and for $\text{V}_6\text{O}_{17}^{-4}$ it was observed at 582 ppm. Alan S. Tracey³³ used ^{51}V NMR spectroscopy to study complexation of vanadium(V) by alpha-hydro carboxylic acids in aqueous solutions.

The α -Hydroxyisobutyric acid formed three major complexes in 1:1, 2:2, and 3:2 vanadium: ligand stoichiometric ratios.

Buglyo et al.³⁴ used ^{51}V NMR spectroscopy and EPR spectroscopy to investigate solution phase complexes of vanadium(V) and vanadium(IV) with deferoxamine B in aqueous solution. They observed complexation of three hydroxamic functional group of deferoxamine B with bare vanadium. They observed that pH effects complexation, because VO(IV) and VO₂(V) oxo complexes are formed upon increasing the pH of solution. Vanadium was interacting with deferoxamine B via one or two hydroxamic functional group of deferoxamine B. Butler et al.³⁵ used ^{51}V NMR spectroscopy to examine vanadium(V) complexation with metal binding sites present in human transferrins.

Booyesen et al.³⁶ showed formation of polynuclear oxovanadium(IV) complex of NH₄VO₃ with 2-hydroxyphenylbenzothiazole(Hobs) in 1:2 stoichiometric ratio having general formula, [VO(obs)₂]_n. They showed formation of mononuclear complex of NH₄VO₃ with 2-hydroxyphenylbenzimidazole(Hobz) containing pyridine with formula, cis-[VO₂(obz)_{py}]. Oxovanadium(IV) complex with 2-pyridylbenzimidazole(Hpbyz) [VO(Hpbyz)₂SO₄].H₂O was also observed upon reaction of (Hpbyz) ligand with VOSO₄ in 2:1 molar ratio.

Fernando et al.³⁷ showed that sodium metavanadate reacts with Hdmpp(3-hydroxy-1,2-dimethyl-4-pyridinone) ligand in presence of KOH and forms a trinuclear oxovanadium(IV) complex at the pH of 4.5. They observed the effect of pH upon oxovanadium(V) complexation. They observed that the trinuclear oxovanadium(V) complex was unstable and hydrolyzes in water at pH >5 resulting in formation of free vanadium(V)

species and a mononuclear complex of vanadium with 1:1 and 1:2 stoichiometric ratios between vanadium and ligand. The trinuclear oxovanadium(V) complex was only stable at certain pH range ($\text{pH} < 5$). Miranda and coworkers^{38, 39} used UV-Visible and ^{51}V NMR spectroscopy to study vanadium(V) complexation with alpha-aminohydroxamic acid. Solution phase complexes of oxovanadium(V) ion, (VO_2^+), and alpha-amino hydroxamate ligand were observed in 1:1 and 1:2 stoichiometric ratios. The 1:1 complex possesses distorted trigonal bipyramidal geometry at pH of 7 and exists as VO_2L . The complex with 1:2 stoichiometric ratio exists in octahedral geometry as $\text{VO}_2\text{H}_2\text{L}_2^+$. In acidic conditions, 1:2 complex exists as $\text{VO}_2\text{H}_3\text{L}_2^+$, and in basic conditions it is formed as VO_2HL_2 .

Kremer et al.⁴⁰ studied vanadium(V) and vanadium(IV) complexes with anionic polysaccharides. Reaction of $[\text{VO}_4]^{-3}$ with polysaccharides, carboxyl methyl cellulose, xanthum gum, and sodium salt of aliginic acid was studied, in the presence of L-ascorbic acid and L-cysteine. The complexes were investigated by using ^{51}V NMR, and EPR spectroscopies. Kelley and coworkers⁴¹ used 4,5-(diamidoximyl)imidazole ligand to understand complexation of UO_2^{+2} and VO_2^+ with amidoxime functional groups. They noticed formation of 1:2 complex by both UO_2^{+2} and VO_2^+ in different geometry. VO_2^+ showed coordination to 4,5-(diamidoximyl)imidazole through an interaction involving single oxygen of oxime functional group and nitrogen of imidazole functional group. However, UO_2^{+2} showed η^2 approach for complexation with 4,5-(diamidoximyl)imidazole coordinating through two oxygens of oxime functional group. Both UO_2^{+2} and VO_2^+ complexes show different geometry due to different modes of interaction.

2.3 Adsorbents for Uranium Extraction from Seawater

Scientists at the US Department of Energy are developing technology for uranium extraction from seawater to maintain a steady supply of uranium for generation of nuclear energy. Various extraction methods for UO_2^{+2} uptake from seawater have been tested, and among all methods, its extraction using amidoxime-based adsorbents is frequently used and has persisted since the 1980's.⁴²⁻⁴⁶ This is because amidoxime-based adsorbents possesses high adsorption capacity, as well as selectivity for uranium. Scientists from different research groups, national laboratories, and universities⁸ are investigating fundamental and practical methods for development of adsorbents that are more selective for UO_2^{+2} adsorption compared to other metal ions present in seawater.^{24, 47, 48}

It is also important to develop an efficient elution process resulting in an improved adsorption capacity upon reuse of adsorbents. Scientists from the Oak Ridge National Lab (ORNL), and the Pacific Northwest National Laboratory (PNNL) are researching the role of grafting, amidoximation conditions, marine testing of different adsorbents, and impact of marine life upon UO_2^{+2} adsorption. Performance evaluation of the adsorbents developed at the Oak Ridge National Lab (ORNL) is conducted by their preliminary testing at the Marine Science Lab (MSL) in Sequim, WA.⁴⁹ Flow through packed columns and recirculating flumes, circulating seawater are used for conducting marine testing of the adsorbents. Natural seawater, at a flow rate greater than 2 cm/sec and temperature of 20 ± 1.5 °C, is delivered to flow through columns.⁵⁰ Effect of environmental conditions, such as temperature, salinity, flow rate, and particulate matter upon uranium extraction efficiency in controlled lab settings and oceans are also studied. The adsorbed uranium and other elements present in seawater

are eluted using acid solution, and adsorption capacity is quantified by ICP-MS and ICP-OES.⁵¹ Time based uranium adsorption (g U/kg of adsorbent) is then calculated.

Recent reports^{24, 47, 48} show results of marine testing on different series of amidoxime-based adsorbents developed at the Oak Ridge National Lab. Depth of the adsorbent deployment in seawater also affects the UO_2^{+2} adsorption. An experiment conducted at the Woods Hole Oceanographic Institution showed high adsorption, 2.3 g uranium/kg of adsorbent, when the adsorbent was placed at 5-meter depth in a steel mesh. Brookhaven National Lab is researching grafting conditions, their effect on substrate fibers, different monomers for polymerization, temperature, and solvents for preparation of the preferred adsorbent. Techniques like mid-IR detection and pulse radiolysis are used for yield evaluation, assessment of rates, and termination of the polymerization reaction. Radiation Induced Graft Polymerization (RIGP) of acrylonitrile into high surface area adsorbent is monitored using FTIR spectroscopy. Designing amidoxime fibers containing two functional groups enhances amidoxime affinity and provides additional coordination site⁵² for UO_2^{+2} uptake. Primary amines were selected for the formation of bifunctional adsorbents because of their high affinity for UO_2^{+2} ion. One of the amines tested to make such bifunctional adsorbent was diethyltriamine (DETA). Diethyltriamine was capable of interacting with amidoxime, and could bind with metal ion. Bifunctional fiber containing amidoxime and diethyltriamine functional group showed excellent UO_2^{+2} adsorption.⁵²

Understanding complexation of UO_2^{+2} with amidoxime ligands using thermodynamic studies¹⁵ and evaluating their binding ability based on chemical structure and properties, aids in preparation of adsorbents with strong UO_2^{+2} selectivity. High temperature improves UO_2^{+2} adsorption efficiency because complexation of UO_2^{+2} with amidoxime is endothermic.^{21, 53}

Computer based techniques for designing and screening ligands for UO_2^{+2} extraction are inexpensive, reliable, rapid, and systematic. Computer based techniques also provide information about solvation of uranium complexes in seawater.^{54,55} In one study, $\text{Ca}_2\text{UO}_2(\text{CO}_3)_2$ complex solvation in water was studied using molecular dynamics simulations because it is a predominant and very stable uranium complex in seawater. It was observed that $\text{Ca}_2\text{UO}_2(\text{CO}_3)_3$ species was water stable and due to hydrogen bonding of water molecules around this complex, two Ca^{+2} ions bind differently in this complex.⁵⁵ Solvation of $\text{Ca}_2\text{UO}_2(\text{CO}_3)_3$ species was also studied⁵⁴ in real seawater containing NaCl because of high concentration of Na^+ and Cl^- ions present in seawater. It was observed that $\text{Ca}_2\text{UO}_2(\text{CO}_3)_3$ complex was positively charged because of Na^+ ions neighboring the $\text{Ca}_2\text{UO}_2(\text{CO}_3)_3$ complex, while Cl^- ions lay farther from the complex.

Molecular dynamics simulations were also performed to understand solvation of vanadium(V) in aqueous solution.⁵⁶ This solvation study will help to further understanding of different species of vanadium(V) in seawater and their role in complexing with amidoxime ligands. The computer-aided studies provide information regarding free energy and binding constant between $\text{UO}_2^{+2}/\text{VO}_2^+$ species with various amidoxime ligands and aid in designing a ligand which is more selective for UO_2^{+2} than VO_2^+ . A previous report⁵⁷ shows formation of vanadium complexes with formamidoximate ligand that possess stable binding because complexation occurs through amine nitrogen and oxime oxygen of an iminohydroxylamine ligand formed by tautomeric rearrangement of amidoxime.

Formation of a complex between amidoxime and vanadium requires proton transfer between oxime oxygen and amine nitrogen. It was observed that η^2 binding mode of formamidoximate-vanadium complexes was less stable than tautomeric rearrangement of

amidoxime complex with vanadium. This observation is of great significance because, unlike vanadium, η^2 binding coordination mode is most stable for UO_2^{+2} binding with amidoxime.²³ Tautomeric rearrangement of amidoxime to iminohydroxylamine enhances formation of amidoximate-vanadium complexes. Therefore, for increasing UO_2^{+2} complexation, by eliminating the feasibility of vanadium binding, this tautomeric rearrangement is prohibited by synthesizing ligands in such a way that the amine hydrogen atoms are replaced by aromatic and aliphatic functional groups. A recent study⁵⁸ shows alkylation of amidoxime groups forming *N,N*-dimethyl substituted amidoxime that cannot undergo tautomeric rearrangement shows higher UO_2^{+2} selectivity. Another recent report⁵⁹ used X-ray absorption fine structure (XAFS) spectroscopy for determining binding of UO_2^{+2} with amidoxime-based adsorbents. Results indicated presence of a transition metal adjacent to uranium coordinating with the adsorbent. This binding was distinct from previously reported tridentate and η^2 coordination concept.

Research is also being conducted in green chemistry for development of an environmental friendly, biodegradable adsorbent for uranium extraction from seawater.⁶⁰ A polymer chitin present in shrimp cells can be used for uranium extraction. Chitin can be transformed into sheets, which attracts uranium. Expensive ionic liquids are required for solubilizing chitin. Substrate produced by using chitin is beneficial because of its high surface area, but it cannot persist in seawater conditions. Professor Alexander H. Slocum and his team at MIT⁶¹ is working towards development of innovative adsorbent deployment techniques. The novel idea is to use wind turbines installed in the ocean and hang the adsorbent braids from the top of the wind turbine. In such a system, the adsorbent circulates in water and rollers preclude it from entangling. Elution of adsorbed uranium can take place at the same site on

each wind turbine, and transit cost for the adsorbent deployment into seawater after UO_2^{+2} recovery is reduced, decreasing the overall cost of uranium extraction from seawater.

Investigation is ongoing upon development of unique adsorbents providing extreme affinity towards uranium. Nanoporous carbon materials providing high surface area were studied for their uranium adsorption at high salinity levels.⁶² Density of amidoxime functional group, and high surface area are crucial factors in determining the uranium adsorption capacity. Pacific Northwest National Lab (PNNL) is exploring problems related to the use of kelp-like adsorbents because deployment of such adsorbents in a large area⁶³ of $\sim 670 \text{ km}^2$ is required for extracting more quantities of uranium. Effect of such deployment on ocean currents, and its effect upon oceanic uranium and other elements present in seawater, shows toxicity to marine life⁶⁴ upon close interaction with the adsorbent material.

Biofouling is a serious hindrance in the process of UO_2^{+2} extraction from seawater.⁶⁵ This reduces UO_2^{+2} adsorption. Formation of a biofilm is caused by undesired microbial activity on the surface of the adsorbent within a very short time of submerging it in seawater. Good results for uranium adsorption were obtained in water with no biofouling.⁶⁵ Biofouling reduces approachability of amidoxime ligands on the adsorbent. Biofouling also affects chemical processes involved in elution of uranium from the adsorbent by interfering with chemical solution used for uranium extraction, and it may also affect the adsorbent reusability. Major microbial activity occurring on the adsorbent surface causes a 20%-30% loss in its UO_2^{+2} adsorption capacity. Experiments were conducted at the Oak Ridge National Lab to understand uranium adsorption as a function of biomass accumulation. The ORNL-AF1, adsorbent showed reduction in adsorption capacity by 30 % after a 42-day exposure of the adsorbent in sunlit water.⁶⁵ However, low to no loss in adsorption capacity was observed in

flume exposed to dark conditions because placing the adsorbent in dark conditions mitigates biofouling, and lessens loss in UO_2^{+2} adsorption capacity.

2.4 Comparison of Different Metal Elution Approaches

The different metal elution approaches tested include a) acid elution, b) carbonate + H_2O_2 elution⁶⁶, c) bicarbonate elution, and d) elution using bicarbonate followed by Tiron (4,5-dihydroxy-1,3-benzenedisulfonic acid disodium salt) elution.⁶⁷ These elution processes were effective for uranium elution from the adsorbent and removed 88% to 90% of uranium after 42 days exposure of the adsorbent in seawater. However, vanadium removal was challenging, and up to 23% of vanadium could be removed. Another leaching process that uses potassium bicarbonate (KHCO_3) was efficient for elution of uranium and magnesium (>85 % elution was observed), but bicarbonate was not effective for elution of iron and could only remove ~22% to 32% of iron. It was observed that Tiron elution was advantageous for iron (~69% to 73 % of iron was removed) compared to acid elution. Reuse of the adsorbent after acid (0.5 M HCl) elution of uranium, followed by KOH reconditioning, reduces its adsorption capacity. Chemical and physical damages occur to the adsorbent upon acid elution, which causes decrease in adsorption capacity because amidoxime groups are hydrolyzed in the presence of acid. A previous report⁶⁶ describes a novel elution technique that causes minimal loss in the adsorbent capacity. Another report⁶⁸ shows that extended KOH conditioning at 80 °C damages the adsorbent because of the degradation of amidoxime groups. Scanning electron microscopy (SEM) is used for characterizing the adsorbents because SEM images can clearly show fractures and the intensity of physical damage taking place in the adsorbent surface.

2.5 Cost Analysis

Development of a cost-effective method for UO_2^{+2} extraction from seawater is very challenging. Since the 1960's, research has been conducted to develop an economically feasible method that can display its competency as a cost-effective substitute compared to the method of mining uranium from terrestrial resources. A recent review¹¹ estimates the cost of uranium production from seawater to be in the range of \$400–\$1000/kg of uranium, which is much greater than its spot market price of \$100/kg of uranium reported for the year 2014. In 2011, the cost to produce uranium was ~\$1230/kg of uranium, using the braid type adsorbent developed by Japanese researchers.¹⁷ However, the cost is now lowered to \$610/kg of uranium because of the increase in uranium adsorption capacity of the amidoxime-based adsorbents. This new improved cost (\$610/kg of uranium) is about half of the cost assessed for Japanese technology (~\$1230/kg of uranium). But the cost still needs to reduce further, and research is still under development. One way to reduce cost is through increasing the adsorbent durability so that it can be reused for multiple UO_2^{+2} loading after several uranium stripping cycles.

Major parameters affecting the cost of uranium extraction from seawater include the gram uranium uptake per kg of adsorbent (adsorption capacity), as well as the duration that the adsorbent is placed in the ocean, because the rate of biofouling in the adsorbent is directly proportional to the duration of the adsorbent in seawater. Biofouling decreases the adsorption capacity of the adsorbent. Water temperature also affects UO_2^{+2} adsorption capacity.⁵³ Higher water temperature increases UO_2^{+2} adsorption capacity, but biofouling is also enhanced at high water temperature. This observation suggests that UO_2^{+2} adsorption capacity can be enhanced by immersing the adsorbent at suitable selected locations, having little bioactivity, and using high water temperature. Biofouling is always a major concern and a severe problem impacting

performance and accuracy of studies conducted in seawater. A study⁶⁹ showed that copper can remarkably reduce biofouling upon windows of optical sensors used for oceanographic studies, as well as increase the accuracy of collected data. To prevent biofouling, research is being conducted on the use copper as an antifouling compound on the adsorbent.

The cost related to the placement of the adsorbent back into seawater after uranium elution cycle remains same, even though the adsorption capacity of the adsorbent decreases upon its reuse. To make this uranium extraction process economically viable, research is being conducted by scientists to develop cost-effective techniques for the adsorbent deployment in seawater.

The development of innovative uranium elution techniques that prevent the adsorbent damage and provide improved adsorption capacity upon the adsorbent reusability is of great significance to make this uranium extraction process profitable and environmental friendly. Reusability of the adsorbent for several uranium adsorption-desorption cycles saves a greater part of the cost required for manufacturing these adsorbents.

2.6 Conclusions

In this literature review, we investigated and described novel approaches explored by different universities, research organizations, and national laboratories for extraction of uranium from seawater. Examination of methods for uranium extraction from seawater and review on cost analyses suggests prime ways to mitigate cost of UO_2^{+2} extraction, include increasing adsorption capacity, developing innovative elution techniques that avoid the adsorbent degradation, increasing the adsorbent recyclability, and the development of long-lasting adsorbent with high UO_2^{+2} selectivity. Economical alternatives for expensive

chemicals and novel adsorbent deployment techniques are required in the future for efficient uranium recovery from seawater. One way for improving the adsorbent performance is the development and synthesis of high surface area adsorbents in different shapes and sizes. Impact of marine life accumulation on the adsorbent performance for extracting uranium from seawater, obstacles associated with the commercial scale adsorbent deployment, and its harmful effects to marine ecosystem also need to be addressed in the future for advancement of this technology.

References

1. Scott, K.; Daly, H.; Barrett, J.; Strachan, N. National climate policy implications of mitigating embodied energy system emissions. *Climatic Change*. **2016**, *136* (2), 325-338.
2. Lu, L.W.; Preckel, P.V.; Gotham, D.; Liu, A.L. An assessment of alternative carbon mitigation policies for achieving the emissions reduction of the Clean Power Plan: Case study for the state of Indiana. *Energy Policy*. **2016**, *96*, 661-672.
3. Van Kooten, G.C.; Duan, J.; Lynch, R. Is There a Future for Nuclear Power? Wind and Emission Reduction Targets in Fossil-Fuel Alberta. *Plos One*. **2016**, *11* (11), 14.
4. Chmielewski, A.G. Dreams or Reality - Fossil Fuels, Renewables or Nuclear Power?. *Ecological Chemistry and Engineering S*. **2010**, *17* (3), 257-261.
5. Nifenecker, H. Future electricity production methods. Part 1: Nuclear energy. *Reports on Progress in Physics*. **2011**, *74* (2).
6. IAEA; OECD, *Uranium 2014: Resources, Production and Demand*; OECD/NEA Publishing: Paris, 2014.
7. Kim, J.; Tsouris, C.; Mayes, R.T.; Oyola, Y.; Saito, T.; Janke, C.J.; Dai, S.; Schneider, E.; Sachde, D. Recovery of Uranium from Seawater: A Review of Current Status and Future Research Needs. *Separation Science and Technology*. **2013**, *48* (3), 367-387.
8. Alexandratos, S.D.; Kung, S. Preface to the special Issue: Uranium in Seawater. *Ind. Eng. Chem. Res*. **2016**, *55* (15), 4101-4102.
9. Leggett, C.J.; Rao, L.F. Complexation of calcium and magnesium with glutarimidodioxime: Implications for the extraction of uranium from seawater. *Polyhedron*. **2015**, *95*, 54-59.

10. Endrizzi, F.; Rao, L.F. Formation of Ca^{+2} and Mg^{+2} complexes with $\text{UO}_2(\text{CO}_3)_3^{4-}$ in aqueous solution: Effect on the speciation of UO_2^{+2} and its extraction from marine environments. *Chem. Eur. J.* **2014**, *20*, 14499-14506.
11. Lindner, H.; Schneider, E. Review of cost estimates for uranium recovery from seawater. *Energy Economics.* **2015**, *49*, 9-22.
12. Astheimer, L.; Schenk, H. J.; Witte, E. G.; Schwochau, K. Development of sorbers for the recovery of uranium from seawater. Part 2. The accumulation of uranium from seawater by resins containing amidoxime and imidoxime functional groups. *Separation Science and Technology.* **1983**, *18* (4), 307-339.
13. Schenk, H. J.; Astheimer, L.; Witte, E. G.; Schwochau, K. Development of sorbers for the recovery of uranium from seawater. 1. Assessment of key parameters and screening studies of sorber materials. *Separation Science and Technology.* **1982**, *17* (11), 1293-1308.
14. Mehio, N.; Ivanov, A. S.; Williams, N. J.; Mayes, R. T.; Bryantsev, V. S.; Hancock, R. D.; Dai, S. Quantifying the binding strength of salicylaldoxime-uranyl complexes relative to competing salicylaldoxime-transition metal ion complexes in aqueous solution: a combined experimental and computational study. *Dalton Transactions.* **2016**, *45* (22), 9051-9064.
15. Endrizzi, F.; Melchior, A.; Tolazzib, M.; Rao, L.F. Complexation of uranium(VI) with glutarimidoxime: thermodynamic and computational studies. *Dalton Transactions.* **2015**, *44* (31), 13835-13844.
16. Tamada, M.; Kasai, N.; Seko, N.; Shimizu, T. Cost estimation of uranium recovery from seawater with system of braid type adsorbent. *Trans. At. Energ. Soc. Japan.* **2006**, *5*, 358-363.

17. Kim, J.; Tsouris, C.; Oyola, Y.; Janke, C.J.; Mayes, R.T.; Dai, S.; Gill, G.; Kuo, L. J.; Wood, J.; Choe, K.Y.; Schneider, E.; Lindner, H. Uptake of Uranium from Seawater by Amidoxime-Based Polymeric Adsorbent: Field Experiments, Modeling, and Updated Economic Assessment. *Industrial & Engineering Chemistry Research*. **2014**, *53* (14), 6076-6083.
18. Sun, X.Q.; Xu, C.; Tian, G.X.; Rao, L.F. Complexation of glutarimidedioxime with Fe(III), Cu(II), Pb(II), and Ni(II), the competing ions for the sequestration of U(VI) from seawater. *Dalton Transactions*. **2013**, *42* (40), 14621-14627.
19. Sun, X.Q.; Tian, G.; Xu, C.; Rao, L.F.; Vukovic, S.; Kang, S.O.; Hay, B.P. Quantifying the binding strength of U(VI) with phthalimidedioxime in comparison with glutarimidedioxime. *Dalton Transactions*. **2014**, *43* (2), 551-557.
20. Tian, G.X.; Teat, S.J.; Rao, L.F. Thermodynamic studies of U(VI) complexation with glutardiamidoxime for sequestration of uranium from seawater. *Dalton Transactions*. **2013**, *42* (16), 5690-5696.
21. Tian, G.X.; Teat, S.J.; Zhang, Z.Y.; Rao, L.F. Sequestering uranium from seawater: binding strength and modes of uranyl complexes with glutarimidedioxime. *Dalton Transactions*. **2012**, *41* (38), 11579-11586.
22. Kang, S. O.; Vukovic, S.; Custelcean, R.; Hay, B. P. Cyclic Imidedioximes: Formation and Hydrolytic Stability. *Industrial & Engineering Chemistry Research*. **2012**, *51* (19), 6619-6624.
23. Vukovic, S.; Watson, L.A.; Kang, S.O.; Custelcean, R.; Hay, B. P. How Amidoximate Binds the Uranyl Cation. *Inorganic Chemistry*. **2012**, *51* (6), 3855-3859.

24. Das, S.; Brown, S.; Mayes, R.T.; Janke, C.J.; Tsouris, C.; Kuo, L.J.; Gill, G.; Dai, S. Novel poly(imidedioxime) sorbents: Development and testing for enhanced extraction of uranium from natural seawater. *Chemical Engineering Journal*. **2016**, 298, 125-135.
25. Kennedy, Z.C.; Cardenas, A.J.P.; Corbey, J.F.; Warner, M.G. 2,6-Diiminopiperidin-1-ol: an overlooked motif relevant to uranyl and transition metal binding on poly(amidoxime) adsorbents. *Chemical Communications*. **2016**, 52 (57), 8802-8805.
26. Xian, L.; Tian, G.X.; Beavers, C.M.; Teat, S.J.; Shuh, D.K. Glutarimidedioxime: A Complexing and Reducing Reagent for Plutonium Recovery from Spent Nuclear Fuel Reprocessing. *Angewandte Chemie-International Edition*. **2016**, 55 (15), 4671-4673.
27. Mustapha, A. M.; Pasilis, S. P. Probing uranyl(VI) speciation in the presence of amidoxime ligands using electrospray ionization mass spectrometry. *Rapid Communications in Mass Spectrometry*. **2013**, 27 (19), 2135-2142.
28. Mustapha, A. M.; Pasilis, S. P. Gas-phase complexes formed between amidoxime ligands and vanadium or iron investigated using electrospray ionization mass spectrometry. *Rapid Communications in Mass Spectrometry*. **2016**, 30 (15), 1763-1770.
29. Pan, H. B.; Kuo, L.J.; Wai, C.M.; Miyamoto, N.; Joshi, R.; Wood, J. R.; Strivens, J.E.; Janke, C.J.; Oyola, Y.; Das, S.; Mayes, R.T.; Gill, G.A. Elution of Uranium and Transition Metals from Amidoxime-Based Polymer Adsorbents for Sequestering Uranium from Seawater. *Industrial & Engineering Chemistry Research*. **2016**, 55 (15), 4313-4320.

30. Suzuki, T.S.; Saito, K.; Sugo, T.; Ogura, H.; Oguma, K. Fractional elution and determination of uranium and vanadium adsorbed on amidoxime fiber from seawater. *Analytical Sciences*. **2000**, *16* (4), 429-432.
31. Leggett, C.J.; Parker, B.F.; Teat, S.J.; Zhang, Z.; Dau, P.D.; Lukens, W.W.; Peterson, S.M.; Cardenas, A.J.P.; Warner, M.G.; Gibson, J.K.; Arnold, J.; Rao, L.F. Structural and spectroscopic studies of a rare non-oxido V(V) complex crystallized from aqueous solution. *Chemical Science*. **2016**, *7* (4), 2775-2786.
32. Habayeb, M.A.; Hileman, O.E. ^{51}V FT NMR investigations of metavanadate ions in aqueous solutions. *Can. J. Chem.* **1980**, *58*, 2255.
33. Tracey, A. S. Applications of ^{51}V NMR spectroscopy to studies of the complexation of vanadium(V) by α -hydroxycarboxylic acids. *Coordination Chemistry Reviews*. **2003**, *237*, 113-121.
34. Buglyo, P.; Culeddu, N.; Kiss, T.; Micera, G.; Sanna, D. Vanadium(IV) and vanadium(V) complexes of deferoxamine-B in aqueous solution. *Journal of Inorganic Biochemistry*. **1995**, *60* (1), 45-59.
35. Butler, A.; Eckert, H. ^{51}V NMR as a probe of vanadium(V) coordination to human apotransferrin. *Journal of the American Chemical Society*. **1989**, *111* (8), 2802-2809.
36. Booyesen, I.N.; Hlela, T.; Akerman, M.P.; Xulu, B. Mono and polynuclear vanadium(IV) and (V) compounds with 2-substituted phenyl/pyridyl heterocyclic chelates. *Polyhedron*. **2015**, *85*, 144-150.
37. Avecilla, F.; Geraldès, C.F.G.C.; Castro, M.M.C.A. A new trinuclear oxovanadium(V) complex with DMPP ligands - Synthesis and structural characterization in the solid state and in aqueous solution. *European Journal of Inorganic Chemistry*. **2001**, (12), 3135-3142.

38. Miranda, C.T.; Carvalho, S.; Yamaki, R.T.; Paniago, E.B.; Borges, R.H.U.; De Bellis, V.M. Formation and structure in aqueous solution of complexes between vanadium(V) and aminohydroxamic acids that potentiates vanadium's insulinomimetic activity: L-glutamic gamma-hydroxamic and L-aspartic-beta-hydroxamic acids. *Inorganica Chimica Acta*. **2010**, *363* (14), 3776-3783.
39. Miranda, C.T.; Carvalho, S.; Yamaki, R.T.; Paniago, E.B.; Borges, R.H.U.; De Bellis, V.M. pH-metric, UV-Vis and ^{51}V NMR study of vanadium(V) coordination to alpha-aminohydroxamic acids in aqueous solutions. *Polyhedron*. **2010**, *29* (2), 897-903.
40. Kremer, L.E.; Mcleod, A.I.; Aitken, J.B.; Levina, A.; Lay, P.A. Vanadium(V) and (IV) complexes of anionic polysaccharides: Controlled release pharmaceutical formulations and models of vanadium biotransformation products. *Journal of Inorganic Biochemistry*. **2015**, *147*, 227-234.
41. Kelley, S.P.; Barber, P.S.; Mullins, P. H. K.; Rogers, R.D. Structural clues to $\text{UO}_2^{2+}/\text{VO}_2^+$ competition in seawater extraction using amidoxime-based extractants. *Chemical Communications*. **2014**, *50* (83), 12504-12507.
42. Egawa, H.; Kabay, N.; Jyo, A.; Hirono, M.; Shuto, T. Recovery of uranium from seawater .15. Development of amidoxime resins with high sedimentation velocity for passively driver fluidized bed adsorbers. *Industrial & Engineering Chemistry Research*. **1994**, *33* (3), 657-661.
43. Egawa, H.; Kabay, N.; Shuto, T.; Jyo, A. Recovery of uranium from seawater .13. Long term stability tests for high performance chelating resins containing amidoxime groups and evaluation of elution process. *Industrial & Engineering Chemistry Research*. **1993**, *32* (3), 540-547.

44. Das, S.; Pandey, A.K.; Athawale, A.; Kumar, V.; Bhardwaj, Y.K.; Sabharwal, S.; Manchanda, V.K. Chemical aspects of uranium recovery from seawater by amidoximated electron-beam-grafted polypropylene membranes. *Desalination*. **2008**, *232* (1-3), 243-253.
45. Kago, T.; Goto, A.; Kusakabe, K.; Morooka, S. Preparation and performance of amidoxime fiber adsorbents for recovery of uranium from seawater. *Industrial & Engineering Chemistry Research*. **1992**, *31* (1), 204-209.
46. Liu, X.Y.; Liu, H.Z.; Ma, H.J.; Cao, C.Q.; Yu, M.; Wang, Z.Q.; Deng, B.; Wang, M.; Li, J.Y. Adsorption of the uranyl ions on an amidoxime based Polyethylene nonwoven fabric prepared by preirradiation induced emulsion graft polymerization. *Industrial and Engineering Chemistry Research*. **2012**, *51* (46), 15089-15095.
47. Das, S.; Oyola, Y.; Mayes, R.T.; Janke, C.J.; Kuo, L.J.; Gill, G.; Wood, J.R.; Dai, S. Extraction of uranium from seawater: Promising AF series adsorbent. *Industrial and Engineering Chemistry Research*. **2016**, *55*(15), 4110-4117.
48. Das, S.; Oyola, Y.; Mayes, R.T.; Janke, C.J.; Kuo, L.J.; Gill, G.; Wood, J.R.; Dai, S. Extracting uranium from seawater: Promising AI series adsorbents. *Industrial & Engineering Chemistry Research*. **2016**, *55*(15), 4103-4109.
49. Kuo, L.J.; Janke, C.J.; Wood, J.R.; Strivens, J.E.; Das, S.; Oyola, Y.; Mayes, R.T.; Gill, G. Characterization and Testing of Amidoxime-Based Adsorbent Materials to Extract Uranium from Natural Seawater. *Industrial & Engineering Chemistry Research*. **2016**, *55* (15), 4285-4293.

50. Gill, G.A.; Kuo, L.J.; Janke, C.J.; Park, J.; Jeters, R.T.; Bonheyo, G.T.; Pan, H. B.; Wai, C.M.; Khangaonkar, T.; Bianucci, L.; Wood, J.R.; Warner, M.G.; Peterson, S.; Abrecht, D.G.; Mayes, R.T.; Tsouris, C.; Oyola, Y.; Strivens, J. E.; Schlafer, N.J.; Addleman, R. S.; Chouyyok, W.; Das, S.; Kim, J.; Buessler, K.; Breier, C.; D'Alessandro, E. The Uranium from Seawater Program at the Pacific Northwest National Laboratory: Overview of Marine Testing, Adsorbent Characterization, Adsorbent Durability, Adsorbent Toxicity, and Deployment Studies. *Industrial & Engineering Chemistry Research*. **2016**, *55* (15), 4264-4277.
51. Wood, J.R.; Gill, G.A.; Kuo, L.J.; Strivens, J.E.; Choe, K.Y. Comparison of Analytical Methods for the Determination of Uranium in Seawater Using Inductively Coupled Plasma Mass Spectrometry. *Industrial & Engineering Chemistry Research*. **2016**, *55* (15), 4344-4350.
52. Alexandratos, S.D.; Zhu, X.P.; Florent, M.; Sellin, R. Polymer-Supported Bifunctional Amidoximes for the Sorption of Uranium from Seawater. *Industrial & Engineering Chemistry Research*. **2016**, *55*(15), 4208-4216.
53. Sekiguchi, K.; Saito, K.; Konishi, S.; Furusaki, S.; Sugo, T.; Nobukawa, H. Effect of seawater temperature on uranium recovery from seawater using amidoxime adsorbents. *Industrial & Engineering Chemistry Research*. **1994**, *33* (3), 662-666.
54. Wu, W.; Priest, C.; Zhou, J.; Peng, C.; Liu, H.; Jiang, D. Solvation of the $\text{Ca}_2\text{UO}_2(\text{CO}_3)_3$ complex in seawater from classical molecular dynamics. *J. Phys. Chem. B*. **2016**, *120* (29), 7227-7233.

55. Priest, C.; Tian, Z.Q.; Jiang, D. E. First-principles molecular dynamics simulation of the $\text{Ca}_2\text{UO}_2(\text{CO}_3)_3$ complex in water. *Dalton Transactions*. **2016**, 45 (24), 9812-9819.
56. Sadoc, A.; Messaoudi, S.; Furet, E.; Gautier, R.; Le Fur, E.; Le Polles, L.; Pivan, J. Y. Structure and stability of VO_2^+ in aqueous solution: A car-parrinello and static ab initio study. *Inorganic Chemistry*. **2007**, 46 (12), 4835-4843.
57. Mehio, N.; Johnson, J.C.; Dai, S.; Bryantsev, V.S. Theoretical study of the coordination behavior of formate and formamidoximate with dioxovanadium(V) cation: implications for selectivity towards uranyl. *Physical Chemistry Chemical Physics*. **2015**, 17 (47), 31715-31726.
58. Ivanov, A.S.; Bryantsev, V.S. Assessing ligand selectivity for uranium over vanadium ions to aid in the discovery of superior adsorbents for extraction of UO_2^{2+} from seawater. *Dalton Transactions*. **2016**, 45 (26), 10744-10751.
59. Abney, C.W.; Mayes, R.T.; Piechowicz, M.; Lin, Z.; Bryantsev, V.S.; Veith, G.M.; Dai, S.; Lin, W. XAFS investigation of polyamidoxime-bound uranyl contests the paradigm from small molecule studies. *Energy & Environmental Science*. **2016**, 9 (2), 448-453.
60. Hanes, R.; Rogers, R.; Gurau, G.; Shamshina, J. 525 Solutions.
<http://uraniumfromseawater.engr.utexas.edu/partners/525-solutions> (accessed Feb 9, 2017).
61. Slocum, A.; Pham, T.; Haji, M.; Hamlet, A.; Gonzalez, J.; Cao, C.; Delmy, C.; Nguyen, T.; Mcentee, T.; Poole, J.; Simms, M.; Wall, J. Massachusetts Institute of Technology. <http://uraniumfromseawater.engr.utexas.edu/partners/massachusetts-institute-technology> (accessed Feb 9, 2017).

62. Yue, Y.; Sun, X.; Mayes, R.T.; Kim, J.; Fulvio, P.F.; Qiao, Z.A.; Brown, S.; Tsouris, C.; Oyola, Y.; Dai, S. Polymer-coated nanoporous carbons for trace seawater uranium adsorption. *Science China Chemistry*. **2013**, *56* (11), 1510-1515.
63. Wang, T.; Khangaonkar, T.; Long, W.; Gill, G. Development of a Kelp-type structure module in a coastal ocean model to assess the hydrodynamic impact of seawater uranium extraction technology. *Journal of Marine Science and Engineering*. **2014**, *2*, 81-92.
64. Park, J.; Jeters, R.T.; Kuo, L.J.; Strivens, J.E.; Gill, G.A.; Schlafer, N.J.; Bonheyo, G.T. Potential Impact of Seawater Uranium Extraction on Marine Life. *Industrial & Engineering Chemistry Research*. **2016**, *55* (15), 4278-4284.
65. Park, J.; Gill, G.A.; Strivens, J.E.; Kuo, L.J.; Jeters, R.T.; Avila, A.; Wood, J.R.; Schlafer, N.J.; Janke, C.J.; Miller, E.A.; Thomas, M.; Addleman, R.S.; Bonheyo, G.T. Effect of Biofouling on the Performance of Amidoxime-Based Polymeric Uranium Adsorbents. *Industrial & Engineering Chemistry Research*. **2016**, *55* (15), 4328-4338.
66. Pan, H.B.; Liao, W.; Wai, C.M.; Oyola, Y.; Janke, C.J.; Tian, G.X.; Rao, L.F. Carbonate-H₂O₂ leaching for sequestering uranium from seawater. *Dalton Transactions*. **2014**, *43* (28), 10713-10718.
67. Gill, G.A.; Kuo, L.J.; Strivens, J.; Wood, J.; Wai, C.M.; Pan, H.B. Investigations into Alternative Desorption Agents for Amidoxime-Based Polymeric Uranium Adsorbents. 2015.
68. Pan, H.B.; Kuo, L.J.; Wood, J.; Strivens, J.; Gill, G.A.; Janke, C.J.; Wai, C.M. Towards understanding KOH conditioning of amidoxime-based polymer adsorbents for sequestering uranium from seawater. *Rsc Advances*. **2015**, *5* (122), 100715-100721.
69. Manov, D.V.; Chang, G.C.; Dickey, T.D. Methods for reducing biofouling of moored optical sensors. *Journal of Atmospheric and Oceanic Technology*. **2004**, *21* (6), 958-968.

Chapter 3: Vanadium and Uranium Coordination with Amidoxime Ligands in Aqueous Solutions

3.1 Abstract

Glutarimidedioxime and glutardiamidoxime are most promising ligands grafted on amidoxime adsorbents with polyethylene substrate used for uranium extraction from seawater. The pH of seawater is around 8.3 and these ligands are known to form strong complexes with (UO_2^{+2}) at this pH. To enhance uranium uptake from seawater, it is vital to understand solution phase complexes of these ligands with UO_2^{+2} and vanadium. Vanadium competes with UO_2^{+2} for binding sites on adsorbent and reduces its UO_2^{+2} adsorption efficiency. Spectroscopic techniques, such as nuclear magnetic resonance (NMR), UV-Visible absorption spectrophotometry, and liquid chromatography–mass spectrometry (LC-MS), are used for characterization of solution phase uranyl and vanadium complexes, and to evaluate relative stabilities of such complexes at different pH values.

3.2 Introduction

Sequestering uranium from seawater has become an active research area in recent years due to concerns about limited land-based uranium ore reserves, which may be depleted by the end of this century due to uranium consumption by nuclear power industry. Our oceans contain more than 1000 times uranium than all known land-based uranium ore reserves. Uranium exists in seawater at a very low concentration, about 3 ppb, and in a very stable form, uranyl tris-carbonato complex [$\text{UO}_2(\text{CO}_3)_3^{4-}$]. Extraction of uranium from seawater requires a highly efficient adsorption material to make this unorthodox uranium production method economically feasible. According to the literature, amidoxime-based polymer adsorbents have been shown to be the most effective material for sequestering uranium from seawater. The concentration factor of uranium from seawater to amidoxime-based adsorbent ($\sim 3 \times 10^{-3}$ g U/g

of sorbent) is typically 6 orders of magnitude in seawater tests. High uranium adsorption capacity and good mechanical strength of amidoxime-based polymer adsorbents make them attractive for extracting uranium from seawater. The amidoxime-based polymer adsorbents are also effective for extracting transition metals from seawater, particularly vanadium. Actually, on a molar basis, vanadium adsorption is much greater than that of uranium from seawater tests utilizing amidoxime-based adsorbents. Vanadium apparently is a major competing element for uranium adsorption from seawater using amidoxime-based adsorbents. There is little information in the literature regarding distribution of vanadium species in seawater. According to one report,¹ vanadium can exist in seawater in two different oxidation states, +4 and +5, and distribution of the two vanadium oxidation species in seawater depends on location and season. Complexation of different vanadium species with amidoxime is also not well known. Knowledge of the coordination chemistry of vanadium with amidoxime molecules is essential for understanding vanadium adsorption by amidoxime-based adsorbents in seawater. However, it should be cautioned that coordination behavior of metal ions with free ligand molecules may not be the same as ligand groups attached to a polymer adsorbent. Nevertheless, this information is still important for designing new amidoxime-based adsorbents which could be more selective for uranyl coordination over vanadium ions and result in higher uranium adsorption capacities. This paper reports results of our recent spectroscopy studies regarding complexation of vanadium species with amidoxime molecules and their competition with uranyl ions in aqueous solution. The information is crucial for understanding competitive adsorption of uranyl and vanadium species on amidoxime-based adsorbents in seawater. This study presents a first look at solution state NMR studies of UO_2^{+2}

complexation with glutarimidedioxime and glutardiamidoxime system in the absence and presence of vanadium.

3.3 Experimental

3.3.1 Chemicals and reagents

Glutarimidedioxime and glutardiamidoxime used for this study were synthesized in our lab by the procedure as described in the literature.² Uranyl (VI) nitrate hexahydrate was purchased from International Bio-Analytical Industries, Inc. (Boca Raton, FL, USA). Sodium orthovanadate Na_3VO_4 (99%) and vanadyl sulfate VO_2SO_4 (99%), were purchased from Acros Organics, a Fisher Scientific brand (NJ, USA). Hydrochloric acid (ACS grade), sodium hydroxide (ACS grade), NaCl (ACS grade), were purchased from EMD Chemicals (Gibbstown, NJ, USA), and NaHCO_3 (ACS grade), was purchased from Fair Lawn (NJ, USA). ^{13}C enriched Na_2CO_3 was purchased from Sigma Aldrich. Distilled water was used. All chemicals were used as received.

3.3.2 Instrumentation

A 500 MHz Bruker Avance NMR spectrometer was used to acquire ^{51}V NMR, ^1H NMR, ^{13}C NMR, and heteronuclear multiple bond coherence (HMBC) spectra. Absorption spectra were acquired using a Model 440 UV-Vis spectrophotometer with a CCD (charge coupled device) array detector (Spectral Instruments Inc., Tucson AZ). ESI mass spectra were collected using a Waters Xevo TQ MS mass spectrometer. The mass spectrometer was programmed to acquire data in positive ion mode between 20 and 1000 Da with a 1.5 sec scan time. The capillary voltage was set to 3.5 kV, cone voltage was 35 V, the collision voltage was 2 V, the desolvation temperature was 300 °C, and desolvation gas flow (nitrogen) was

300 L/Hr. Liquid chromatography was done using a gradient of water with 0.1% formic acid (Solvent A) and methanol with 0.1% formic acid (Solvent B) at a flow rate of 0.2 mL/min. The solvent composition was 97% A and 3% B at injection. For the first 2 minutes, elution was isocratic. At 2 minutes, gradient began, with composition reaching 100% B at 12 minutes. The ratio of A and B was held at 100% B for 3 minutes, brought back to 97% A and 3% B over the next four minutes, and held at 97/3 for the next 6 minutes prior to the next injection. The column used was a Waters Acquity BEH C18 column with dimensions 2.1 mm i.d. X 50 mm length and 1.7 μ m particle size (P/N 186002350). The column was maintained at 32 degrees, and the injection volume was 10 μ L. Detection was done using an Acquity Photodiode array detector set to acquire spectra from 200 to 500 nm.

3.3.3 *Sample preparation*

20 mM stock solutions of uranyl(VI) nitrate hexahydrate, sodium orthovanadate, and glutardiamidoxime were prepared by dissolving an appropriate amount of each compound, and diluting with 0.05 M NaCl solution of D₂O/H₂O to give final concentration. 10 mM stock solutions of glutarimidedioxime, EDTA, and vanadyl sulfate were prepared in the same way. Appropriate ratios of metal and ligand stock solutions were combined to give final required concentrations. The pH of sample solutions was adjusted with HCl or NaOH. The pH measurements of the solutions were made using an Orion ROSS combination pH electrode (Thermo Fisher Scientific, Pittsburg, PA, USA). The pH electrode calibration was performed using pH 4.0, 7.0, and 10.0 buffers traceable to the NIST pH activity scale. Simulated seawater was prepared by dissolving 25.6 gram of sodium chloride, and 193 mg of sodium bicarbonate in a 1000 mL volumetric flask. Stock solutions and samples were prepared on the day of use. A coaxial NMR tube insert containing benzene-d₆/acetone-d₆ was inserted into each sample

tube before NMR analyses and was used for magnetic field lock. ^{51}V NMR chemical shifts were referenced to an external VOCl_3 signal at 0 ppm. ^{13}C chemical shifts were referenced to signals arising from acetone- d_6 , and ^1H chemical shifts were referenced to a signal arising from residual C_6H_6 at 7.16 ppm.

3.4 Results and Discussion

One method of synthesizing amidoxime-based fiber is by Radiation Induced Graft Polymerization (RIGP) technique, which involves grafting acrylonitrile ($\text{CH}_2=\text{CH}-\text{CN}$) onto polyethylene fabrics followed by chemical conversion of the $-\text{CN}$ groups with hydroxylamine (NH_2OH) to amidoxime groups. The amidoxime groups formed in the polymer adsorbent by the synthesis method described in Chapter 4 can exist in different structures², including the open-chain diamidoxime and cyclic imidedioxime illustrated in Figure 3.1. Both the cyclic imidedioxime (H_2A) and the open-chain diamidoxime (H_2B) on the adsorbent can form strong complexes with uranium. Rao and co-workers reported that the open-chain diamidoxime is a weaker ligand than the cyclic imidedioxime for complexing with uranyl ions under seawater conditions (pH ~ 8.3 , 2.3 mM total carbonate).³ The seawater uranium sequestering process may be illustrated by the following reaction.



where H_2A and H_2B represent glutarimidedioxime and glutardiamidoxime shown in Figure 3.1, respectively.

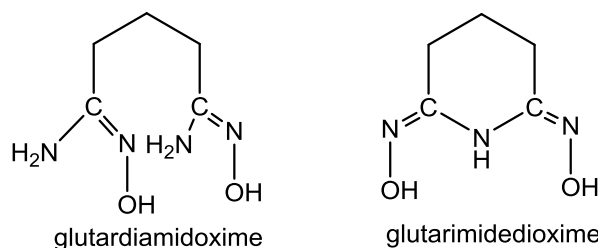


Figure 3.1 Structures of open-chain diamidoxime (left) and cyclic imidedioxime (right)

A recent publication⁴ reports that vanadium in the +5 oxidation state as Na_3VO_4 dissolved in water at pH 8 reacts only with cyclic glutarimidedioxime, and not with open-chain glutardiamidoxime according to the ^{51}V NMR spectroscopy. Former research colleague Dr. Naomi Miyamoto did preliminary experiments on studying vanadium complexation with glutarimidedioxime and glutardiamidoxime using ^{51}V NMR spectroscopy. Results indicate formation of 1:1 complex between vanadium(V) and cyclic glutarimidedioxime using low concentrations (0.2 mM) of Na_3VO_4 .

The ^{51}V NMR spectrum for free vanadium(V) gives a ^{51}V NMR peak at -549 ppm. Upon addition of cyclic glutarimidedioxime to vanadium(V), the ^{51}V NMR peak shifts to -413 ppm. Shift in the ^{51}V NMR signal of vanadium(V) upon the addition of cyclic glutarimidedioxime, shows complexation of vanadium(V) with cyclic glutarimidedioxime. However, no complexation of vanadium(V) with open-chain glutardiamidoxime was observed. Upon addition of open-chain glutardiamidoxime to vanadium(V), the ^{51}V NMR peak appears at -548 ppm. No significant shift in the ^{51}V NMR signal of vanadium(V) upon the addition of open-chain glutardiamidoxime shows that vanadium(V) does not react with open-chain glutardiamidoxime. The ^{51}V NMR spectra for this study are shown in Figure 3.2a-c.

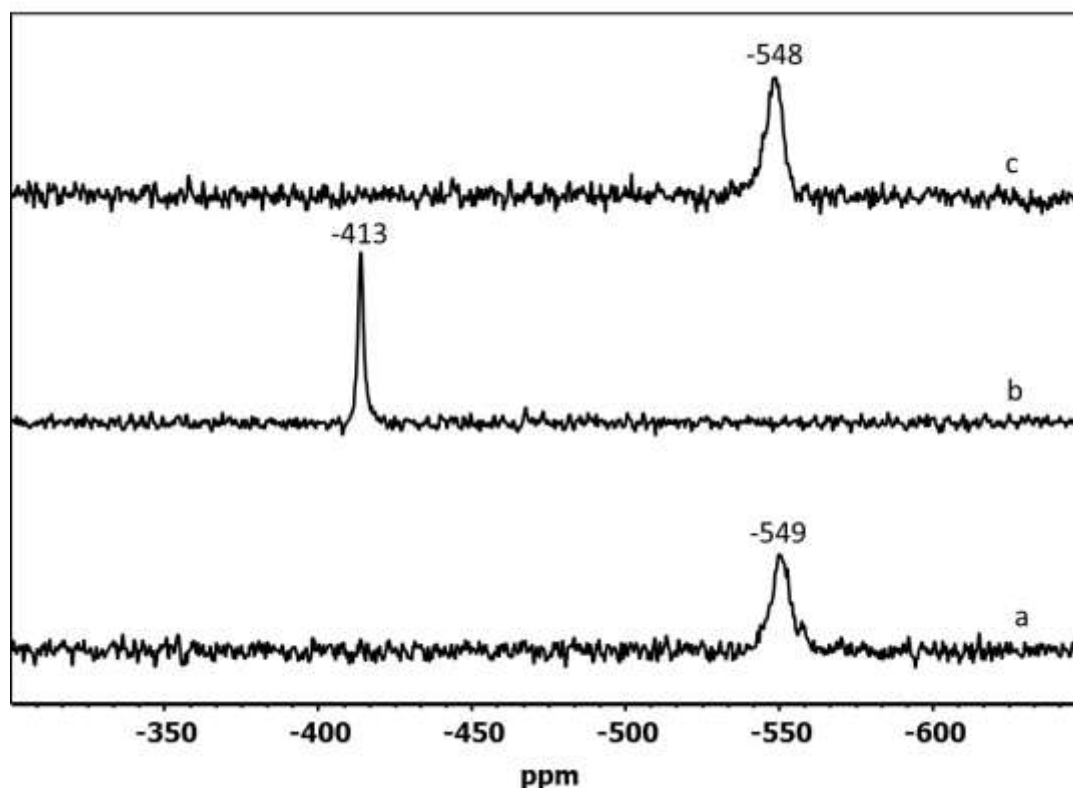


Figure 3.2 ^{51}V NMR spectra of 0.2 mM vanadium(V) in simulated seawater (a) without any ligand, (b) with 0.2 mM of cyclic glutarimidedioxime, and (c) with 0.2 mM of open-chain glutardiamidoxime.

Miyamoto further studied the coordination between vanadium and cyclic glutarimidedioxime for determining the stoichiometric ratio of coordination between vanadium and cyclic glutarimidedioxime using ^{51}V NMR spectroscopy. The ^{51}V NMR spectra for this study are shown in Figure 3.3. The ^{51}V NMR peak for free vanadium(V) without addition of glutarimidedioxime was observed at -548 ppm. This peak belongs to free vanadates (H_2VO_4^- and HVO_4^{2-}), at the pH of 8.3, and is consistent with previous literature.⁵⁻⁷ Upon addition of cyclic glutarimidedioxime in concentrations of less than 0.2 mM, the ^{51}V NMR peak for both complexed and free vanadium(V) were observed at ~ -411 ppm and ~ -548 ppm respectively. When 0.2 mM cyclic glutarimidedioxime was added to solution containing 0.2 mM vanadium(V) such that vanadium(V):cyclic glutarimidedioxime

mole ratio was 1:1, only one ^{51}V NMR peak at -411 ppm was observed. This observation confirms the formation of a 1:1 complex between vanadium(V) and cyclic glutarimidedioxime.

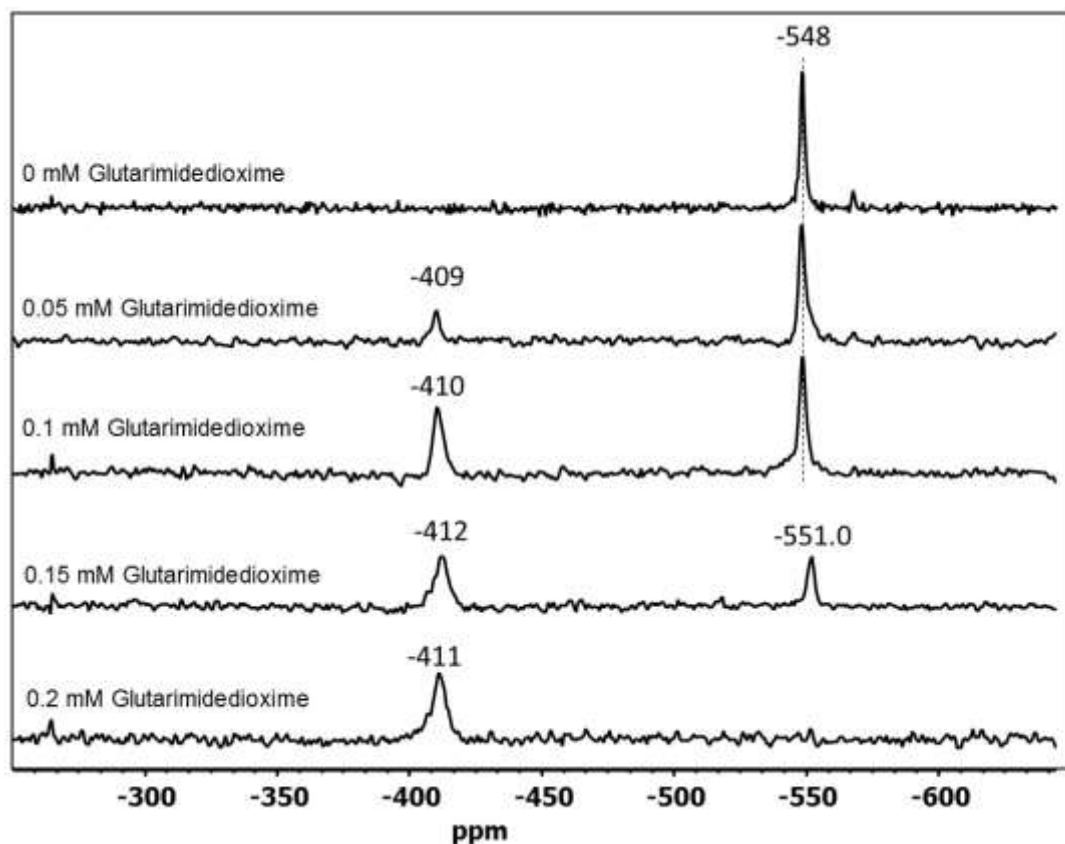


Figure 3.3 ^{51}V NMR spectra of 0.2 mM vanadium(V) followed by addition of different concentrations of cyclic glutarimidedioxime. All samples in 0.5 M NaCl aqueous solution at pH 8.3.

This work was further expanded by detailed spectroscopic investigation of vanadium(V) interactions with cyclic glutarimidedioxime and open-chain glutardiamidoxime using ^{51}V NMR, ^1H NMR, ^{13}C NMR, heteronuclear multiple bond coherence (HMBC), liquid chromatography-mass spectrometry (LC-MS), and UV-Visible absorption spectroscopy. The effect of changes in vanadium(V) concentrations above 0.2 mM, and varying vanadium(V)-glutarimidedioxime mole ratio, and time-based formation of 1:1 and 1:2 complex in solutions

containing cyclic glutarimidedioxime, and open-chain glutardiamidoxime was also investigated using the above mentioned spectroscopic techniques.

3.4.1 Complexation of vanadium(V) with glutarimidedioxime

Figure 3.4a-d, shows ^{51}V NMR spectra acquired using 0.2 mM vanadium(V), and increasing glutarimidedioxime concentration from 0.4 mM to 2.0 mM. The peak at the chemical shift ranging from -417.3 ppm to -418.8 ppm (Figure 3.4a-d) indicates the formation of 1:1 complex between vanadium(V) and glutarimidedioxime. The ^{51}V NMR spectra shows no significant change on chemical shift upon increasing glutarimidedioxime concentration. Only 1:1 complex was observed in the ^{51}V NMR spectra for all the samples, because 1:1 complex is stable and forms immediately.

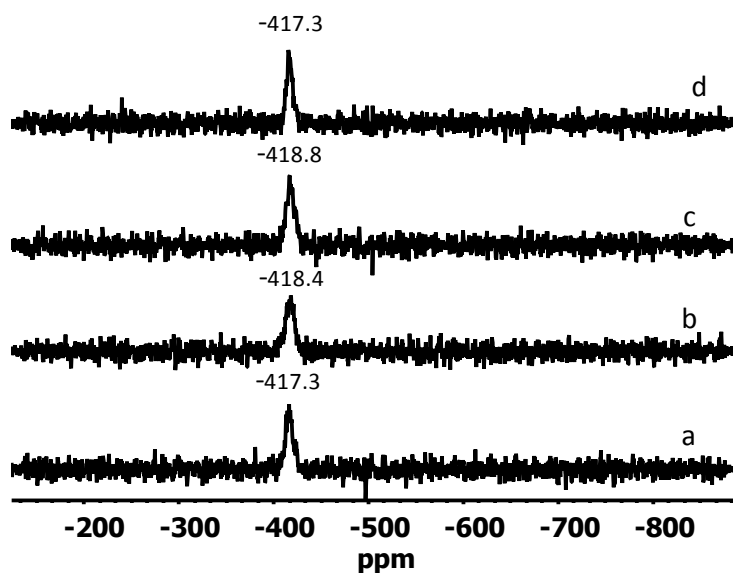


Figure 3.4 ^{51}V NMR spectra of 0.2 mM vanadium(V) followed by addition of different molar concentrations of glutarimidedioxime, (a) 0.4 mM, (b) 0.8 mM, (c) 1.2 mM, and (d) 2.0 mM. All samples in 0.05 M NaCl aqueous solution at pH 8.3.

The 1:2 complex was not detected for samples containing low concentration (0.2 mM) of Na_3VO_4 , even by increasing the molar ratio of vanadium(V):glutarimidedioxime from 1:1 to 1:10, and reanalyzing the samples after 7 days. This observation indicates that only 1:1 complex was detected at low vanadium concentration, and high ligand concentration do not facilitate the formation of 1:2 complex between vanadium(V) and glutarimidedioxime.

The complex formation between vanadium(V) and glutarimidedioxime at low vanadium(V) concentration (0.2 mM) was also investigated using mass spectrometry. Figure 3.5 shows the mass spectrum acquired for solutions containing glutarimidedioxime and vanadium(V) at the molar ratio of 1:1 using 0.2 mM Na_3VO_4 and 0.2 mM glutarimidedioxime. Protonated glutarimidedioxime can be seen at $m/z \sim 144$, along with fragment ions resulting from water loss at $m/z \sim 126$. Evidence of 1:1 vanadium-glutarimidedioxime complex, at $m/z \sim 226$, was observed in the mass spectrum.

The peaks observed at $m/z \sim 247.8$, $m/z \sim 269.7$, $m/z \sim 291.8$, were due to $[(\text{VO}_2+\text{glutarimidedioxime}+\text{Na})^+]$, $[(\text{VO}_2+\text{glutarimidedioxime}+2\text{Na}-\text{H}^+)]$, and $[(\text{VO}_2+\text{glutarimidedioxime}+3\text{Na}-2\text{H}^+)]$, respectively.

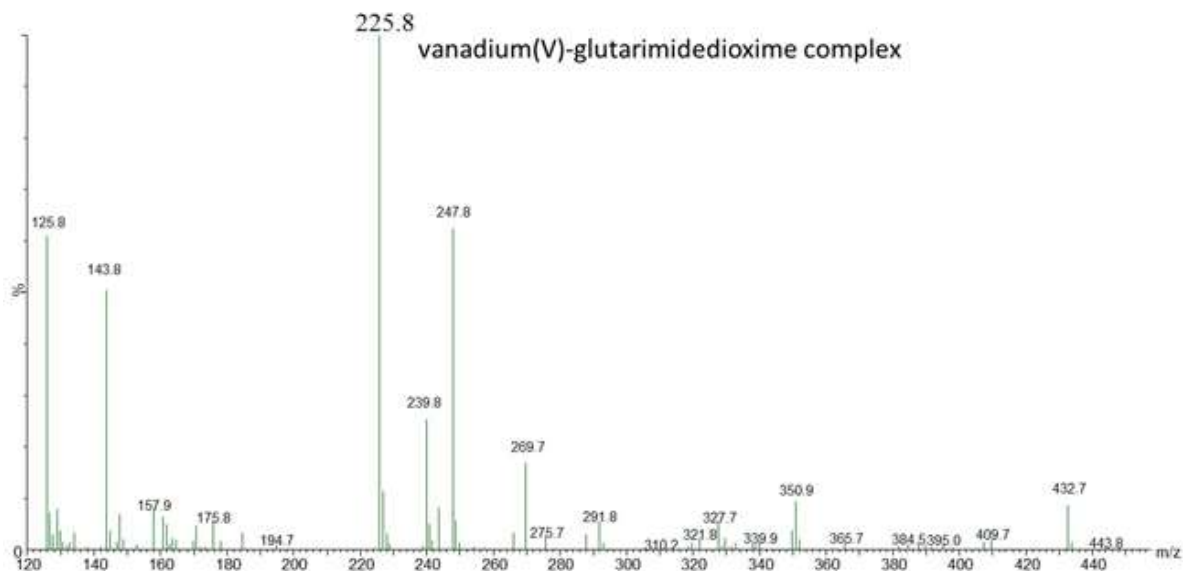


Figure 3.5 Positive-ion ESI mass spectrum of a solution containing 0.2 mM vanadium(V) and 0.2 mM glutarimidedioxime in 0.05 M NaCl aqueous solution at pH 8.3.

Figure 3.6 shows chromatogram acquired for solutions containing free glutarimidedioxime without any vanadium, and glutarimidedioxime with vanadium(V) at a molar ratio of 1:1. The peak at the retention time of 1.75 minutes is due to free glutarimidedioxime. Evidence of 1:1 vanadium(V)-glutarimidedioxime complex was observed at the retention time of 0.77 minutes in the chromatogram.

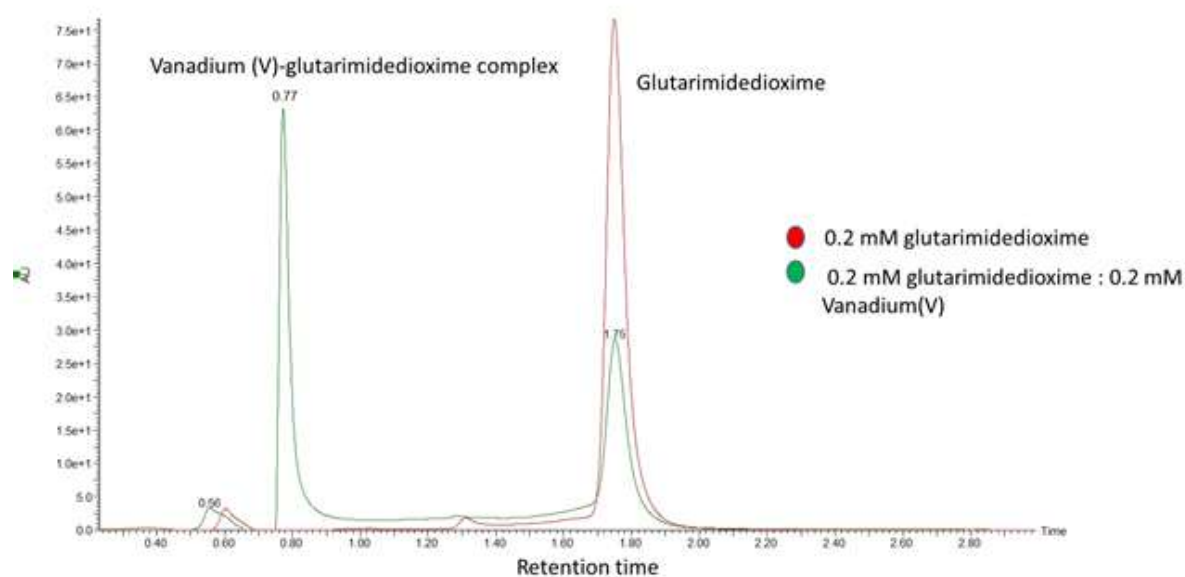


Figure 3.6 Chromatogram for solutions containing 0.2 mM glutarimidedioxime only, and 0.2 mM glutarimidedioxime:0.2 mM vanadium(V) in 0.05 M NaCl aqueous solution at pH 8.3.

The mass spectrum was acquired for solution containing 0.1 mM free glutarimidedioxime (Figure.3.7). Protonated glutarimidedioxime can be seen at m/z ~144 along with fragment ions resulting from water loss at m/z ~126.⁸

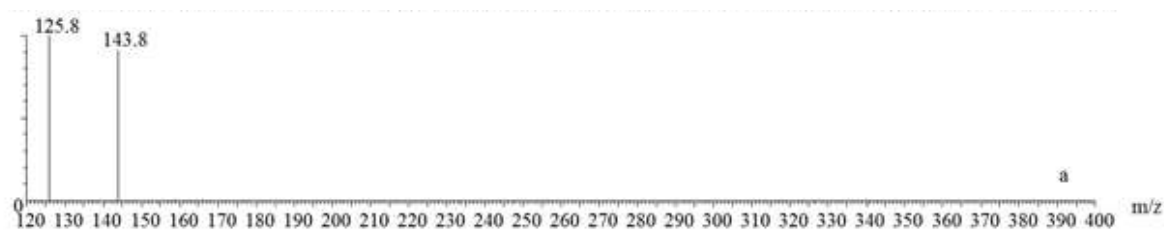


Figure 3.7 Positive-ion ESI-MS mass spectrum acquired from a solution containing 0.1 mM glutarimidedioxime in 0.05 M NaCl aqueous solution at pH 8.3.

Due to low natural abundance of ^{13}C nucleus, it is very time-consuming to acquire ^{13}C NMR spectra at low glutarimidedioxime concentration. Also, the quaternary carbon of

complexed glutarimidedioxime cannot be observed at low concentration of glutarimidedioxime. The quaternary carbon has a long T1 relaxation time, and it relaxes slowly, and displays a ^{13}C NMR signal with reduced intensity. Hence, high concentration of vanadium(V) (5 mM), and glutarimidedioxime (5 mM), in the stoichiometric ratio of 1:1 was used for the detection of 1:1 complex between vanadium(V) and glutarimidedioxime using ^{13}C NMR spectroscopy. ^1H NMR spectra were also acquired for these samples.

Figure 3.8a, shows ^{13}C NMR signals for free glutarimidedioxime without any vanadium belonging to $-\text{CH}_2-\text{CH}_2-\text{CH}_2-$, at 19 ppm, 1C; $-\text{CH}_2-\text{CH}_2-\text{CH}_2-\text{C}(\text{NOH})-$, at 25 ppm, 2C; and $\text{HON}-\text{C}-(\text{NH})-\text{C}-\text{NOH}$, at 149 ppm, 2C; (Figure.3.8a). The 1:1 complex of vanadium(V) with glutarimidedioxime was observed (Figure.3.8b) because along with ^{13}C signals assigned for free glutarimidedioxime new ^{13}C signals for complexed carbons of glutarimidedioxime were observed (Figure.3.8b) $-\text{CH}_2-\text{CH}_2-\text{CH}_2-$, at 20 ppm, 1C; $-\text{CH}_2-\text{CH}_2-\text{CH}_2-\text{C}(\text{NOH})-$, at 22 ppm, 2C; and $\text{HON}-\text{C}-(\text{NH})-\text{C}-\text{NOH}$, at 160 ppm, 2C.

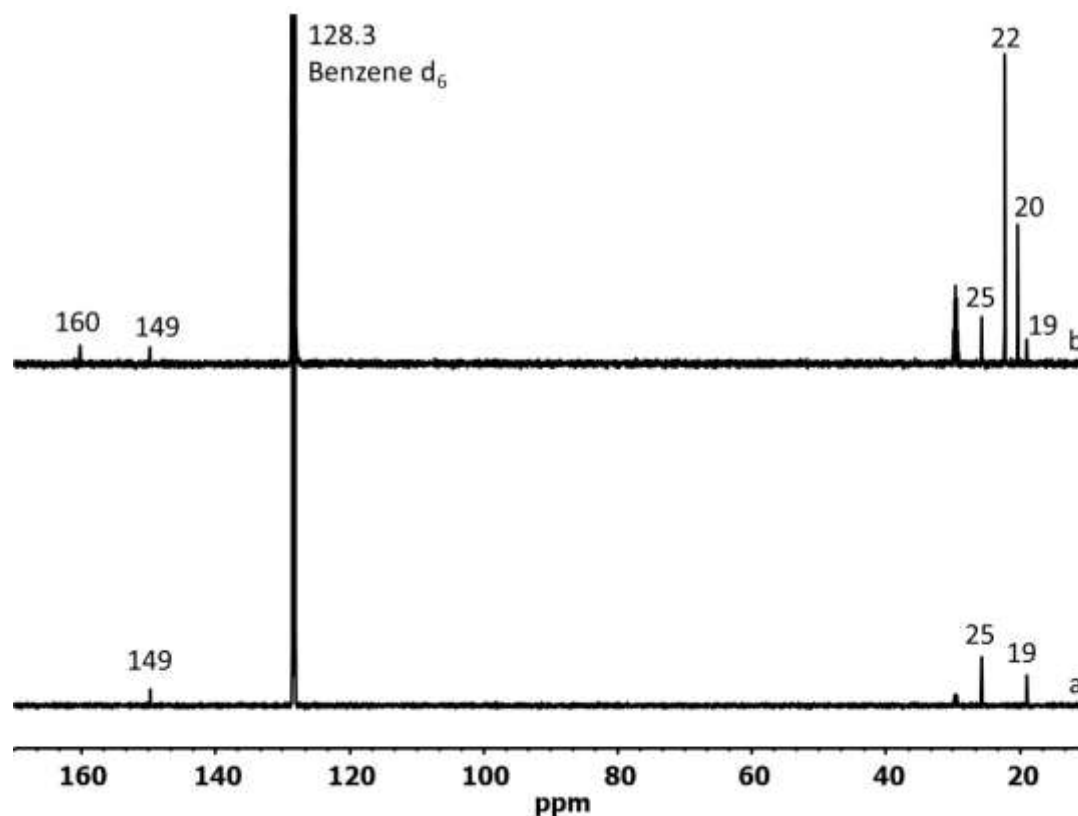


Figure 3.8 ¹³C NMR spectra of (a) 5 mM glutarimidedioxime, and (b) 5 mM vanadium(V):5 mM glutarimidedioxime. All samples in 0.05 M NaCl aqueous solution at pH 8.3. The ¹³C NMR signal at 128.3 ppm is due to benzene-d₆ used for magnetic field lock.

¹H NMR spectra for solutions containing free glutarimidedioxime without any vanadium and vanadium(V)-glutarimidedioxime complex in the molar ratio of 1:1 are shown in Figure 3.9a-b. Free glutarimidedioxime without any vanadium shows a triplet for —CH₂—CH₂—CH₂—C(NOH)—, at 2.49 ppm, 4H; and a quintet for —CH₂—CH₂—CH₂—, at 1.8 ppm, 2H; (Figure 3.9a). However, upon addition of 5 mM vanadium(V) to 5 mM glutarimidedioxime formation of a 1:1 complex between vanadium(V) and glutarimidedioxime was observed. The ¹H NMR signals for glutarimidedioxime in complexed

state, shows a triplet for $-\text{CH}_2-\text{CH}_2-\text{CH}_2-\text{C}(\text{NOH})-$, at 2.54 ppm, 4H; and a quintet for $-\text{CH}_2-\text{CH}_2-\text{CH}_2-$, at 1.9 ppm, 2H; (Figure 3.9b).

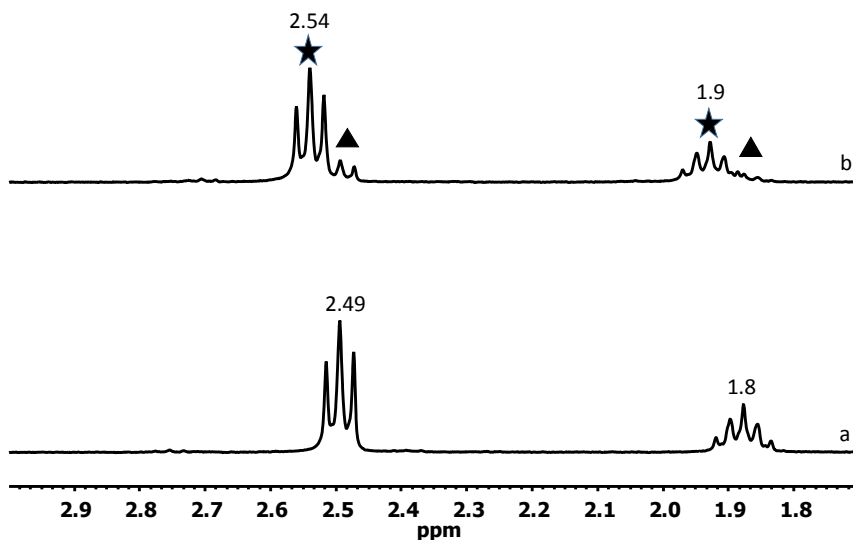


Figure 3.9 ^1H NMR spectra of (a) 5 mM glutarimidedioxime, and (b) 5 mM vanadium(V):5 mM glutarimidedioxime. All samples in 0.05 M NaCl aqueous solution at pH 8.3.

The above results for investigation of vanadium(V) complexation with glutarimidedioxime using different spectroscopic techniques shows formation of 1:1 complex, at low vanadium(V) concentration (0.2 mM). Further investigation on the formation of 1:1, and 1:2 complex between vanadium(V) and glutarimidedioxime was performed using high concentration (0.5 mM) of Na_3VO_4 followed by addition of different concentrations of glutarimidedioxime. Figure 3.10, shows the ^{51}V NMR spectra acquired using 0.5 mM vanadium(V) and increasing glutarimidedioxime concentration from 1 mM to 5.0 mM. The peak at the chemical shift ranging from -416.2 ppm to -418.3 ppm (Figure 3.10a-d) indicates the formation of 1:1 complex between vanadium(V) and glutarimidedioxime. The 1:2

complex was not observed for these samples containing 0.5 mM of Na_3VO_4 even by increasing the molar ratio of vanadium(V):glutarimidedioxime from 1:2 to 1:10.

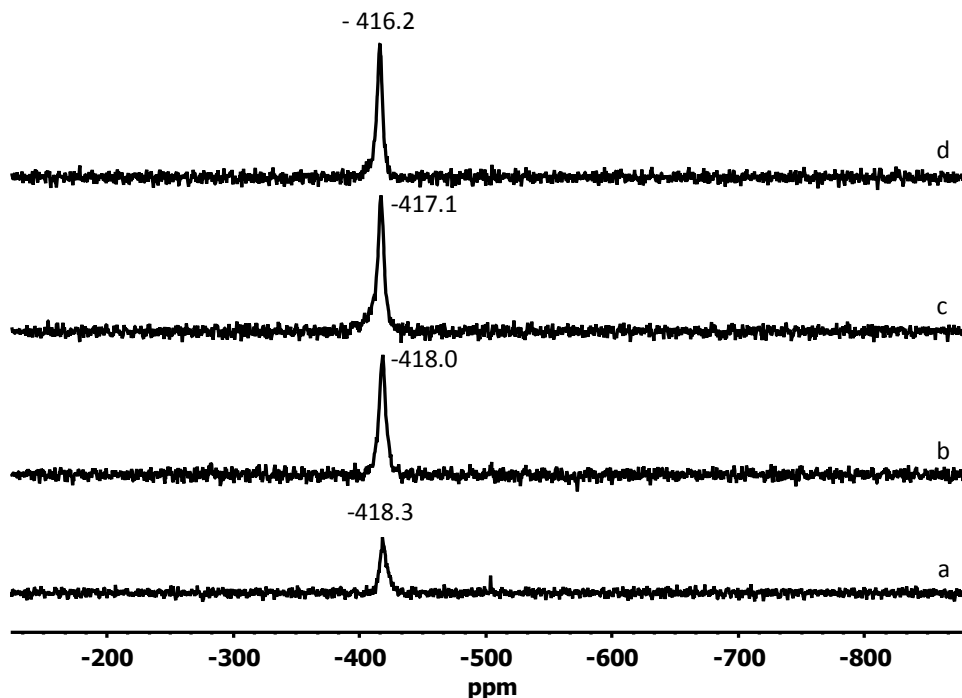


Figure 3.10 ^{51}V NMR spectra of 0.5 mM vanadium(V) followed by addition of different millimolar concentrations of glutarimidedioxime (a) 1.0 mM, (b) 2.0 mM, (c) 3.0 mM, and (d) 5.0 mM. All samples in 0.05 M NaCl aqueous solution at pH 8.3.

When concentration of vanadium(V) was 0.5 mM, and concentration of glutarimidedioxime was 1 mM, the chemical shift of complexed vanadium(V) shifted with time, as observed in the ^{51}V NMR spectrum, shown in Figure 3.11a-e. However, at low concentration (0.2 mM) of vanadium(V) and low concentration (0.4 mM) of glutarimidedioxime, the chemical shift of complexed vanadium(V) does not shift with time. Initially a ^{51}V NMR peak for vanadium(V) complexed with glutarimidedioxime was observed at the chemical shift of -416.1 ppm, along with two other signals at -499.3 ppm and -515.2 ppm (Figure 3.11a-b), probably due to resonances of decavanadate as reported by Rehder et al.⁶ We observed that the ^{51}V NMR signal for complexed vanadium(V) shifted from -416.1

ppm to -428.7 ppm till 9.5 hours, and then it remained unchanged till 2 days (Figure 3.11 a-e). Time dependent disappearance of ^{51}V NMR signal at the chemical shift of -499.3 ppm and -515.2 (Figure 3.11 a-b) was also observed; it may be because the polynuclear vanadium species (decavanadate) could form other stable complexes. The coordination chemistry of vanadium(V) with glutarimidedioxime at high vanadium concentration appears complicated and is difficult to understand at the present time.

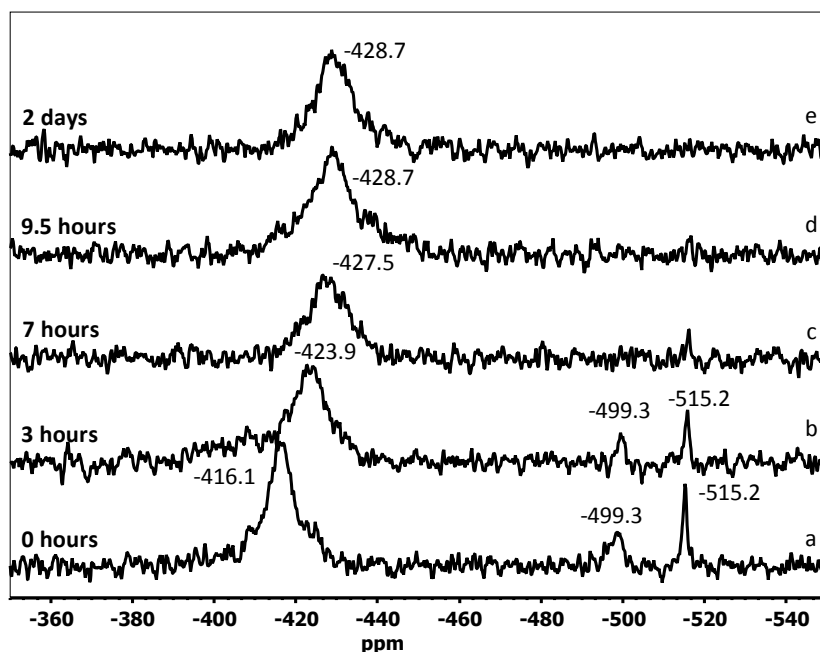


Figure 3.11 ^{51}V NMR spectra of a solution containing 0.5 mM vanadium(V):1 mM glutarimidedioxime observed with time. All samples in 0.05 M NaCl aqueous solution at pH 8.3.

The above complexation of 0.5 mM vanadium(V) with 1 mM glutarimidedioxime was also studied using ^{13}C NMR spectroscopy. The ^{13}C NMR spectrum was obtained for sample solution containing 0.5 mM vanadium(V):1 mM glutarimidedioxime after 2 days of sample preparation to form a stable complex. The obtained ^{13}C NMR spectrum (Figure 3.12b) was compared to the ^{13}C NMR spectrum obtained using 1 mM free glutarimidedioxime without any vanadium (Figure 3.12a). The ^{13}C signals for complexed carbons of glutarimidedioxime,

due to the formation of vanadium(V)-glutarimidedioxime complex in 1:1 stoichiometric ratio were observed at, $\text{---CH}_2\text{---}\mathbf{CH}_2\text{---CH}_2\text{---}$, at 20.1 ppm, 1C and at $\text{---}\mathbf{CH}_2\text{---CH}_2\text{---}\mathbf{CH}_2\text{---C(NOH)---}$, at 22.1 ppm, 2C (Figure 3.12 b-c). The ^{13}C signals for 1:2 complex between vanadium(V) and glutarimidedioxime were not detected by ^{13}C NMR spectroscopy because the complex takes more time to form and was not formed at this reaction condition. Figure 3.12c is the zoomed version of ^{13}C NMR spectrum obtained in Figure 3.12b, highlighting peaks observed in the region of 15 ppm to 35 ppm, which are otherwise obscured. We see ^{13}C NMR signals for carbons belonging to free glutarimidedioxime without any vanadium, at 19.0 ppm for $\text{---CH}_2\text{---CH}_2\text{---CH}_2\text{---}$, 25.7 ppm for $\mathbf{CH}_2\text{---CH}_2\text{---}\mathbf{CH}_2\text{---}$, and 149.8 ppm for, $\text{HON---C---(NH)---C---NOH}$ (Figure 3.12a). Figure 3.12c, shows several ^{13}C NMR signals at 13.8 ppm, 19.3 ppm, 20.1 ppm, 21.4 ppm, 22.1 ppm, 31 ppm, and 33 ppm for a solution containing 0.5 mM vanadium(V), and 1 mM glutarimidedioxime. This may indicate that glutarimidedioxime is complexed with vanadium at different binding sites in a polynuclear vanadium species, giving different ^{13}C NMR signals, which can't be assigned. Signals for uncomplexed glutarimidedioxime, as assigned earlier for Figure 3.12a, were also observed for this solution. The ^{13}C NMR signals at 128.3 ppm and 29.6 ppm are the ^{13}C signals from benzene-d₆ and trace amount of acetone-d₆, respectively, present in the insert used for magnetic field lock.

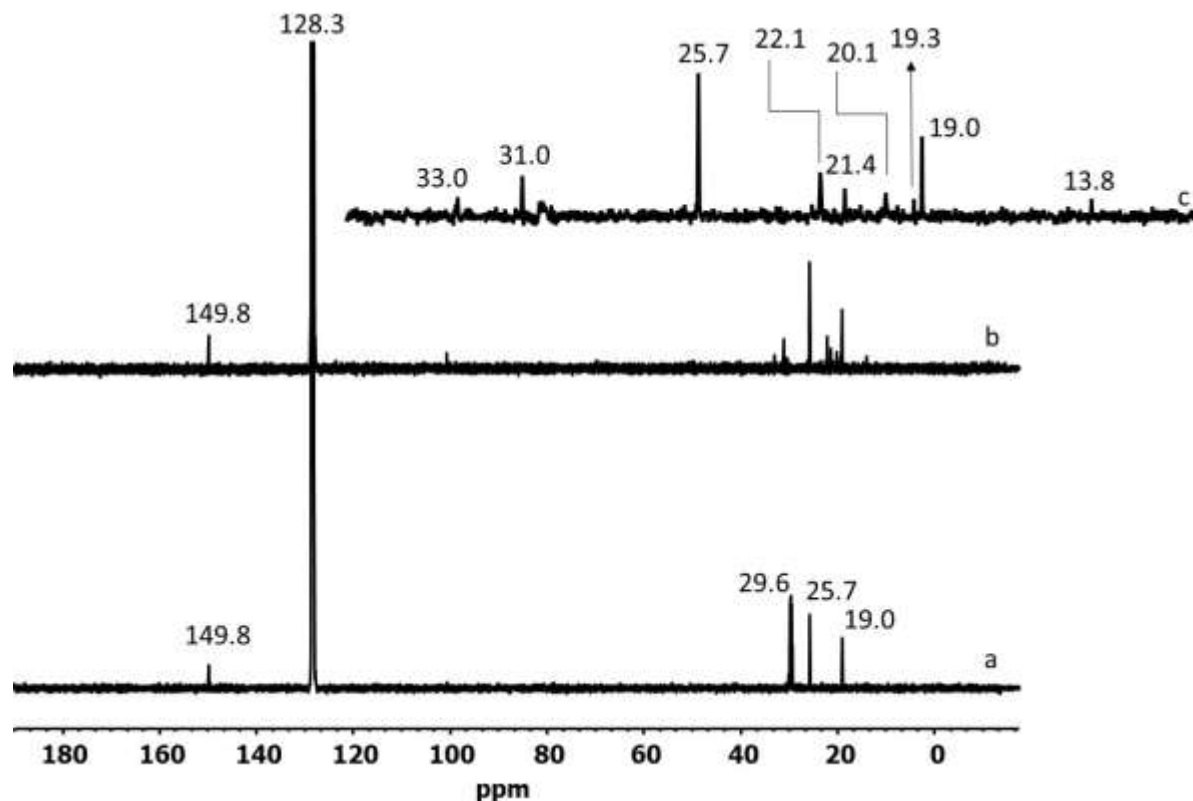


Figure 3.12 ^{13}C NMR spectra of solution containing (a) 1 mM glutarimidedioxime only, (b) 0.5 mM vanadium(V):1 mM glutarimidedioxime, and (c) spectrum b, zoomed in the region of 15-35 ppm. All samples in 0.05 M NaCl aqueous solution at pH 8.3. The signal at 128.3 is due to benzene d₆ insert used for magnetic field lock.

To understand this complexation mass spectrum was acquired for this study. The mass spectrum shown in Figure 3.13 shows most abundant peak at m/z of ~ 226 , corresponding to a 1:1 complex between vanadium(V) and glutarimidedioxime. The peak at m/z of 144 corresponds to protonated glutarimidedioxime.⁸ The mass spectrum in Figure 3.13 shows no formation of 1:2 complex in the mass spectrum, which may be because the 1:2 complex between vanadium(V) and glutarimidedioxime is not formed in this short time.

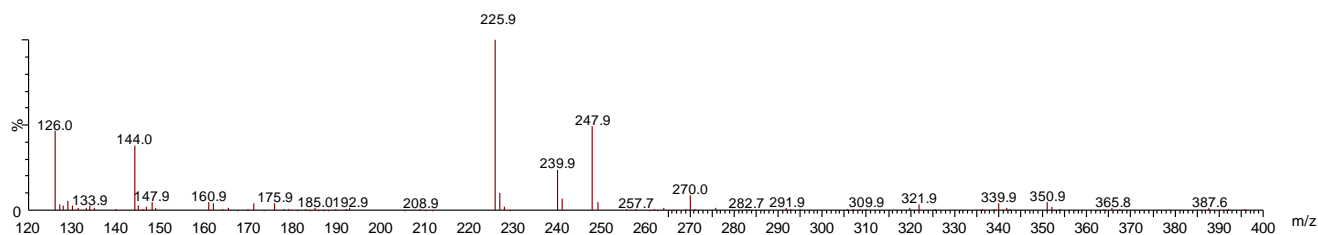


Figure 3.13 Positive-ion ESI mass spectrum acquired from a solution containing 0.5 mM vanadium(V), and 1 mM glutarimidedioxime in 0.05 M NaCl, at pH 8.3.

The complexation of 0.5 mM vanadium(V) with 1 mM glutarimidedioxime was also studied using liquid chromatography (LC). Figure 3.14 shows the chromatogram acquired for this solution. Immediate analysis of sample solution shows only two peaks in LC chromatogram. A peak at the retention time of 1.79 minute is assigned to free glutarimidedioxime. Vanadium(V)-glutarimidedioxime complex in 1:1 stoichiometry was observed at the retention time of 0.82 minutes (Figure 3.14). The same solution was reanalyzed after two days because earlier ^{51}V NMR results for this sample solution (Figure 3.11 a-e) shows the formation of a stable complex between vanadium(V) and glutarimidedioxime in 2 days. The chromatogram for this solution (Figure 3.14) shows a new peak at the retention time of 2.65 minutes, along with earlier assigned peaks at the retention time of 0.82 minutes and 1.79 minutes.

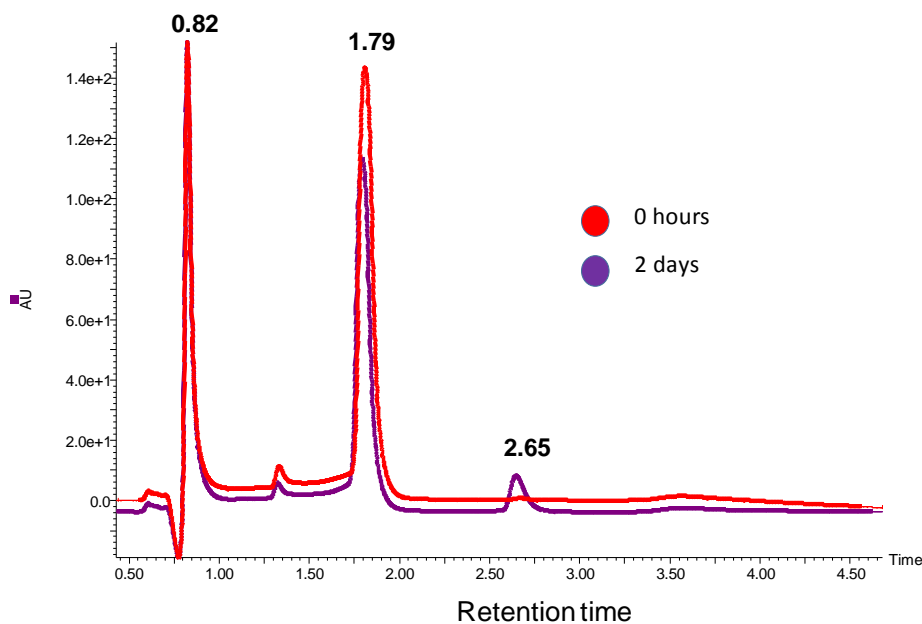


Figure 3.14 Chromatogram of a solution containing 0.5 mM vanadium(V) and 1 mM glutarimidedioxime analyzed immediately (0 hours) and after 2 days in 0.05 M NaCl aqueous solution at pH 8.3.

A recent report⁹ published about gas phase complexes formed between amidoxime ligands and vanadium shows that m/z of 333.1 corresponds to a complex between vanadium(V) and glutarimidedioxime with water loss $[\text{VO}_2+2(\text{DHIP})-2(\text{H}_2\text{O})]^+$, where glutarimidedioxime is named as DHIP. This indicates that the peak at the retention time of 2.65 minutes (Figure 3.14), is due to a vanadium(V)-glutarimidedioxime complex, $[\text{VO}_2+2(\text{DHIP})-2(\text{H}_2\text{O})]^+$ because the mass of m/z 333.1 was observed for the peak at the retention time of ~ 2.65 minutes (Figure 3.15). Vanadium in its higher oxidation state forms polynuclear vanadium species known as polyoxovanadate ions.^{6, 10-13} They are anionic vanadium-oxygen clusters. Different polynuclear species are formed depending upon the pH, concentration and ionic strength of solutions prepared using sodium orthovanadate. At high concentrations of vanadium, polynuclear species of vanadium are formed, and glutarimidedioxime can bind to different vanadium sites, forming a polynuclear complex of

vanadium with glutarimidedioxime. Due to the formation of this polynuclear complex, the stoichiometric ratio of vanadium and glutarimidedioxime may not be 1:1.

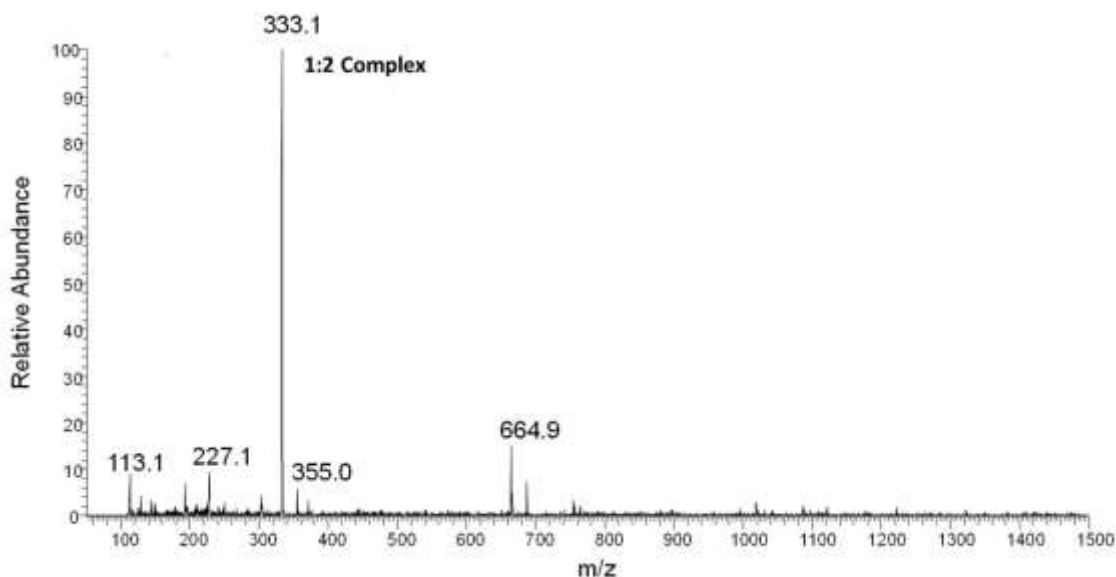


Figure 3.15 Positive-ion ESI mass spectrum of a solution containing 0.5 mM vanadium(V) and 1 mM glutarimidedioxime in 0.05 M NaCl aqueous solution at pH 8.3. The spectrum shows m/z 333.1 for the peak at the retention time of 2.65 minutes shown in Figure 3.14.

Liquid chromatography-mass spectrometry (LC-MS) results indicate time dependent formation of 1:2 complex between vanadium(V) and glutarimidedioxime. Previous ^{51}V NMR experiments using 0.5 mM vanadium(V) with varying glutarimidedioxime concentration do not show formation of 1:2 complex because the time required for the formation and detection of 1:2 complex between vanadium(V) and glutarimidedioxime remained unnoticed. Later, formation of 1:2 complex was detected for solution containing 0.5 mM vanadium(V) and 1.0 mM glutarimidedioxime using ^{51}V NMR spectroscopy. The 1:2 complex was observed after a minimum of 4 days at the chemical shift of +738.0 ppm (Figure. 3.16b), along with a 1:1 complex at the chemical shift of -418 ppm (Figure. 3.16a) for samples containing high concentration (0.5 mM) of vanadium(V).

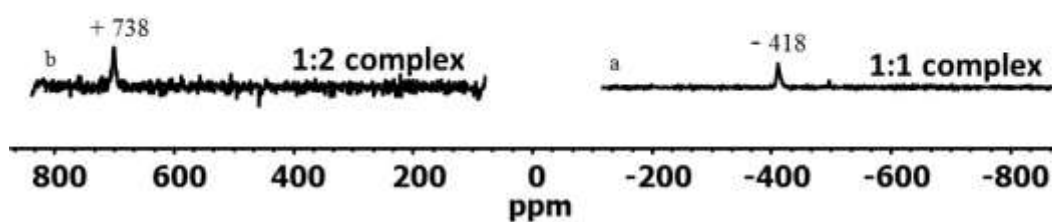


Figure 3.16 ^{51}V NMR spectra of 0.5 mM vanadium(V) followed by the addition of 1.0 mM glutarimidedioxime showing the formation of (a) 1:1, and (b) 1:2, vanadium(V)-glutarimidedioxime complex in 0.05 M NaCl aqueous solution at pH 8.3.

Results from the above study indicate that formation of 1:2 complex between vanadium(V) and glutarimidedioxime depends upon time and concentration of vanadium(V). The 1:1 complex forms right away. However, formation of 1:2 complex is time dependent and takes a minimum of 4 days to be detected by ^{51}V NMR spectroscopy (Figure. 3.16) and 2 days to be detected by liquid chromatography (Figure. 3.14). At a high concentration (0.5 mM) of vanadium(V), both 1:1, and 1:2 complex were observed in the ^{51}V NMR spectra (Figure 3.16a-b). It is of interest to see that the formation of 1:2 complex depends upon concentration of vanadium(V). At 0.5 mM vanadium(V), less intense ^{51}V NMR signal for dimeric vanadium species, $\text{H}_2\text{V}_2\text{O}_7^{-2}$ was observed, along with an intense ^{51}V NMR signal for dominant monomeric vanadium species, H_2VO_4^- (Figure. 3.51).⁵⁻⁷ Coordination chemistry for the formation of 1:2 complex between vanadium(V) and glutarimidedioxime appears difficult to

understand at the present time. Recent discussion about understanding interactions of seawater ions with amidoxime through X-Ray crystallography, by Professor Robin D. Rogers from the University of Alabama, suggests that polynuclear vanadium species $[V_{10}O_{28}]^{-6}$ clusters are sandwiched between bilayers of amidoxime ligands and interact with each other through non-covalent O-H \cdots O hydrogen bonds. The amidoxime ligands interact with each other through π - π stacking interactions and N-H \cdots O hydrogen bonds. A recent report¹⁴ suggests formation of an unusual 1:2 complex between vanadium(V) and glutarimidedioxime in aqueous solutions. This unusual complex formation involves non-oxido vanadium(V). The formation of this complex is concentration and time dependent, unlike formation of a more stable 1:1 complex, that forms immediately. In real seawater, 1:1 complex between vanadium(V) and glutarimidedioxime is more likely to form than 1:2 complex, due to low vanadium concentration of about 1.6 ppb in real sea water.

3.4.2 *Complexation of vanadium(V) with glutarimidedioxime in presence of UO_2^{+2} at the pH of 8.3.*

We used 1H NMR spectroscopy to investigate interactions of glutarimidedioxime with vanadium(V) and UO_2^{+2} mixtures. Figure 3.17 shows 1H NMR spectra obtained when vanadium(V) was added to UO_2^{+2} -glutarimidedioxime solution at pH of 8.3, to investigate competition of vanadium(V) with UO_2^{+2} for complexation with glutarimidedioxime. For this study, 0.2 mM UO_2^{+2} and 0.2 mM glutarimidedioxime was mixed in 0.05 M NaCl aqueous (D_2O) solution. The solution was stirred overnight, and the pH of the solution was adjusted to 8.3. The 1H NMR spectrum for ligand in the presence of UO_2^{+2} (Figure 3.17a) was same as the 1H NMR spectrum of free ligand without UO_2^{+2} (Figure 3.9a). This may occur due to the precipitation of uranyl hydroxides at the pH of 8.3 caused by the hydrolysis of UO_2^{+2} . After

obtaining the ^1H NMR spectrum for UO_2^{+2} -glutarimidedioxime system, 0.2 mM vanadium(V) was added to solution containing 0.2 mM UO_2^{+2} and 0.2 mM glutarimidedioxime, the solution was stirred overnight, and pH of the solution was adjusted to 8.3. ^1H NMR spectrum was obtained for 0.2 mM UO_2^{+2} :0.2 mM glutarimidedioxime:0.2 mM vanadium(V) (Figure 3.17b). Formation of 1:1 complex between vanadium(V) and glutarimidedioxime (Figure 3.17b) was observed, with the appearance of a more intense triplet at the chemical shift of 2.50 ppm and a quintet at 1.9 ppm. A less intense triplet at 2.45 ppm and a quintet at 1.8 ppm are due to trace amount of free glutarimidedioxime (Figure 3.17b).

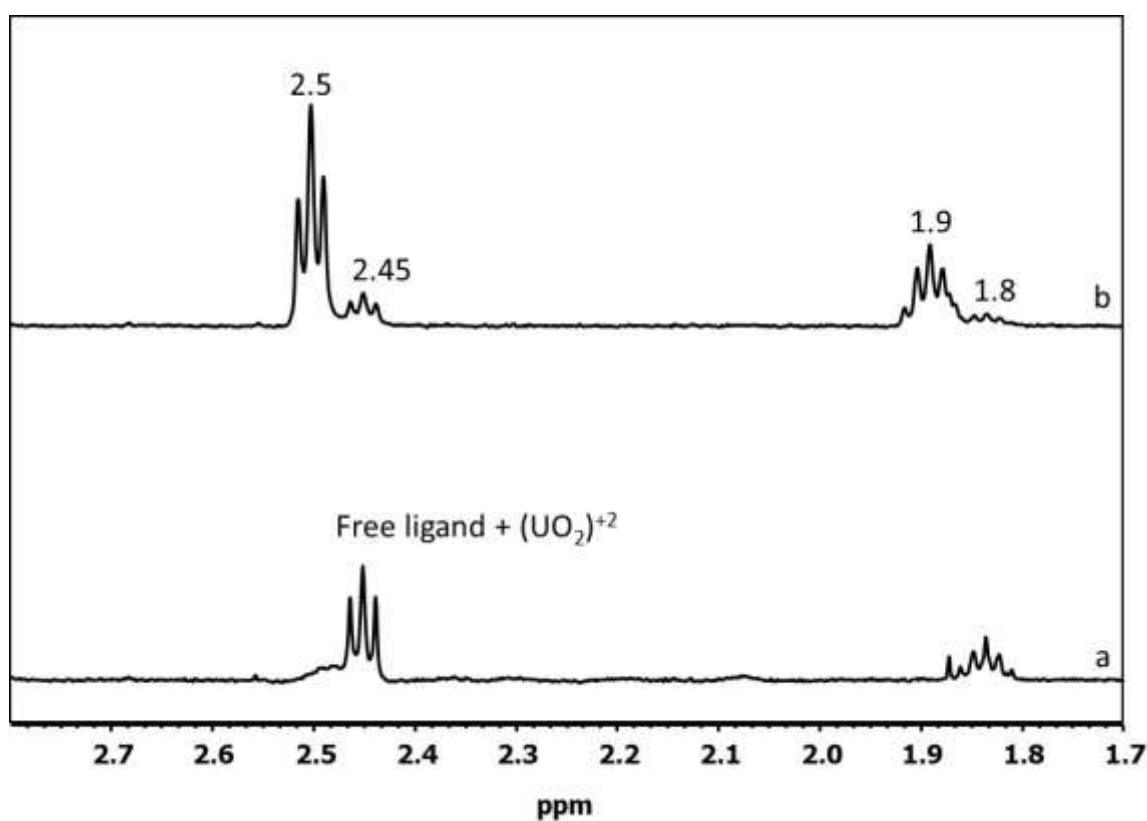


Figure 3.17 ^1H NMR spectra demonstrating vanadium(V)-glutarimidedioxime complex formation in the presence of UO_2^{+2} . Solutions labels (a) 0.2 mM UO_2^{+2} :0.2 mM glutarimidedioxime, (b) 0.2 mM UO_2^{+2} :0.2 mM glutarimidedioxime upon the addition of 0.2 mM vanadium(V). All samples in 0.05 M NaCl in D_2O at pH 8.3.

Vanadium(V) complexation with glutarimidedioxime in presence of UO_2^{+2} was further investigated using ^{51}V NMR spectroscopy. ^{51}V NMR spectra were acquired for solutions containing 0.2 mM UO_2^{+2} :0.2 mM glutarimidedioxime:0.2 mM vanadium(V) (Figure 3.18). The formation of 1:1 complex between vanadium(V) and glutarimidedioxime was observed by ^{51}V NMR peak at the chemical shift of ~ -417 ppm. 1:2 complex of vanadium(V) and glutarimidedioxime at +738.0 ppm was not observed for this system.

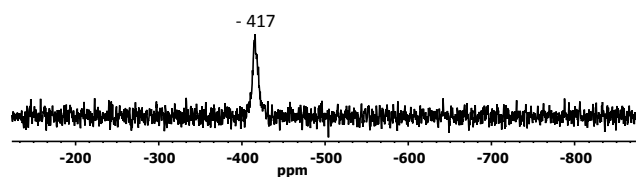


Figure 3.18 ^{51}V NMR spectrum demonstrating vanadium(V)-glutarimidedioxime complex formation in the presence of UO_2^{+2} upon the addition of 0.2 mM vanadium(V) to a solution containing 0.2 mM UO_2^{+2} :0.2 mM glutarimidedioxime, at pH 8.3.

We used ^{51}V NMR spectroscopy to confirm the formation of 1:1 complex of vanadium(V) with glutarimidedioxime in presence of UO_2^{+2} at the pH of 8.3. For this study 0.2 mM vanadium(V) was added to a solution containing 0.1 mM UO_2^{+2} and 0.1 mM glutarimidedioxime. The ^{51}V NMR spectrum for this solution is shown in Figure 3.19. The spectrum shows two signals for complexed, and free vanadium with peak area of $\sim 50\%$ for each signal. The stoichiometry of vanadium to glutarimidedioxime was 2:1. Half of the vanadium(V) was in complexed state, forming a 1:1 complex with glutarimidedioxime in the presence of UO_2^{+2} , and half of it was uncomplexed. However, in the ^{51}V NMR spectra

obtained in Figure 3.18, when the stoichiometry of vanadium(V) to glutarimidedioxime was 1:1, only one ^{51}V NMR signal for the completely complexed vanadium(V) was observed. This suggests that vanadium(V) forms 1:1 complex with glutarimidedioxime.

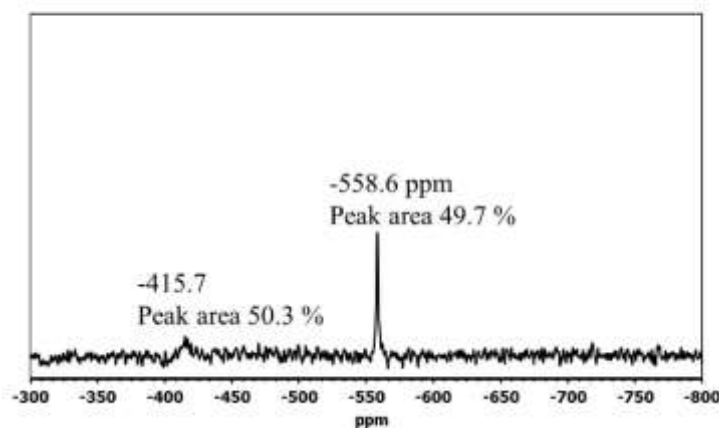


Figure 3.19 ^{51}V NMR spectrum demonstrating vanadium(V)-glutarimidedioxime complex formation in presence of UO_2^{+2} , upon addition of 0.2 mM vanadium(V) to a solution containing 0.1 mM UO_2^{+2} : 0.1 mM glutarimidedioxime, at pH 8.3.

Results from this study confirms that, at the pH of seawater (8.3), vanadium(V) complexation with glutarimidedioxime can be observed in presence of UO_2^{+2} . However, the complexation of UO_2^{+2} with glutarimidedioxime was not observed at this pH. Further investigation for understanding UO_2^{+2} complexation with glutarimidedioxime was performed, followed by a competition study between UO_2^{+2} and vanadium(V) to complex with glutarimidedioxime discussed in sections 3.4.3 and 3.4.4 below.

3.4.3 *Glutarimidedioxime complexation with UO_2^{+2}*

Uranyl complexation with amidoxime ligands have been extensively studied in solution phase. 1:1, and 1:2 metal/ligand complexes have been reported.^{2, 3, 8} Kouimtzis¹⁵ used potentiometry and observed 1:1, and 1:2 complex of benzanilidoxime with UO_2^{+2} . Hirotsu et al.¹⁶ investigated complexation of UO_2^{+2} with acetamidoxime, and observed the formation of

1:1 and 1:2 UO_2^{+2} -acetamidoxime complexes in aqueous solution. A previous report¹⁷ suggests use of ^1H NMR and ^{13}C NMR spectroscopy to determine UO_2^{+2} -benzamidoxime complexes. ^1H NMR spectra of solutions containing UO_2^{+2} and glutarimidedioxime were acquired at various pH keeping a molar ratio of UO_2^{+2} :glutarimidedioxime constant.

Complexation of UO_2^{+2} with glutarimidedioxime was monitored from pH of 2.3 to 8.3 (Figure 3.20a-f). Previous reports suggest that amidoxime ligands can be either protonated or deprotonated in aqueous solution based on pH.^{2,3} Our results show that both cyclic glutarimidedioxime and open-chain glutardiamidoxime used in the study are effective in binding with UO_2^{+2} at pH around 3.4.

When pH of the solution was increased above 3.4, UO_2^{+2} -glutarimidedioxime complex starts to disappear due to precipitation of uranyl hydroxides at pH's higher than 3.4. At pH of 2.3, UO_2^{+2} -glutarimidedioxime complex was not observed because the complex dissociates in strongly acidic conditions² due to competition of H^+ with UO_2^{+2} . The ^1H NMR spectrum for UO_2^{+2} -cyclic glutarimidedioxime solutions at the pH of 8.2 (Figure 3.21f) shows the ^1H NMR signals for free cyclic glutarimidedioxime only. At higher pH's, OH^- competes with cyclic glutarimidedioxime for UO_2^{+2} and leads to the formation of insoluble UO_2^{+2} species. A previous report¹⁸ suggests precipitation of uranyl hydroxides at $\text{pH} > 4.5$. Hence, the complexation of UO_2^{+2} with cyclic glutarimidedioxime is too weak to be effectively detected by ^1H NMR spectroscopy at the pH of 8.2 due to an increase in the hydrolysis UO_2^{+2} and formation of uranyl hydroxides. Precipitation of UO_2^{+2} -acetamidoxime¹⁶ complex was observed above pH 6. ^1H NMR spectra of UO_2^{+2} -glutarimidedioxime solutions at pH 3.4, (Figure 3.20c) shows, two sets of signals, a triplet for free glutarimidedioxime — $\text{CH}_2\text{—CH}_2\text{—CH}_2\text{—C}(\text{NOH})$ —, at 2.5 ppm, 4H; and a triplet for complexed glutarimidedioxime — $\text{CH}_2\text{—}$

$\text{CH}_2\text{-CH}_2\text{-C}(\text{NOH})\text{-}$, at 3.01 ppm, 4H. Another set of signal shows, a quintet for free glutarimidedioxime $\text{-CH}_2\text{-CH}_2\text{-CH}_2\text{-}$, at 1.8 ppm, 2H; and a quintet for complexed glutarimidedioxime $\text{-CH}_2\text{-CH}_2\text{-CH}_2\text{-}$, at 2.2 ppm, 2H; (Figure 3.20c). Integration of peaks for free triplet at 2.5 ppm and complexed triplet at 3.01 ppm (Figure 3.20c), shows ~ 0.14 mM or $\sim 67.5\%$ of the glutarimidedioxime is complexed with UO_2^{+2} and ~ 0.07 mM or 32.5% of the glutarimidedioxime is in uncomplexed state.

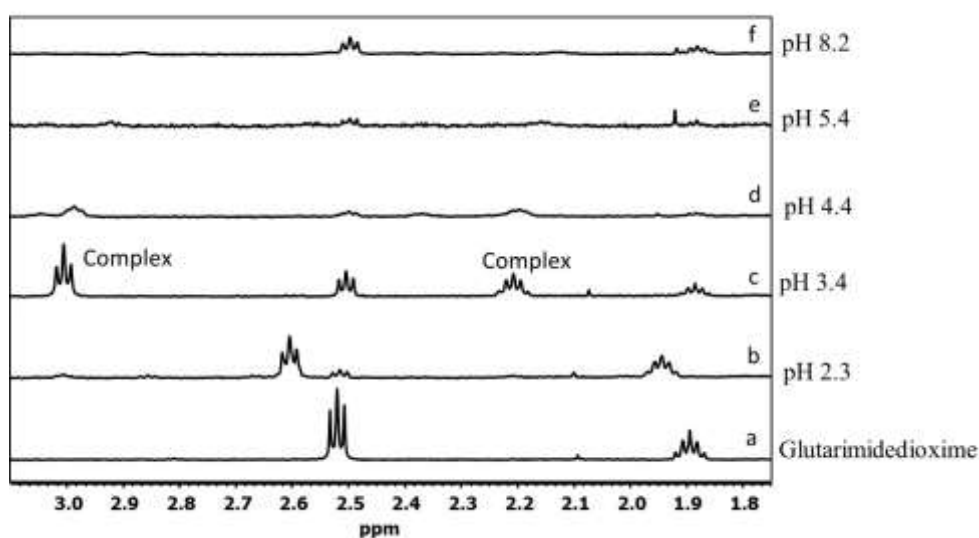


Figure 3.20 ^1H NMR spectra of solutions containing 0.2 mM glutarimidedioxime with (a) no UO_2^{+2} , at pH 3.4, (b) 0.2 mM UO_2^{+2} , at pH 2.3, (c) 0.2 mM UO_2^{+2} , at pH 3.4, (d) 0.2 mM UO_2^{+2} , at pH 4.4, (e) 0.2 mM UO_2^{+2} , at pH 5.4, and (f) 0.2 mM UO_2^{+2} , at pH 8.2. All samples in 0.05 M NaCl in D_2O .

Complete complexation of glutarimidedioxime was not observed because the reaction takes a long time to complete. The reaction is very slow because even in the presence of excess UO_2^{+2} complete complexation was not observed and ^1H NMR signal for uncomplexed glutarimidedioxime was observed. To understand time dependent complexation of glutarimidedioxime with UO_2^{+2} , 0.1 mM glutarimidedioxime was complexed with excess 0.2 mM UO_2^{+2} at pH of 3.4. ^1H NMR spectra were acquired after 24 hours (Figure 3.21a) and 7

days (Figure 3.21b) for same sample solution. After 24 hours, 36.9 % or 0.04 mM free glutarimidedioxime, showing a ^1H NMR signal at 2.5 ppm, and 63.1 % or 0.06 mM of complexed glutarimidedioxime, showing ^1H NMR signal at 2.96 ppm was observed in the ^1H NMR spectrum shown in Figure 3.21a. However, after 7 days ^1H NMR spectrum was acquired again, and 15.1 % or 0.02 mM of free glutarimidedioxime, showing a ^1H NMR signal at 2.5 ppm, and 84.9% or 0.08 mM of complexed glutarimidedioxime, showing a ^1H NMR signal at 2.96 ppm, was observed.

This decrease in percentage of free glutarimidedioxime, and increase in percentage of complexed glutarimidedioxime after 7 days confirms that complexation of glutarimidedioxime with UO_2^{+2} is time dependent and complete complexation will take a very long time. This study shows the reason behind observing free glutarimidedioxime peak for most of the analyzed samples with varying molar ratio of UO_2^{+2} :glutarimidedioxime using ^1H NMR spectroscopy.

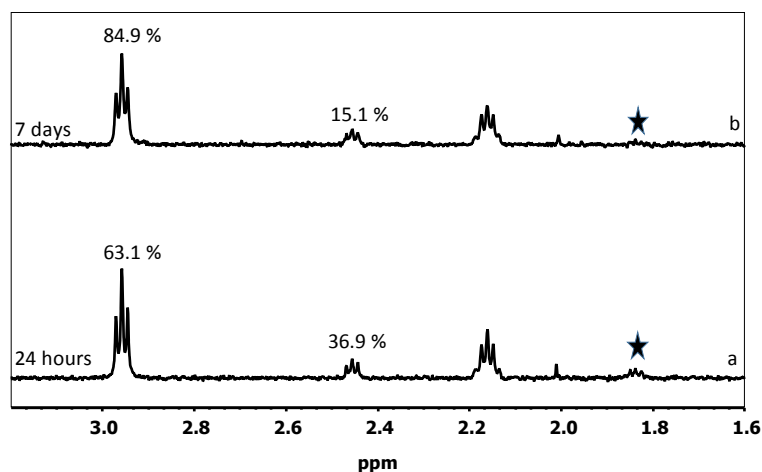


Figure 3.21 ^1H NMR spectra of solutions containing 0.2 mM UO_2^{+2} and 0.1 mM glutarimidedioxime after (a) 24 hours, and (b) 7 days. All samples in 0.05 M NaCl in D_2O at pH 3.4.

Further complexation of UO_2^{+2} with cyclic glutarimidedioxime was studied by keeping concentration of uranium constant and varying ligand concentration. At 0.2 mM UO_2^{+2} , and 0.05 mM cyclic glutarimidedioxime (Figure 3.22b), ~19.5% or 0.01 mM of cyclic glutarimidedioxime was free, giving a triplet for $\text{CH}_2\text{-CH}_2\text{-CH}_2\text{-}$, 4H; at 2.5 ppm, and 80.5% or 0.04 mM cyclic glutarimidedioxime was complexed, giving a triplet at ~3.0 ppm. Further, upon addition of 0.3 mM UO_2^{+2} to 0.05 mM glutarimidedioxime, only two signals, a triplet at ~3.0 ppm, and a quintet at 2.16 ppm (Figure 3.22c), for completely complexed glutarimidedioxime were observed. To identify ^1H NMR signals belonging to free and complexed glutarimidedioxime, the ^1H NMR spectrum obtained in Figure 3.22b and Figure 3.22c was compared with the ^1H NMR spectrum of free glutarimidedioxime without any UO_2^{+2} (Figure 3.22a). Free glutarimidedioxime gives only two signals in the ^1H NMR spectrum, a triplet at 2.5 ppm, and a quintet at 1.9 ppm (Figure 3.22a).

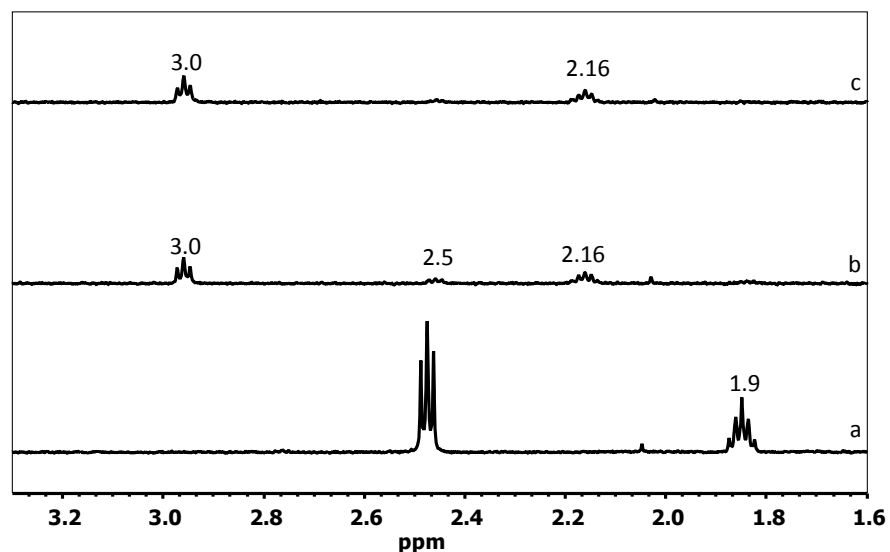


Figure 3.22 ¹H NMR spectra of (a) 0.2 mM cyclic glutarimidedioxime only, (b) 0.2 mM UO₂⁺²:0.05 mM cyclic glutarimidedioxime, and (c) 0.3 UO₂⁺²:0.05 mM cyclic glutarimidedioxime in 0.05 M NaCl in D₂O at pH 3.4.

The complexation of UO₂⁺² with glutarimidedioxime was confirmed by heteronuclear multiple bond coherence (HMBC) experiment. In HMBC spectrum (Figure 3.23). The ¹H NMR peaks for free glutarimidedioxime at ~1.9 ppm, and ~2.5 ppm, and the peaks for complexed glutarimidedioxime, at ~3.0 ppm and ~2.2 ppm were observed. The ¹H NMR peaks were correlated with ¹³C NMR peaks for free glutarimidedioxime at 19 ppm and 25 ppm, and for complexed glutarimidedioxime at 18 ppm and 22 ppm.

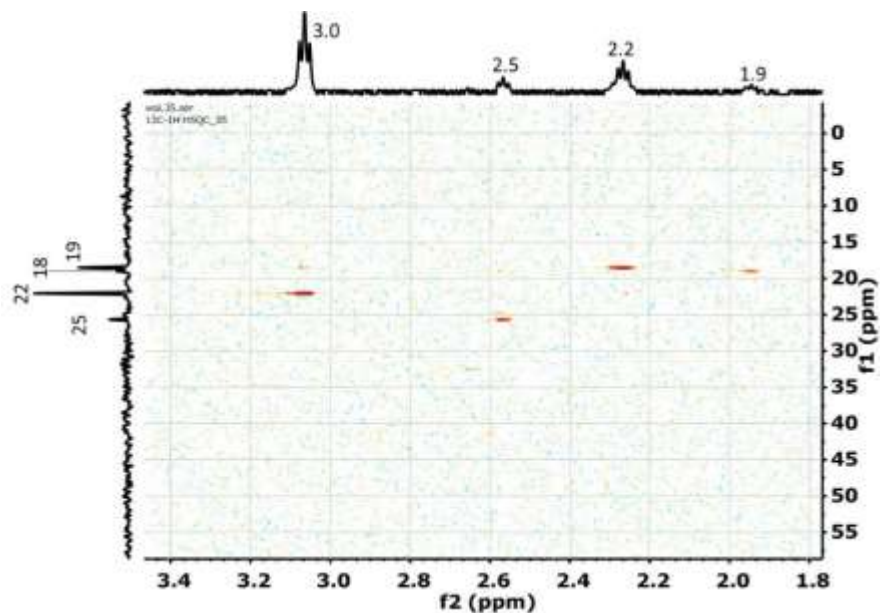


Figure 3.23 Heteronuclear Multiple Bond Coherence (HMBC) spectra for 0.2 mM UO_2^{+2} :0.2 mM glutarimidedioxime in 0.05 M NaCl in D_2O at pH 3.4.

3.4.4 Complexation of vanadium(V) with glutarimidedioxime in presence of UO_2^{+2}

From an earlier ^1H NMR study, it was observed that UO_2^{+2} forms complex with cyclic glutarimidedioxime at pH of 3.4. Competition of vanadium(V), and UO_2^{+2} to complex with glutarimidedioxime was studied further. Similar concentration (0.2 mM) of UO_2^{+2} , and vanadium(V) was used for understanding their competition for complexing with glutarimidedioxime. Glutarimidedioxime concentrations ranging from 0.05 mM to 0.8 mM were used. ^1H NMR spectrum for 0.2 mM glutarimidedioxime, shown in Figure 3.24a, shows two signals at 1.9 ppm, and 2.5 ppm. Upon addition of 0.05 mM glutarimidedioxime to 0.2 mM UO_2^{+2} , appearance of two new signals were observed, a triplet at ~ 3.0 ppm, and a quintet 2.2 ppm (Figure 3.24b). For this solution, $\sim 19.5\%$ of glutarimidedioxime was free, and $\sim 80.5\%$ was complexed with UO_2^{+2} . Further, to investigate the competition of vanadium(V) with UO_2^{+2} for complexation with glutarimidedioxime, 0.2 mM vanadium(V) was added to UO_2^{+2} -glutarimidedioxime complex. Significant changes in ^1H NMR spectra were observed

upon the addition of vanadium(V). New ^1H NMR signals at different chemical shift, a triplet, at 2.7 ppm, and a quintet at 2.0 ppm for glutarimidedioxime complexed with vanadium was observed (Figure 3.24c). Complete complexation of glutarimidedioxime with vanadium(V) was observed, because ^1H NMR signals corresponding to free glutarimidedioxime were not detected. When concentration of glutarimidedioxime was increased further from 0.1 mM to 0.8 mM, relative intensity of the peak assigned to free glutarimidedioxime increased due to excess glutarimidedioxime. As described earlier in Figure 3.21b, at 0.1 mM ligand about 84.9 % of glutarimidedioxime was complexed with UO_2^{+2} and about 15.1% was free. Our result suggests the formation of 1:1 complex between UO_2^{+2} and glutarimidedioxime. The complexation of 0.05 mM UO_2^{+2} with 0.1 mM glutarimidedioxime was observed through UV-Visible spectroscopy and is described in a later part of the discussion. The acquired UV-Visible spectrum for the complex is shown in Figure 3.28. The formation of 1:2 complex between UO_2^{+2} and glutarimidedioxime is described in the literature using UV-Visible spectroscopy.² At 0.2 mM UO_2^{+2} and 0.2 mM glutarimidedioxime, a triplet at ~ 3.0 ppm and a quintet at ~ 2.2 ppm was observed for glutarimidedioxime complexed with UO_2^{+2} , and another triplet at 2.5 ppm and a quintet at 1.9 ppm was observed for free glutarimidedioxime (Figure 3.24f). At 0.2 mM glutarimidedioxime ~ 64.3 % or ~ 0.13 mM glutarimidedioxime was complexed with UO_2^{+2} , and ~ 35.7 % or 0.07 mM was free. Upon addition of 0.2 mM vanadium(V) to this sample, signals for glutarimidedioxime complexed with vanadium were observed at 2.7 ppm and 2.0 ppm. (Figure 3.24g). At 0.3 mM glutarimidedioxime, 58.8 % or about 0.18 mM of the glutarimidedioxime was complexed with UO_2^{+2} , and 41.2% or about 0.12 mM glutarimidedioxime was free. The complexed and free triplet were observed at 3.0 ppm and 2.5 ppm, respectively (Figure 3.24h). Upon addition of 0.2 mM vanadium(V), new

peaks, a triplet at 2.7 ppm and a quintet at 2.0 ppm for glutarimidedioxime complexed with vanadium(V) were observed (Figure 3.24i). At 0.3 mM glutarimidedioxime, 72.0 % or about 0.21 mM of glutarimidedioxime was complexed with 0.2 mM vanadium and 28.0% or about 0.08 mM of glutarimidedioxime was free. This observation suggests that vanadium(V) forms 1:1 complex with glutarimidedioxime.

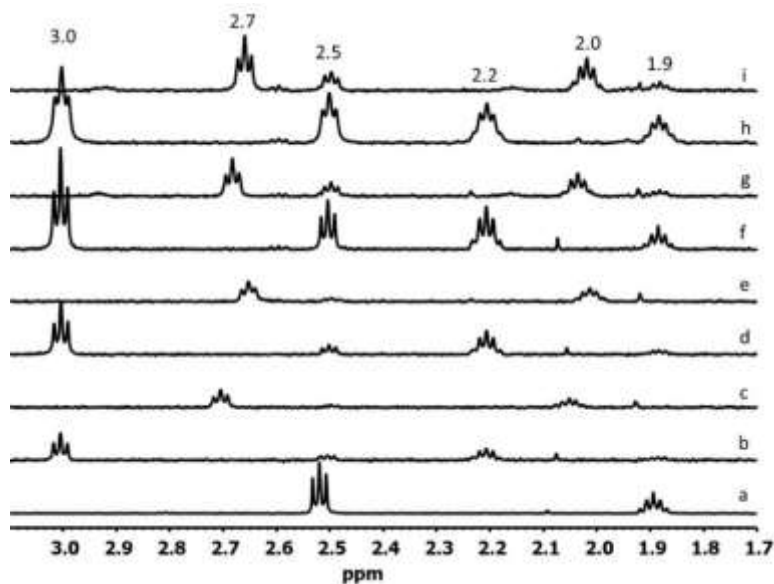


Figure 3.24 ^1H NMR spectra of (a) 0.2 mM cyclic glutarimidedioxime only, at pH \sim 3.4, (b) 0.2 mM UO_2^{+2} :0.05 mM cyclic glutarimidedioxime, at pH \sim 3.4, (c) 0.2 mM UO_2^{+2} :0.05 mM cyclic glutarimidedioxime:0.2 mM vanadium(V), at pH \sim 6.5, (d) 0.2 mM UO_2^{+2} :0.1 mM cyclic glutarimidedioxime, at pH \sim 3.4, (e) 0.2 mM UO_2^{+2} :0.1 mM cyclic glutarimidedioxime:0.2 mM vanadium(V), at pH \sim 7.1, (f) 0.2 mM UO_2^{+2} :0.2 mM cyclic glutarimidedioxime, at pH \sim 3.4, (g) 0.2 mM UO_2^{+2} :0.2 mM cyclic glutarimidedioxime:0.2 mM vanadium(V), at pH \sim 6.8, (h) 0.2 mM UO_2^{+2} :0.3 mM cyclic glutarimidedioxime, at pH \sim 3.4, (i) 0.2 mM UO_2^{+2} :0.3 mM cyclic glutarimidedioxime:0.2 mM vanadium(V), at pH \sim 7.1.

The formation of UO_2^{+2} -glutarimidedioxime complex and vanadium(V)-glutarimidedioxime complex was also observed upon addition of 0.4 mM, 0.5 mM, 0.6 mM, and 0.8 mM of glutarimidedioxime (Figure 3.25a-i).

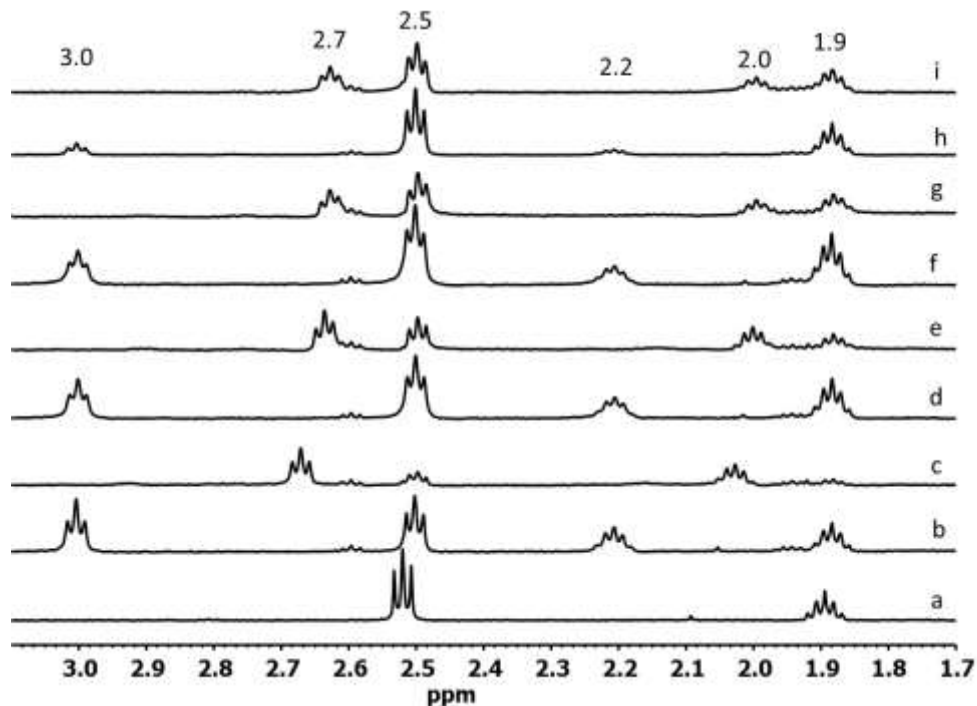


Figure 3.25 ¹H NMR spectra of (a) 0.2 mM cyclic glutarimidedioxime only, at pH ~3.4, (b) 0.2 mM UO₂⁺²:0.4 mM cyclic glutarimidedioxime, at pH ~3.4, (c) 0.2 mM UO₂⁺²:0.4 mM cyclic glutarimidedioxime:0.2 mM vanadium(V), at pH ~6.8, (d) 0.2 mM UO₂⁺²:0.5 mM cyclic glutarimidedioxime, at pH ~3.4, (e) 0.2 mM UO₂⁺²:0.5 mM cyclic glutarimidedioxime:0.2 mM vanadium(V), at pH ~7.3, (f) 0.2 mM UO₂⁺²:0.6 mM cyclic glutarimidedioxime, at pH ~3.4, (g) 0.2 mM UO₂⁺²:0.6 mM cyclic glutarimidedioxime:0.2 mM vanadium(V), at pH ~7.24, (h) 0.2 mM UO₂⁺²:0.8 mM cyclic glutarimidedioxime, at pH ~3.4, and (i) 0.2 mM UO₂⁺²:0.8 mM cyclic glutarimidedioxime:0.2 mM vanadium(V), at pH ~7.4.

The formation of 1:1 complex between vanadium(V) and glutarimidedioxime was also confirmed by ⁵¹V NMR spectroscopy. ⁵¹V NMR spectra were acquired after addition of vanadium(V), to solutions containing UO₂⁺²-glutarimidedioxime complex. The acquired ⁵¹V NMR spectra are shown in Figure 3.26a-d and Figure 3.27a-d.

The ⁵¹V NMR spectra shows vanadium(V) chemical shifts, ranging from -459 ppm to -481 ppm for vanadium(V)-glutarimidedioxime complex, in presence of UO₂⁺² (Figure 3.26a-d and Figure 3.27a-d). Upon addition of vanadium(V) to a solution containing UO₂⁺²-glutarimidedioxime complex, glutarimidedioxime is displaced from UO₂⁺²-

glutarimidedioxime complex, as vanadium(V) complex with glutarimidedioxime forms preferentially. This ^{51}V NMR signal is the average of signals arising from the exchange of vanadium between free vanadium(V), vanadium(V) complexed with glutarimidedioxime, and vanadium(V) displacing glutarimidedioxime from UO_2^{+2} -glutarimidedioxime complex.

The ^{51}V NMR peak for free vanadium(V) was observed at -549 ppm (Figure 3.2a), and the ^{51}V NMR peak for vanadium(V) complexed with glutarimidedioxime was observed at chemical shift ranging from -417.3 ppm to -418.8 ppm (Figure 3.4a-d). However, the ^{51}V NMR peak for vanadium(V) displacing glutarimidedioxime from UO_2^{+2} -glutarimidedioxime complex, and itself forming vanadium(V)-glutarimidedioxime complex, was observed at the chemical shift ranging from -459 ppm to -481 ppm (Figure 3.26a-d and Figure 3.27a-d). As the concentration of glutarimidedioxime increases, we observe a systematic downfield shift for the ^{51}V NMR peak (Figure 3.26a-d and Figure 3.27a-d), because vanadium-glutarimidedioxime interaction grow in significance at high concentration of glutarimidedioxime. The ^{51}V NMR peak at +738 ppm, for 1:2 complex of vanadium(V) with glutarimidedioxime was not observed in the presence of UO_2^{+2} at this low concentration (0.2 mM) of vanadium(V).

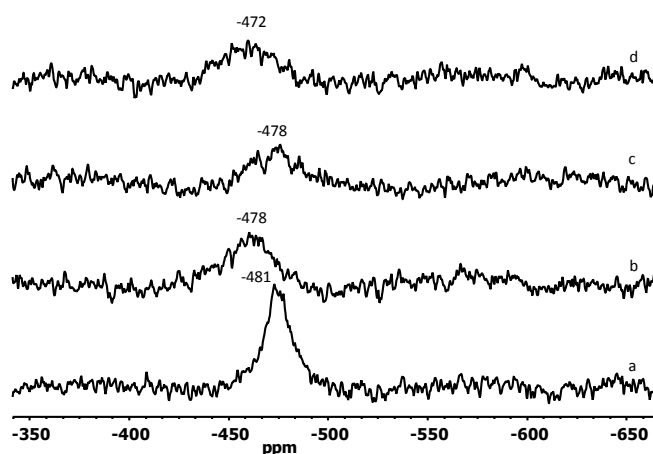


Figure 3.26 ^{51}V NMR spectra of (a) 0.2 mM UO_2^{+2} :0.05 mM cyclic glutarimidedioxime:0.2 mM vanadium(V), at pH \sim 6.5, (b) 0.2 mM UO_2^{+2} :0.1 mM cyclic glutarimidedioxime:0.2 mM vanadium(V), at pH \sim 7.1, (c) 0.2 mM UO_2^{+2} :0.2 mM cyclic glutarimidedioxime:0.2 mM vanadium(V), at pH \sim 6.8, and (d) 0.2 mM UO_2^{+2} :0.3 mM cyclic glutarimidedioxime:0.2 mM vanadium(V), at pH \sim 7.1.

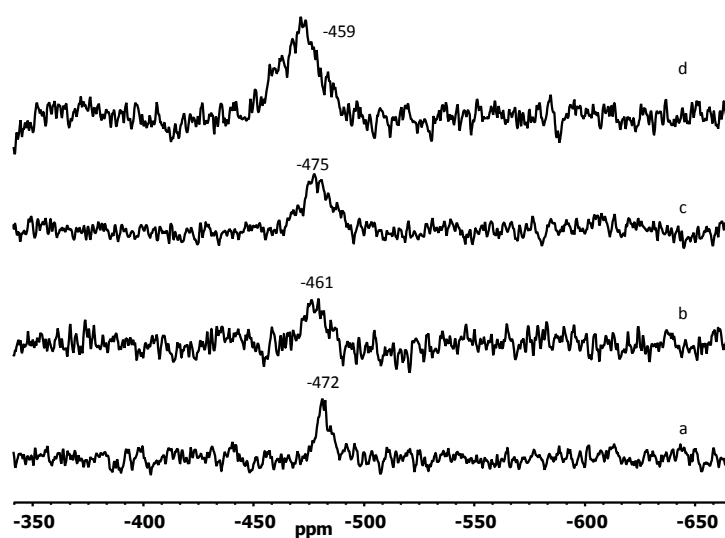


Figure 3.27 ^{51}V NMR spectra of (a) 0.2 mM UO_2^{+2} :0.4 mM cyclic glutarimidedioxime:0.2 mM vanadium(V), at pH \sim 6.8, (b) 0.2 mM UO_2^{+2} :0.5 mM cyclic glutarimidedioxime:0.2 mM vanadium(V), at pH \sim 7.3, (c) 0.2 mM UO_2^{+2} :0.6 mM cyclic glutarimidedioxime:0.2 mM vanadium(V), at pH \sim 7.24, and (d) 0.2 mM UO_2^{+2} :0.8 mM cyclic glutarimidedioxime:0.2 mM vanadium(V), at pH \sim 7.4.

Uranyl-glutarimidedioxime complex can be clearly observed in the UV-Visible spectrum with the absorption band at the wavelength of 280 nm, using 0.05 mM UO_2^{+2} and 0.1 mM glutarimidedioxime at the pH of 8.3 as shown in Figure 3.28 below. The experiments for the detection of UO_2^{+2} -glutarimidedioxime complex at a pH of 8.3 were successful at this low concentration of UO_2^{+2} and glutarimidedioxime² because the UO_2^{+2} speciation in solution changes with concentration,¹⁹ and upon decreasing the UO_2^{+2} concentration the precipitation of uranyl hydroxides is too weak to effectively compete with the complexation of UO_2^{+2} with glutarimidedioxime.

UV-Visible spectroscopy was used to observe effect of vanadium(V) addition upon the complexation of UO_2^{+2} with glutarimidedioxime. Figure 3.28 shows that upon the addition of 0.05 mM vanadium(V) to UO_2^{+2} -glutarimidedioxime complex, slight disappearance of the 280 nm band for UO_2^{+2} -glutarimidedioxime complex was observed, and further addition of 0.1 mM vanadium(V) to UO_2^{+2} -glutarimidedioxime complex, complete disappearance of the band at 280 nm was observed. This indicates that vanadium(V) displaces glutarimidedioxime from UO_2^{+2} -glutarimidedioxime complex and forms a 1:1 vanadium(V)-glutarimidedioxime complex in presence of UO_2^{+2} .

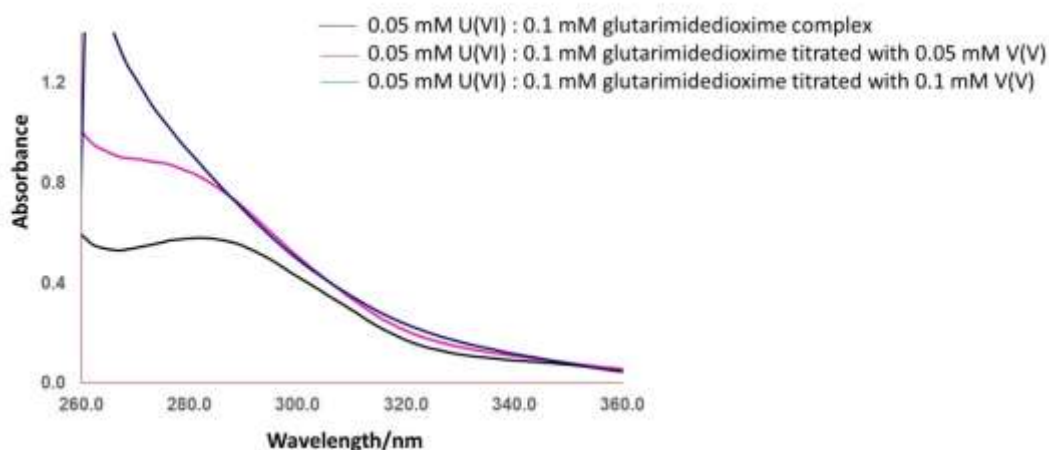


Figure 3.28 UV-Visible absorption spectra showing complexation of UO_2^{+2} with glutarimidedioxime, and effect of vanadium(V) upon complexation of UO_2^{+2} with glutarimidedioxime at pH 8.3.

Uranium and vanadium competition was also studied by adding UO_2^{+2} to a solution containing vanadium(V)-glutarimidedioxime complex. Figure 3.29a, shows that when 0.05 mM UO_2^{+2} was added to the solution containing 0.05 mM vanadium(V):0.1 mM glutarimidedioxime, an absorption band at 280 nm was observed due to the formation of UO_2^{+2} complex with glutarimidedioxime. A gradual stepwise increase in the intensity of the absorption band at 280 nm for UO_2^{+2} -glutarimidedioxime complex was observed from 1/2 hour to 7 hours (Figure 3.29a). UO_2^{+2} at a concentration of 0.05 mM can complex with glutarimidedioxime in the presence of vanadium(V), because after the formation of 1:1, vanadium(V)-glutarimidedioxime complex, there is an excess of 0.05 mM glutarimidedioxime in the system. However, Figure 3.29b shows that when 0.05 mM UO_2^{+2} was added to a solution containing 0.05 mM vanadium(V), and 0.05 mM glutarimidedioxime, no formation of UO_2^{+2} -glutarimidedioxime complex was observed because all glutarimidedioxime is now complexed with vanadium(V), forming a 1:1, vanadium(V)-glutarimidedioxime complex, and no free glutarimidedioxime is present to form complex with

UO_2^{+2} . No change in the UV-Visible absorption spectra (Figure 3.29b) was observed from the start of the reaction till 12 hours. It was observed that UO_2^{+2} -glutarimidedioxime complexes are less likely to form when vanadium(V) is present in solution at a pH of 8.3, as vanadium(V) complex with glutardiamidoxime forms preferentially.

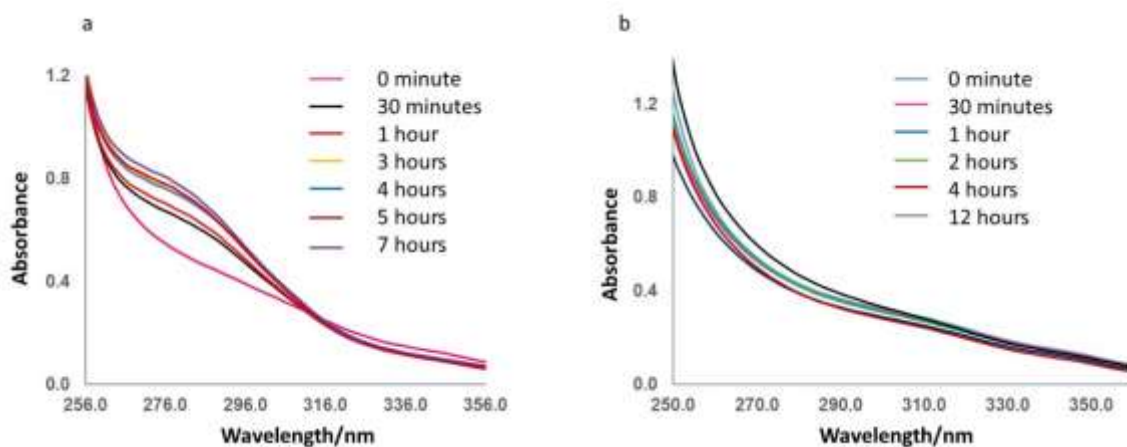


Figure 3.29 UV-Visible absorption spectra acquired at pH 8.3 from solutions containing (a) 0.05 mM vanadium(V):0.1 mM glutardiamidoxime to which 0.05 mM UO_2^{+2} was added, (b) 0.05 mM vanadium(V):0.05 mM glutardiamidoxime to which 0.05 mM UO_2^{+2} was added.

3.4.5 Open-chain glutardiamidoxime complexation with UO_2^{+2}

The solution state complexation of UO_2^{+2} with open-chain glutardiamidoxime was studied using ^1H NMR, and ^{13}C NMR spectroscopy. Open-chain glutardiamidoxime is an acyclic isomer of cyclic glutardiamidoxime as illustrated in Figure 3.1. Other research groups have reported complexation of UO_2^{+2} by open-chain glutardiamidoxime^{2,3,8} using thermodynamic and electrospray ionization mass spectrometric techniques. The complexation of open-chain glutardiamidoxime with UO_2^{+2} at different pH's was observed. ^1H NMR spectrum was acquired for solutions containing free open-chain glutardiamidoxime without any UO_2^{+2} , and 0.2 mM UO_2^{+2} with 0.2 mM open-chain glutardiamidoxime at different pH's ranging from 2.3 to 8.2 (Figure 3.30 a-g). ^1H NMR spectrum of free glutardiamidoxime

without any UO_2^{+2} was taken at each pH and was compared with complexed glutardiamidioxime.

The ^1H NMR spectrum for UO_2^{+2} -(open-chain glutardiamidioxime) solutions (Figure 3.30b) resembles with the ^1H NMR spectrum acquired for free open-chain glutardiamidioxime (Figure 3.30 a) at the pH of 8.2. This is caused by the precipitation of uranyl hydroxides at $\text{pH} > 4.5$ as reported by Endrizzi et al.¹⁸ At higher pH's, OH^- competes with glutardiamidioxime for UO_2^{+2} and leads to the formation of insoluble UO_2^{+2} species. Hence, the complexation of UO_2^{+2} with open-chain glutardiamidioxime is too weak to be effectively detected by ^1H NMR spectroscopy.

The complexation between UO_2^{+2} and open-chain glutardiamidioxime was not detected by ^1H NMR spectroscopy at the pH of 2.3 (Figure 3.30g) because at lower pH's, the UO_2^{+2} -glutardiamidioxime complex dissociates in strongly acidic conditions due to the competition of H^+ with UO_2^{+2} . However, UO_2^{+2} -(open-chain glutardiamidioxime) complexation was observed at the pH's of 4.4 and 3.4. Slight differences in the chemical shift values were observed for complexed glutardiamidioxime at the pH's of 4.4 and 3.4 (Figure 3.30d and f). This is because the chemical shift of the non-exchangeable protons is pH dependent. Chemical shift perturbation occurs at different pH's due to presence of different protonation states at different pH values. At the pH of 4.4, ^1H NMR spectrum of free open-chain glutardiamidioxime differs from ^1H NMR spectrum of complexed glutardiamidioxime. Free glutardiamidioxime shows a triplet for 4H; $-\text{CH}_2-\text{CH}_2-\text{CH}_2-$, at ~ 2.5 ppm and a quintet for $\text{CH}_2-\text{CH}_2-\text{CH}_2-$, 2H; at ~ 2.0 ppm (Figure 3.30c). However, complexed glutardiamidioxime shows three signals in the ^1H NMR spectra (Figure 3.30d).

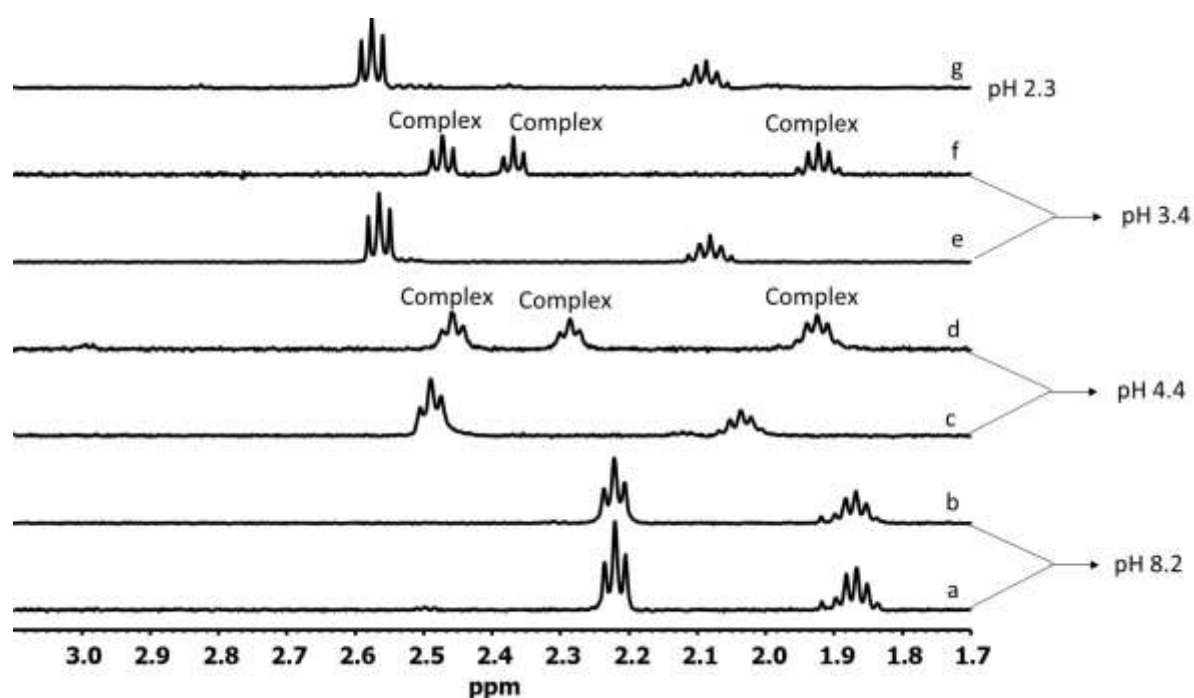


Figure 3.30 ^1H NMR spectra of solutions containing (a) 0.2 mM open-chain glutardiamidoxime, at pH 8.2, (b) 0.2 UO_2^{+2} :0.2 mM open-chain glutardiamidoxime, at pH 8.2, (c) 0.2 mM open-chain glutardiamidoxime, at pH 4.4, (d) 0.2 mM UO_2^{+2} :0.2 mM open-chain glutardiamidoxime, at pH 4.4, (e) 0.2 mM open-chain glutardiamidoxime, at pH 3.4, (f) 0.2 mM UO_2^{+2} :0.2 mM open-chain glutardiamidoxime, at pH 3.4, and (g) 0.2 mM UO_2^{+2} :0.2 mM open-chain glutardiamidoxime, at pH 2.3. All samples in 0.05 M NaCl in D_2O .

At the pH of 3.4, free glutardiamidoxime shows two clear ^1H NMR signals, a triplet at ~ 2.5 ppm and a quintet at ~ 2.0 ppm (Figure 3.30e). However, complexed glutardiamidoxime shows three clear ^1H NMR signals. The complexation of UO_2^{+2} -glutardiamidoxime occurs from one side of the oxime group, and the three CH_2 's ($-\text{CH}_2-\text{CH}_2-\text{CH}_2-$) become nonequivalent and give three different ^1H NMR signals (Figure 3.30f). The integration ratio for the three different CH_2 's in the NMR spectrum in Figure 3.30f also

shows 1:1:1 ratio for the three CH₂'s, confirming that these signals are from the complexed CH₂'s of glutardiamidioxime.

The ¹H NMR spectrum that was acquired immediately after the addition of 0.2 mM UO₂⁺² to 0.2 mM open-chain glutardiamidioxime, shows only two signals, a triplet and a quintet (Figure 3.31a), and resembles with the ¹H NMR spectrum for free glutardiamidioxime. ¹H NMR spectrum was acquired again, after 24 hours of sample preparation. Intermediate stage with incomplete reaction was observed after 24 hours. In the intermediate stage, two sets of signals for complexed and free CH₂'s of glutardiamidioxime were observed. A signal at 2.53 ppm is a mixture of signals from free and complexed ligand. Another signal at 2.39 ppm is for the complexed ligand in the intermediate state (Figure 3.31b). Another set of signals, a quintet for free, and complexed ligand at 2.06 ppm and 1.96 ppm, respectively, was observed in the intermediate stage. This observation suggests that complex between UO₂⁺², and open-chain glutardiamidioxime (Figure 3.31b) starts to form in 24 hours. After a minimum of 4-7 days, glutardiamidioxime was completely complexed with UO₂⁺², and three signals for three non-equivalent completely complexed CH₂'s of open-chain glutardiamidioxime were clearly observed (Figure 3.31c). ¹H NMR signals show a downfield triplet at 2.47 ppm, for CH₂ closer to the site of complexation, and an upfield triplet at 2.36 ppm, at the site of no complexation. The signal for complexed quintet, CH₂-**CH**₂-CH₂-, 2H, is observed at 1.92 ppm. The ¹H NMR spectrum was acquired again after 10 days for the same sample, and it was observed that the spectrum remains unchanged after 10 days. This observation suggests a complete and stable complexation of UO₂⁺² with glutardiamidioxime at the pH of 3.4.

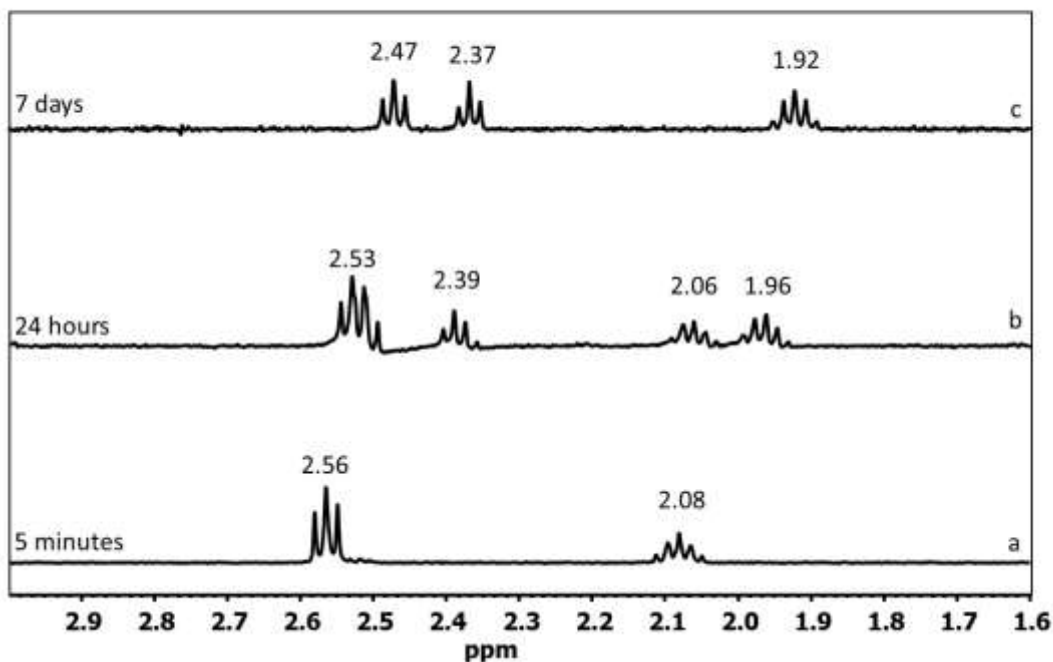


Figure 3.31 ^1H NMR spectra of solutions containing 0.2 mM UO_2^{+2} and 0.2 mM open-chain glutardiamidioxime in 0.05 M NaCl in D_2O at pH 3.4 (a) 5 minutes, (b) 24 hours, and (c) 7 days.

Figure 3.32a-c shows the ^1H NMR spectra acquired by lowering the concentration of glutardiamidioxime to 0.05 mM and 0.1 mM and keeping the concentration of UO_2^{+2} constant to 0.2 mM and adjusting the pH of the sample to 3.4 (Figure 3.32a-c). This study was performed to investigate complexation of UO_2^{+2} with glutardiamidioxime at lower concentrations of glutardiamidioxime. As a general observation, the ^1H NMR spectra shown in Figure 3.32 resembles with previously shown ^1H NMR spectra in Figure 3.31. This observation suggests that complexation between UO_2^{+2} and glutardiamidioxime can be observed at lower concentrations of glutardiamidioxime. Glutardiamidioxime in the complexed state shows appearance of three ^1H NMR peaks for the three CH_2 's of glutardiamidioxime in the complexed state which becomes nonequivalent upon complexation with UO_2^{+2} . The complexation takes a minimum of 4 to 7 days to form. Based upon the

formation constants of resulting species, and previous reports on abundance of UO_2^{+2} -glutardiamidoxime vs. UO_2^{+2} -glutarimidedioxime complexes in the ESI spectra,^{2, 3, 8} it has been shown that open-chain glutardiamidoxime compared to cyclic glutarimidedioxime forms complexes with UO_2^{+2} less effectively.^{3, 8} This may be the reason for time dependent formation of a solution state complex between UO_2^{+2} and glutardiamidoxime because it takes a minimum of 4 to 7 days to detect UO_2^{+2} -glutardiamidoxime complex. However; UO_2^{+2} -glutarimidedioxime complex was observed within 24 hours.

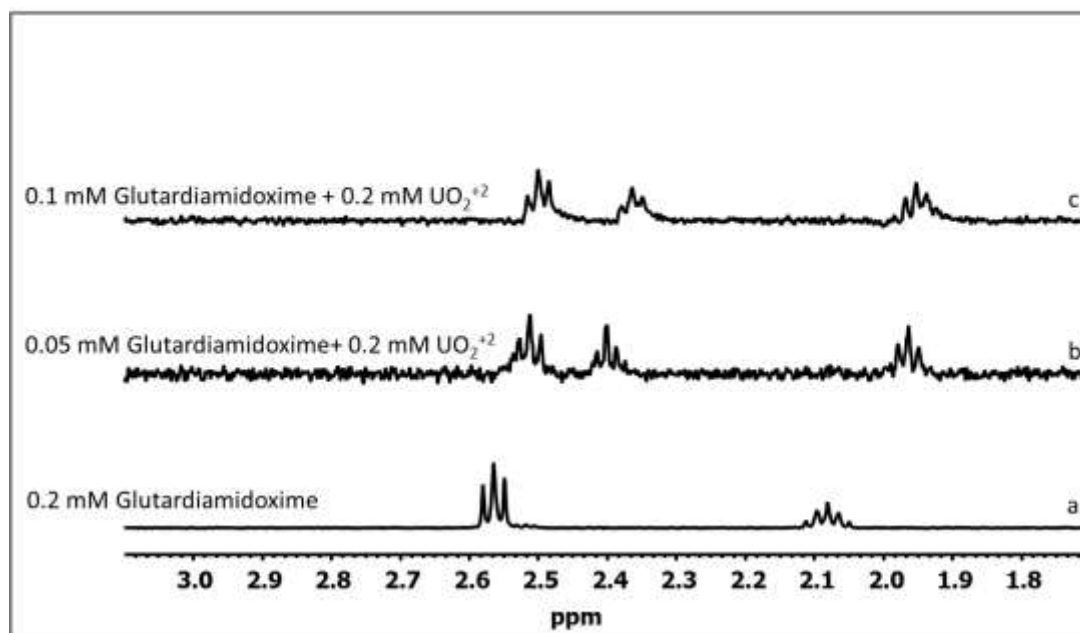


Figure 3.32 ^1H NMR spectra of solutions containing (a) 0.2 mM open-chain glutardiamidoxime, (b) 0.05 mM open-chain glutardiamidoxime:0.2 mM UO_2^{+2} , and (c) 0.1 mM open-chain glutardiamidoxime:0.2 mM UO_2^{+2} . All samples in 0.05 M NaCl in D_2O at pH 3.4.

The complexation of UO_2^{+2} with open-chain glutardiamidoxime was studied through ^{13}C NMR spectroscopy. Free open-chain glutardiamidoxime shows two peaks in the ^{13}C NMR spectra for its two different CH_2 's. A ^{13}C NMR signal at 23.9 ppm for carbon belonging to,

$-\text{CH}_2-\text{CH}_2-\text{CH}_2-$, and another signal at 28.3 ppm for carbon belonging to, $-\text{CH}_2-\text{CH}_2-\text{CH}_2-$ (Figure 3.33a). The signal for quaternary carbon belonging to $\text{C}(\text{NH}_2)=\text{NOH}$ was observed at 163 ppm with poor intensity, and it is not shown in the spectrum (Figure 3.33a) for clarity. The quaternary carbon has a longer T1 relaxation time than the primary, secondary, and tertiary carbon's; it relaxes slowly and displays a ^{13}C NMR signal with reduced intensity. Upon addition of UO_2^{+2} to open-chain glutardiamidoxime, the complexation was observed. Three different ^{13}C NMR signals were observed for three non-equivalent carbons, $-\text{CH}_2-\text{CH}_2-\text{CH}_2-$, of open-chain glutardiamidoxime because the three CH_2 's become non-equivalent upon complexation with UO_2^{+2} (Figure 3.33b). The signal for complexed quaternary carbon belonging to $\text{C}(\text{NH}_2)=\text{NOH}$ was not observed in Figure 3.33b. Quaternary carbon [$\text{C}(\text{NH}_2)=\text{NOH}$] is closest to the site of complexation, and its signal broadens up and gets buried in noise, upon complexation with UO_2^{+2} .

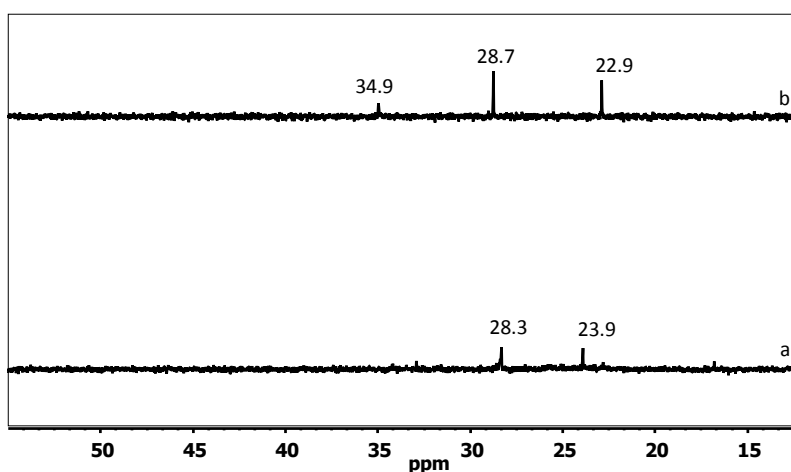


Figure 3.33 ^{13}C NMR spectra of solution containing (a) 1 mM open-chain glutardiamidoxime, (b) 1 mM UO_2^{+2} :1 mM open-chain glutardiamidoxime in 0.05 M NaCl in D_2O at pH 3.4.

3.4.6 Competition of glutardiamidoxime and carbonate for complexation with UO_2^{+2}

Uranium in sea water exist mainly in the form of uranyl tris-carbonato complex²⁰ $UO_2(CO_3)_3^{4-}$ and amidoxime functional groups can displace the carbonate $UO_2(CO_3)_3^{4-}$ because they can strongly bind to UO_2^{+2} and are stable at the pH of seawater. The competition of open-chain glutardiamidoxime with carbonate to complex with UO_2^{+2} was studied. For this study, ^{13}C enriched sodium carbonate (Na_2CO_3) was used with 23% enrichment. Different species of carbonate were studied at the pH of 11 and pH of 8. At the pH of 11, carbonate mainly exists in the form of CO_3^{-2} and shows a ^{13}C signal at 167.5 ppm (Figure 3.34b). At the pH of 8, carbonate exists in the form of bicarbonate HCO_3^{-1} , giving rise to a ^{13}C signal at 160.4 ppm (Figure 3.34c). The peaks at 206.6 ppm and 29.9 ppm are ^{13}C signals from acetone-d6 used for magnetic field lock. A coaxial NMR tube insert containing acetone-d6 was inserted into each sample tube before ^{13}C NMR analyses. Open-chain glutardiamidoxime was characterized by ^{13}C NMR using acetone-d6 insert, and the ^{13}C signals at 24.0 ppm for $[-CH_2-CH_2-C(NOH)NH_2]$, 29.0 ppm for $[-CH_2-CH_2-C(NOH)NH_2]$ and 157 ppm for $[-CH_2-CH_2-C(NOH)NH_2]$ were observed (Figure 3.34a).

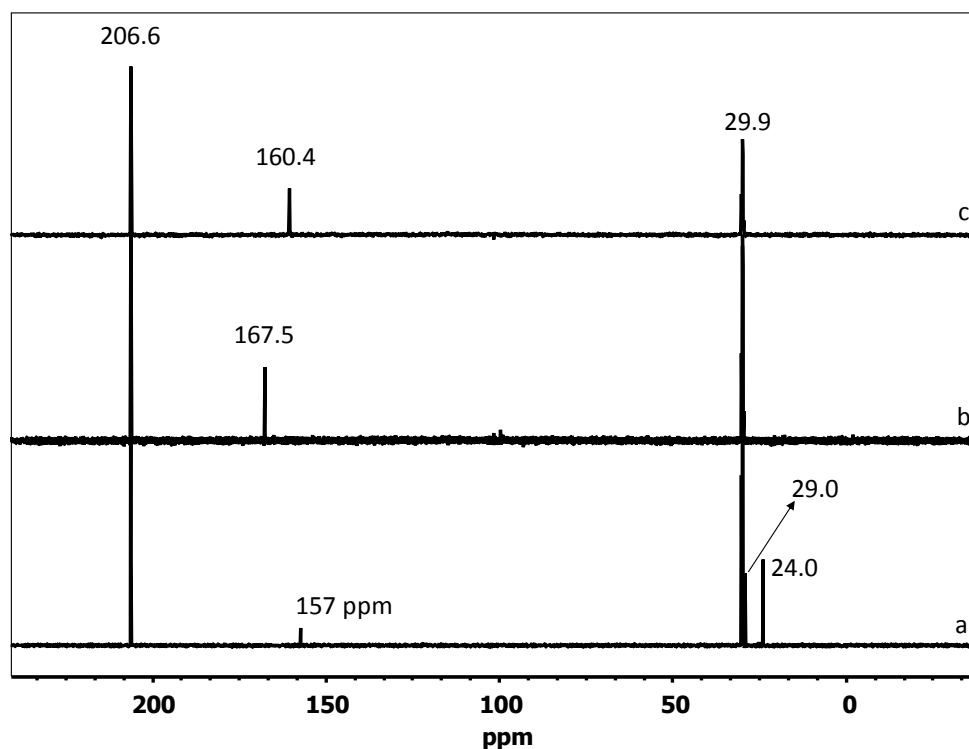


Figure 3.34 ¹³C NMR spectra of (a) open-chain glutardiamidoxime, (b) Na₂CO₃ at pH 11, and (c) Na₂CO₃ at pH 8. The ¹³C signals at 206.6 ppm and 29.9 ppm are due to acetone-d₆ insert used for magnetic field lock.

To understand displacement of carbonate by open-chain glutardiamidoxime, UO₂(CO₃)₃⁴⁻ was prepared by using uranyl(VI) nitrate hexahydrate and ¹³C enriched Na₂CO₃, in 1:3 molar ratio. The ¹³C NMR spectra were acquired at low temperature of +3 °C to observe free and complexed carbonate species by slowing down the rate of exchange between them. ¹³C NMR spectra were acquired for solution containing UO₂(CO₃)₃⁴⁻ only (Figure 3.35a), and for solutions containing UO₂(CO₃)₃⁴⁻ with open-chain glutardiamidoxime in concentrations ranging from 10 mM to 140 mM at the pH of 8 (Figure 3.35b-e). The effect of increasing open-chain glutardiamidoxime concentration on peak area of various ¹³C signals can be observed in the ¹³C NMR spectra shown in Figure 3.35b-e. Initially, a ¹³C signal at 167.7 ppm belonging to free carbonate species present in UO₂(CO₃)₃⁴⁻ was observed (Figure 3.35a) for the solution containing UO₂(CO₃)₃⁴⁻ only, at the pH of 8. The percentage area of this ¹³C

NMR signal was ~100%. As the open-chain glutardiamidoxime concentrations increase from 10 mM to 140 mM in a solution containing $\text{UO}_2(\text{CO}_3)_3^{4-}$, changes in the ^{13}C NMR spectra were observed. When 10 mM open-chain glutardiamidoxime was added to the solution containing $\text{UO}_2(\text{CO}_3)_3^{4-}$, it starts to displace carbonate in $\text{UO}_2(\text{CO}_3)_3^{4-}$, and three signals in the ^{13}C NMR spectra (Figure 3.35b) were observed. A signal at 167.7 ppm for free carbonate species, a signal at 167.2 ppm for combined complex of $\text{UO}_2(\text{CO}_3)_3^{4-}$ with open-chain glutardiamidoxime, and a signal at 160.6 ppm for carbonate displaced from $\text{UO}_2(\text{CO}_3)_3^{4-}$ upon addition of 10 mM open-chain glutardiamidoxime (Figure 3.35b) were observed. The peak area for the ^{13}C NMR signal for free carbonate species $\text{UO}_2(\text{CO}_3)_3^{4-}$ decreased to 62% upon addition of 10 mM open-chain glutardiamidoxime. Open-chain glutardiamidoxime starts to complex with UO_2^{+2} giving a new signal at 167.2 ppm for the combined complex of $\text{UO}_2(\text{CO}_3)_3^{4-}$ with open-chain glutardiamidoxime, with a peak area of 19.7%. The displaced carbonate was observed at 160.6 ppm with a peak area of 18.3%. When open-chain glutardiamidoxime concentration increased from 20 mM to 140 mM (Figure 3.35c-e), a new ^{13}C NMR signal at 157 ppm was observed in the ^{13}C NMR spectra, belonging to free open-chain glutardiamidoxime, along with the appearance of three previously described signals for the three different carbonate species. Other ^{13}C signals for free glutardiamidoxime, at 24 ppm, and 29 ppm, as described in Figure 3.34a, were also observed, but that region is not covered in the spectrum shown in Figure 3.35(c-e). As the concentration of open-chain glutardiamidoxime increases (Figure 3.35c-e), its interaction with UO_2^{+2} also increases, and more combined complex of $\text{UO}_2(\text{CO}_3)_3^{4-}$ with open-chain glutardiamidoxime takes place. The peak area for the ^{13}C signal at 167.2 ppm increases from 30% to 39% (Figure 3.35c-e). This study shows that UO_2^{+2} can form stable complex with open-chain glutardiamidoxime in the

presence of carbonate at the pH of 8. No precipitation of the complex was observed. This indicates that carbonate stabilizes UO_2^{+2} -glutardiamidoxime complex may be by forming a stable UO_2^{+2} -(glutardiamidoxime) $_2$ carbonate complex²¹. Upon increasing the concentration of open-chain glutardiamidoxime, more carbonate is being displaced from $\text{UO}_2(\text{CO}_3)_3^{4-}$; hence the peak area of the signal for free $\text{UO}_2(\text{CO}_3)_3^{4-}$ at 167.7 ppm decreases from 45.6 % to 14.2 % (Figure 3.35c-e). The peak area of the ^{13}C signal for the displaced carbonate species at 160.6 ppm increases from 24.4% to 46.8% (Figure 3.35c-e). This observation confirms the displacement of carbonate from $\text{UO}_2(\text{CO}_3)_3^{4-}$ upon increasing open-chain glutardiamidoxime concentration. The signal at 157 ppm belonging to open-chain glutardiamidoxime also increases in intensity as the concentration of glutardiamidoxime increases (Figure 3.35c-e).

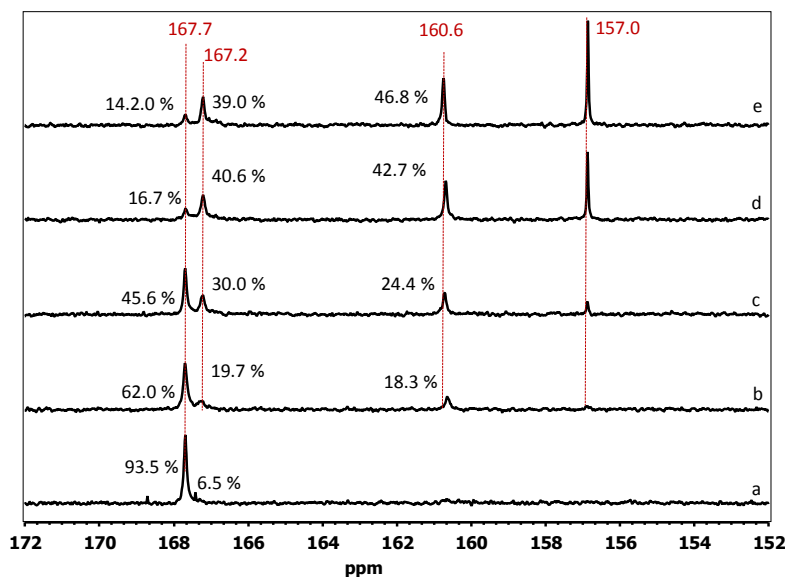


Figure 3.35 ^{13}C NMR spectra of (a) $\text{UO}_2(\text{CO}_3)_3^{4-}$ prepared using 10 mM uranyl (VI) nitrate hexahydrate and 30 mM Na_2CO_3 , (b) $\text{UO}_2(\text{CO}_3)_3^{4-}$ in 10 mM open-chain glutardiamidoxime, (c) $\text{UO}_2(\text{CO}_3)_3^{4-}$ in 20 mM open-chain glutardiamidoxime, (d) $\text{UO}_2(\text{CO}_3)_3^{4-}$ in 100 mM open-chain glutardiamidoxime, and (e) $\text{UO}_2(\text{CO}_3)_3^{4-}$ in 140 mM open-chain glutardiamidoxime at pH 8 and +3 °C.

3.4.7 Vanadium(V) complexation with open-chain glutardiamidoxime

^{51}V NMR results (Figure. 3.16a, 3.16b) described earlier shows that cyclic glutarimidedioxime reacts with vanadium(V) forming 1:1 and 1:2 complex, but open-chain glutardiamidoxime does not react with vanadium(V) in simulated seawater conditions. Complexation of open-chain glutardiamidoxime with vanadium(V) using ^{13}C NMR and ^1H NMR spectroscopic techniques was further studied. The ^{51}V NMR spectra for open-chain glutardiamidoxime without and with vanadium(V) are shown earlier in Figure 3.2a-c. To further study complexation between glutardiamidoxime and vanadium(V), ^1H NMR spectra was acquired for solutions containing 5 mM vanadium(V):5 mM open-chain glutardiamidoxime, in 0.05 M NaCl in D_2O solution. The ^1H NMR spectra for free open-chain glutardiamidoxime without any vanadium shows two ^1H NMR signals, a quintet for $[-\text{CH}_2-\text{CH}_2-\text{CH}_2-]$; 2H, at ~1.8 ppm, and a triplet for $[-\text{CH}_2-\text{CH}_2-\text{CH}_2-]$ 4H; at 2.2 ppm (Figure 3.36a). Upon addition of vanadium(V) to open-chain glutardiamidoxime, the ^1H NMR signals for CH_2 's of glutardiamidoxime remain at the same position as that of free glutardiamidoxime without any vanadium (Figure 3.36a-b). This observation suggests that open-chain glutardiamidoxime does not react with vanadium(V).

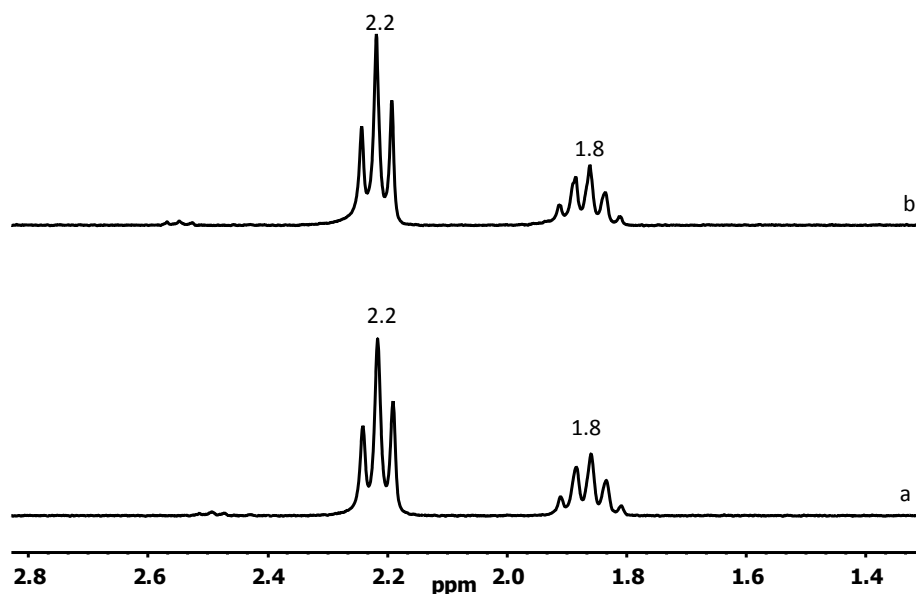


Figure 3.36 ¹H NMR spectra demonstrating no formation of vanadium(V)-(open-chain glutardiamidoxime) complex. Solutions labels (a) 5 mM open-chain glutardiamidoxime only, and (b) 5 mM vanadium(V):5 mM open-chain glutardiamidoxime.

To investigate interactions of open-chain glutardiamidoxime with vanadium(V), ¹³C NMR spectroscopy was also used. Free open-chain glutardiamidoxime shows ¹³C NMR signals at chemical shift of 24.6 ppm, 29.6 ppm, and 157.8 ppm for carbon's belonging to $-\text{CH}_2-\text{CH}_2-\text{CH}_2-$; $-\text{CH}_2-\text{CH}_2-\text{CH}_2-$ and, $-\text{C}(\text{NH}_2)=\text{NOH}$, respectively (Figure 3.37a). Upon addition of 5 mM vanadium(V) to open-chain glutardiamidoxime, ¹³C NMR spectra was acquired, and ¹³C NMR peaks for carbons of glutardiamidoxime remain at the same peak position (Figure 3.37b) as that of free glutardiamidoxime without any vanadium(V) (Figure 3.37a). This observation again suggests that open-chain glutardiamidoxime does not complex with vanadium(V). The peak at 49.6 ppm (Figure 3.37b) is due to the impurity of methanol present in sample. Methanol may come from D₂O used for sample preparation or from the NMR tubes because methanol was used for cleaning the NMR tubes.

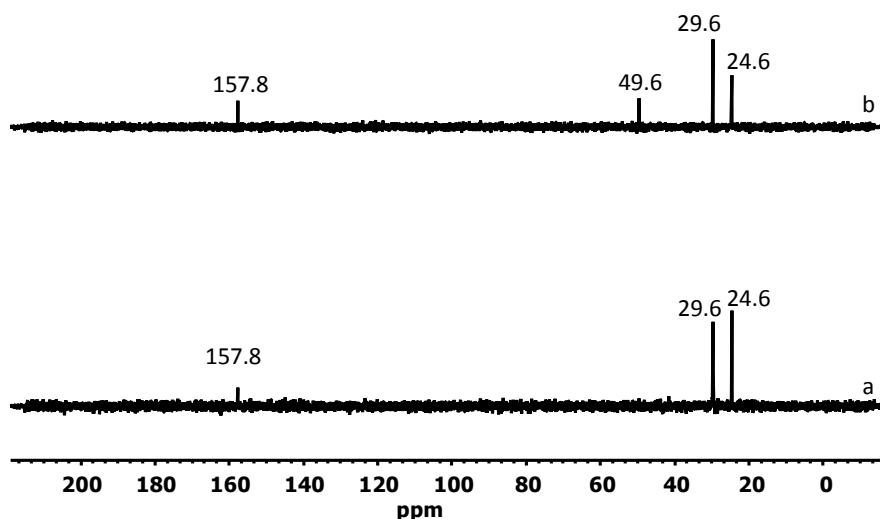


Figure 3.37 ^{13}C NMR spectra demonstrating no formation of vanadium(V)-(open-chain glutardiamidoxime) complex. Solutions labels (a) 5 mM open-chain glutardiamidoxime only, and (b) 5 mM vanadium(V):5 mM open-chain glutardiamidoxime.

The complexation of vanadium(V) with open-chain glutardiamidoxime in presence of UO_2^{+2} was also studied. When vanadium(V) was added to a solution containing 0.2 mM UO_2^{+2} :0.2 mM open-chain glutardiamidoxime, no complexation was observed. The observed signals in the ^1H NMR spectra for 0.2 mM UO_2^{+2} :0.2 mM open-chain glutardiamidoxime:0.2 mM vanadium(V) (Figure 3.38b) resembles the ^1H NMR signals of free glutardiamidoxime at 2.0 and 2.5 ppm. (Figure 3.38a). The pH of solutions was adjusted to 3.4. The chemical shift of the ^1H NMR signal depends upon analyte concentration. For 0.2 mM of free glutardiamidoxime the ^1H NMR signals were observed at 2.0 and 2.5 ppm (Figure 3.38a). However, for 5 mM open-chain glutardiamidoxime, ^1H NMR signals were observed at 1.8 and 2.2 ppm (Figure 3.36a).

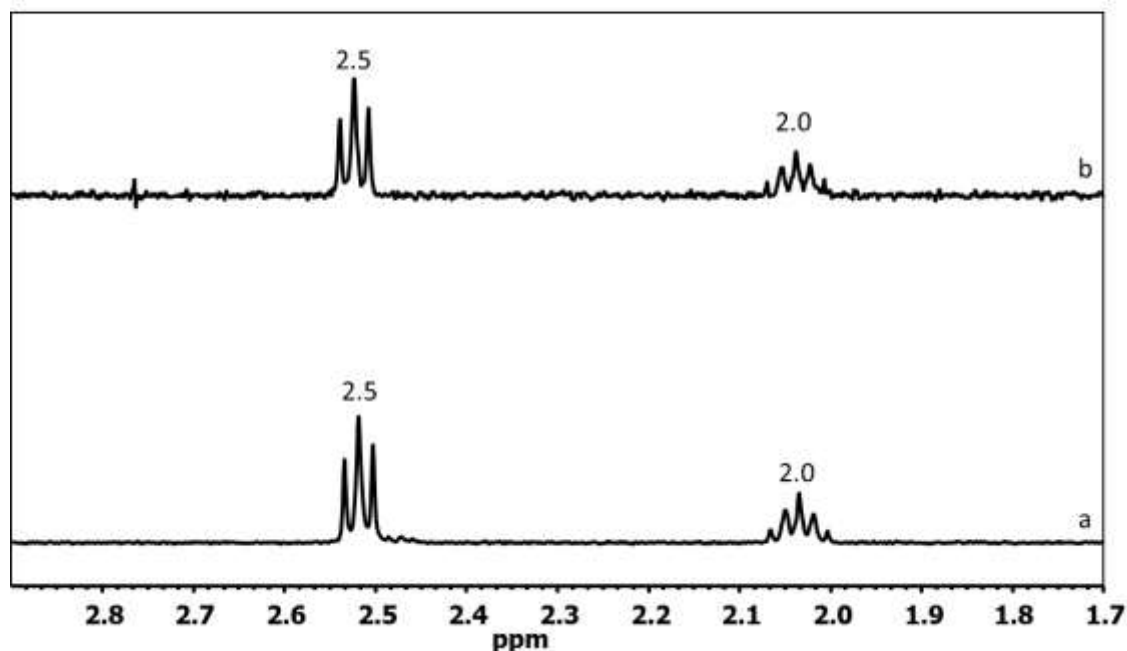


Figure 3.38 ^1H NMR spectra demonstrating no formation of vanadium(V)-(open-chain glutardiamidoxime) complex in the presence of UO_2^{+2} . Solutions labels (a) 0.2 mM open-chain glutardiamidoxime only, and (b) 0.2 mM UO_2^{+2} :0.2 mM open-chain glutardiamidoxime:0.2 mM vanadium(V). All samples in 0.05 M NaCl in D_2O at pH 3.4.

^{51}V NMR spectra were acquired from solution containing 0.2 mM UO_2^{+2} :0.2 mM open-chain glutardiamidoxime:0.2 mM vanadium(V) to study vanadium(V)-(open-chain glutardiamidoxime) interactions (Figure 3.39a-b). Initially, a peak for uncomplexed vanadium(V) was observed at the chemical shift of -551 ppm (Figure 3.39a). ^{51}V NMR spectra for the solution was acquired again after 24 hours, and no vanadium(V) peak was detected (Figure 3.39b). This observation suggests that vanadium(V) is reduced to vanadium(IV) because vanadium(IV) nucleus is paramagnetic in nature and gives no signal in the ^{51}V NMR spectra. A previous report suggests that amidoxime molecules are reducing agents²² and acidic conditions can reduce vanadium(V) to vanadium(IV).

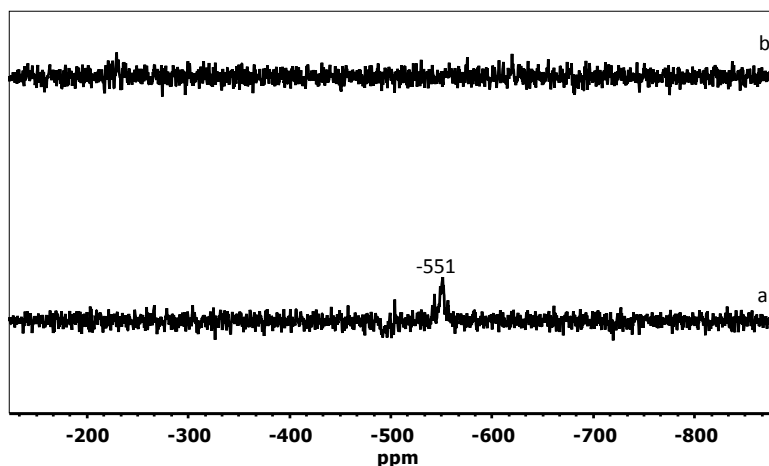


Figure 3.39 ^{51}V NMR spectra acquired from a solution containing 0.2 mM UO_2^{+2} :0.2 mM vanadium(V):0.2 mM open-chain glutardiamidoxime observed after (a) 5 minutes, and (b) 24 hours. Sample was prepared in 0.05 M NaCl in D_2O at pH 3.4.

3.4.8 Vanadium(IV) complexation with glutarimidedioxime and glutardiamidoxime

Vanadium(IV) interactions are mainly examined by EPR and UV-Visible spectroscopy because vanadium(IV) nucleus is paramagnetic and cannot be observed in NMR. UV-Visible spectroscopy was used to monitor interactions of vanadium(IV) with cyclic glutarimidedioxime and open-chain glutardiamidoxime. Electron paramagnetic resonance (EPR) spectroscopy was used to monitor stabilization of vanadium(IV) oxidation state. Oxidation of vanadium(IV) to vanadium(V) was observed using ^{51}V NMR spectroscopy because vanadium(V) nucleus is diamagnetic and can be studied by ^{51}V NMR spectroscopy. For UV-Visible study, concentrations of vanadium(IV) were varied from 0.25 mM to 2.0 mM, and constant concentration (2.0 mM) of cyclic glutarimidedioxime was used. The pH of the solution was ~ 8 . The UV-Visible spectrum of free glutarimidedioxime is featureless. However, the solution containing vanadium(IV) and glutarimidedioxime shows the wavelength of most intense UV-Visible absorption at 445.0 nm (Figure 3.40), for 0.5 mM

vanadium(IV). This suggests the presence of enough glutarimidedioxime in the system so that vanadium(IV), and vanadium(V) formed by the oxidation of vanadium(IV) can form stable complex with glutarimidedioxime. The vanadium(V)-glutarimidedioxime complex was not observed in the UV-Visible spectrum. At low concentration 0.25 mM of vanadium(IV), the absorbance at 445.0 nm decreases because vanadium(IV)-glutarimidedioxime complex is formed in low abundance. In such a system, there is an excess of glutarimidedioxime; hence, vanadium(V)-glutarimidedioxime complex is more favourable to form because vanadium(V) has a higher binding affinity for glutarimidedioxime than vanadium(IV). At high concentrations (1 mM and 2 mM) of vanadium(IV), the absorbance at 445.0 nm wavelength decreases (Figure 3.40) upon increasing vanadium(IV) concentration. This decrease in absorbance is caused by oxidation of vanadium(IV) to vanadium(V). At higher concentrations, more vanadium(IV) oxidizes to vanadium(V) and the formed vanadium(V) complexes with cyclic glutarimidedioxime and effectively displaces glutarimidedioxime from vanadium(IV)-glutarimidedioxime complex. This causes decrease in the absorbance of vanadium(IV)-cyclic glutarimidedioxime complex. The stoichiometry of vanadium(IV) complexation with glutarimidedioxime appears complicated to understand at the present time.

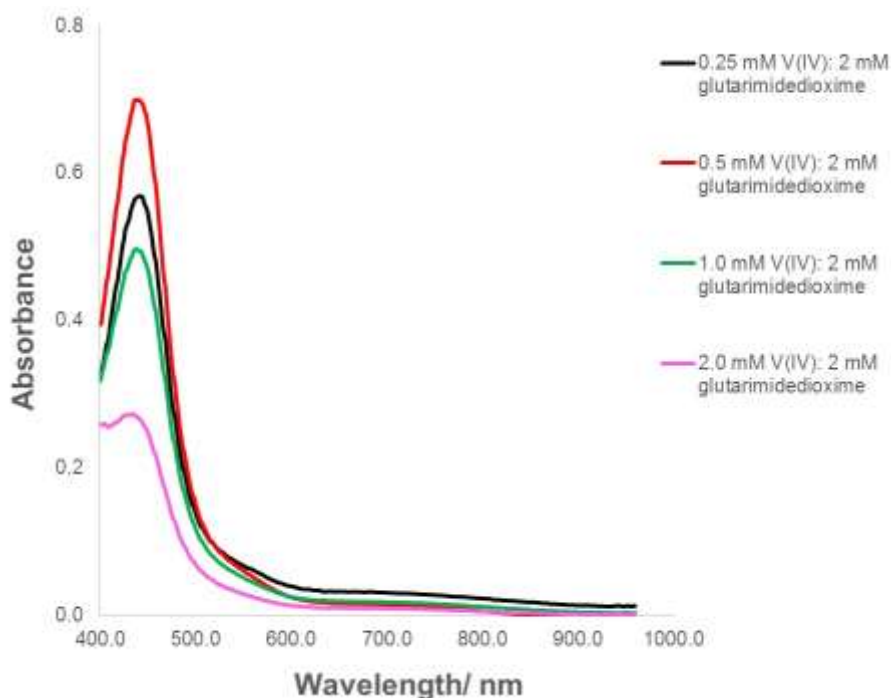


Figure 3.40 UV-Visible absorption spectra using vanadium(IV) and its complexation with glutarimidedioxime.

The oxidation of vanadium(IV) to vanadium(V) was confirmed using ^{51}V NMR spectroscopy for the above solutions showing the lowest absorbance for the solution containing 2 mM vanadium(IV) and 2 mM glutarimidedioxime, and the highest absorbance for the solution containing 0.5 mM vanadium(IV) and 2 mM glutarimidedioxime. The acquired ^{51}V NMR spectra are shown in (Figure 3.41 a-b). ^{51}V NMR peaks were observed for samples containing vanadium(IV)-glutarimidedioxime because vanadium(IV) was oxidized to vanadium(V). The ^{51}V NMR signal for vanadium(V) complexed with glutarimidedioxime was observed at -421 ppm, and the ^{51}V NMR signal for free vanadium(V) was observed at -518 ppm, and -558 ppm (Figure 3.41b). Two peaks were observed at -518 ppm and -558 ppm, probably due to the presence of $\text{H}_2\text{V}_{10}\text{O}_{28}^{4-}$ and H_2VO_4^- respectively, as reported by Rehder et al⁶. At high concentration (2 mM) vanadium(IV), more vanadium(V) is formed by oxidation of vanadium(IV), and the ^{51}V NMR peaks for free vanadium(V) species, along with

the ^{51}V NMR peak for complexed vanadium at -421ppm (Figure 3.41b), were observed. However, at low concentration (0.5 mM) vanadium(IV), the vanadium(V) formed by oxidation of vanadium(IV), is completely complexed with cyclic glutarimidedioxime, giving one ^{51}V NMR signal at - 424 ppm (Figure 3.41a).

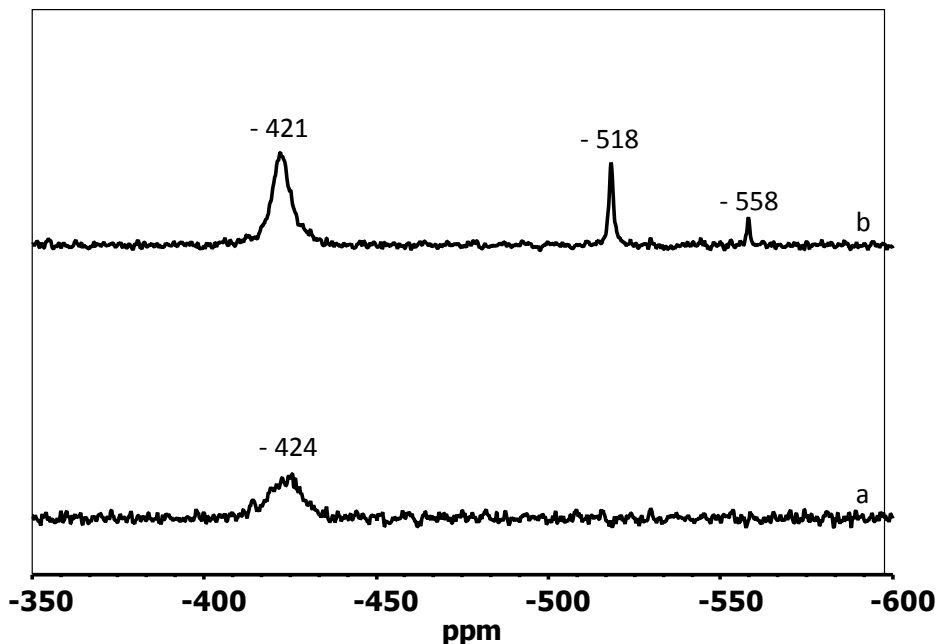


Figure 3.41 ^{51}V NMR spectra of (a) 0.5 mM vanadium(IV) in 2 mM glutarimidedioxime, and (b) 2 mM vanadium(IV) in 2 mM glutarimidedioxime.

To understand the complexation of vanadium(IV) with glutarimidedioxime, the stabilization of vanadium(IV) was required. A previous report by Britton et al.²³ on effect of sodium hydroxide on solutions containing vanadyl sulphate showed that addition of NaOH facilitates oxidation of vanadium(IV) to vanadium(V). It was observed that, even in the absence of NaOH, vanadium(IV) was oxidized to vanadium(V). For the solutions containing vanadium(IV)-glutarimidedioxime at different molar ratio in the absence of NaOH, the ^{51}V NMR spectra (Figure 3.42a-c) show peaks at -485 ppm, -489 ppm, and -491 ppm, due to vanadium(V) complexation with glutarimidedioxime. The ^{51}V NMR signal shifts from -485

ppm to -491 ppm, due to different concentrations of vanadium(IV) present in the analyzed samples. NMR chemical shift depends upon concentration of analyte because change in concentration produces a change in environment surrounding the analyte. The observed signals are due to the oxidation of vanadium(IV) to vanadium(V).

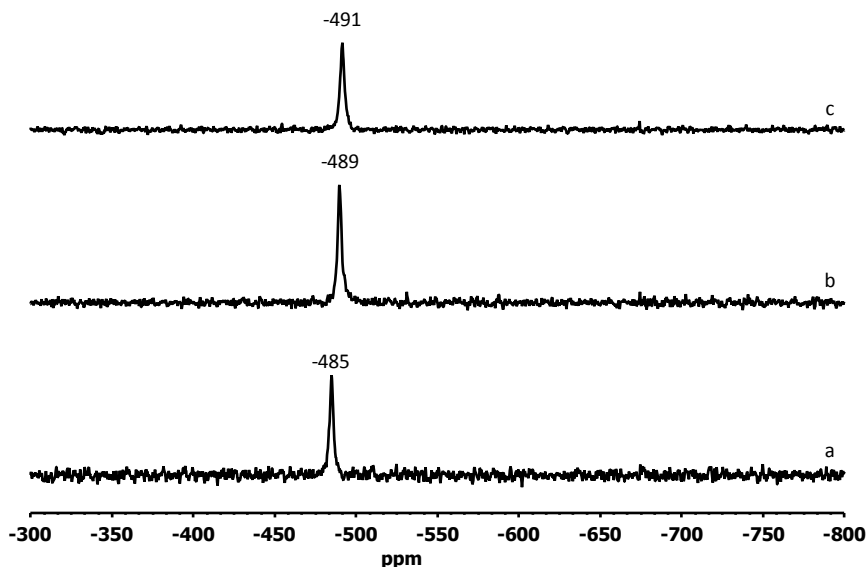


Figure 3.42 ^{51}V NMR spectra in the absence of NaOH (a) 0.5 mM vanadium(IV) in 2 mM glutarimidedioxime, (b) 1 mM vanadium(IV) in 2.0 mM glutarimidedioxime, and (c) 2.0 mM vanadium(IV) in 2 mM glutarimidedioxime.

The different stabilizing agents known for stabilization of vanadium(IV) oxidation state include polygalactouronic acid, tunichromes, 3,4-dihydroxyphenylalanine (DOPA) containing peptides, vanadobin, strain of *saccharomyces cerevisiae*, reduced glutathione GSH, exopolysaccharides produced by marine bacteria, saccharides, ascorbic acid, fulvic acid, catechol, polyaminocarboxylic acid like ethylenediaminetetraacetic acid (EDTA), and diethylenetriaminepentaacetic acid (DTPA).²⁴⁻³⁵ Readily available stabilizing agents, such as fulvic acid, catechol, and polyaminocarboxylic acids, such as EDTA and DTPA were tried. Solutions containing vanadium(IV)-fulvic acid, and vanadium(IV)-catechol were tested at

different pH's, and they were able to stabilize vanadium(IV) at the pH of ~ 3.1 and ~ 3.2 , respectively. Stabilization of vanadium(IV) was evident through “no” ^{51}V NMR signal for these solutions (Figure 3.43b, d). However, fulvic acid, and catechol were not able to stabilize vanadium(IV) at pH 8 because ^{51}V NMR signals that are probably due to free vanadium(V) species⁶ at -558 ppm, -572 ppm, and -577 ppm for H_2VO_4^- , $\text{H}_2\text{V}_2\text{O}_7^{2-}$, and $\text{V}_4\text{O}_{12}^{4-}$, respectively, were observed for these solutions (Figure 3.43 a, c).

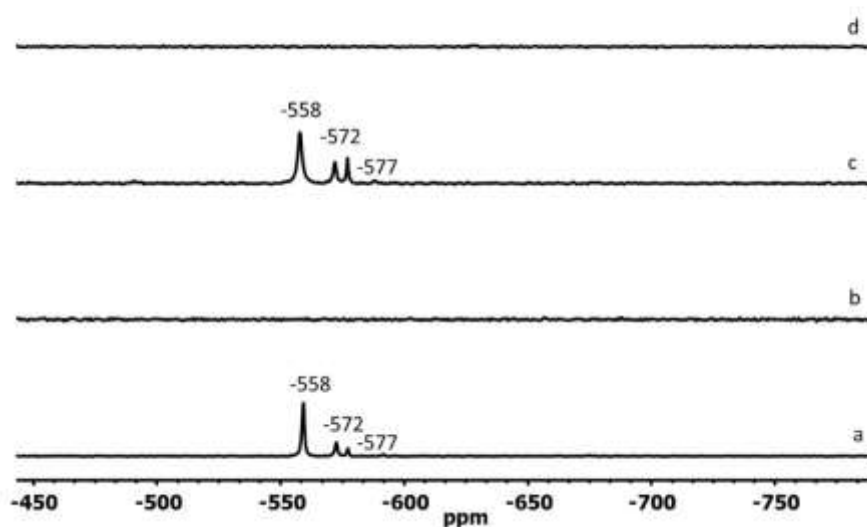


Figure 3.43 ^{51}V NMR spectra of (a) 2 mM vanadium(IV):2 mM fulvic acid, at pH 8.0, (b) 2 mM vanadium(IV):2 mM fulvic acid, at pH 3.14, (c) 10 mM vanadium(IV):10 mM catechol, at pH 8.0, and (d) 10 mM vanadium(IV):10 mM catechol, at pH 3.2.

To study complexation of vanadium(IV) with amidoxime ligands and formation of UO_2^{+2} -glutarimidedioxime complex in the presence of vanadium(IV), it was important to stabilize vanadium(IV) and prevent its oxidation to vanadium(V) at the pH of seawater. Polyaminocarboxylic acids like EDTA, and DTPA both stabilized vanadium(IV) at seawater pH of 8.3. Evidence for stabilization of vanadium(IV) oxidation state was observed through “no” NMR signal for vanadium(IV) complexed with EDTA (Figure 3.44b-c) because

vanadium(IV) is paramagnetic in nature and cannot be observed in high resolution NMR. Vanadium(IV) in water oxidizes to vanadium(V), at pH of 8.3, and ^{51}V NMR signal for vanadium(V) was observed at -558 ppm (Figure 3.44a) because vanadium(V) is a NMR active nucleus. In this study, EDTA was used to stabilize vanadium(IV) because EDTA is a simpler molecule than DTPA and forms 1:1 complex with vanadium(IV).³³ The $[\text{VO}(\text{EDTA})]^{-2}$ complex has a larger formation constant, $\log K = 18.0$, than $[\text{VO}_2(\text{EDTA})]^{-3}$ complex, $\log K = 15.5$ ^{36, 37}

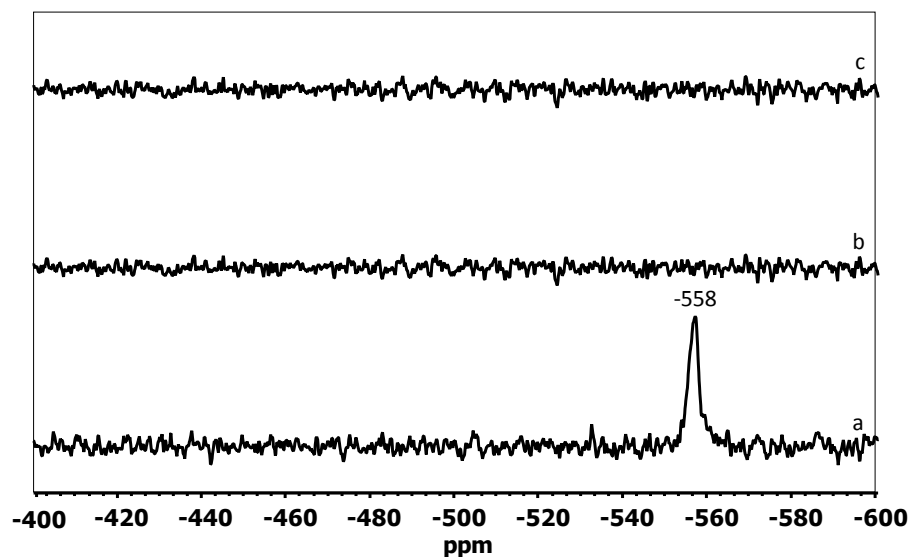


Figure 3.44 ^{51}V NMR spectra of (a) 10 mM vanadium(IV) in water, at pH 8.3, (b) 10 mM vanadium(IV) in ethylenediaminetetraacetic acid (EDTA), at pH 8.3, and (c) 10 mM vanadium(IV) in diethylenetriaminepentaacetic acid (DTPA), at pH 8.3.

EPR is a useful technique for characterization and investigation of vanadium(IV) complexes, such as vanadium(IV) complex with tripeptide glutathione³⁸, vanadyl polyphenolate complexes,³⁹ and nonoxido vanadium(IV) compounds.⁴⁰ Vanadium(IV) nucleus is EPR active and gives an eight-line EPR pattern typical of oxo vanadium(IV) species.⁴¹ The unpaired electron on vanadium(IV) experiences $spin = 7/2$ from vanadium

nucleus, and the number of lines originating from the hyperfine interaction is determined by the formula $(2NI+1)$, where N is the number of equivalent nuclei and I is the nuclear spin. Hence, 8 signals $(2 \times 1 \times 7/2 + 1)$ for vanadium(IV) nucleus were observed in the EPR spectra (Figure 3.45). This observation, as well as “no” NMR signal in ^{51}V NMR spectroscopy, strongly indicates that vanadium(IV) oxidation state is stabilized using EDTA.

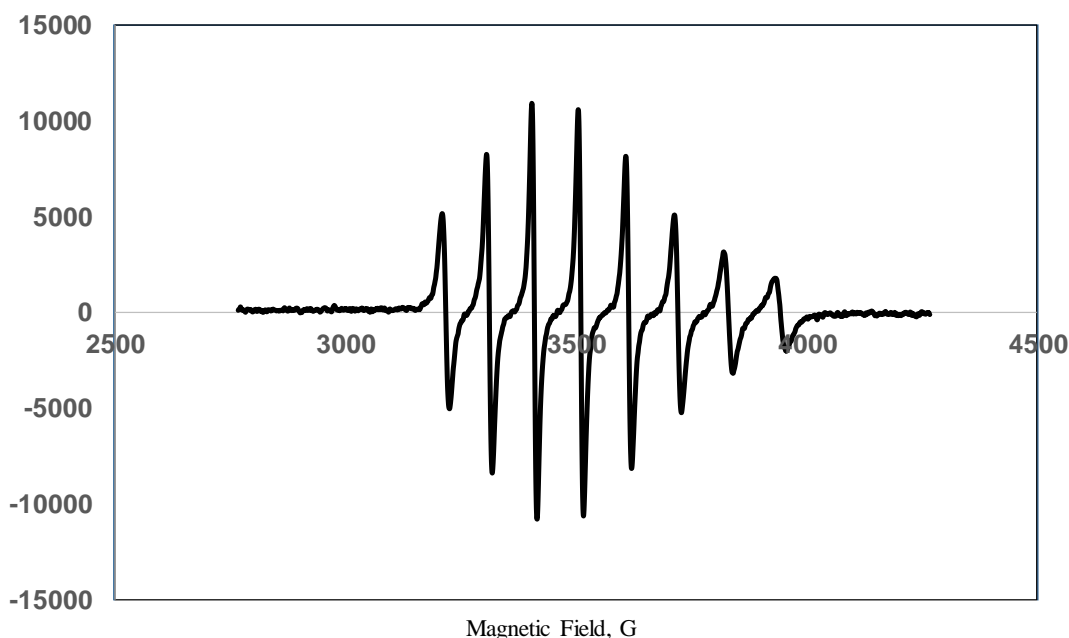


Figure 3.45 EPR spectrum of 5 mM vanadium(IV):5 mM EDTA in water at pH 8.0.

At low concentration (0.05 mM UO_2^{+2} and 0.1 mM glutarimidedioxime), at the pH of 8 (Figure 3.28), UO_2^{+2} -glutarimidedioxime complex, with an absorption band at 280 nm, was clearly observed in the UV-Visible spectrum.² Rao et al.⁴² reported the formation of UO_2^{+2} -EDTA complex in stoichiometric ratio of 2:1 using spectrophotometric study. Wavelength range 240 nm – 270 nm was used to study UO_2^{+2} -EDTA complex using uranyl perchlorate-EDTA and uranyl acetate-EDTA mixtures. Influence of pH on stability of UO_2^{+2} -EDTA complex was also studied. The complex was stable at pH 6, with no precipitation in 6 days. At pH 7 and pH 8, turbidity starts after 6 days and 5 days, respectively. However, at pH 8.5

and 9.5, turbidity starts after 24 hours and 4 hours, respectively. After stabilization of vanadium(IV) oxidation state using EDTA, competition of vanadium(IV) and UO_2^{+2} for complexation with glutarimidedioxime was studied. For this study, a solution containing 0.05 mM of vanadium(IV)-EDTA was first complexed with 0.1 mM glutarimidedioxime, and then 0.05 mM UO_2^{+2} was added to this solution. The pH of the solution was adjusted to 8. The UV-Visible spectrum initially shows no formation of UO_2^{+2} -glutarimidedioxime complex because UO_2^{+2} takes time to displace glutarimidedioxime from vanadium(IV)-glutarimidedioxime complex. A gradual stepwise increase in the intensity of the absorption band at 280 nm for UO_2^{+2} -glutarimidedioxime complex was observed from the start of the reaction till 16 hours (Figure 3.46). The absorption band at 280 nm belongs to UO_2^{+2} -glutarimidedioxime complex as reported by Tian et al.² Complete UO_2^{+2} -glutarimidedioxime complex can be observed in 16 hours (Figure 3.46). This observation indicates that UO_2^{+2} can form stable UO_2^{+2} -glutarimidedioxime complex in the presence of vanadium(IV). ^{51}V NMR spectrum was acquired for solution containing 0.05 mM vanadium(IV):0.05 mM UO_2^{+2} :0.1 mM glutarimidedioxime to confirm stabilization of vanadium(IV) oxidation state. The ^{51}V NMR spectra were acquired at start of the reaction and after 16 hours. No peaks were observed in the ^{51}V NMR spectra, confirming that vanadium(IV) was not oxidized to vanadium(V) during this time. However, “no” UO_2^{+2} -glutarimidedioxime complex was observed in the presence of vanadium(V) (Figure 3.29b) because UO_2^{+2} cannot compete with vanadium(V) for complexation with glutarimidedioxime, as strong vanadium(V)-glutarimidedioxime complex forms preferentially.

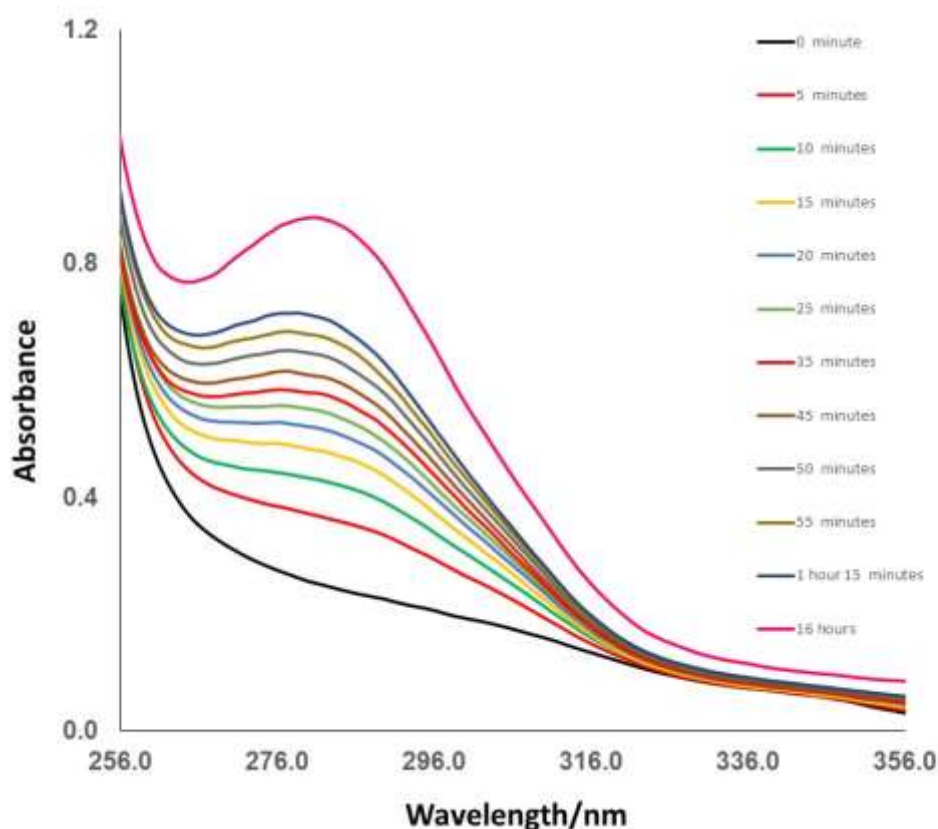


Figure 3.46 UV-Visible absorption spectra acquired upon the addition of UO_2^{+2} to vanadium(IV)-EDTA solution, showing complexation of UO_2^{+2} with glutarimidedioxime.

Similar UV-Visible studies were carried out for solutions containing 0.05 mM UO_2^{+2} and 0.1 mM glutarimidedioxime. Different concentrations of vanadium(IV) (Figure 3.47) were added to UO_2^{+2} -glutarimidedioxime complex. Decrease in the 280 nm band for UO_2^{+2} -glutarimidedioxime complex upon addition of different concentrations of vanadium(IV) ranging from 0.05 mM to 0.8 mM was observed (Figure 3.47). However, complete disappearance of the band at 280 nm was observed upon addition of 0.8 mM vanadium(IV), indicating disappearance of UO_2^{+2} -glutarimidedioxime complex and formation of vanadium(IV)-glutarimidedioxime complex. High concentration (0.8 mM) of vanadium(IV) was required to destabilize formed UO_2^{+2} -glutarimidedioxime complex. However, when vanadium(V) was added to solution containing 0.05 mM UO_2^{+2} and 0.1 mM

glutarimidedioxime as shown earlier in Figure 3.28, it was observed that lower concentration of vanadium(V) (0.1 mM) can destabilize the formed UO_2^{+2} -glutarimidedioxime complex because of the higher formation constant of vanadium(V)-glutarimidedioxime complex than the formation constant of 1:1, and 1:2, UO_2^{+2} -glutarimidedioxime complexes with ML [$\log \beta=17.8$] and ML_2 [$\log \beta =27.5$]³, respectively.

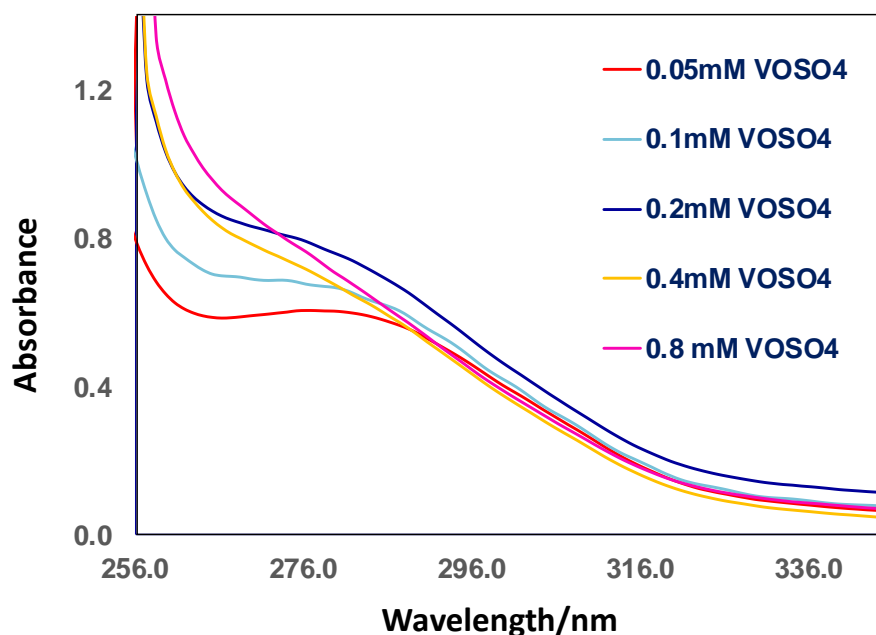


Figure 3.47 UV-Visible absorption spectra showing the effect of increasing vanadium(IV) concentrations on UO_2^{+2} complexation with glutarimidedioxime.

The complexation of vanadium(IV) stabilized using EDTA, with glutarimidedioxime was further studied. Previous reports^{37, 43} suggest absorption bands observed at 780 nm and 591 nm are characteristics of vanadium(IV) complexes with various amino carboxylates ligands, d-d transitions, d_{xy} to $d_{xz, yz}$ (777 nm) and d_{xy} to $d_{x^2-y^2}$ (585 nm). The position for wavelength of maximum absorbance depends upon the pH of the mixture. The absorption bands at 791 nm and 602 nm were observed in the UV-Visible spectrum for solutions

containing vanadium(IV)-EDTA and vanadium(IV)-EDTA-glutarimidedioxime (Figure 3.48). These absorption bands are assigned to vanadium(IV) complexes with amino carboxylate ligand (EDTA), caused by d-d transitions, d_{xy} to $d_{xz, yz}$ (791 nm) and d_{xy} to $d_{x^2-y^2}$ (602 nm). Upon the addition of 20 mM glutarimidedioxime to a solution containing vanadium(IV) and EDTA, a third absorbance at 445 nm was observed due to complexation of vanadium(IV)-EDTA with glutarimidedioxime. The spectrum was recorded for a period of 1 hour, and complex formation between glutarimidedioxime and vanadium(IV)-EDTA increased with time, causing an increase in the intensity of absorbance at 445 nm.

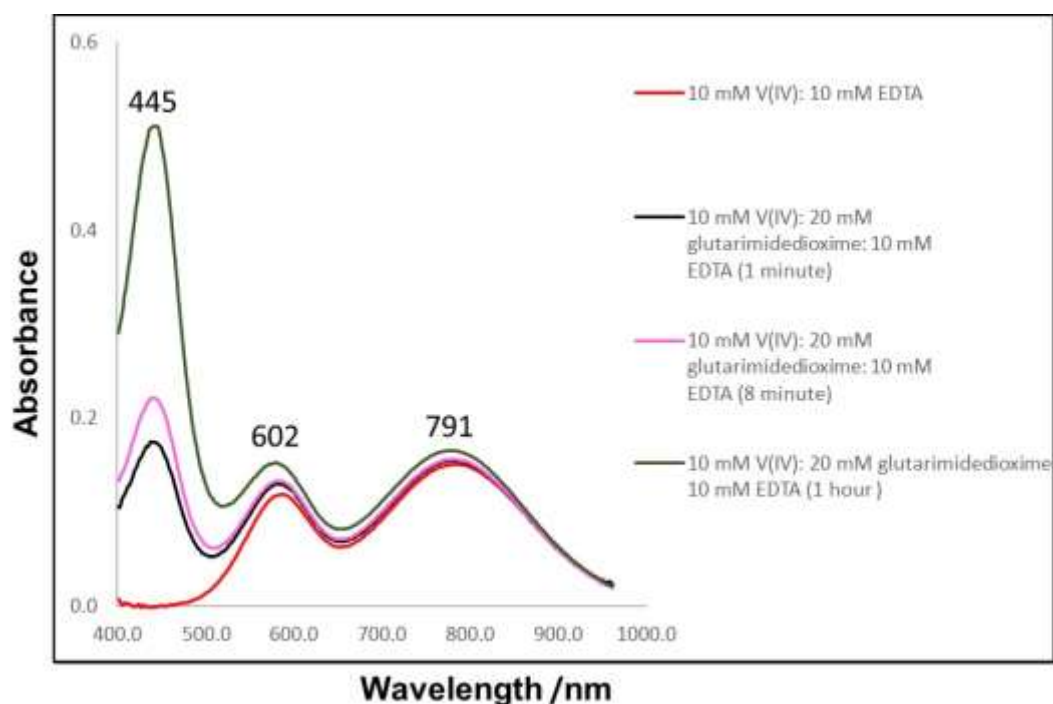


Figure 3.48 UV-Visible absorption spectra acquired for vanadium(IV)-EDTA solution, showing its complexation with glutarimidedioxime.

Stabilization of vanadium(IV) by DTPA and complexation of vanadium(IV)-DTPA solution with glutarimidedioxime was also studied. Figure 3.49 shows UV-Visible spectrum obtained by using vanadium(IV): DTPA solution, in molar ratio of 1:1. The absorption band

at 585 nm and 778 nm were observed (Figure 3.49) characteristics of vanadium(IV) complexes with DTPA (d-d transitions). Upon addition of glutarimidedioxime, emergence of a new absorption band at ~439 nm was observed, due to complexation of vanadium(IV):DTPA solution with glutarimidedioxime.

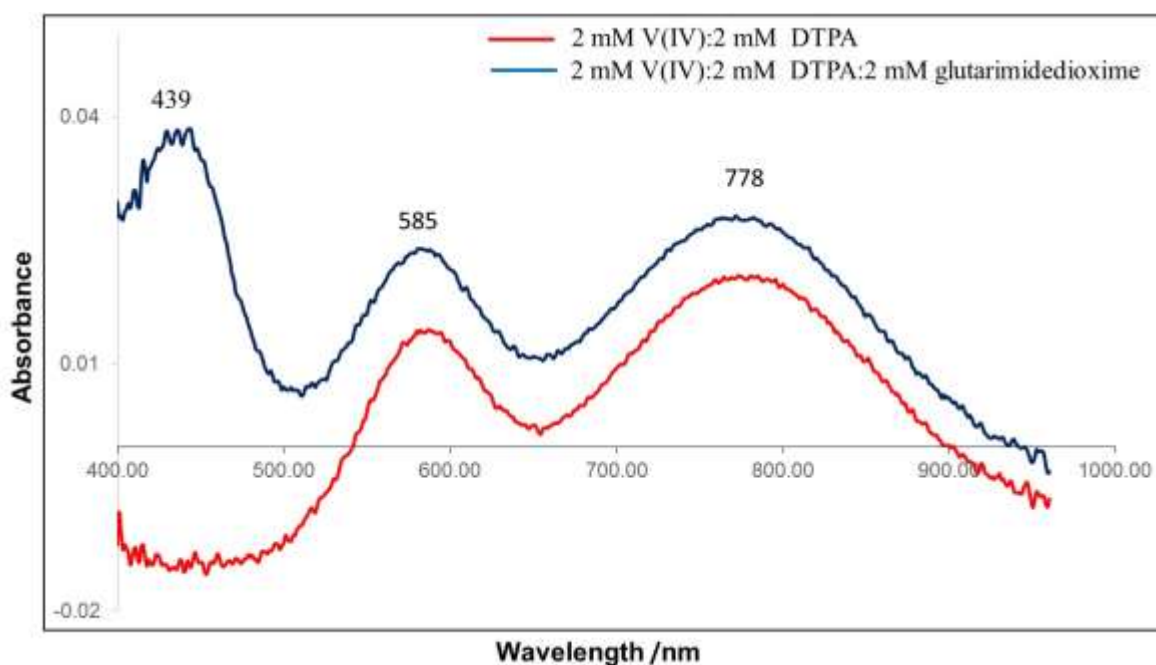


Figure 3.49 UV-Visible absorption spectra using vanadium(IV):DTPA solution and its complexation with glutarimidedioxime.

Complexation of open-chain glutardiamidoxime with vanadium(IV) was studied using UV-Visible spectroscopy, and UV-Visible spectra were recorded for solution containing vanadium(IV) and open-chain glutardiamidoxime in 1:1 molar ratio. Vanadium(IV) oxidation state was stabilized using EDTA. The pH of the sample was adjusted to 8.0. The UV-Visible spectrum acquired after ~10 minutes of sample preparation is shown in Figure 3.50. The sample was reanalyzed after 5 hours, and the acquired spectrum resembles the spectrum shown in Figure 3.50. This observation suggests that open-chain glutardiamidoxime does not form complex with vanadium(IV) because absorbances at 587 nm and 783 nm, corresponding

to d-d transitions of vanadium(IV) complexes with EDTA, were only observed even in the presence of open-chain glutardiamidoxime.

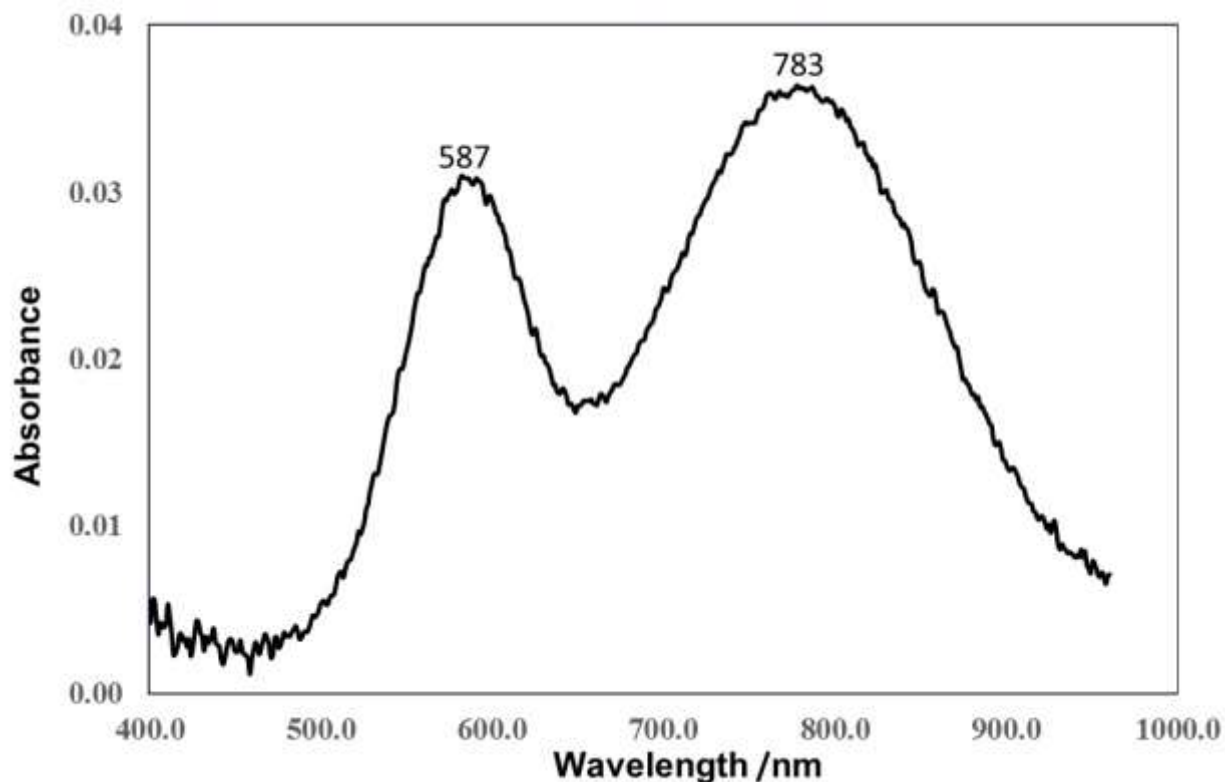


Figure 3.50 UV-Visible absorption spectrum acquired from a solution containing 2 mM vanadium(IV):2 mM EDTA:2 mM open-chain glutardiamidoxime at pH 8.0.

3.4.9 *Glutarimidedioxime complexation with vanadium(V) using LC-MS and formation of polynuclear vanadium species*

Sodium orthovanadate (Na_3VO_4), when dissolved in water, forms different inorganic vanadium species. ^{51}V NMR spectroscopy was used to investigate speciation of inorganic vanadium compounds at different concentrations of sodium orthovanadate ranging from 0.2 mM to 1.0 mM (Figure 3.51a-e). Effect of increasing Na_3VO_4 concentration on the ^{51}V NMR chemical shift can be seen in the NMR spectra shown in Figure 3.51a-e. At vanadate concentration of 0.2 mM, an intense ^{51}V NMR signal appears at the chemical shift of -556

ppm, and the least intense signal was observed at -574 ppm (Figure 3.51a). When vanadate concentration increased from 0.2 mM to 1.0 mM, the intensity of the ^{51}V NMR peaks at the chemical shift of -556 ppm and -574 ppm increased. However, when vanadate concentration increased to 1.0 mM, a third ^{51}V NMR signal was observed at the chemical shift of -579 ppm (Figure 3.51e), and the intensity of the signals at -556 ppm and -574 ppm also increased (Figure 3.51a-e). The ^{51}V NMR signals at -556 ppm and -560 ppm are probably due to monomeric form of vanadium H_2VO_4^- . The ^{51}V NMR signal for H_2VO_4^- shifts from -556 ppm to -560 ppm, upon increasing vanadate concentration from 0.2 mM to 1.0 mM, because NMR chemical shift vary with concentration. The ^{51}V NMR signals at -574 ppm, and -579 ppm, can be due to dimeric $\text{H}_2\text{V}_2\text{O}_7^{2-}$, and tetrameric $\text{V}_4\text{O}_{12}^{4-}$, vanadium species, respectively, according to the literature.⁶

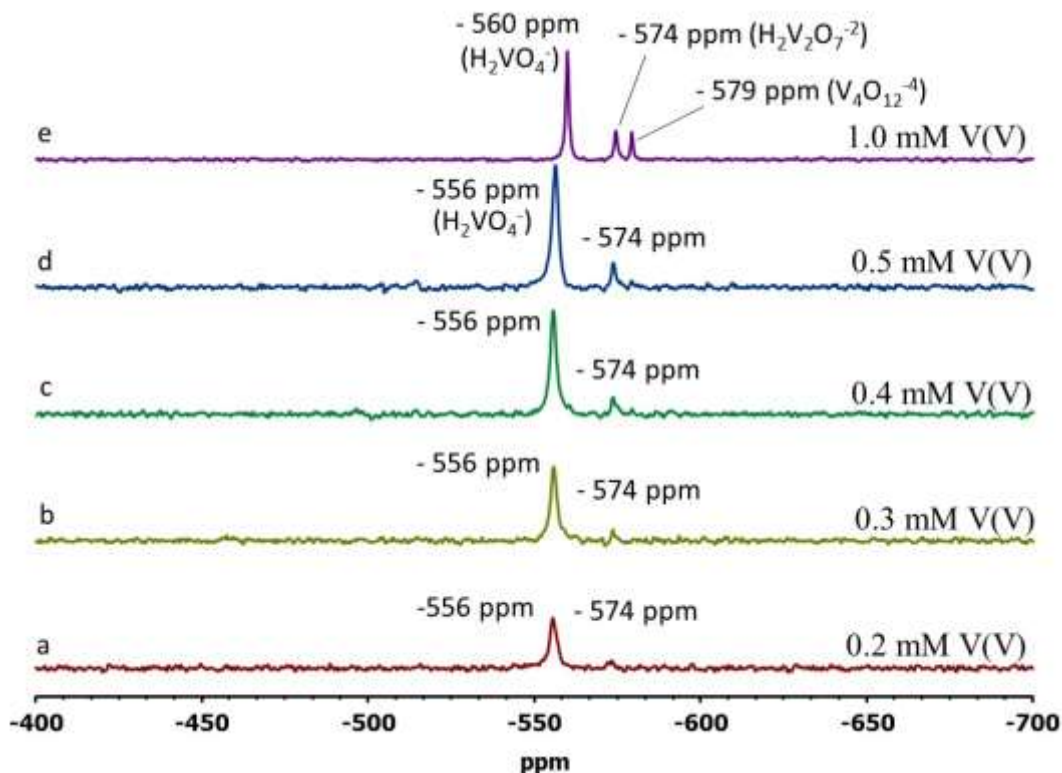


Figure 3.51 ^{51}V NMR spectra acquired from solutions containing varying concentrations of vanadium(V). All samples in 0.05 M NaCl aqueous solution at pH 8.3.

At high concentrations of vanadium(V), more polynuclear vanadium species are formed. Vanadium(V) complexes with cyclic glutarimidedioxime were further studied using liquid chromatography. For this study two different concentrations of vanadium(V), a low concentration of 0.2 mM and a high concentration of 0.5 mM, were used. The chromatogram was obtained using 0.2 mM vanadium(V) with varying glutarimidedioxime concentrations. Vanadium(V):glutarimidedioxime, molar ratio of 1:1.5, 1:2, 1:4, and 1:10 were used in this study. The acquired chromatogram is shown in Figure 3.52. The peak at the retention time ~ 0.8 minutes is related to a 1:1, vanadium(V)-glutarimidedioxime complex. This complex between vanadium(V) with glutarimidedioxime was discussed earlier using mass spectrum shown earlier in Figure 3.5 and the extracted ion chromatogram shown in Figure 3.6. The peak at the retention time of ~ 1.8 minutes (Figure 3.52) belongs to free glutarimidedioxime. This

peak was also observed earlier for free glutarimidedioxime in the extracted ion chromatogram, shown in Figure 3.6. When the concentration of glutarimidedioxime was increased from 0.4 mM to 2 mM, the relative intensity of the peak assigned to free glutarimidedioxime at the retention time of ~ 1.8 increased significantly (Figure 3.52). A very small peak at the retention of ~ 2.7 minutes was observed in the chromatogram. The peak area of this peak increased (Figure 3.52) upon increasing the concentration of glutarimidedioxime.

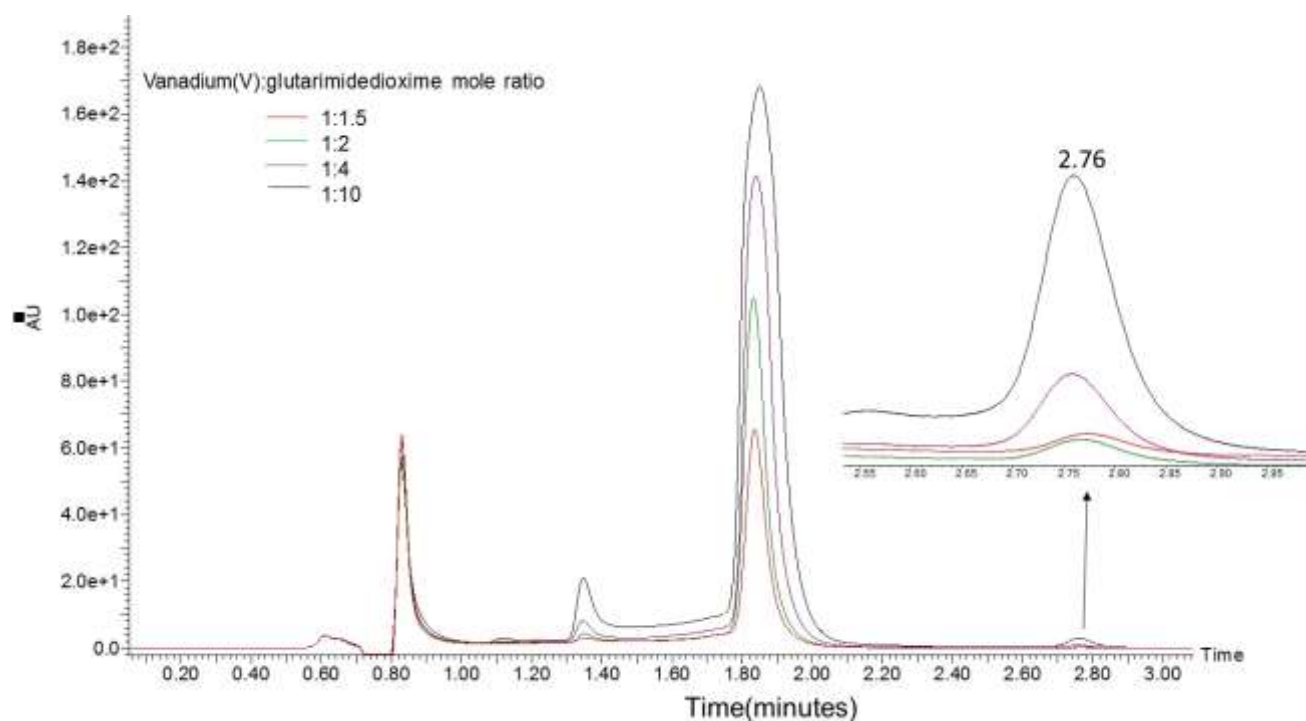


Figure 3.52 Chromatogram acquired from solutions containing 0.2 mM vanadium(V) and varying concentrations of glutarimidedioxime. The vanadium(V):glutarimidedioxime molar ratio of 1:1.5, 1:2, 1:4, and 1:10 were used in this study. All samples in 0.05 M NaCl aqueous solution at pH 8.3.

The mass spectrum shown in Figure 3.53 shows the m/z 333.1, corresponding to the peak at the retention time of ~ 2.7 minutes. This may indicate the formation of a 1:2 complex of vanadium(V) with glutarimidedioxime. A recent report⁹ on gas phase complexes formed between amidoxime ligands and vanadium(V) shows that the peak at m/z 333.1 belongs to a

1:2 complex of vanadium(V) with glutarimidedioxime $[\text{VO}_2+2(\text{DHIP})-2(\text{H}_2\text{O})]^+$ where DHIP stands for glutarimidedioxime.

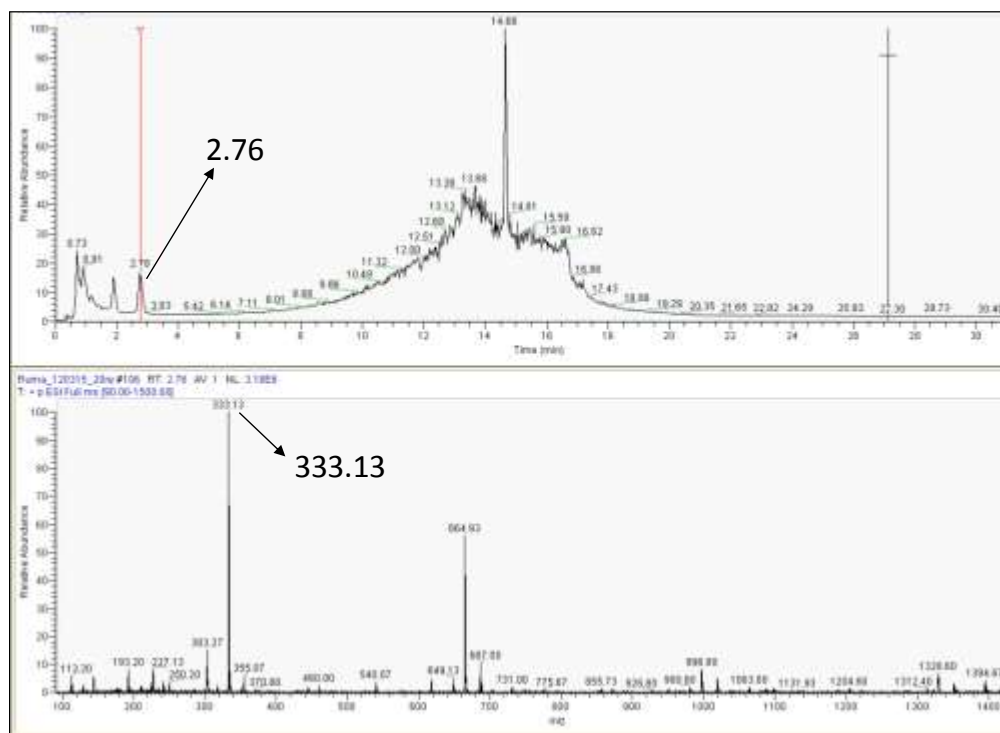


Figure 3.53 Positive-ion ESI mass spectrum acquired from a solution containing 0.2 mM vanadium(V) and 2 mM glutarimidedioxime showing m/z 333.13 for the peak at the retention time of 2.76 minutes. Sample was prepared in 0.05 M NaCl aqueous solution at pH 8.3.

The chromatogram obtained using liquid chromatography, at high concentration (0.5 mM), of vanadium(V), with varying vanadium(V):glutarimidedioxime molar ratio is shown in Figure 3.54. The peaks at the retention time of ~0.8 minutes, ~1.8 minutes, and ~2.7 minutes were observed in the chromatogram (Figure 3.54). These peaks were described earlier while discussing the chromatogram obtained in Figure 3.52. However, the chromatogram obtained using 0.5 mM vanadium(V), shown in Figure 3.54, shows significant increase in intensity and peak area of the peak at the retention time of ~2.7 minutes. This observation suggests formation of 1:2 complex between vanadium(V) and glutarimidedioxime in high abundance.

The mass corresponding to the peak at ~2.7 minutes shows formation of 1:2 complex⁹ between vanadium(V) and glutarimidedioxime (DHIP), $[\text{VO}_2+2(\text{DHIP})-2(\text{H}_2\text{O})]^+$ at m/z 333.1.

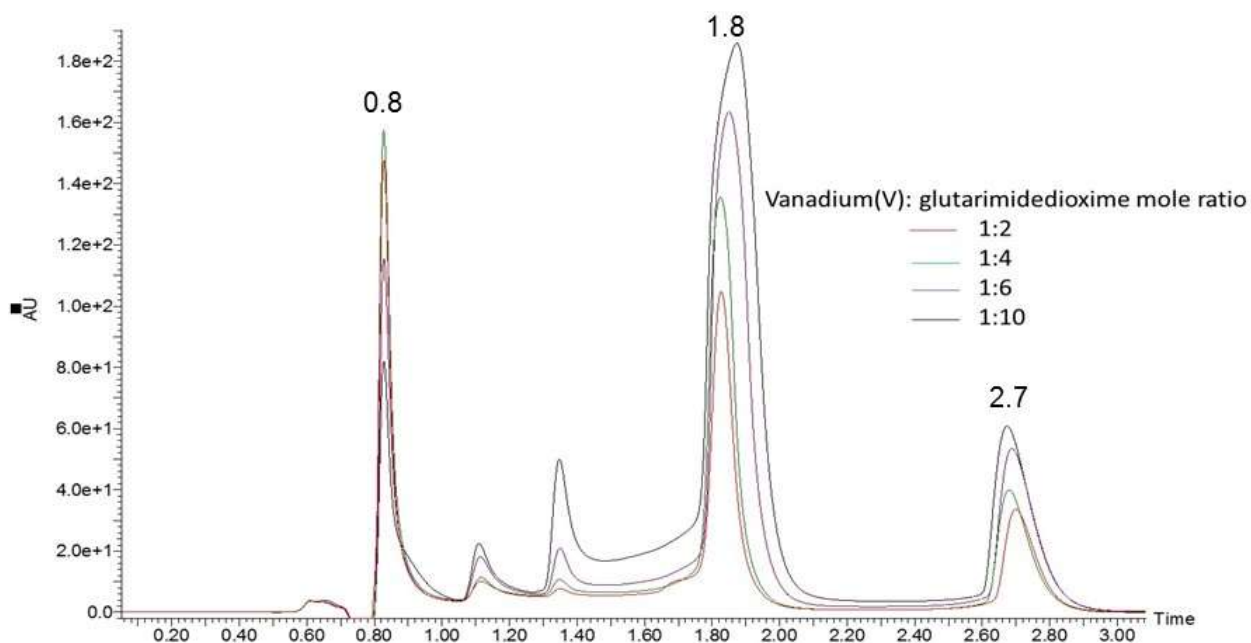


Figure 3.54 Chromatogram acquired from solutions containing 0.5 mM vanadium(V) and varying concentrations of glutarimidedioxime. The vanadium(V):glutarimidedioxime molar ratio of 1:2, 1:4, 1:6, and 1:10 were used in this study. All samples in 0.05 M NaCl aqueous solution at pH 8.3.

3.5 Conclusions

The solution phase complexes of UO_2^{+2} , VO_2^+ , and VO^{+2} with amidoxime ligands glutarimidedioxime and open-chain glutardiamidoxime were characterized using NMR, UV-Visible, and ESI-MS spectroscopy. The effect of changes in metal and ligand concentration, metal/ligand mole ratio, and solution pH on UO_2^{+2} -amidoxime, VO_2^+ -amidoxime, and VO^{+2} -amidoxime, solution phase complexes was also investigated. Glutarimidedioxime and open-chain glutardiamidoxime are the main complexing agents in the adsorbent used for uranium extraction from sea water.

Results from NMR spectroscopy show the formation of 1:1, vanadium(V)-glutarimidedioxime complex at low vanadium concentration of 0.2 mM. The 1:1

vanadium(V)-glutarimidedioxime complex is stable and forms immediately. However, the formation of 1:2, vanadium(V)-glutarimidedioxime complex is time and concentration dependent. Formation of 1:2, vanadium(V)-glutarimidedioxime complex requires a minimum of 4 days, and high vanadium(V) concentration (0.5 mM), for its detection using ^{51}V NMR spectroscopy. Results from ^1H NMR spectroscopy shows the formation of 1:1 UO_2^{+2} -glutarimidedioxime and UO_2^{+2} -glutardiamidoxime complexes at pH 3.4. Results from ^{13}C NMR spectroscopy indicates that carbonate stabilizes UO_2^{+2} -glutardiamidoxime complex, at pH 8, may be by forming a stable UO_2^{+2} -(glutardiamidoxime) $_2$ carbonate complex²¹. The formation of 1:2 UO_2^{+2} -glutarimidedioxime complex at low concentrations of UO_2^{+2} (0.05 mM) and glutarimidedioxime (0.1 mM) was observed using UV-Visible spectroscopy.²

The nature of glutarimidedioxime coordination with UO_2^{+2} was different from open-chain glutardiamidoxime. The CH_2 's [$-\text{CH}_2-\text{CH}_2-\text{CH}_2-\text{C}=\text{NOH}$] of glutarimidedioxime remain equivalent upon complexation with UO_2^{+2} . A triplet for two equivalent CH_2 's [$-\text{CH}_2-\text{CH}_2-\text{CH}_2-\text{C}=\text{NOH}$], and a quintet for a CH_2 [$-\text{CH}_2-\text{CH}_2-\text{CH}_2-$] was observed in the ^1H NMR spectrum of complexed glutarimidedioxime. UO_2^{+2} -glutarimidedioxime complex was formed within 24 hours. However, it took a minimum of 4 to 7 days to observe open-chain glutardiamidoxime complex with UO_2^{+2} . Glutarimidedioxime binds to UO_2^{+2} more effectively than open-chain glutardiamidoxime forming a tridentate complex with UO_2^{+2} binding via the oxime oxygens and imide nitrogen.² In the chemical structure of open-chain glutardiamidoxime, the two amidoxime groups are separated by 4 C-C bonds; hence, it is less effective for UO_2^{+2} coordination. Open-chain glutardiamidoxime binds with UO_2^{+2} in such a way that the three CH_2 's become non-equivalent upon complexation with UO_2^{+2} . Three different ^1H NMR signals for each CH_2 [$-\text{CH}_2-\text{CH}_2-\text{CH}_2-$] was observed. This

observation suggests that glutardiamidoxime may be binding through only one side of the two oxime oxygens and may be binding with UO_2^{+2} through η^2 coordination to the N–O bond.⁴⁴

It is important to study VO_2^+ , and VO^{+2} complexation with glutarimidedioxime and open-chain glutardiamidoxime to understand the effect of vanadium, on solution phase complexes of UO_2^{+2} with amidoxime ligands. It was observed that UO_2^{+2} -glutarimidedioxime complex was less likely to form in the presence of VO_2^+ because VO_2^+ -glutarimidedioxime complex has more stable configuration, and VO_2^+ has higher affinity for glutarimidedioxime than UO_2^{+2} .

Uranyl and VO_2^+ bind to glutarimidedioxime by different coordination modes. Different values of chemical shifts were observed for VO_2^+ -glutarimidedioxime and UO_2^{+2} -glutarimidedioxime complex in the ^1H NMR spectra. High concentrations of VO_2^+ ~1.6 ppb in sea water suggests that it will outcompete UO_2^{+2} , and reduce UO_2^{+2} binding sites on the adsorbent. UV–Visible studies on solutions containing VO^{+2} -glutarimidedioxime in presence of UO_2^{+2} shows formation of 1:2, UO_2^{+2} -glutarimidedioxime complex in the presence of VO^{+2} . However, the formation of 1:2, UO_2^{+2} -glutarimidedioxime complex was not observed in the presence of VO_2^+ . Both VO^{+2} and VO_2^+ were observed to form complex with glutarimidedioxime. However, both of them do not form complex with open-chain glutardiamidoxime. UO_2^{+2} forms complex with both glutarimidedioxime and open-chain glutardiamidoxime.

References

1. Wang, D.; Wilhelmy, S.A.S. Vanadium speciation and cycling in coastal waters. *Marine Chemistry*. **2009**, *117* (1-4), 52-58.
2. Tian, G.X.; Teat, S.J.; Zhang, Z.Y.; Rao, L.F. Sequestering uranium from seawater: binding strength and modes of uranyl complexes with glutarimidedioxime. *Dalton Transactions*. **2012**, *41* (38), 11579-11586.
3. Tian, G.X.; Teat, S.J.; Rao, L.F. Thermodynamic studies of U(VI) complexation with glutardiamidoxime for sequestration of uranium from seawater. *Dalton Transactions*. **2013**, *42* (16), 5690-5696.
4. Pan, H.B.; Kuo, L.J.; Wai, C.M.; Miyamoto, N.; Joshi, R.; Wood, J.R.; Strivens, J. E.; Janke, C.J.; Oyola, Y.; Das, S.; Mayes, R.T.; Gill, G.A. Elution of Uranium and Transition Metals from Amidoxime-Based Polymer Adsorbents for Sequestering Uranium from Seawater. *Industrial & Engineering Chemistry Research*. **2016**, *55* (15), 4313-4320.
5. Heath, E.; Howarth, O.W. ^{51}V and ^{17}O Nuclear magnetic resonance study of vanadate(V) equilibria and kinetics. *J. Chem. Soc., Dalton Trans.* **1981**, (5), 1105-1110.
6. Rehder, D.; Polenova, T.; Buhl, M. Vanadium-51 NMR. *Annual Reports on Nmr Spectroscopy*. **2007**, *62*, 49-114.
7. Sadoc, A.; Messaoudi, S.; Furet, E.; Gautier, R.; Le Fur, E.; Le Polles, L.; Pivan, J. Y. Structure and stability of VO_2^+ in aqueous solution: A car-parrinello and static ab initio study. *Inorganic Chemistry*. **2007**, *46* (12), 4835-4843.
8. Mustapha, A.M.; Pasilis, S.P. Probing uranyl(VI) speciation in the presence of amidoxime ligands using electrospray ionization mass spectrometry. *Rapid Communications in Mass Spectrometry*. **2013**, *27* (19), 2135-2142.

9. Mustapha, A.M.; Pasilis, S.P. Gas-phase complexes formed between amidoxime ligands and vanadium or iron investigated using electrospray ionization mass spectrometry. *Rapid Communications in Mass Spectrometry*. **2016**, *30* (15), 1763-1770.
10. Greenwood, N. N.; Earnshaw, A. *Chemistry of the Elements*, 2nd ed.; Butterworth-Heinemann: Oxford, 1997.
11. Cotton, F. A.; Wilkinson, G.; Murillo, C.A.; Bochmann, M. *Advanced Inorganic Chemistry*, 6th ed.; Wiley: New York, 1999.
12. Pope, M.T.; Muller, A. Polyoxometalate chemistry- an old field with new dimensions in several disciplines. *Angewandte Chemie-International Edition in English*. **1991**, *30* (1), 34-48.
13. Bouhedja, L.; Steunou, N.; Maquet, J.; Livage, J. Synthesis of polyoxovanadates from aqueous solutions. *Journal of Solid State Chemistry*. **2001**, *162* (2), 315-321.
14. Leggett, C.J.; Parker, B.F.; Teat, S.J.; Zhang, Z.; Dau, P.D.; Lukens, W.W.; Peterson, S.M.; Cardenas, A.J.P.; Warner, M.G.; Gibson, J.K.; Arnold, J.; Rao, L.F. Structural and spectroscopic studies of a rare non-oxido V(V) complex crystallized from aqueous solution. *Chemical Science*. **2016**, *7* (4), 2775-2786.
15. Manoussakis, G.; Kouimtzis, T. Study on complexes of Fe^{3+} , Cu^{2+} and UO_2^{2+} with benzanilidoxime. *J. Inorg. Nucl. Chem.* **1969**, *31* (12), 3851.
16. Hirotsu, T.; Katoh, S.; Sugasaka, K.; Seno, M.; Itagaki, T. Binding ability of acetamide oxime with proton, copper(II) and dioxouranium(VI) in aqueous solutions. *Journal of the Chemical Society, Dalton Transactions*. **1986**, (8), 1609-1611.

17. Kim, S.Y.; Harada, M.; Tomiyasu, H.; Ikeda, Y.; Park, Y.Y. Structure and kinetic studies of U(VI)-benzamidoxime complex in non-aqueous solutions by ^1H and ^{13}C NMR. *Progress in Nuclear Energy*. **2000**, *37* (1-4), 399-404.
18. Endrizzi, F.; Melchior, A.; Tolazzi, M.; Rao, L.F. Complexation of uranium(VI) with glutarimidodioxime: thermodynamic and computational studies. *Dalton Transactions*. **2015**, *44* (31), 13835-13844.
19. Muller, K.; Brendler, V.; Foerstendorf, H. Aqueous uranium(VI) hydrolysis species characterized by attenuated total reflection fourier-transform infrared spectroscopy. *Inorganic Chemistry*. **2008**, *47*, 10127-10134.
20. Davies, R.V.; Kennedy, J.; Hill, K.M.; McIlroy, R.W.; Spence, R. Extraction of uranium from seawater. *Nature*. **1964**, *203* (495), 1110.
21. Pan, H.B.; Liao, W.; Wai, C.M.; Oyola, Y.; Janke, C.J.; Tian, G.X.; Rao, L.F. Carbonate- H_2O_2 leaching for sequestering uranium from seawater. *Dalton Transactions*. **2014**, *43* (28), 10713-10718.
22. Xian, L.; Tian, G.X.; Beavers, C.M.; Teat, S.J.; Shuh, D.K. Glutarimidedioxime: A Complexing and Reducing Reagent for Plutonium Recovery from Spent Nuclear Fuel Reprocessing. *Angewandte Chemie-International Edition*. **2016**, *55* (15), 4671-4673.
23. Britton, H.T.S. Physicochemical studies of complex acids Part XIII. The constitution of quinquevalent and quadrivalent vanadium solutions; with a note on their respective reduction and oxidation. *Journal of the Chemical Society*. **1934**, 1842-1846.
24. Baran, E.J. Oxovanadium(IV) and oxovanadium(V) complexes relevant to biological systems. *Journal of Inorganic Biochemistry*. **2000**, *80* (1-2), 1-10.

25. Hassler, C.S.; Alasonati, E.; Nichols, C.A.M.; Slaveykova, V.I. Exopolysaccharides produced by bacteria isolated from the pelagic Southern Ocean - Role in Fe binding, chemical reactivity, and bioavailability. *Marine Chemistry*. **2011**, *123* (1-4), 88-98.
26. Gutierrez, T.; Biller, D.V.; Shimmield, T.; Green, D.H. Metal binding properties of the EPS produced by *Halomonas* sp. TG₃₉ and its potential in enhancing trace element bioavailability to eukaryotic phytoplankton. *Biometals*. **2012**, *25* (6), 1185-1194.
27. Gessa, C.; De Cherchi, M.L. The Reduction of Fe(III) to Fe(II) and V(V) to V(IV) by polygalacturonic acid: a Reduction and Complexation Mechanism of Biochemical Significance. *Inorganica Chimica Acta*. **1983**, *80*, L53-L55.
28. Sreedhara, A.; Susa, N.; Patwardhan, A.; Rao, C.P. One electron reduction of vanadate(V) to oxovanadium(IV) by low-molecular-weight biocomponents like saccharides and ascorbic acid: Effect of oxovanadium(IV) complexes on pUC18 DNA and on lipid peroxidation in isolated rat hepatocytes. *Biochemical and Biophysical Research Communications*. **1996**, *224* (1), 115-120.
29. Bisconti, L.; Pepi, M.; Mangani, S.; Baldi, F. Reduction of vanadate to vanadyl by a strain of *Saccharomyces cerevisiae*. *Biometals*. **1997**, *10* (4), 239-246.
30. Oltz, E.M.; Bruening, R.C.; Smith, M.J.; Kustin, K.; Nakanishi, K. The tunichromes a class of reducing blood pigments from sea squirts isolation, structures and vanadium chemistry. *Journal of the American Chemical Society*. **1988**, *110* (18), 6162-6172.
31. Kutter, V.; Montes-Bayon, M.; Sella, S.M.; Sanz-Medel, A.; Silva-Filho, E. Vanadium-Binding Protein in Marine Plankton from Tropical South Atlantic Ocean. *Journal of the Brazilian Chemical Society*. **2014**, *25* (6), 1116-1123.

32. Michibata, H.; Morita, A.; Kanamori, K. Vanadobin a vanadium-binding substance, extracted from the blood-cells of an ascidian, can reduce vanadate(V) to vanadyl(IV). *Biological Bulletin*. **1991**, *181* (1), 189-194.
33. Coetzee, P.P.; Fischer, J.L.; Hu, M.S. The separation and simultaneous determination of V(IV) and V(V) species complexed with EDTA by IC-ICP-OES. *Water SA*. **2002**, *28* (1), 37-44.
34. Komarova, T.V.; Obrezkov, O.N.; Shpigun, O.A. Ion Chromatographic behavior of anionic EDTA complexes of Vanadium(IV) and Vanadium(V). *Analytica Chimica Acta*. **1991**, *254*, 61-63.
35. Ferrer, E.G.; Baran, E.J. Reduction of Vanadium(V) with ascorbic acid and isolation of the generated oxovanadium(IV) species. *Biological Trace Element Research*. **2001**, *83* (2), 111-119.
36. Mishra, A.P.; Khan, R.; Pandey, R.R. Kinetic studies on effects of EDTA and surfactants on reduction of vanadium(V) to vanadium(IV) in sulphuric acid medium. *Indian Journal of Chemistry, Section A*. **2009**, *48*, 1228-1234.
37. Sasaki, Y.; Okazaki, K.; Nagasawa, A.; Saito, K.; Kanamoto, M. Kinetics of the oxidation of an ethylenediaminetetraacetate complex of the oxovanadium(IV) ion with hexachloroiridate(IV) in aqueous solution. *Inorganic Chemistry*. **1985**, *24* (5), 772-775.
38. Dessi, A.; Micera, G.; Sanna, D. EPR investigation of the oxovanadium(IV) complexes formed by the tripeptide glutathione and some related ligands in aqueous solution. *Journal of Inorganic Biochemistry*. **1993**, *52* (4), 275-286.

39. Soshnikov, I.E.; Semikolenova, N.V.; Shubin, A.A.; Bryliakov, K.P.; Zakharov, V. A.; Redshaw, C.; Talsi, E.P. EPR Monitoring of Vanadium(IV) Species Formed upon Activation of Vanadium(V) Polyphenolate Precatalysts with AlR_2Cl and AlR_2Cl /Ethyltrichloroacetate ($\text{R} = \text{Me}, \text{Et}$). *Organometallics*. **2009**, 28 (23), 6714-6720.
40. Sanna, D.; Sciortino, G.; Ugone, V.; Micera, G.; Garribba, E. Nonoxido V(IV) Complexes: Prediction of the EPR Spectrum and Electronic Structure of Simple Coordination Compounds and Amavadin. *Inorganic Chemistry*. **2016**, 55 (15), 7373-7387.
41. Islam, M.K.; Tsuboya, C.; Kusaka, H.; Aizawa, S.; Ueki, T.; Michibata, H.; Kanamori, K. Reduction of vanadium(V) to vanadium(IV) by NADPH, and vanadium(IV) to vanadium(III) by cysteine methyl ester in the presence of biologically relevant ligands. *Biochimica Et Biophysica Acta-General Subjects*. **2007**, 1770 (8), 1212-1218.
42. Rao, G.G.; Somidevamma, G. Studies in uranium(VI) complexes with organic ligands. *Z.Anal.Chem.* **1957**, 157, 1-27.
43. Mishra, A.P.; Khan, R.; Pandey, R.R. Biological aspects kinetic analysis of the vanadium(V) to vanadium(IV) by EDTA in sulphuric acid medium. *National Academy Science Letters-India*. **2010**, 33(5-6), 149-152.
44. Vukovic, S.; Watson, L.A.; Kang, S.O.; Custelcean, R.; Hay, B.P. How Amidoximate Binds the Uranyl Cation. *Inorganic Chemistry*. **2012**, 51 (6), 3855-3859.

Chapter 4: Spectroscopic Characterization of Amidoxime Based Polymer Adsorbents and Probing Vanadium Adsorption by ICP-MS

4.1 Abstract

Polymer adsorbents containing amidoxime functional groups have been widely used since the 1980's for uranium extraction from seawater because of their uranophilicity. A novel amidoxime functionalized "LCW" adsorbent material was prepared using polyacrylic fiber as starting material. The LCW adsorbent mainly contains open-chain glutardiamidoxime. Design and development strategies for the LCW adsorbent was based to have low vanadium adsorption, thereby resulting in efficient uranium chelation. This adsorbent is durable and requires no KOH conditioning for its reuse. This chapter describes and compares vanadium adsorption capacity of the LCW adsorbent synthesized in our lab and the ORNL-AF1 adsorbent produced at the Oak Ridge National Laboratory. ^{13}C CP/MAS (Cross-polarization with Magic Angle Spinning), solid state NMR, and fourier transform infrared (FTIR) spectroscopy were used for the characterization of these adsorbents. ^{13}C CP/MAS spectroscopy was used to confirm the formation of glutarimidedioxime, and glutardiamidoxime in the synthesized adsorbents. ^{51}V solid state NMR spectroscopy was used to characterize sodium orthovanadate. Inductively coupled plasma mass spectrometry (ICP-MS) was used to evaluate vanadium adsorption efficiency of these adsorbents in simulated seawater experiments, with vanadium concentration of 10 ppm at pH of 8.3-8.5. LCW adsorbent showed lower vanadium (10.3 mg vanadium/g of adsorbent) adsorption capacity than ORNL-AF1 adsorbent, which showed higher vanadium (63.3 mg vanadium/g of adsorbent) adsorption capacity in 24 hours.

4.2 Introduction

Development and evaluation of various amidoxime-based polymer adsorbents for uranium extraction from seawater has been attracting a lot of interest for decades because of the importance of uranium required for nuclear power generation. Solid state NMR (SSNMR) spectroscopy is a very useful technique for characterization and examination of powdered or crystalline chemical compounds, interactions in different polymers, solid state inorganic, and biological materials. Solid state NMR technique helps in studying the structural environment of polymers which are insoluble in commonly used aprotic solvents, such as dimethyl sulfoxide (DMSO), acetone, and N-N dimethylformamide (DMF). Chemical shift observed for different nuclei provides valuable information about the structure and coordination environment of the molecule. The first NMR experiments on condensed material were carried out by Gorter et al.¹ in 1936. Lithium nuclei were studied using crystalline lithium fluoride, but the experiments were unsuccessful. Later in 1945, Purcell et al.² at Harvard University conducted the first successful NMR experiment on solid paraffin wax. NMR signals for protons present in paraffin wax were observed. The key feature of solid state NMR is that, spin interactions are anisotropic, change in sample orientation, changes spin interactions; hence, the NMR spectrum changes as well. In liquids, the orientation dependent interactions are averaged to zero by tumbling of molecules experiencing different molecular orientations with equal probability. Therefore, for liquid sample, the method of NMR tube placement does not matter. Due to this averaging, the acquisition of solution state NMR spectra is more simple and straightforward than solid state NMR. The environment of molecule in solid state is very different from solution state. In a crystal, the environment of each molecule depends upon crystal structure and its symmetry. However, in solution the molecules are surrounded by

solvent, creating a random environment. In a powdered sample, molecules orient in different directions, giving a broad NMR signal with reduced intensity. The NMR signal is the sum of signals from each crystallite in powder form, and superimposition of these different NMR frequencies gives rise to a pattern called “powder pattern”.

In Chapter 3, interactions of vanadium and uranium with glutarimidedioxime and glutardiamidoxime were studied in solution state using NMR spectroscopy. However, in this chapter, a newly developed amidoxime-carboxylate containing LCW adsorbent is characterized using solid state NMR spectroscopy. The method development for synthesis of this adsorbent is still under development. In solid fiber, the molecules are fixed with no random motion. Hence, the fiber possesses unique structural-adsorption characteristics. Solid state NMR provides a novel approach for characterization of polymer adsorbents that are used to extract uranium from seawater. The information and knowledge gained from spectroscopic results of this technique will aid in the development of efficient, robust, and cost effective adsorbents. Designing uranyl selective adsorbents with high uranium adsorption capacity and developing cost effective and efficient uranium elution techniques is a research subject of considerable interest to the U.S. Department of Energy at the present time. In the last 4 years (2012-2016), there has been a significant increase in uranium adsorption capacity. The adsorption capacity has increased from 3.30 g U/kg of adsorbent to ~6.56 g U/kg of adsorbent, by the best adsorbent tested so far. The LCW adsorbent shows high uranium uptake of 5 – 6 g U/kg of adsorbent in a 56-day exposure to seawater.³ The LCW adsorbent shows low V/U ratio of ~1.0 because it mainly contains open-chain glutardiamidoxime. Compared to cyclic glutarimidedioxime, open-chain glutardiamidoxime does not form complex with vanadium(V) as described in Chapter 3. Uranium extraction from seawater using LCW

adsorbent, will decrease vanadium(V) competition for binding sites on adsorbent, enhancing its UO_2^{+2} adsorption capacity. The ORNL-AF1 (Oak Ridge National Laboratory) adsorbent shows high V/U ratio of ~ 3.0 because this adsorbent mainly contains cyclic glutarimidedioxime (Figure 4.10a) possessing higher vanadium affinity than open-chain glutardiamidoxime. High vanadium adsorption by the ORNL-AF1 adsorbent decreases its UO_2^{+2} extraction efficiency. The ORNL-AF1 adsorbent requires KOH conditioning to make it effective for sequestering uranium from seawater. However, no KOH conditioning is necessary for the LCW adsorbent. Among different adsorbents tested for uranium adsorption capacity, LCW adsorbent reached half saturation in about half of the time taken by other adsorbents. This suggests that the LCW adsorbent shows fast uranium uptake and reaches equilibrium faster compared to other adsorbents. Fast uranium uptake at lesser seawater exposure time will cause less biofouling on this adsorbent, resulting in increased uranium adsorption capacity, effective uranium elution, and increased adsorbent reusability. Development of adsorbents with high uranium adsorption capacity is important for cost-effective uranium extraction from seawater. Solid state NMR has proven to be a very useful tool for characterization of vanadium containing materials.⁴⁻⁸ However, challenges are involved in using solid state NMR technique for understanding vanadium adsorption by polymer adsorbents. Low concentration of adsorbed vanadium may not be detected by using this technique. Understanding vanadium adsorption will require an adsorbent saturated with vanadium because high concentration of vanadium may show a peak in the ^{51}V solid state NMR spectrum. Different batches of LCW adsorbent after metal uptake will be required to fill the rotor for solid state NMR analysis. This will lead to inaccurate sampling and may

introduce uncertainty. The basic principles and applications of solid state NMR spectroscopy are introduced in sections below.

4.2.1 *Type of interactions in solid state NMR*

In section 4.2.1, basic principles of solid state NMR spectroscopy are introduced. Various interactions in solid state NMR includes Zeeman interaction, radiofrequency interaction, quadrupolar interaction, chemical shielding anisotropy, dipolar interaction, J coupling, and spin rotation interaction. Out of all NMR interactions, Zeeman and radiofrequency interactions are external interactions. However, all other interactions are internal interactions because they originate in sample itself. Out of all NMR interactions, J coupling and spin rotation interaction affect the solid NMR spectrum to a very little extent because they are the smallest interactions.⁹

a) Zeeman interaction

Zeeman interaction is the largest interaction out of all NMR interactions.⁹ It is a direct interaction between nuclear spin, and magnetic field (B_0) along z axis.

b) Radiofrequency interaction

This is an external interaction. It is the interaction of the nucleus with the radiofrequency field.⁹ The radiofrequency field is generally chosen along x axis while the magnetic field is along the z axis.

c) Quadrupolar interaction

Quadrupolar interaction involves interaction of nuclear spin with electric field gradient (EFG). This interaction is electronic in origin, whereas other interactions are magnetic in nature. Quadrupolar nuclei are nuclei with spin $> \frac{1}{2}$.⁹ The electric charge distribution in the nucleus of a quadrupolar nuclei is non spherical. This gives rise to an electric quadrupole

moment.¹⁰ Interaction of electric quadrupole moment with electric field gradient (EFG) is called quadrupolar interaction which intensely effects the NMR spectrum.¹¹ Spin energy levels are affected by quadrupolar interaction depending upon the magnitude of quadrupole moment and the strength of electric field gradient (EFG). Nuclei with spin 1/2 are spherically symmetric, and for such nuclei, the quadrupolar interaction is zero. Based on quadrupolar frequency, there are two types of quadrupolar interactions: first order quadrupolar interactions and second order quadrupolar interactions.¹² The first order quadrupolar interactions give rise to shift in transitions and shifts the signal to a broad range of frequency. The first order quadrupolar interactions are averaged to zero by magic angle spinning.⁹ However, second order quadrupolar interactions are not averaged to zero by magic angle spinning and lead to quadrupolar line broadening. Effects of second order quadrupolar splitting for nuclei with smaller coupling constant can be reduced by several techniques, such as dirotation, variable angle spinning, dynamic angle spinning, and multiple quantum magic angle spinning (MQMAS).^{9, 11, 13}

d) Chemical shielding interaction

The interaction of electrons surrounding the nucleus with magnetic field is called chemical shielding. The nucleus is surrounded by electrons, which results in a secondary field, called the induced field. The induced field contributes to the total effective field felt at the nucleus because the net magnetic field experienced by the nucleus is the total of the applied magnetic field and the induced magnetic field, $[B_{\text{total}} = B_{\text{applied}} + B_{\text{induced}}]$. The magnetic field produced by circulation of electrons surrounding the nucleus (the induced field) leads to a shielding interaction.¹⁴ The shift of the sample relative to the reference material due to the total magnetic field felt at the nucleus is called chemical shift.¹⁴

e) Dipolar interaction

The interaction between two nuclear spins is called dipolar coupling. Each of the nuclear spins generates a magnetic field. The magnetic field generated by the first nuclear spin is experienced by the second nuclear spin and vice versa. In liquid samples, the dipolar coupling is not observed because the samples are tumbling isotropically. However, in solid samples the dipolar coupling is the main source of line broadening.^{9, 12, 14}

4.2.2 Techniques used in solid state NMR

a) Magic Angle Spinning (MAS)

The most common technique used in solid state NMR spectroscopy is called magic angle spinning. This technique was first introduced by Andrew and Lowe.^{15, 16} During magic angle spinning, the sample is placed in a rotor and is rotated rapidly at an angle of 54.74° (magic angle), relative to the axis of external magnetic field, as shown in Figure 4.1.¹⁴ The NMR spectrum of a powdered sample is a broad line due to anisotropic interactions, such as the quadrupolar interaction present in the quadrupolar nuclei, dipolar coupling, and the chemical shielding anisotropy. Nuclei in different orientations give different transition frequencies, which give rise to a broad signal. The technique of magic angle spinning was invented to remove magnetic shift anisotropy. Mathematical expression for the angular dependence of anisotropic interactions is represented by $3\cos^2\theta - 1$. The angle θ represent different orientations of the quadrupolar tensor, dipolar interaction tensor, and the chemical shift tensor. At the magic angle, this expression is averaged to zero,^{9, 14} thus averaging out various anisotropic interactions and giving a single peak resembling the peak as observed for solution state NMR. Averaging of anisotropic interactions also depends upon the rotation

frequency. High frequency of sample rotation or high spinning rate is required for complete averaging of anisotropic interactions, and mitigation of quadrupolar broadening.¹²

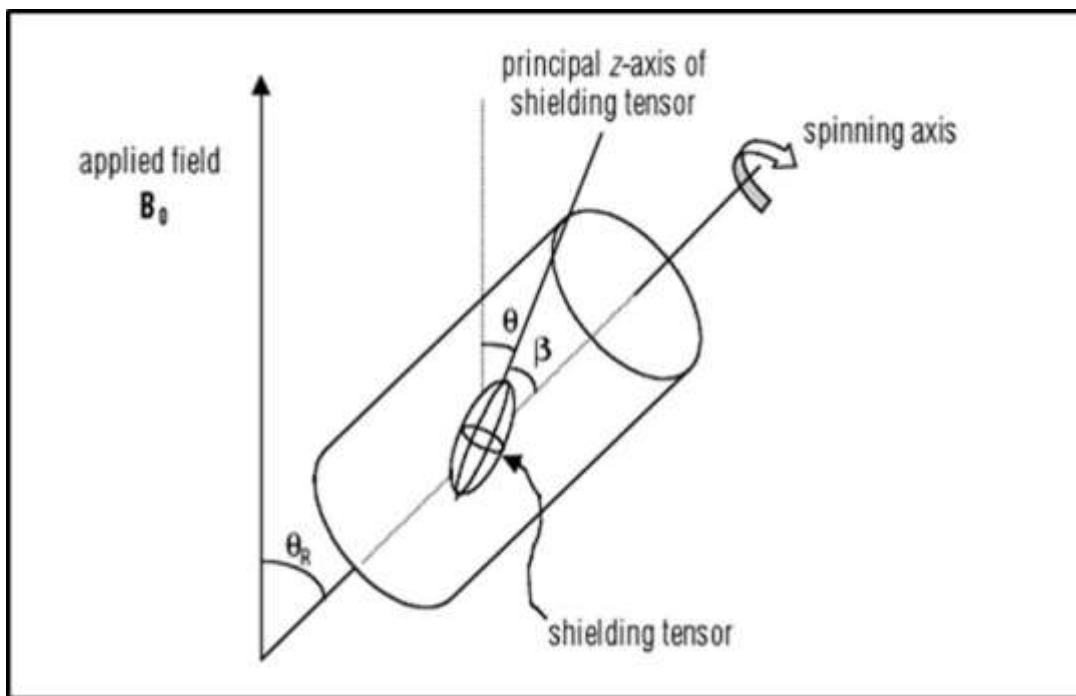


Figure 4.1 Geometry of sample showing magic angle ($\beta = 54.74^\circ$) with respect to the applied magnetic field. (Figure adapted from reference 14)

b) Cross-polarization with magic angle spinning (CP/MAS) NMR

Cross-polarization with the magic angle spinning technique (CP/MAS) was first introduced by Pines et al.¹⁷ Hartmann and Hahn¹⁸ developed the theory of cross-polarization. The nuclei with low natural abundance, e.g. ^{13}C and ^{15}N , are called dilute nuclei in NMR.¹² In such nuclei, the homonuclear dipole-dipole interactions are absent. Therefore, such nuclei have a very long spin lattice relaxation time (T_1).^{12, 14} Such nuclei are less sensitive due to their low net polarization. It takes a very long time to acquire solid state NMR spectra for such nuclei. Cross-polarization with magic angle spinning technique (CP/MAS) solves the problem of acquiring NMR spectrum of dilute spins with long relaxation time. This technique enhances

weak signals obtained from dilute nuclei. In solid state NMR when both abundant and dilute nuclei are present, the technique of polarization transfer is applied for signal enhancement of dilute nuclei. The steps include excitation of the abundant ^1H nuclei, followed by polarization transfer to dilute ^{13}C nuclei, and proton decoupling during the process of data acquisition. Polarization transfer from abundant, ^1H nuclei to dilute, ^{13}C nuclei is done via dipolar interaction.^{12, 14} Hence, for polarization transfer the two nuclei must have dipolar interaction. The cross polarization time depends upon the strength of ^1H - ^{13}C dipolar interaction.

4.2.3 *Advantages and drawbacks of using solid state NMR*

Solid state NMR is an advanced and full-fledged technique used for characterization of solid compounds. It is a well-established technique for characterization of pharmaceutical compounds, such as cimetidine, an active pharmaceutical agent present in the drug with the brand name Tagamet, that show polymorphism.¹⁹ It is not possible to get appropriate crystals for such compounds; hence, traditionally used XRD (X-ray diffraction) technique can't be used for their characterization.¹⁹ Solid state NMR spectroscopy provides structural information and is used for examining short range atomic environment. However, XRD technique provides structural information from medium to long range atomic order and has drawbacks in examination of local interactions and the interactions involving elements like hydrogen.^{20, 21} Sometimes in the analysis using X-ray diffraction technique, inappropriate information about molecular structure can be obtained due to peak overlap in the diffraction pattern.²² In such cases, solid state NMR spectroscopy provides more accurate structural information. X-ray diffraction technique provides valuable information about the dimension and space group, but calculations for atomic positions are time consuming and complicated. Solid state NMR spectroscopy provides valuable information for the molecules that do not

form crystals; it is nucleus specific, nondestructive, and non-invasive. However, drawbacks of using solid state NMR include analysis cost, longer analysis time, challenging automation, and expertise for proper usage.

4.2.4 *Applications of solid state NMR*

Solid state NMR spectroscopy is used as an excellent means for examining molecular structures of crystalline materials,^{23, 24} noncrystalline materials, and insoluble chemical compounds. It provides valuable information about the intra and intermolecular motions, local symmetry, and bond character.²¹ Results from this technique are sometimes compared with the results from other conventional techniques, such as single-crystal XRD and powder XRD. This helps to get deeper insights on structural properties of polycrystalline organic materials. Therefore, this technique aids in the refinement of results obtained from other techniques.²⁵ In most cases, results from solid state NMR spectroscopy agree with the results from other techniques. Solid-state NMR technique is mostly used for probing the structures and coordination environments of polymers,²⁶⁻²⁸ self-assembled monolayers (SAMs),²⁹ support materials, heterogeneous catalysts,³⁰ zeolitic materials,^{28, 31} glasses,^{28, 32, 33} biological materials,^{28, 34-36} and mesoporous composite materials.^{37,38}

4.3 **Experimental**

4.3.1 *Chemicals and reagents*

Deionized (DI) water was used for the preparation of different samples, such as 1:1(v/v) methanol/water solution containing about 3 wt% to 6 wt% hydroxylamine and 1M NaOH solution. Sodium orthovanadate, Na₃VO₄ (99%), was purchased from Acros Organics, a Fisher Scientific brand (NJ, USA). Sodium hydroxide (ACS grade), Potassium hydroxide

(ACS grade), and NaCl (ACS grade) were purchased from EMD Chemicals (Gibbstown, NJ, USA). Sodium bicarbonate (NaHCO_3 , ACS Reagent, Aldrich) was used to prepare simulated seawater solution. A 1000 ppm vanadium standard solution used for the preparation of ICP standards, hydroxylamine, and methanol were obtained from Sigma-Aldrich. All chemicals were used as received.

4.3.2 Instrumentation

Solid-state ^{51}V NMR and ^{13}C NMR spectra were acquired on a Bruker Avance NMR spectrometer operating at 500 MHz. In general, ~ 100 mg of sample was loaded into a 4 mm o.d. Si_3N_4 rotor. For each compound, the ^{51}V NMR and the ^{13}C NMR spectra were acquired at several spinning frequencies between 8 and 11 kHz. The spinning frequencies were controlled within ≤ 5 Hz. The chemical shifts of vanadium were referenced to neat VOCl_3 as an external standard. The ^{13}C chemical shifts were referenced using adamantane as an external standard. Magic angle was set by maximizing number of rotational echoes observed in the ^{79}Br NMR free induction decay of solid KBr. Vanadium MAS spectra were acquired using single pulse excitation. A short 1.5 μs pulse was used for vanadium to excite central transitions. For ^{13}C NMR, cross polarization technique was used. Recycle delay time of 10 seconds was used. A total of ~ 4000 complex data points were acquired. Data was processed by fourier transformation. Mestre-nova NMR data processing software was used for baseline correction. ICP-MS was used to study vanadium adsorption by LCW adsorbent in simulated seawater. A Nicolet Magna 760 fourier transform infrared (FTIR) spectrometer equipped with a deuterated triglycine sulfate (DTGS) detector was used for the acquisition of infrared spectra. A split beam attenuated total reflectance accessory (Harrick Scientific) was used for making FTIR measurements. A silicon internal reflection element was used as a reflection

medium. FTIR spectra were acquired using 500 coadded scans at 2 cm^{-1} resolution with Norton-Beer “medium” apodization function. The spectra were normalized to 1451.9 cm^{-1} peak to facilitate comparison.

4.3.3 *Sample preparation*

- a) Preparation of amidoxime and carboxylate containing ORNL-AF1 polymer adsorbent.

The information for the preparation of ORNL-AF1 polymer adsorbent is taken from Pan et al.³⁹ but is expressed in my own words. Radiation Induced Graft Polymerization (RIGP) method as shown in Figure 4.2 is used for the preparation of amidoxime-based ORNL-AF1 polymer adsorbent. Steps for this process are described below.

- i) Irradiation of polyethylene fibers.

The fibers were kept in a plastic bag and were sealed under nitrogen. The bag was then kept in an insulated container placed on top of dry ice. A dose of 200 kGy using 4.9 MeV electrons and a current of 1 mA was used for the irradiation of polyethylene fibers.

- ii) Grafting of polymerizable monomers containing nitrile, and hydrophilic groups.

A flask containing a previously de-gassed solution of acrylonitrile and methacrylic acid in dimethylsulfoxide was used to immerse the irradiated fibers. Immersed fibers were placed for about 18 hours in an oven at $65\text{ }^{\circ}\text{C}$. After completion of grafting reaction, fibers were taken out from the solution and were washed using dimethylformamide (DMF). To remove dimethylformamide, fibers were washed with methanol and were dried for 72 hours under vacuum at $50\text{ }^{\circ}\text{C}$.

iii) Conversion of nitrile groups to amidoxime groups.

10% hydroxylamine hydrochloride in 50/50 (w/w), water–methanol solution was used for conversion of nitrile groups to amidoxime groups. The irradiated fibers were kept in this solution at 80 °C for 72 hours. After this, the fibers were washed with DI water. The fibers were then rinsed with methanol and were dried at 50 °C under vacuum for 72 hours.

iv) Alkaline conditioning of grafted fibers.

The amidoximated fibers were immersed in a solution containing 2.5% KOH and heated at 80 °C for 20 minutes at the ratio of 0.5 ml KOH per mg of adsorbent. The fibers were washed with deionized water until the pH was neutral. The fibers were then immersed in deionized water, prior to vanadium adsorption experiments.

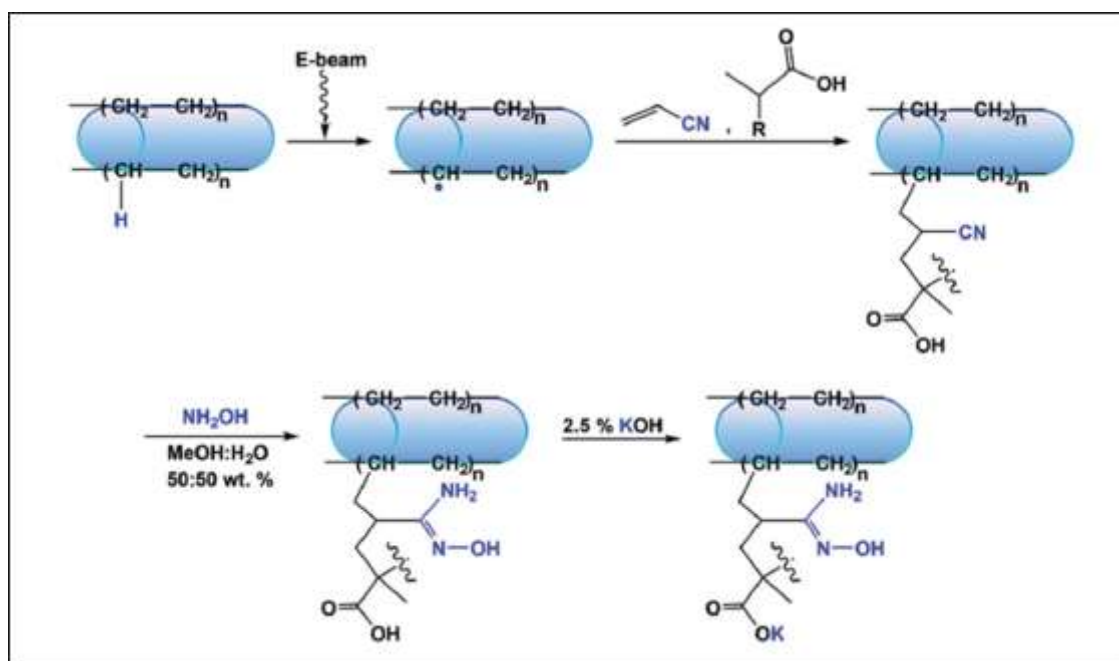


Figure 4.2 Reaction scheme for preparation of amidoxime-based ORNL-AF1 polyethylene fibers. (Figure adapted from reference 39)

b) Preparation of LCW adsorbents derived from acrylic fibers

Amidoxime-based LCW adsorbent fibers were prepared by Dr. Horng-Bin Pan according to the method as shown in Figure 4.3a-c. The acrylic fibers were cut into 4.2-4.5 cm pieces, each piece weighing ~25 mg. About 100 mg (4 pieces) of acrylic fibers were weighed. The fibers were then immersed in a vial containing 10 ml of 1:1(v/v) methanol/water solution containing about 3 wt% to 6 wt% hydroxylamine at room temperature. The vial containing fibers was sonicated for about 10 minutes followed by soaking for 24 hours at room temperature. After 24 hours, the vial (containing 100 mg of acrylic fibers in 10 ml of 1:1(v/v) methanol/water solution containing about 3 wt% to 6 wt% hydroxylamine) was heated at 70 °C (oil bath temperature 80 °C) for 30 minutes and 20 minutes for the fibers soaked in a solution containing 3 wt% hydroxylamine and 6 wt% hydroxylamine, respectively. This step is amidoximation step. After amidoximation, the vial was removed from the oil bath. The amidoximated fibers were removed from the vial and fibers were washed with DI water to remove residual hydroxylamine solution. The fibers were then stored in DI water. 10 ml of 1 M NaOH solution were prepared, and the amidoximated fibers were placed in this alkaline solution and left to sit for 24 hours (for fibers prepared using 3 wt% and 6 wt% hydroxylamine) at room temperature. After reaction, the fibers were removed from NaOH solution and were rinsed with DI water to remove residual NaOH. The fibers were then stored in DI water. The fibers were air dried before spectroscopic analysis.

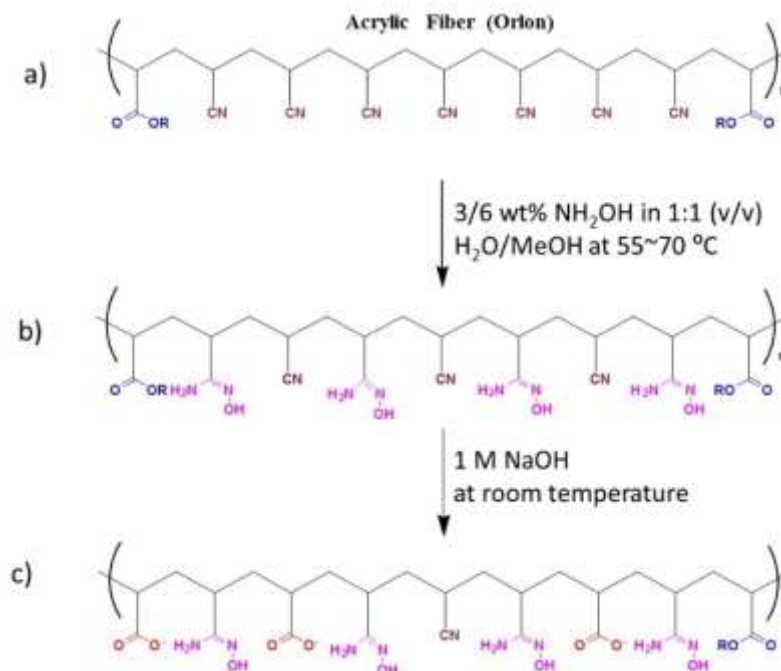


Figure 4.3 Chemical structure of (a) pure acrylic fiber, (b) amidoximated LCW adsorbent, and (c) alkaline treated LCW adsorbent. (From Horng-Bin Pan unpublished)

c) Preparation of samples for instrumental analysis

Figure 4.4 shows sample preparation accessories used for solid-state NMR spectroscopy. The sample was packed into a thick-walled rotor. Before sample filling the rotor surface was checked for scratches and roughness. The empty, undamaged rotor was placed inside the funnel, and this assembly was placed in a flat table surface. Small amount of sample was placed inside the funnel. A sample densification tool was used for densifying the sample in rotor by using gentle pressure. This process was repeated 4-5 times until the rotor was filled to a correct height. The filling height was checked, to ensure space for the cap. If more sample was required, the rotor was refilled with sample, using funnel and densification tool. The cap was then inserted into the rotor, ensuring no gap between cap and rotor. Using a black sharpie marker, half of the bottom edge of rotor was marked. The rotor was checked for cleanliness before inserting it into NMR spectrometer. The rotor was then inserted into the NMR

spectrometer for solid-state NMR analysis. For analysis using FTIR ~20 mg of the air-dried adsorbent was placed directly on silicon internal reflection element, and FTIR measurements were made. For analysis using ICP-MS, three standard solutions of 10 ppb, 50 ppb, and 100 ppb in 2% nitric acid solution were prepared from 1000 ppm vanadium standard. The blank solution and collected sample aliquots were diluted with 2% nitric acid solution to give final concentration of 92 ppb. The samples were then analyzed using ICP-MS spectrometry. Washouts using 2% nitric acid solution were monitored between the samples in order to ensure no vanadium was carried over into the next analysis.

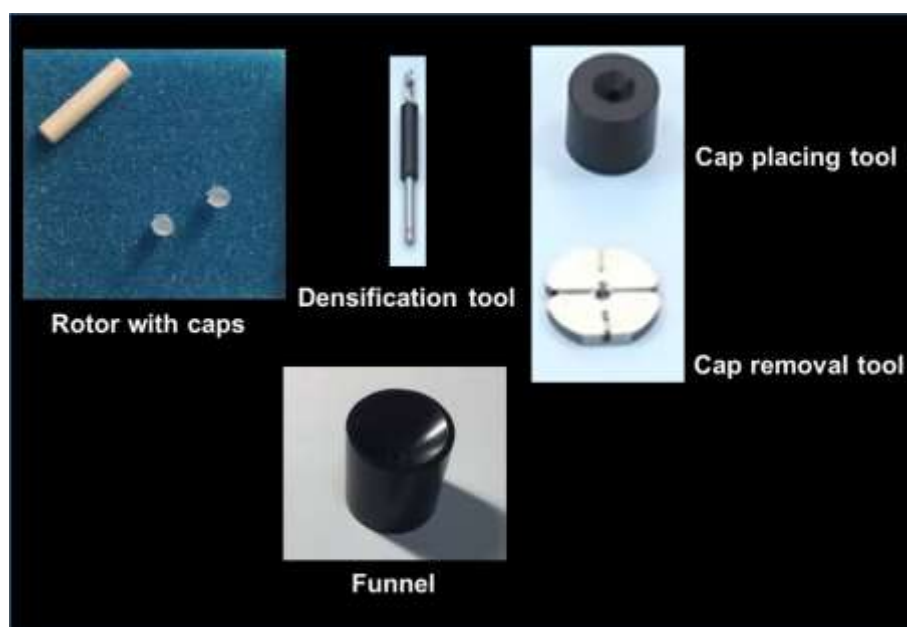


Figure 4.4 Sample preparation accessories for solid state NMR (SSNMR)

4.4 Results and Discussion

4.4.1 Characterization of glutarimidedioxime and glutardiamidoxime using ^{13}C CP/MAS solid state NMR spectroscopy

Figure 4.5 shows the ^{13}C CP/MAS solid state NMR spectrum of Adamantane ($\text{C}_{10}\text{H}_{16}$). Adamantane is commonly used as an external standard for ^{13}C CP/MAS solid state NMR spectroscopy. Adamantane helps in determination of suitable spectral width and resonance frequency. It is used as a standard for chemical shift referencing in solid state NMR spectroscopy. The spectrum in Figure 4.5 shows two distinct well resolved ^{13}C signals, a peak at 28.6 ppm corresponding to methine carbon atoms of adamantane, and a signal at 37.7 ppm corresponding to methylene carbon atoms of adamantane.

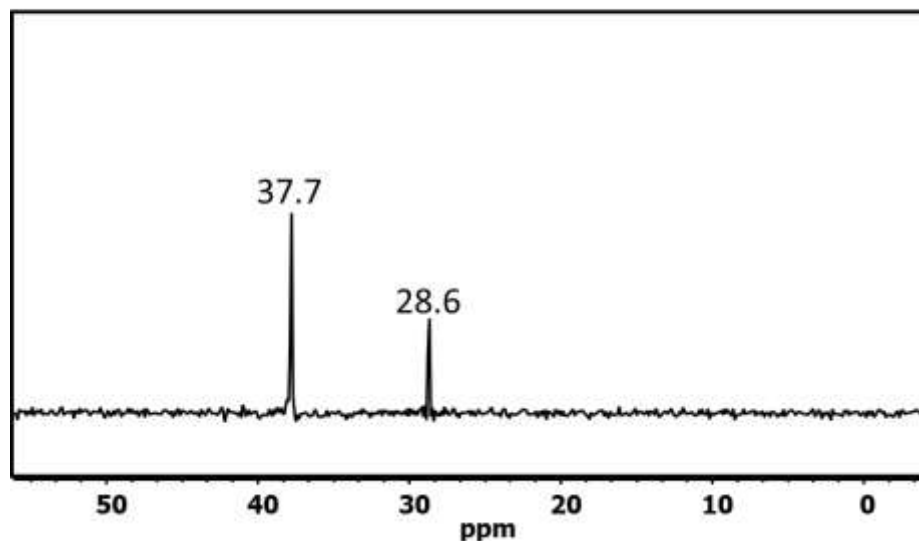


Figure 4.5 ^{13}C CP/MAS solid state NMR spectrum of Adamantane.

Figure 4.6 shows ^{13}C CP/MAS solid state NMR spectra acquired for glutarimidedioxime and glutardiamidoxime. The structures of glutarimidedioxime and glutardiamidoxime are previously shown in Chapter 3, Figure 3.1. Open-chain

glutardiamidoxime shows ^{13}C signals for $[-\text{CH}_2-\text{CH}_2-\text{C}(\text{NOH})\text{NH}_2]$ at 22 ppm, for $[-\text{CH}_2-\text{CH}_2-\text{C}(\text{NOH})\text{NH}_2]$ at 31 ppm, and for $[-\text{CH}_2-\text{CH}_2-\text{C}(\text{NOH})\text{NH}_2]$ at 155 ppm (Figure 4.6a). The ^{13}C solid state NMR signals belonging to $\text{CH}_2-\text{CH}_2-\text{CH}_2-$ at 20 ppm, $-\text{CH}_2-\text{CH}_2-\text{CH}_2-\text{C}(\text{NOH})$ at 24 ppm and for $\text{C}=\text{N}-\text{OH}$ at 147 ppm (Figure 4.6b) were observed for carbons present in the structure of cyclic glutarimidedioxime. The signals at 20 and 24 ppm (Figure 4.6b) and the signals at 22 and 31 ppm (Figure 4.6a) are not well resolved, and a broad signal was observed. This is caused by $^{13}\text{C}-^1\text{H}$ dipolar interactions. There was not enough power in our instrument for resolution of these signals because, to resolve these signals, high power irradiation at proton resonance frequency for decoupling $^{13}\text{C}-^1\text{H}$ interaction is required.

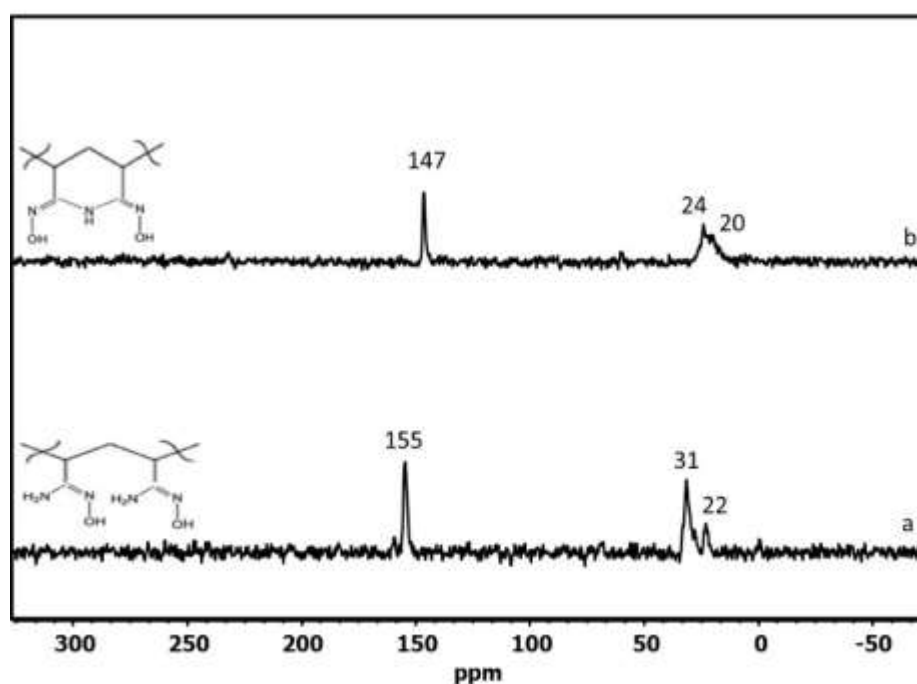


Figure 4.6 ^{13}C CP/MAS solid state NMR spectra of (a) open-chain glutardiamidoxime, and (b) cyclic glutarimidedioxime.

Figure 4.7 shows ^{51}V solid state NMR spectrum acquired for sodium orthovanadate (Na_3VO_4). ^{51}V has a spin of $7/2$, and it falls in the category of quadrupolar nuclei (nuclei with

spin $> 1/2$). The quadrupolar nuclei possess first and second order quadrupolar interactions.

The different satellite and central transitions for ^{51}V nuclei are shown as below.

$$m_1 = \pm 7/2 \leftrightarrow \pm 5/2, \pm 5/2 \leftrightarrow \pm 3/2, \pm 3/2 \leftrightarrow \pm 1/2. \text{ (Satellite transitions)}$$

$$m_1 = + 1/2 \leftrightarrow -1/2 \text{ (Central transitions)}$$

First order quadrupolar interaction mainly affect satellite transitions, and lead to broad NMR signal extended over a wide frequency range. The first order quadrupolar terms can be averaged by magic angle spinning (MAS)^{9, 14} and give spinning sidebands. Second order quadrupolar interactions in vanadium nucleus acts on both satellite as well as central transitions. Second order quadrupolar interactions give lesser broadening of NMR signal than the first order quadrupolar interactions but cannot be averaged by the magic angle spinning technique. The quadrupolar interactions and chemical shielding anisotropy affects the ^{51}V NMR spectra. In the ^{51}V solid state NMR spectrum shown in Figure 4.7, the peaks are caused by central transitions of ^{51}V quadrupolar nuclei. The ^{51}V solid state NMR spectrum of sodium orthovanadate (Figure 4.7) shows a broad signal ranging from -555 ppm to -543 ppm. The broad peak is observed because of different chemical sites and different chemical shift tensors of vanadium in sodium orthovanadate. The broad signal is caused by quadrupolar interactions because of asymmetric environment around the vanadium nucleus, and, due to second order quadrupolar interactions, that broaden central transitions and gives rise to a pattern of broad signals (Figure 4.7) known as the powder pattern.¹² Chemical shielding anisotropy also causes broadening of the signal and results in asymmetric line shape of the NMR signal. The ^{51}V solid state NMR signal observed at -505 ppm (Figure 4.7), is caused by vanadium in a symmetric environment giving rise to an isotropic chemical shift at -505 ppm. In powder form, the NMR signal is the sum of signals from each crystallite, and the signal depends upon the orientation of each crystallite.

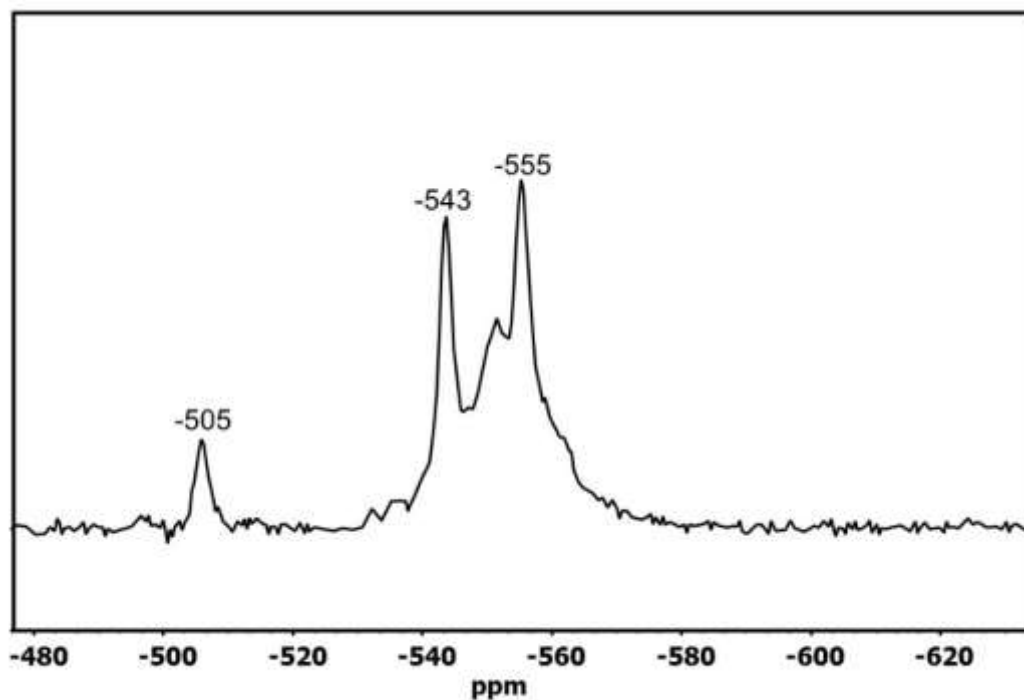


Figure 4.7 ^{51}V solid state NMR spectrum of sodium orthovanadate (Na_3VO_4)

4.4.2 *Characterization of amidoxime and carboxylate containing polymer adsorbents using ^{13}C CP/MAS solid state NMR and FTIR spectroscopy*

^{13}C CP/MAS solid state NMR spectroscopy was used to characterize different functional groups present in pure acrylic fiber and in amidoxime-based polymer adsorbents prepared by using different reaction conditions. Effective adsorption of uranium from seawater depends upon population of carboxylate and amidoxime functional groups present in the polymer adsorbent. Solid state NMR spectroscopy has an advantage over FTIR technique because ^{13}C CP/MAS solid state NMR technique can differentiate between population of cyclic glutarimidedioxime and open-chain glutardiamidoxime present in the polymer adsorbent. The interference between different nuclei is not observed in solid state NMR. Figure 4.8a shows ^{13}C CP/MAS solid state NMR spectrum acquired for pure acrylic

fiber used as a starting material for preparation of LCW adsorbent. The chemical structure of the pure acrylic fiber is shown in Figure 4.3a. The acrylic fibers are polyacrylonitrile fibers containing ester copolymers. Figure 4.8b shows ^{13}C CP/MAS solid state NMR spectrum of amidoximated LCW polymer adsorbent prepared using 3 wt% hydroxylamine in 1:1(v/v) methanol/water solution at 55 to 70 °C and reaction time of 45 minutes. In amidoximation reaction, nitrile groups present in the acrylic fiber are converted to amidoxime. Hydroxylamine converts nitrile groups to amidoxime. The amidoximated fibers were then immersed in 1 M NaOH solution at room temperature for 24 hours. In alkaline solution, the nitrile groups are converted to carboxylate to provide hydrophilicity to the LCW polymer adsorbent and to minimize its physical damage. Some of the nitrile $\text{C}\equiv\text{N}$ groups are left unconverted to preserve mechanical strength in the polymer adsorbent. The ^{13}C CP/MAS solid state NMR spectrum acquired for the fibers after alkaline treatment is shown in Figure 4.8c.

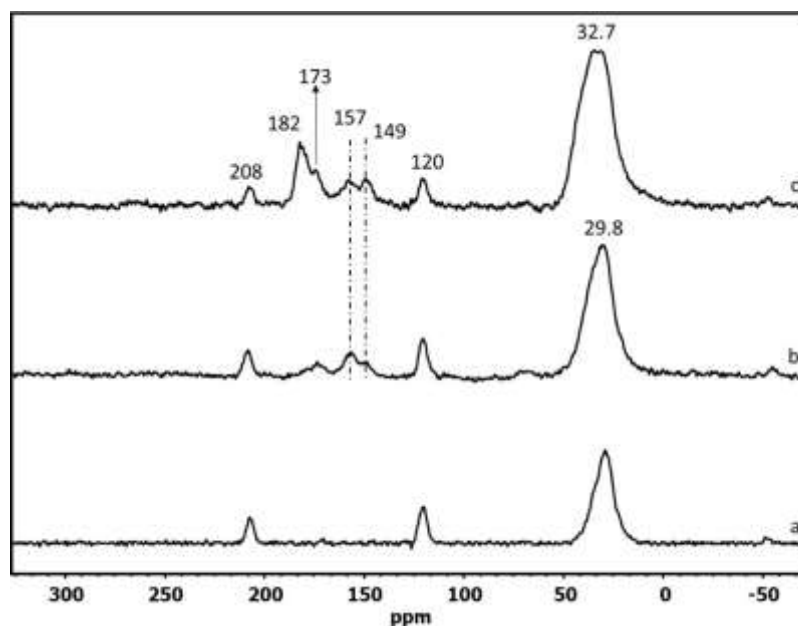


Figure 4.8 ^{13}C CP/MAS solid state NMR spectra of (a) pure acrylic fiber, (b) amidoximated (using 3 wt% hydroxylamine) LCW adsorbent, and (c) alkaline treated LCW adsorbent.

The peak at 29.8 ppm (Figure 4.8a-b) and the peak at 32.7 ppm (Figure 4.8c) belongs to sp^3 hybridized carbon atoms present in polymer adsorbent. The peak at 120 ppm (Figure 4.8a-c) belongs to nitrile $\text{C}\equiv\text{N}$ group present in the polymer adsorbent. The peak at 149 ppm, and 157 ppm (Figure 4.8b-c) are assigned to cyclic glutarimidedioxime [$\text{C}=\text{N}-\text{OH}$] and open-chain glutardiamidoxime [$-\text{CH}_2-\text{CH}_2-\text{C}(\text{NOH})\text{NH}_2$], respectively.^{40, 41} This observation shows formation of both cyclic glutarimidedioxime and open-chain glutardiamidoxime in a ratio of $\sim 1:1$ in the final adsorbent (Figure 4.8c) under these reaction conditions. Das et al.⁴² used ^{13}C CP/MAS solid state NMR technique to investigate effect of heat treatment upon amidoximated, ORNL-AF1 adsorbent. Cyclization of open-chain glutardiamidoxime into cyclic glutarimidedioxime, after treating amidoximated ORNL-AF1 adsorbent with DMSO at 130°C for 3 hours, was observed. In the spectrum shown in Figure 4.8c, two different types of the carbonyl groups in different environments were observed giving rise to two different

signals at chemical shift of 182 ppm and 173 ppm.^{43, 44} The peak at 208 ppm (Figure 4.8a-c) is a spinning side band for the peak at 120 ppm.

Figure 4.9 shows the ¹³C CP/MAS solid state NMR spectra acquired for polymer adsorbent prepared using different reaction conditions using 6 wt% hydroxylamine in 1:1(v/v) methanol/water solution at 55-70 °C. Figure 4.9a, shows ¹³C CP/MAS solid state NMR spectrum of pure acrylic fiber. The spectrum has been explained previously, and shown in Figure 4.8a. It is shown again in Figure 4.9a for the ease of comparison. Figure 4.9b shows the ¹³C CP/MAS solid state NMR spectrum obtained for the amidoximated LCW fibers and chemical structure of amidoximated fiber is shown in Figure 4.3b. Figure 4.9c shows the ¹³C CP/MAS solid state NMR spectrum obtained for fiber after alkaline treatment with 1 M NaOH for 24 hours at room temperature. The chemical structure of the fiber after alkaline treatment is shown in Figure 4.3c. The spectra in Figure 4.9a-c shows ¹³C peaks at 36.4 ppm, 32.2 ppm and 29.2 ppm due to sp³ hybridized carbon atoms present in the polymer adsorbent. The peaks observed at 120 ppm, 173 ppm, 182 ppm, and 208 ppm (Figure 4.9a-c) have been previously explained and shown in Figure 4.8a-c. It is of interest to observe the signal at 157 ppm (Figure 4.9b-c) for open-chain glutardiamidoxime carbon [-CH₂-CH₂-C(NO₂)NH₂]. This observation is likely due to the formation of mainly the open-chain glutardiamidoxime under these reaction conditions.

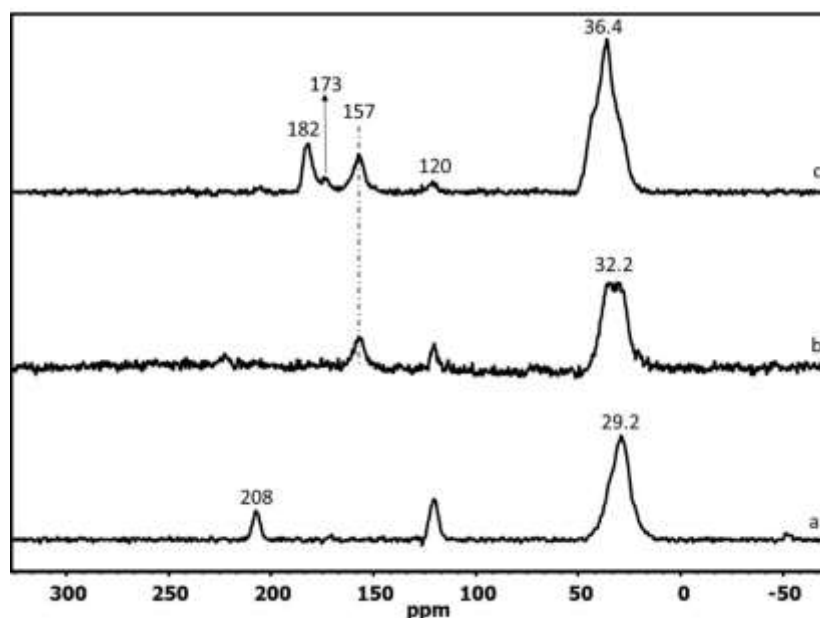


Figure 4.9 ^{13}C CP/MAS solid state NMR spectra of (a) pure acrylic fiber, (b) amidoximated (using 6 wt% hydroxylamine) LCW adsorbent, and (c) alkaline treated LCW adsorbent.

Previous reports suggest that vanadium(V) is one of the greatest competing ions for amidoxime in seawater.⁴⁵⁻⁴⁷ A recent report⁴⁸ using ^{51}V NMR spectroscopy in solution state shows that vanadium(V) does not form complex with open-chain glutardiamidoxime but can complex with the cyclic glutarimidedioxime. The uncomplexation of vanadium(V) with open-chain glutardiamidoxime is previously explained in Chapter 3 and shown in Figure 3.2c, Figure 3.36, and Figure 3.37 using ^{51}V NMR, ^1H NMR, and ^{13}C NMR spectroscopy, respectively. Using cyclic glutarimidedioxime, vanadium uptake from seawater was the same as that of uranium. Iron and vanadium are the two major transition metals competing with uranium for adsorption to amidoxime-based adsorbents in real seawater.^{49,50} Vanadium, which exists in +4 oxidation state as VO^{+2} and +5 oxidation state as VO_2^+ in seawater, has been observed to bind strongly to amidoxime-functionalized adsorbent, reducing adsorption sites available for UO_2^{+2} binding.^{50,51} Elution of vanadium from amidoxime-based adsorbents is

difficult because vanadium binds strongly to the amidoxime groups. However, this vanadium adsorption onto the adsorbent decreases its uranium extraction efficiency and has critical impact on economic feasibility of uranium extraction from ocean. One solution for less vanadium uptake by the amidoxime-functionalized adsorbent is to synthesize a polymer adsorbent containing only the open-chain glutardiamidoxime, because vanadium(V) has less affinity for open-chain glutardiamidoxime, than cyclic glutarimidedioxime. To prepare polymer adsorbent that contains only the open-chain glutardiamidoxime, reaction conditions were modified. Figure 4.10b shows ^{13}C CP/MAS solid state NMR spectrum acquired for the final product (amidoximated and alkaline treated adsorbent) using 3 wt% hydroxylamine in 1:1(v/v) methanol/water solution at 70 °C and reaction time of 30 minutes. The spectrum shows formation of mainly the open-chain glutardiamidoxime evident by the ^{13}C solid state NMR peak at 157 ppm. Other peaks at 36.4 ppm, 120 ppm, and 182 ppm are ascribed to sp^3 hybridized carbon atoms, nitrile $\text{C}\equiv\text{N}$ group, and carboxylate group, respectively (Figure. 4.10a-c). Figure 4.10c shows the ^{13}C CP/MAS spectrum obtained for the amidoximated and alkaline treated adsorbent using 6 wt% hydroxylamine in 1:1(v/v) methanol/water solution at 70 °C, and short reaction time of 20 minutes. This is the best recipe so far for the preparation of LCW adsorbent. The spectrum shows a peak at 157 ppm, suggesting the formation of only the open-chain glutardiamidoxime under these reaction conditions. ^{13}C CP/MAS solid state NMR spectra were also acquired for the AF series adsorbent obtained from the Oak Ridge National Lab (ORNL-AF1), in order to compare it with the LCW polymer adsorbent. The ^{13}C CP/MAS spectrum for the (ORNL-AF1) polymer adsorbent (Figure 4.10a) shows the formation of both cyclic glutarimidedioxime and open-chain glutardiamidoxime evident through a signal at 149 ppm and a shoulder at 157 ppm, respectively. The peak at 30.3 ppm

(Figure 4.10a) corresponds to the sp^3 hybridized carbon atoms present in the structure of ORNL-AF1 polymer adsorbent.

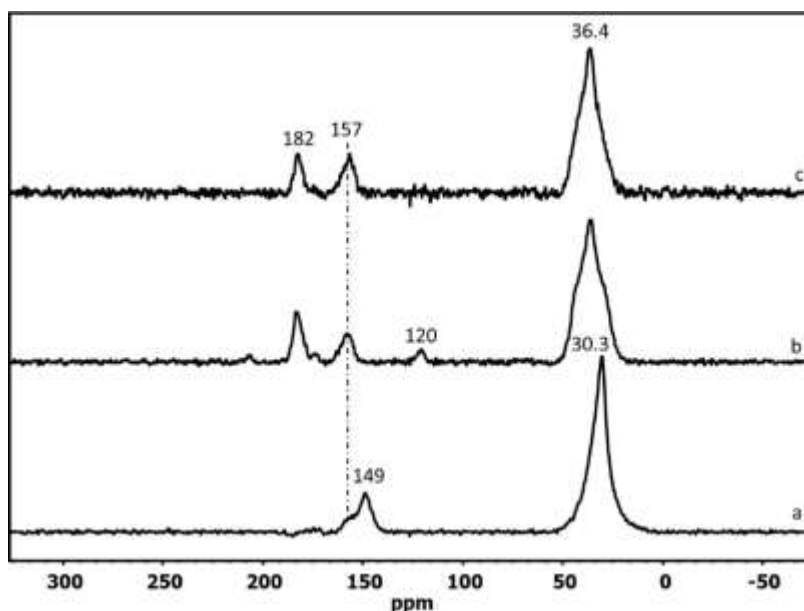


Figure 4.10 ^{13}C CP/MAS solid state NMR spectra of (a) ORNL-AF1 adsorbent, (b) amidoximated (using 3 wt% hydroxylamine) and alkaline treated LCW adsorbent, and (c) amidoximated (using 6 wt% hydroxylamine) and alkaline treated LCW adsorbent.

Commonly used ORNL-AF1 polymer adsorbent for uranium extraction from seawater contains amidoxime and carboxylic acid functional groups. Radiation Induced Graft Polymerization (RIGP) technique is used to graft nitrile and carboxylic acid group into the polyethylene fibers. The adsorbent needs KOH conditioning before exposing them to real seawater for uranium adsorption. KOH conditioning makes the fiber more hydrophilic. This is achieved by removal of a proton from the carboxylic acid grafted in the polyethylene fiber. FTIR results show conversion of amidoxime to carboxylate by the process of KOH conditioning.⁵² KOH conditioning causes physical damage to the structure of polymer adsorbent and results in reduction of uranium adsorption capacity. The use of sodium carbonate and hydrogen peroxide (1 M Na_2CO_3 containing 0.1 M H_2O_2)³⁹ has been suggested

for the elution of uranium from the ORNL-AF1 adsorbents. These eluting agents cause less damage to the adsorbent, resulting in less reduction in uranium adsorption capacity of the adsorbents. The adsorbents can be reused without KOH reconditioning by using the above-mentioned eluting agents. However, no KOH conditioning is necessary for the LCW adsorbent. Mild reaction conditions, at 70 °C, and a short reaction time of 20 minutes was used for the preparation of LCW adsorbent using 6 wt% hydroxylamine. A reaction time of 30 minutes was used for the preparation of LCW adsorbent using 3 wt% of hydroxylamine. It is of interest to observe the ^{13}C CP/MAS solid state NMR spectrum for the LCW adsorbent prepared using 3 wt%, and 6 wt% of hydroxylamine at different reaction times (Figure 4.10b-c) looks identical, with both showing the formation of open-chain glutardiamidoxime, evident through the ^{13}C signal at 157 ppm. However, they show different adsorption capacity in real seawater experiments. The ^{13}C CP/MAS solid state NMR spectrum acquired for the adsorbent prepared using 6 wt% hydroxylamine shows complete disappearance of the nitrile $\text{C}\equiv\text{N}$ group (Figure 4.10c) at the chemical shift of 120 ppm. Disappearance of the nitrile, $\text{C}\equiv\text{N}$ group, and appearance of the ^{13}C solid state NMR signal at the chemical shift of 182 ppm for the carboxylate $[\text{COO}^-]$, group confirms the conversion of nitrile to carboxylate after alkaline treatment of adsorbent.

FTIR spectroscopy was used to examine relative population of amidoxime, carboxylate, and nitrile groups present in the synthesized LCW adsorbent. Figure 4.11 shows the FTIR spectra of pure acrylic fiber, amidoximated (using 3 wt% hydroxylamine), and alkaline treated fiber. The FTIR spectra shown in Figure 4.11 were acquired by Dr. Horng-Bin Pan. In the FTIR spectrum acquired for the pure acrylic fiber the stretching frequency at 2242cm^{-1} represents the nitrile $\text{C}\equiv\text{N}$ group, and the stretching frequency at 1736cm^{-1} is

representative of the C=O group. The FTIR spectrum of the amidoximated adsorbent (Figure 4.11) shows the stretching frequency at 1652 cm^{-1} ascribed to the C=N group and the stretching frequency at 1594 cm^{-1} representative of the N-H bending mode. This observation suggests the amidoximation of the polymer adsorbent because most of the nitrile groups are converted to amidoxime in presence of hydroxylamine. Slight reduction in signal intensity for the nitrile [C≡N] group was observed at the stretching frequency at 2242 cm^{-1} indicating the conversion of nitrile to amidoxime. The FTIR spectrum of polymer adsorbent after the treatment with NaOH shows the appearance of carboxylate [COO⁻] group, at the stretching frequency of 1558 cm^{-1} . This observation clearly suggests the conversion of nitrile to carboxylate using alkaline solution. Reduction in the signal intensity for the C=N group and C≡N group at the stretching frequencies of 1652 cm^{-1} and 2242 cm^{-1} , respectively was observed. Reduction in signal intensity for the C≡N group, after the treatment of polymer adsorbent with NaOH, indicates conversion of nitrile to carboxylate.

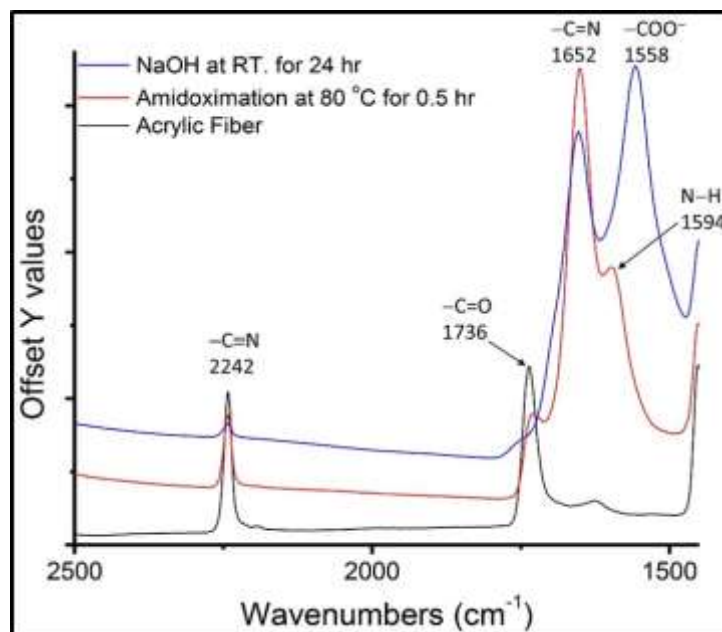


Figure 4.11 FTIR spectra showing the characteristic absorption bands for the LCW adsorbent prepared using 3 wt% hydroxylamine.

The FTIR spectra were acquired for the amidoximated (using 6 wt% hydroxylamine) and alkaline treated polymer adsorbent using a reaction time of 20 minutes at 70 °C are shown in Figure 4.12. No significant change was observed in the FTIR spectra acquired using 3 wt% and 6 wt% hydroxylamine at different reaction conditions. However, the FTIR spectra acquired for adsorbent prepared using 6 wt% hydroxylamine shows complete disappearance of the nitrile $C\equiv N$ group (Figure 4.12) at the stretching frequency of 2236 cm^{-1} . The disappearance of the nitrile $C\equiv N$ group and the appearance of the carboxylate $[COO^-]$ group at the stretching frequency of 1553 cm^{-1} confirms complete conversion of nitrile to carboxylate after treatment of the adsorbent with alkaline solution.

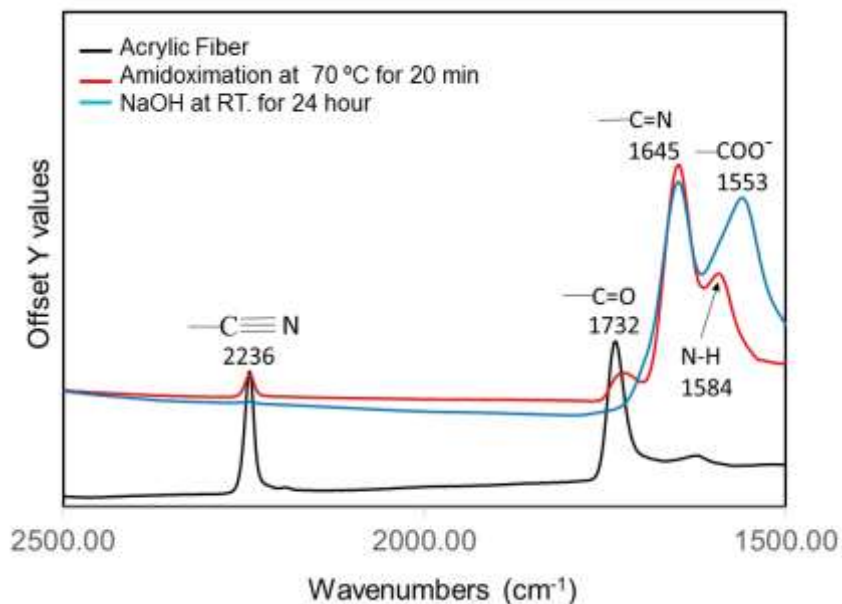


Figure 4.12 FTIR spectra showing the characteristic absorption bands for the LCW adsorbent prepared using 6 wt% hydroxylamine.

4.4.3 Vanadium adsorption in simulated seawater by the LCW adsorbent without and with NaOH treatment

Results for mg of vanadium adsorbed upon simulated seawater exposure of the LCW adsorbent without NaOH treatment are shown in Table 4.1. LCW adsorbent without NaOH treatment shows negligible vanadium adsorption. Without alkaline (NaOH) treatment, the fiber is hydrophobic (Figure 4.13), and, therefore, it does not pick up any vanadium from vanadium stock solution. Results from this study (Table 4.1) indicate that mg vanadium (ranging from 3.4 mg to 3.8 mg), in 400 ml of simulated seawater spiked with 10 ppm vanadium containing the LCW adsorbent is almost the same as that of mg vanadium (3.3 mg) present in 400 ml vanadium stock solution without any adsorbent. This observation suggests that there is no vanadium uptake by the LCW fiber without alkaline treatment. Slight variations in the ICP-MS results with a standard deviation of 0.1673, and percentage relative

standard deviation (%RSD) of 4.6 is caused by instrumental error, may be because of inadequate rinsing of the instrument between vanadium stock solution and samples.

Table 4.1 ICP-MS results on mg of vanadium adsorption by the LCW adsorbent without NaOH treatment in simulated seawater spiked with 10 ppm vanadium.

Sample Details	(mg) Vanadium in 400 ml simulated sea water from ICP-MS
Vanadium stock solution (10 ppm vanadium in simulated sea water without adding adsorbent)	3.3
Simulated seawater exposure time (minutes) of LCW adsorbent without NaOH treatment	
15	3.4
30	3.7
60	3.7
180	3.4
300	3.8
1440	3.6
Mean	3.6
Sample standard deviation	0.16733
% RSD	4.6

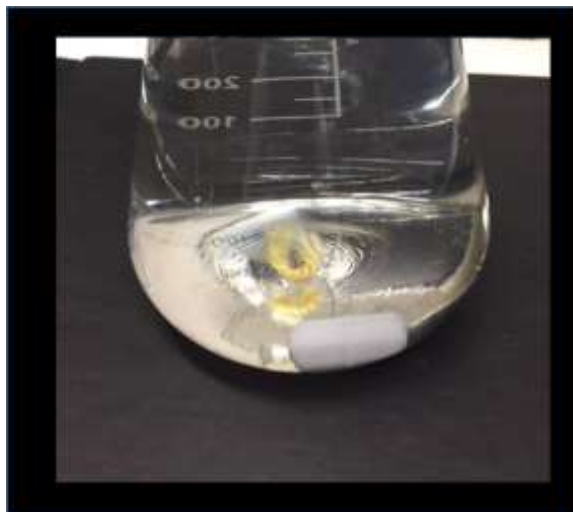


Figure 4.13 LCW adsorbent without NaOH treatment in simulated seawater spiked with 10 ppm vanadium.

The LCW polymer adsorbent was tested for vanadium adsorption using simulated seawater conditions. Simulated seawater solution was prepared using 193 mg of sodium bicarbonate and 25.6 g of sodium chloride. 10 ppm of vanadium was prepared in simulated seawater using sodium orthovanadate. The solution pH was approximately 8.3. Vanadium stock solution (without adding adsorbent) was collected before addition of amidoximated (prepared using 6 wt% hydroxylamine, 20 minutes reaction time) and alkaline treated LCW adsorbent. It was observed that hydrophilic colorless gel like fiber (Figure 4.14a) became yellowish (Figure 4.14b) after exposing it to simulated seawater containing 10 ppm vanadium solution. The fiber picks up vanadium, becomes heavier, and settles on the bottom of the flask (Figure 4.14b). After 24 hours of exposing the fiber to 10 ppm vanadium solution, it turned light brown after vanadium uptake (Figure 4.14c).

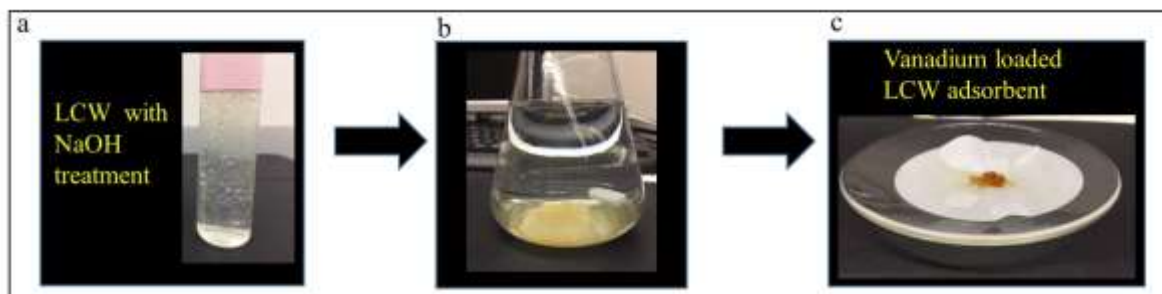


Figure 4.14 Colours of the LCW fiber at different stages. Left, LCW fiber with NaOH treatment in water, hydrophilic forming hydrogel; middle, LCW fibers after ~1-2 hours of exposure in 10 ppm vanadium solution in simulated seawater (yellowish); right, LCW fibers after 24 hours of exposure in 10 ppm vanadium solution in simulated seawater (light brown)

A 10 ppm of vanadium stock solution was equilibrated for ~12 hours to determine the initial vanadium concentration prior to vanadium adsorption experiments conducted by immersing adsorbents into a 400 ml of this solution. 14 mg of adsorbent was equilibrated with 400 ml of simulated seawater solution at room temperature for about 1440 minutes or 24 hours with constant stirring at ~ 290 rpm. An aliquot of sample solution was collected over time. The vanadium stock solution (without adding adsorbent) and the collected sample aliquots were diluted with 2% nitric acid solution to give final concentration of 92 ppb. Samples were then analyzed using ICP-MS spectrometry. The detection limits of ICP-MS are much lower than ICP-OES. ICP-OES has been commonly used by researchers for analysis and quantification of uranium and other elements eluted from the adsorbent by using acid solution.^{42, 53, 54}

Table 4.2, and Figure 4.15, shows time-dependent quantification for vanadium adsorption capacity (mg vanadium/g of adsorbent) by amidoximated (prepared using 6 wt% hydroxylamine, 20 minutes reaction time) and alkaline treated LCW adsorbent. Figure 4.15 shows immediate uptake of 5.2 mg of vanadium /g of adsorbent within 60 minutes. After 300 minutes (5 hours), vanadium uptake by the LCW fiber increased to 10.3 mg vanadium/g of

adsorbent. No significant increase in vanadium adsorption was observed (Figure. 4.15) till 1440 minutes (24 hours).

Table 4.2 Time dependent vanadium uptake by LCW adsorbent exposed to 10 ppm vanadium in simulated seawater.

Simulated seawater exposure time (minutes) of LCW adsorbent with NaOH treatment	(mg) Vanadium adsorbed/g LCW adsorbent
0	0.0
60	5.2
300	10.3
1440	10.3

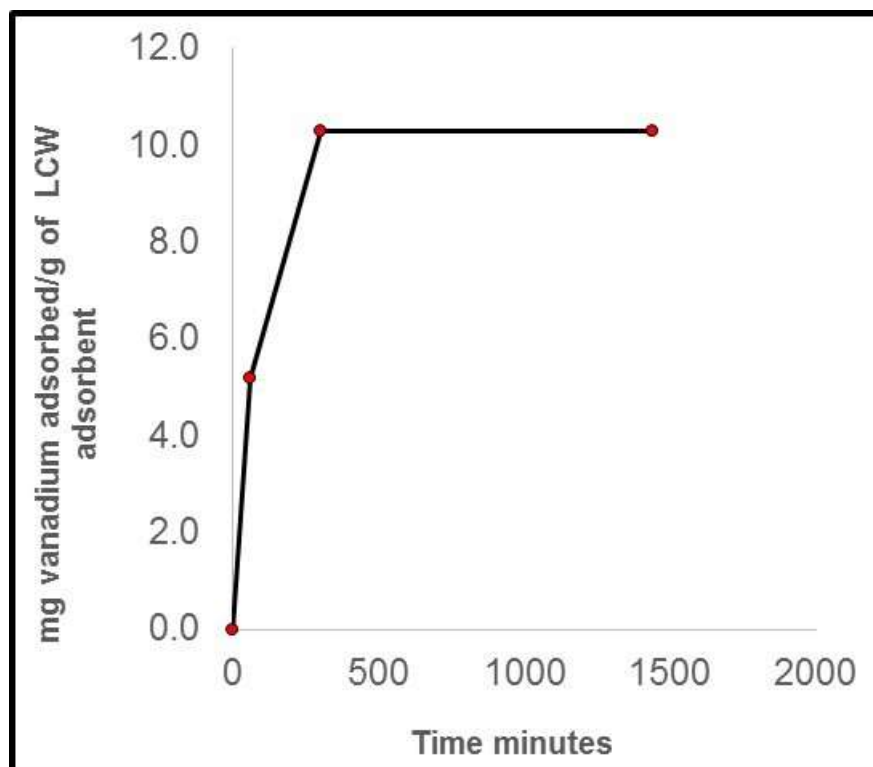


Figure 4.15 Time dependent measurements of vanadium adsorption capacity (mg vanadium/g of adsorbent) by LCW adsorbent exposed to 10 ppm vanadium in simulated seawater.

4.4.4 Vanadium adsorption in simulated seawater by ORNL adsorbent after KOH conditioning

Amidoxime-based ORNL-AF1 adsorbent developed at the Oak Ridge National Lab using Radiation Induced Graft Polymerization (RIGP) method on polyethylene fibers was tested for time dependent vanadium uptake in simulated seawater solution containing 10 ppm vanadium. The original white ORNL-AF1 fibers are shown in Figure 4.16a. The fibers became light brown (Figure 4.16b) after immersing them in simulated seawater containing 10 ppm of vanadium solution. Finally, they turned dark brown (Figure 4.16c) after 24 hours of exposure to 10 ppm vanadium solution in simulated seawater.

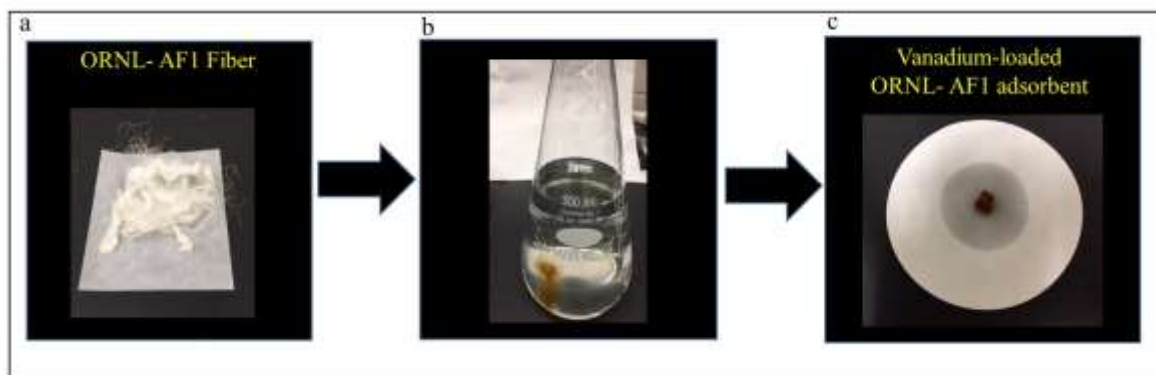


Figure 4.16 Colours of the ORNL-AF1 fiber at different stages. Left, ORNL-AF1 fiber (white); middle, ORNL-AF1 after ~1-2 hours of exposure in 10 ppm vanadium solution in simulated seawater (light brownish); right, ORNL-AF1 fibers after 24 hours of exposure in 10 ppm vanadium solution in simulated seawater (dark brown)

20 mg of ORNL-AF1 adsorbent after KOH conditioning was immersed in 10 ppm vanadium solution in simulated seawater with consistent stirring at 290 rpm for 24 hours at room temperature. Sample aliquots were collected over time and were analyzed by ICP-MS spectrometry. Prior to ICP-MS analysis all samples were diluted with 2% nitric acid solution to give final concentration of 92 ppb. Table 4.3, and Figure 4.17 shows time-dependent measurement for vanadium uptake (mg vanadium/g of adsorbent) by the ORNL-AF1 adsorbent. Figure 4.17 shows increase in vanadium uptake with time. 9.0 mg of vanadium /g of adsorbent was adsorbed by the ORNL-AF1 adsorbent within 20 minutes. A significant increase of 63.3 mg of vanadium/g of adsorbent was observed in 1440 minutes (24 hours). Increase in vanadium adsorption capacity over time by the ORNL-AF1 adsorbent is caused by the presence of cyclic glutarimidedioxime in ORNL-AF1 adsorbent (Figure 4.10a) because it binds strongly to vanadium.

Table 4.3 Time dependent vanadium uptake by the ORNL-AF1 adsorbent exposed to 10 ppm of vanadium in simulated seawater.

Simulated seawater exposure time (minutes) of ORNL-AF1 adsorbent with KOH treatment	(mg) Vanadium adsorbed/g ORNL-AF1 adsorbent
0	0.0
20	9.0
60	22.6
180	45.2
300	49.7
1440	63.3

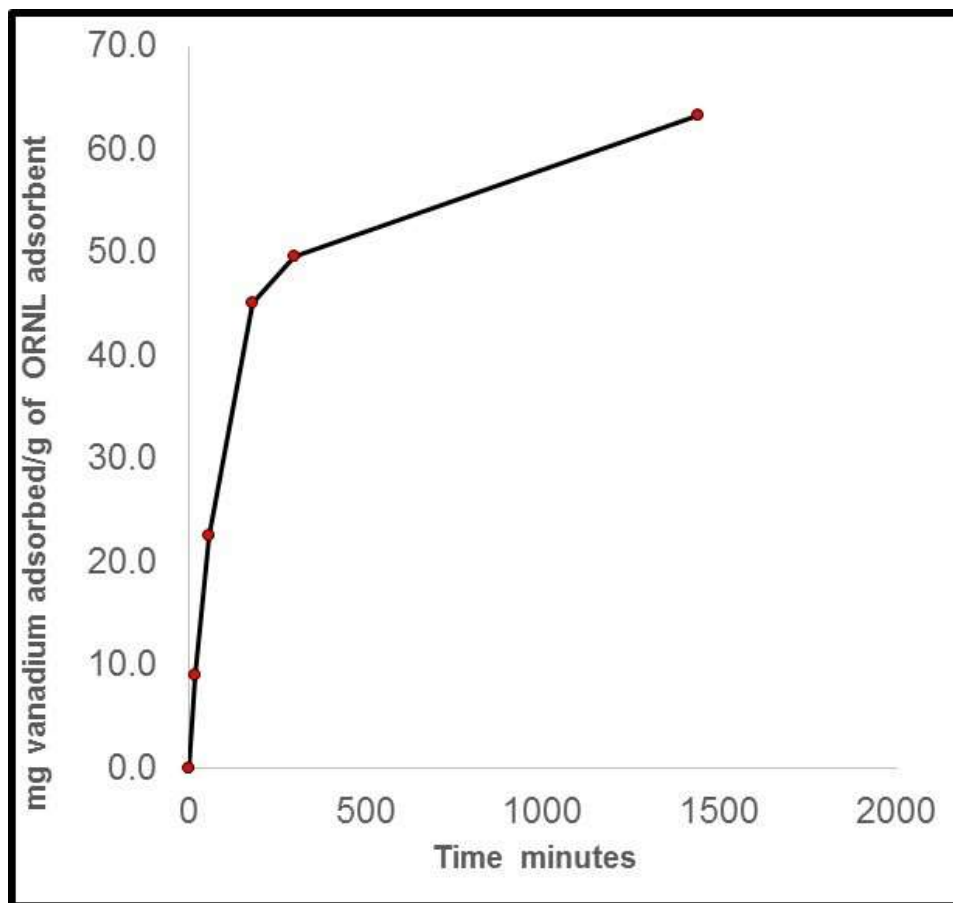


Figure 4.17 Time dependent measurements of vanadium adsorption capacity (mg vanadium/g of adsorbent) by the ORNL-AF1 adsorbent exposed to 10 ppm vanadium in simulated seawater.

4.5 Conclusions

LCW polymer adsorbent was successfully prepared from acrylic fibers as starting material. Acrylic fibers were amidoximated, using 3 wt% and 6 wt% hydroxylamine for 30 and 20 minutes, respectively, at 70 °C, in a solution of 1:1 methanol and water. The amidoximated fibers were treated with an alkaline solution for 24 hours at room temperature. The fibers were air dried before spectroscopic analysis. Formation of mainly open-chain glutardiamidoxime and cyclic glutarimidedioxime in LCW and ORNL-AF1 adsorbent, respectively, was confirmed by ^{13}C CP/MAS solid state NMR spectroscopy. Relative

concentrations of carboxylate, amidoxime, and nitrile groups in the adsorbent were monitored by FTIR spectroscopy. Fast vanadium adsorption kinetics was observed by the LCW adsorbent, upon its exposure to simulated seawater solution spiked with 10 ppm vanadium.

Comparison of vanadium adsorption capacity between LCW and ORNL-AF1 adsorbent shows lower vanadium uptake (10.3 mg vanadium/g of adsorbent) by the LCW adsorbent. The ORNL-AF1 adsorbent shows significantly higher vanadium uptake (63.3 mg vanadium/g of adsorbent). Vanadium adsorption by these adsorbents has been successfully demonstrated by results from ICP-MS analysis.

References

1. Gorter, C.J. Negative result of an attempt to detect nuclear magnetic spins. *Physica*. **1936**, 3, 995-998.
2. Purcell, E.M.; Torrey, H.C.; Pound, R.V. Resonance absorption by nuclear magnetic moments in a solid. *Physical Review*. **1946**, 69 (1-2), 37-38.
3. Wai, C.M.; Pan, H.B. LCW Technologies.
<http://uraniumfromseawater.engr.utexas.edu/partners/lcw-technologies> (accessed Feb 9, 2017).
4. Huang, L.H.; Kao, H.M.; Lii, K.H. Novel vanadium(V) compounds with a layer structure: Synthesis, crystal structures, and solid state NMR spectroscopy of $(VO_2)(2)(4,4\text{-bpy})(0.5)(4,4\text{-Hbpy})(XO_4) \cdot H_2O$ (X = P and As). *Inorganic Chemistry*. **2002**, 41 (11), 2936-2940.
5. Chary, K.V.R.; Rao, V.V.; Mastikhin, V.M. Characterization of vanadium-oxide catalysts supported on $\gamma\text{-Al}_2\text{O}_3$ by ^{51}V solid-state NMR spectroscopy. *Journal of the Chemical Society-Chemical Communications*. **1989**, (3), 202-204.
6. Narsimha, K.; Reddy, B.M.; Rao, P.K.; Mastikhin, V.M. Characterization of vanadium oxide catalysts supported on SnO_2 by ^{51}V and ^1H solid state NMR spectroscopy. *Journal of Physical Chemistry*. **1990**, 94 (19), 7336-7337.
7. Deoliveira, P.G.P.; Lefebvre, F.; Eon, J.G.; Volta, J.C. Characterization of AlNBO_4 and vanadium-oxide catalysts supported on AlNBO_4 by ^{27}Al and ^{51}V solid-state NMR spectroscopy. *Journal of the Chemical Society-Chemical Communications*. **1990**, (21), 1480-1482.

8. Lecoustumer, L.R.; Taouk, B.; Lemeur, M.; Payen, E.; Guelton, M.; Grimblot, J. Characterization by ^{51}V solid-state NMR, Laser Raman and X-ray photoelectron spectroscopy of vanadium species deposited on gamma- Al_2O_3 . *Journal of Physical Chemistry*. **1988**, 92 (5), 1230-1235.
9. Apperley, D.C. *Solid State NMR Basic Principles & Practice*, Momentum Press: Highland Park, 2012.
10. Cohen, M.H.; Reif, F. Quadrupole effects in nuclear magnetic resonance studies of solids. *Solid State Physics*. **1957**, 5, 321-438.
11. Smith, M. E.; Van Eck, E.R.H. Recent advances in experimental solid state NMR methodology for half-integer spin quadrupolar nuclei. *Progress in Nuclear Magnetic Resonance Spectroscopy*. **1999**, 34 (2), 159-201.
12. Balhmutoy, V.I. *Solid-State NMR in Materials Science Principles and Applications*, Taylor and Francis: Hoboken, 2011.
13. Kentgens, A.P.M. A practical guide to solid-state NMR of half-integer quadrupolar nuclei with some applications to disordered systems. *Geoderma*. **1997**, 80 (3-4), 271-306.
14. Duer, M. J. *Solid State NMR Spectroscopy: Principles and Applications (1)*, Wiley-Blackwell: 2008.
15. Andrew, E.R.; Bradbury, A.; Eades, R.G. Removal of dipolar broadening of nuclear magnetic resonance spectra of solids by specimen rotation. *Nature*. **1959**, 183 (4678), 1802-1803.
16. Lowe, I.J. Free induction decays of rotating solids. *Physical Review Letters*. **1959**, 2 (7), 285-287.

17. Pines, A.; Gibby, M.G.; Waugh, J.S. Proton-enhanced NMR of dilute spins in solids. *J. Chem. Phys.* **1973**, *59*, 569.
18. Hartmann, S.R.; Hahn, E.L. Nuclear Double Resonance in the Rotating Frame. *Phys. Rev.* **1962**, *128*, 2042.
19. Pacilio, J.E.; Tokarski, J.T.; Quinones, R.; Iuliucci, R.J. High-Resolution Solid-State NMR spectroscopy: Characterization of Polymorphism in Cimetidine, a Pharmaceutical Compound. *Journal of Chemical Education.* **2014**, *91* (8), 1236-1239.
20. Fernandes, J.A.; Sardo, M.; Mafra, L.; Choquesillo-Lazarte, D.; Masciocchi, N. X-ray and NMR Crystallography Studies of Novel Theophylline Cocrystals Prepared by Liquid Assisted Grinding. *Crystal Growth & Design.* **2015**, *15* (8), 3674-3683.
21. Martins, I.C.B.; Santos, S.M.; Sardo, M.; Fernandes, A.; Antunes, A.; Andre, V.; Mafra, L.; Duarte, T. Packing Interactions and Physicochemical Properties of Novel Multicomponent Crystal Forms of the Anti-Inflammatory Azelaic Acid Studied by X-ray and Solid-State NMR. *Crystal Growth & Design.* **2016**, *16* (1), 154-166.
22. Smith, E.D.L.; Hammond, R.B.; Jones, M.J.; Roberts, K.J.; Mitchell, J.B.O.; Price, S.L.; Harris, R.K.; Apperley, D.C.; Cherryman, J.C.; Docherty, R. The determination of the crystal structure of anhydrous theophylline by X-ray powder diffraction with a systematic search algorithm, lattice energy calculations and ^{13}C and ^{15}N solid-state NMR: A question of polymorphism in a given unit cell. *Journal of Physical Chemistry B.* **2001**, *105* (24), 5818-5826.
23. Lemaitre, V.; Smith, M. E.; Watts, A. A review of oxygen-17 solid state NMR of organic materials towards biological applications. *Solid State Nuclear Magnetic Resonance.* **2004**, *26* (3-4), 215-235.

24. Bryce, D.L.; Sward, G.D. Solid-state NMR spectroscopy of the quadrupolar halogens: chlorine-35/37, bromine-79/81, and iodine-127. *Magnetic Resonance in Chemistry*. **2006**, *44* (4), 409-450.
25. Watts, A.E.; Maruyoshi, K.; Hughes, C.E.; Brown, S.P.; Harris, K.D.M. Combining the Advantages of Powder X-ray Diffraction and NMR Crystallography in Structure Determination of the Pharmaceutical Material Cimetidine Hydrochloride. *Crystal Growth & Design*. **2016**, *16* (4), 1798-1804.
26. Andreis, M.; Koenig, J.L. Poly Soaps/Stabilizers/Nitrogen-15 NMR. In *Advances in Polymer Science*; Springer Verlag: Berlin, 1995; Vol. 124; pp 191-237.
27. Brus, J.; Abbrent, S.; Kobera, L.; Urbanova, M.; Cuba, P. Advances in ^{27}Al MAS NMR Studies of Geopolymers. *Annual Reports on NMR Spectroscopy*. **2016**, *88*, 79-147.
28. Dybowski, C.; Bai, S.; Vanbramer, S. Solid-State Nuclear Magnetic Resonance. *Analytical Chemistry*. **2004**, *76* (12), 3263-3267.
29. Badia, A.; Lennox, R.B.; Reven, L. A dynamic view of self-assembled monolayers. *Accounts of Chemical Research*. **2000**, *33* (7), 475-481.
30. Wachs, I.E. Recent conceptual advances in the catalysis science of mixed metal oxide catalytic materials. *Catalysis Today*. **2005**, *100* (1-2), 79-94.
31. Suib, S.L. Zeolitic and layered materials. *Chemical Reviews*. **1993**, *93* (2), 803-826.
32. Eckert, H. Structural characterization of non-oxide chalcogenide glasses using solid-state NMR. *Angewandte Chemie-International Edition in English*. **1989**, *28* (12), 1723-1732.
33. Eckert, H. Structural characterization of noncrystalline solids and glasses using solid-state NMR. *Prog. Nucl. Magn. Reson. Spectrosc.* **1992**, *24*, 159-293.

34. Legrand, A.P.; Bresson, B.; Guidoin, R.; Famery, R. Mineralization followup with the use of NMR spectroscopy and others. *Journal of Biomedical Materials Research*. **2002**, *63*(4), 390-395.
35. Hong, M. Oligomeric structure, dynamics, and orientation of membrane proteins from solid-state NMR. *Structure*. **2006**, *14* (12), 1731-1740.
36. Baldus, M. Molecular interactions investigated by multi-dimensional solid-state NMR. *Current Opinion in Structural Biology*. **2006**, *16* (5), 618-623.
37. Anderson, M.W. Solid-state NMR as a probe of porous catalysts and catalytic processes. *Topics in Catalysis*. **1996**, *3* (1-2), 195-220.
38. Smith, M.E. Solid State NMR. In *Nuclear Magnetic Resonance*; Webb, G.A., Ed.; Royal Society of Chemistry: 2000; Vol. 29; pp 251-283.
39. Pan, H.B.; Liao, W.S.; Wai, C.M.; Oyola, Y.; Janke, C.J.; Tian, G.X.; Rao, L.F. Carbonate-H₂O₂ leaching for sequestering uranium from seawater. *Dalton Transactions*. **2014**, *43* (28), 10713-10718.
40. Kobuke, Y.; Tanaka, H.; Ogoshi, H. Imidedioxime as a significant component in so called amidoxime resin for uranyl adsorption from seawater. *Polymer Journal*. **1990**, *22* (2), 179-182.
41. Kawakami, T. Structural changes of compounds containing cyano groups by hydroxylamine treatment. *Transactions of the Materials Research Society of Japan*. **2002**, *27*(4), 783-786.
42. Das, S.; Brown, S.; Mayes, R.T.; Janke, C.J.; Tsouris, C.; Kuo, L.J.; Gill, G.; Dai, S. Novel poly(imidedioxime) sorbents: Development and testing for enhanced extraction of uranium from natural seawater. *Chemical Engineering Journal*. **2016**, *298*, 125-135.

43. Finley, J.W. *NMR applications in biopolymers*, 1st ed.; Schmidt S.J., Finley, J.W., Serianni, A.S., Eds.; Plenum Press: Newyork, 1990.
44. Lambert, J. B. *The Multinuclear Approach to NMR Spectroscopy*, 1st ed.; D.Reidel Publishing: Dodrecht, Holland, 1983.
45. Mustapha, A.M.; Pasilis, S.P. Gas-phase complexes formed between amidoxime ligands and vanadium or iron investigated using electrospray ionization mass spectrometry. *Rapid Communications in Mass Spectrometry*. **2016**, 30 (15), 1763-1770.
46. Leggett, C.J.; Parker, B.F.; Teat, S.J.; Zhang, Z.; Dau, P.D.; Lukens, W.W.; Peterson, S.M.; Cardenas, A.J.P.; Warner, M.G.; Gibson, J.K.; Arnold, J.; Rao, L.F. Structural and spectroscopic studies of a rare non-oxido V(V) complex crystallized from aqueous solution. *Chemical Science*. **2016**, 7 (4), 2775-2786.
47. Kelley, S.P.; Barber, P.S.; Mullins, P.H.K.; Rogers, R.D. Structural clues to UO_2^{2+}/VO_2^+ competition in seawater extraction using amidoxime-based extractants. *Chemical Communications*. **2014**, 50 (83), 12504-12507.
48. Pan, H. B.; Kuo, L.J.; Wai, C.M.; Miyamoto, N.; Joshi, R.; Wood, J.R.; Strivens, J.E.; Janke, C.J.; Oyola, Y.; Das, S.; Mayes, R.T.; Gill, G.A. Elution of Uranium and Transition Metals from Amidoxime-Based Polymer Adsorbents for Sequestering Uranium from Seawater. *Industrial & Engineering Chemistry Research*. **2016**, 55 (15), 4313-4320.
49. Kim, J.; Tsouris, C.; Oyola, Y.; Janke, C.J.; Mayes, R.T.; Dai, S.; Gill, G.; Kuo, L. J.; Wood, J.; Choe, K.Y.; Schneider, E.; Lindner, H. Uptake of Uranium from Seawater by Amidoxime-Based Polymeric Adsorbent: Field Experiments, Modeling, and Updated Economic Assessment. *Industrial & Engineering Chemistry Research*. **2014**, 53 (14), 6076-6083.

50. Suzuki, T.; Saito, K.; Sugo, T.; Ogura, H.; Oguma, K. Fractional elution and determination of uranium and vanadium adsorbed on amidoxime fiber from seawater. *Analytical Sciences*. **2000**, *16* (4), 429-432.
51. Kim, J.; Tsouris, C.; Mayes, R.T.; Oyola, Y.; Saito, T.; Janke, C.J.; Dai, S.; Schneider, E.; Sachde, D. Recovery of Uranium from Seawater: A Review of Current Status and Future Research Needs. *Separation Science and Technology*. **2013**, *48* (3), 367-387.
52. Pan, H.B.; Kuo, L.J.; Wood, J.; Strivens, J.; Gill, G.A.; Janke, C.J.; Wai, C.M. Towards understanding KOH conditioning of amidoxime-based polymer adsorbents for sequestering uranium from seawater. *Rsc Advances*. **2015**, *5* (122), 100715-100721.
53. Das, S.; Oyola, Y.; Mayes, R.T.; Janke, C.; Kuo, L.J.; Gill, G.A.; Wood, J.R.; Dai, S. Extracting uranium from seawater: Promising AI series adsorbents. *Industrial & Engineering Chemistry Research*. **2016**, *55*(15), 4103-4109
54. Das, S.; Oyola, Y.; Mayes, R.T.; Janke, C.J.; Kuo, L.J.; Gill, G.A.; Wood, J.R.; Dai, S. Extraction of uranium from seawater: Promising AF series adsorbent. *Industrial and Engineering Chemistry Research*. **2016**, *55*(15), 4110-4117.